FINITE ELEMENT ANALYSIS OF BUILDING DEFORMATIONS DUE TO DEEP EXCAVATIONS

Master Thesis

Harrouni, Mohamed Chakir

19 January 2022

TU Delft Delft University of Technology

FINITE ELEMENT ANALYSIS OF BUILDING DEFORMATIONS DUE TO DEEP EXCAVATIONS

MASTER THESIS

BY

MOHAMED CHAKIR HARROUNI

JANUARY 2022

TO OBTAIN THE DEGREE OF MASTER OF SCIENCE

DELFT UNIVERSITY OF TECHNOLOGY

FACULTY OF CIVIL ENGINEERING

DEPARTMENT OF HYDRAULIC ENGINEERING

SECTION OF HYDRAULIC STRUCTURES & FLOOD RISK

AUTHOR:
MOHAMED CHAKIR HARROUNI
4322967

GRADUATION COMMITTEE:

CHAIRMAN

ASS. PROF. IR. M KORFF	–	SECTION OF GEOTECHNICAL ENGINEERING

COMMITTEE MEMBERS

ASS. PROF. IR. M KORFF	–	SECTION OF GEOTECHNICAL ENGINEERING
IR. W.F. MOLENAAR	–	SECTION OF HYDRAULIC ENGINEERING
IR. P.A. KORSWAGEN	–	SECTION OF STRUCTURAL ENGINEERING

ABSTRACT

Over the past decades an increase in underground construction is observed. Deep excavations are among the structures used for underground construction. The construction of such structures often affects nearby existing structures and causes possibly even damages.

The prediction of these damages is usually done by following these steps:

1. Determining the free-field ground displacements
2. Imposing the displacements on the structure
3. Determining the deformations of the structure
4. Assess potential damages following these deformations

The ground and the structure are often modelled separately taking no (LTSM) or a factor (Relative Stiffness Method) into account for interaction between soil and structure. Taking no interaction into account is particularly conservative when looking at vertical displacements. The non-linear behaviour of structural elements is neglected by these methods. This could lead to errors when assessing deformations of a masonry building due to the extreme non-linear behaviour of masonry structures.

The objective of this thesis is to get a better understanding of the effect of deep excavations on adjacent (piled buildings) by using integrated 2D modelling. This is done by remodelling the construction of the building pit in PLAXIS.

Based on the analysis performed in Section 4 the load on the pile is the largest contributor to the vertical and horizontal displacements of the pile relative to the soil around the pile. The diameter and stiffness of the pile are also very important factor determining the vertical movement of the pile.

The difference in the soil between a free-field situation and a situation with foundation piles (and a building) the piles stiffen the soil around the piles. Especially, when these piles are in a group. This effect increases when the piles are coupled by a structure. Vertical displacements are more smeared out over the length of the pile. This is less the case for horizontal displacements. Foundation piles undergo negative skin friction as a result of the settlements of the upper soil layers leading to stress in the soil beneath the pile tip. The stress in the soil beneath piles increases with increasing load and skin friction on the pile. This increased stress results in more horizontal stress, which in close proximity to a retaining wall could lead to increased deformations in the retaining wall and therefore the soil.

The results of the numerical calculations and the analytic calculations are analysed and compared in Section 6. In the numerical models both linear elastic as non-linear material properties have been assigned to the masonry building façade in different models. The numerical model with linear elastic material properties for masonry showed stiff response of the building to the induced soil deformations, underestimating the potential damages. The numerical model with non-linear material properties assigned to masonry showed more realistic results. These results are in line with the established analytical models.

Integrated numerical modelling could be a viable solution for future projects where potential building damage is assessed next to deep excavation. it could help to identify weak points within a structure which need addressing during the construction of an adjacent deep excavation. This study has shown that it is possible to do damage assessment in a fully integrated model. The important factors in assessing such projects are the overall soil deformation. Secondly, the relation between the soil and foundation of the structure needs to be analysed. Thirdly, the interface between the foundation and the structure is important.

ACKNOWLEDGEMENTS

I would like to thank my supervisors and committee members Mandy Korff, Wilfred Molenaar and Paul Korswagen for their support during the formation of this thesis. Their guidance and assistance have played an essential part in the formation of this thesis.

I would like to thank Mandy Korff for her support and involvement whenever I faced challenging problems. Her participation from the start has been crucial, by providing the necessary input and guidance. Special thanks goes to Wilfred Molenaar for his involvement and critical thinking during the research period. His tendency to return to the basics and work from a structured plot was very helpful. I would also like to thank Paul Korswagen for his critical thinking and in-depth knowledge of modelling masonry, which have been crucial for this thesis

Furthermore, I would like to thank my former colleague Richard Roggeveld and Richard de Nijs for providing essential information which has been used as input and as a reference in this thesis.

Finally, I would like to thank my family and friends for their support and encouragements throughout the thesis and my studies as a whole. Above all, I want to praise and thank Allah the almighty for blessing me with the opportunity and strength to complete this research.

TABLE OFF CONTENT

LIST OF TABLES

LIST OF FIGURES

1 INTRODUCTION

Urban areas have seen a large increase in their size over the past decades or even centuries. This has led to a large pressure on existing free space in these urban areas. At a certain point in time these available spaces will vanish and the question should be asked whether this has been an efficient manner to make use of available space. That's why over the past decades increase in underground building can be seen. Infrastructural elements as tunnels and parking facilities have increasingly been constructed underground. Also, a whole network of cables and pipes is now operative outside of the civilian eye. A portal to a new world has been opened.

1.1 USE OF UNDERGROUND SPACE

Use of underground space has showed to be an efficient method to make use of the already scarcely available space. When moving functionalities to the underground above ground extra pace is generated for other purposes. By moving infrastructure underground, the number of bottlenecks and intersections can be reduced, which is favourable for congestion and safety. Also, noise disturbance and air pollution in urban areas can be reduced significantly. It improves the quality-of-life above ground.

Construction below ground also has got its disadvantages. It's costlier and there is also more risk. It requires knowledge and experience to avoid damage to the existing buildings and the future construction.

1.2 GEOTECHNICAL MODELLING

In the past and present, a lot of analytical design methods are developed to assess the effect of underground construction. The increasing amount of research, boundaries and stakeholders has led to an evenly increasing complexity of these analytical design methods. This has led to an increase of use of computer programs for these types of analysis.

The most complete computer programs are those who make use of finite element method (FEM). FEM has made it possible to get accurate results in a rather simplistic way. FEM programs are nowadays commonly used in (civil) engineering. All claim to be capable of modelling aspects in engineering. Modelling soil behaviour is one of those aspects. PLAXIS has been the widely used FEM-program for geotechnical problems (including modelling building pits) in the Netherlands. PLAXIS has shown to be a reliable and rather accurate tool for analysing soil behaviour, deformation and stability of soil structures. The modelling of buildings and structures is often performed using divergent designated computer programs. In practice, this means that the modelling of structures above surface level and beneath the surface is often separated even if a project regards both fractions.

1.3 ORGANIZATION OF THE THESIS

The introduction to this thesis is presented in Section 1. The thesis outline is explained in Section 2. This is followed up by a literature review in Section 3 in which the modelling methods at hand will be reviewed. In the literature review the focus has been mainly the prediction of ground deformations due to deep excavations and sequentially the building deformation caused by excavations. Also, background information is provided about the case to be reviewed and used. In Section 4 the important parameters foundation piles next to deep excavations is assessed. In Section 5 the effect of the presence of a building on the overall soil behaviour next to deep excavations is analysed. In Section

6 the possibilities of modelling a building next to the deep excavation is asses. Different parameters are varied in order to be able to formulate these important parameters. In Section 7 the conclusions are presented and recommendations for future research are given.

2 THESIS OUTLINE

2.1 OBJECTIVE

The objective of this thesis is to get a better understanding of the effect of deep excavations on adjacent piled buildings. The state-of-the-art design and prediction methods for the prediction of building deformations and potential damages will be reviewed. It is intended to formulate guidelines and recommendations for the prediction of building deformations and damages using 2D Finite Element Analysis in future projects. In order to do so the research can basically be split in two sequential parts:

- Formulate recommendations for 2D numerical modelling of piled buildings adjacent to excavations.
- Validate these recommendations and the state-of-the-art Finite Element Analysis and analytical design methods by back analysis of a well monitored case and comparing these results with real data.

The first part of this research aims to get a better understanding of important parameters for numerical modelling of the behaviour of structures next to building pits. This study aims to include these buildings into numerical models and to modify the properties and dimensions to replicate a real situation as accurately as possible.

The second part of this research aims to validate the state-of-the-art design methods. Both numerical and analytical design methods will be reviewed and set up. The analytical and numerical results of the expected building deformations will be compared to the actual building deformations.

2.2 RESEARCH QUESTION

The literature study has presented a large insight in structural behaviour of structures next to building pits. However, the literature review has also shown that there are still some questions unanswered in the field. Section 2.2.1 contains an overview of the knowledge gaps. Section 2.2.2 describes the aim of the research and in Section 2.2.3 the research question is be formulated.

2.2.1 Knowledge Gaps

- The effect of lateral displacement of piles on the strains in piled building is poorly understood. The strains are mostly determined using (modified) Limiting Tensile Strain Method (LTSM). The interaction between the piles, the soil and the building due to imposed horizontal ground movements, determine the transfer of horizontal strains to the building and the possible lateral pile loading. Netzel (2009) stated that this interaction needs further investigation.

- The actual needed building detail input remains unknown. In most cases, the building is modelled as a weightless, rectangular, isotropic elastic beam. Anisotropy is accounted for by modifying the Poisson's ratio. It is questionable whether the building is modelled properly using this method. Can anisotropy or differences in shape be modelled differently and give more accurate results?

- The validation of the numerical and analytical damage predictions with well-defined monitoring data of differential ground and building deformations is an ongoing future challenge. The clear registration of pre- and post-construction building damage would help

to contribute to adjust conventional methods. The procedure of validation of the modified LTSM method using actual observed damage and monitoring data should be carried out. Although, the LTSM method has shown to deliver the desired work, it is still a rather conservative approach.

- The behaviour of old timber piles proved to deviate from new timber piles or new foundation piled in general. The structural properties of these timber piles degrade over time. The behaviour of these old timber piles is still poorly understood and a prevalent topic.
- The monitoring results collected from the Amsterdam deep excavations can be used for validations and analyses related to the response of buildings to the construction of deep excavations. The actual building deformations and resulting damage should be compared to the theoretical building damage indicators.

2.2.2 Aim of Research

The relevant knowledge gaps are formulated. Based on these knowledge gaps the aim of the research can be proposed. The overall aim of this research is to get a better understanding of important parameters for numerical modelling of the behaviour of structures next to building pits. Especially anisotropy of structures is often modelled in a rather schematic manner. This study aims to include these structures into numerical models and modify the properties and dimensions to replicate a real situation as accurate as possible. Parallel to these numerical models, analytical models will be set up to be able to compare numerical results with analytical results. The analytical models are set up by formulating the free-field ground movements, which will give deflections that are induced on to the building. These free-field ground movements will be modelled using both analytical and numerical approaches. The analytical and numerical results of the expected building deformations will be compared to the actual building deformations. The resemblances and differences will be documented so conclusions can be drawn. This should result in recommendations on predicting building deformations using integrated 2D numerical modelling. The result should give an alternative for using LTSM by focusing on its supposed shortcomings.

The data set used is the one obtained from the Vijzelgracht Station building pit, part of the Amsterdam North South Line metro project. Since, the buildings around this project have mainly timber piled foundations of which some are more than a century old, the main focus will be on these types of buildings. The old timber piles behave different from the new ones. The effect of the aging process on the structural properties of timber piles has been poorly understood and is a relevant aspect of this project. This thesis aims to give some answers regarding this topic. Especially, on how to model the effective pile dimensions and modified Young's modulus.

The Numerical models will be set up in a 2D plane using PLAXIS. PLAXIS is a Finite Element Method Program widely used in The Netherlands for modelling geotechnical problems. A validation is made of the Numerical models and the results should be more easily adopted and extrapolated to other methods or programs in numerical modelling.

2.2.3 Research questions and sub-questions

Based on the literature review, knowledge gaps and the research aim a research question is formulated to define what question this research is aiming to answer:

"What are the important parameters for predicting building deformation next to deep excavations using integrated 2D numerical modelling?"

In order to answer this research question, the following sub questions will need to be answered:

1. **What is the state of the art of predicting building deformations?**
   An assessment should be made the available and used methods on predicting building deformations. Decoupled methods have been addressed in the literature study. Special attention should go to integrated methods.

2. **What are important parameters in modelling piled foundations using 2D Finite Element Analysis?**
   Deep excavations are in most cases a 3D problem. However, excavations with a significant length can be brought back to a 2D cases. The adjacent building is also simplified to a 2D case. If this structure has a piled foundation, this needs also to be simplified to a 2D model. The important parameters need to be identified to get an acceptable 2D representation. Which structural details are of importance and which do not have significant effect on the results?

3. **How do foundation loads and or building stiffness impact soil deformations next to deep excavation?**
   The difference of modelling uncoupled and (partially) coupled is being assessed. The effect of the presence of a piled structure on the soil deformations is analysed.

4. **What are the forces acting on a building foundation during every excavation step?**
   The forces acting on a building foundation are analysed during every excavation step. It could be possible that a foundation is critically loaded in a phase prior to the final excavation step.

5. **What is possible in modelling masonry buildings into PLAXIS and how do these compare?**
   The design choices and simplifications should be mapped. This will help assigning suitable material properties to masonry elements in PLAXIS. Especially, the non-linear behaviour of masonry is of importance.

6. H**ow do the numerical and analytical models compare to real data?**
   A comparison is made between the different calculation method. This is done by comparing both finite element models and analytic models with real monitoring data. It is very interesting to look at the supposed conservative approach of the LTSM method. Also, the neglected horizontal movement of the soil is interesting.

2.3 RESEARCH METHOD

The research question and sub questions will be assessed using the following path described in Figure 2-1 and followed by a further description of the steps:

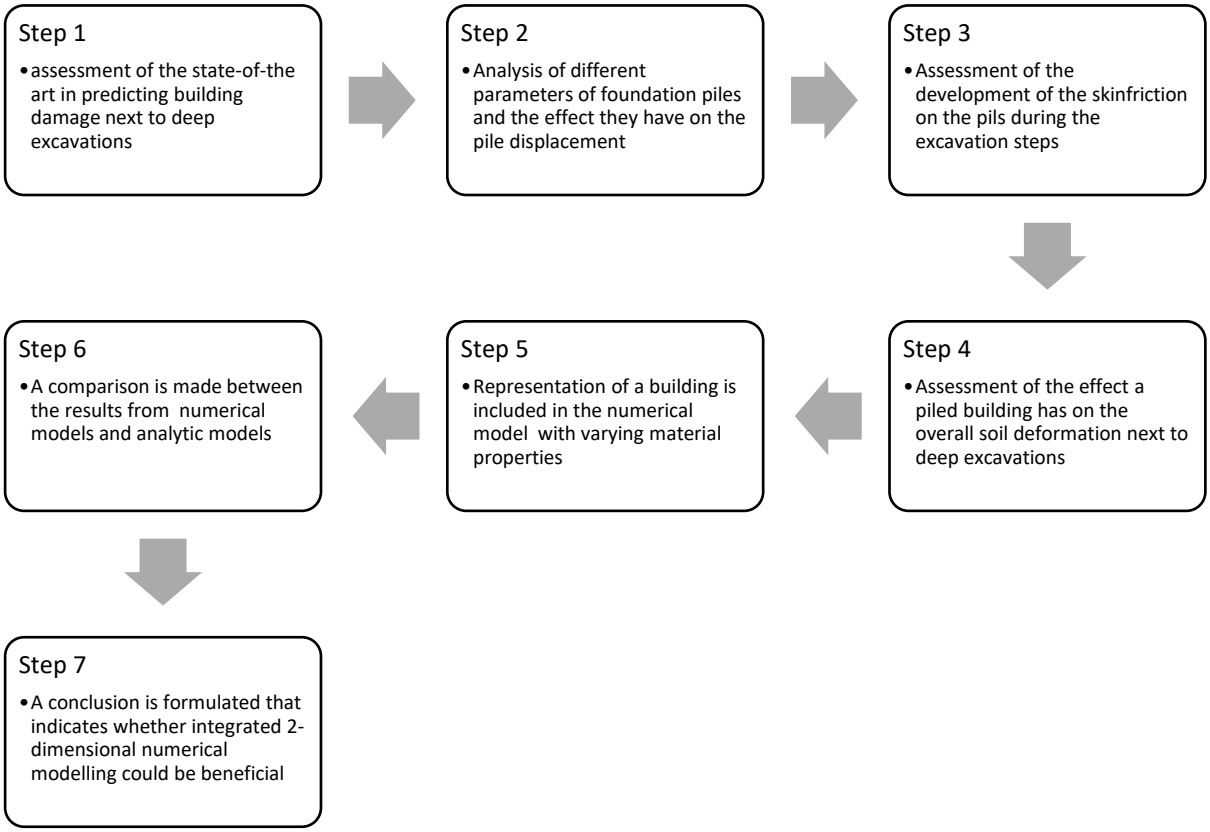

Figure 2-1 Steps of the Limiting Tensile Strain Method

1. The state-of-the-art in predicting building deformations next to deep excavations needs to be assessed. The assumptions used in these methods are of importance. Also, the short comings should be addressed.
2. The building pit will be modelled using PLAXIS. The structural details of the foundation will be analysed. Adjustments will be needed in order to optimize certain elements. This adjusting process should be documented.
    - The simplification of the foundation of the adjacent building is of great importance and should thus be documented in detail. This will be done by looking at the following parameters of old wooden piles.
        - Tapering: The old timber piles are predominantly tapered in shape. The tip is in most cases around 110 mm in diameter and the head is on average around 220 mm in diameter. In PLAXIS these piles are modelled as embedded beam rows in a 2D plane. This means that the piles need to be brought back to a line element. This is done by making 3 models with different pile diameters:
            - 220 mm (this is the maximum value)
            - 110 mm (this is the minimum value)
            - 180 mm (this is a widely used average)

- Youngs modulus: The literature provides a variety of literature concerning this parameter for old timber piles. Old Timber piles behave very different from new piles that's why this is rather interesting to look at:
    - 15000 MPa (new stiff pile)
    - 6000 MPa (aged Pine wood)
    - 3000 MPa (low value found for aged Scot's pine wood)
- The distance of the pile from the excavation: The distance of a pile from the excavation is also of importance for its response. Piles are loaded differently during every construction stage, depending on their distance to the excavation. Piles at 3 different distances from the excavation are analysed.
    - 8 m distance
    - 14 m distance
    - 20 m distance
- Loads: in the literature there is an indication that the load in a pile influences its behaviour significantly. To investigate these 4 separate situations will be analysed to determine the influence of different loads on pile displacements:
    - Self-weight
    - Self-weight + 50 kN
    - Self-weight + 100 kN
    - Self-weight + 200 kN

3. Now the effect of the different excavation steps on the piled foundation is assessed. The excavation induces soil settlements. These settlements cause on their turn an extra load on the piles in the form of negative skin friction. This load varies every excavation step. The following aspects will be analysed:
    - Skin friction action on the piles
4. The effect of the presence of a piled building on the soil deformations is assessed. It is interesting to analyse how the presence of a building effects the settlements and horizontal soil displacement. This will give brighter insight in the disproportion of using uncoupled methods. This will be done by comparing three cases:
    - The green-field settlements: This is a model built without the inclusion of structural elements, other than the structural elements present in the deep excavation.
    - Loaded model: This is a model which includes loaded piles. The output of point 2. is used to assign to the piles their structural properties. Furthermore, each individual pile will get an additional load, representing the vertical load present in the pile coming from a building.
5. Integrated model: This is a model which includes a piled building. Again, the output of point 2. is used to the give the piles their structural properties, the building modelled at this point should resemble the same building aimed to model in the Loaded model. Based on the study performed in Section 3 a set of coupled models are set-up and modelled in PLAXIS. These variants should include different methods modelling a piled masonry structure in PLAXIS.
6. A comparison is needed between the coupled models and the decoupled models. For this, several analytical modes need to be set up.
7. The end goal of this research is to formulate recommendations on modelling piled masonry buildings adjacent to (deep) excavations using integrated 2-dimensional numerical modelling. The settlement effects are of great importance. The steps towards a proper model should be mapped. The following aspects should be described in further detail:

- The parameters used for the foundation need to be assessed. The parameter describing the soil-structure interaction best should be set out.
- A comparison needs to be made between the numerical models and the analytical models for soil deformation by looking at the monitoring data.
- A comparison needs to be made between the numerical models and the analytical models for building deformation by looking at the monitoring data.

3 LITERATURE STUDY

3.1 GROUND DISPLACEMENT DUE TO CONSTRUCTION OF BUILDING PITS

The construction of building pits in urban surrounding implies several sources of ground movements (Netzel, 2009):

- Installation and removal of retaining walls
- Groundwater lowering due to leakage of a retaining wall or due to construction dewatering
- Excavation and as a consequence the deformation of the retaining wall of the building pit

Retaining walls are an essential part in today's construction of building pits. These are rigid (in comparison to the soil) structures which mainly need to provide lateral soil stability. More specific, sheet pile walls are mainly used in the construction of building pits. Well used installation and removal methods of sheet piles are jacking, vibratory driving and impact driving. Due to its economic advantage, vibratory driving is the most used installation method in the Netherlands. In 70 to 80 % of the cases vibratory driving is used as an installation method in the Netherlands (NVAF and PSD, 2002).

Vibratory driving also has its downsides. It reportedly causes vibrations in the soil, noise and settlements. To avoid or reduce these negative side effects other installation methods are used. A more environmentally friendly installation method is pressing of the sheet pile. The alternatives aren't only restricted in installation methods. It is also optional to choose a different type of retaining wall, such as diaphragm walls.

Lot of research is done on the lateral displacements of a retaining wall due to different excavation depths, installation methods and soil conditions. However, it is not so much this parameter but rather the distribution of the (differential) ground movements of the soil mass behind the retaining walls that is of interest to the damage prediction of surrounding buildings (Netzel, 2009).

3.1.1 Peck

The foundation for the assessment and prediction of vertical ground movement next to excavations was laid by Peck (1969). Data was collected of ground surface settlement next to soldier piled structures and (braced) sheet pile walls. The compiled data was presented in a chart on which Peck (1969) drew the ground settlement through. On the chart the relative maximum ground settlement is plotted against the relative distance from the excavation. Peck (1969) has distinguished 3 categories. These classifications are made based on soil condition and the margin of safety against basal stability. Pecks method has been described as a rather conservative approach by Netzel, 2009.

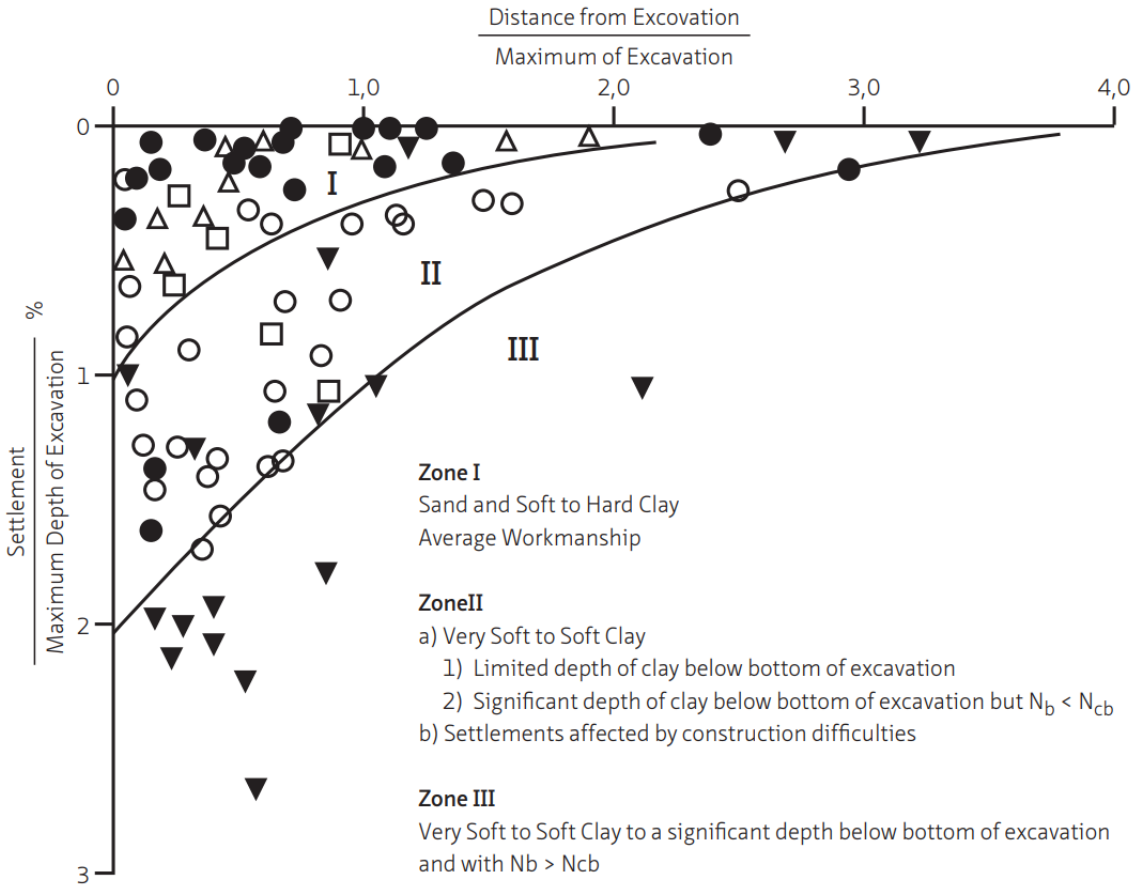

Figure 3-1 Peck's ground settlement trough (Peck, 1969)

3.1.2 Clough & O'Rourke

Clough et al. (1990) has further analysed Peck's work. Additional data and information have been included in the analysis. Also, this work has been supported using several non-linear finite element analyses. The presented displacements are all due the excavation of the building pits and the installation of walls and struts. This study covered sheet piles and soldier piles with struts. The lateral expected displacement is depicted in Figure 3-2.

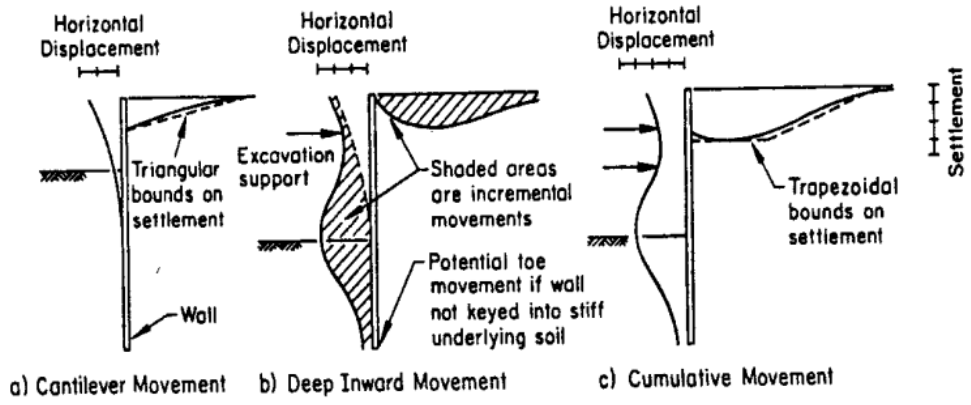

Figure 3-2 Typical displacement profiles for braced and tied-back walls (Clough and O'Rourke, 1990)

It was found that the maximum vertical ground movement was approximately 0,3 % of the excavation depth H for sandy soils and very stiff clays. This is substantially lower than the value found by Peck

(1969), 1,0 % red. According to Clough et al. the differences are the result of development of existing and new methods in the control of the excavation, installation and strutting processes. This had a large effect on the more recent gathered data. For medium and soft clays larger settlements were found. These values corresponded with values found by Peck (1969). The maximum vertical ground movement was varied between 0.5 % and 2.0 % of the excavation depth H depending on the stiffness and safety factor (Netzel, 2009).

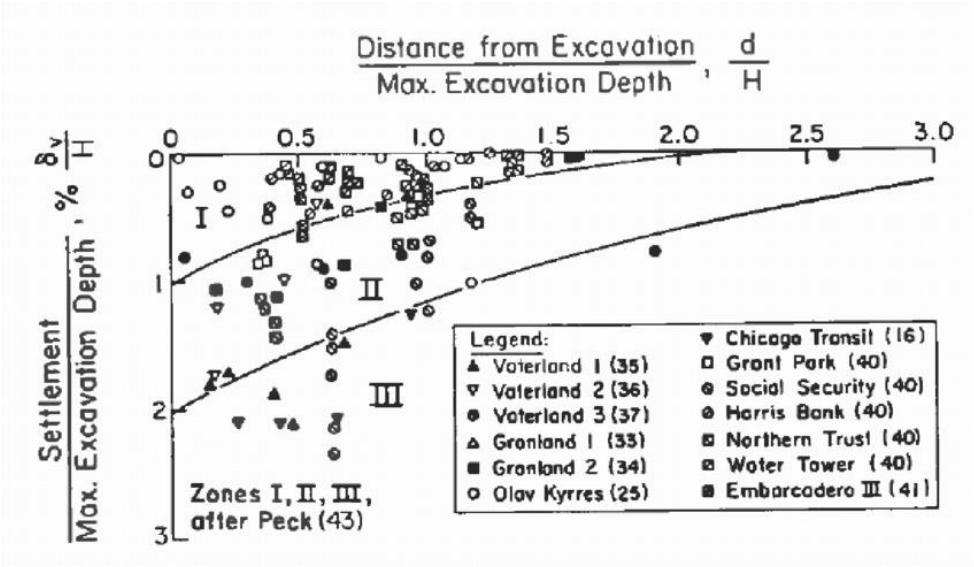

Figure 3-3 Ground settlement trough for medium to soft clays according to Clough et al. (1990)

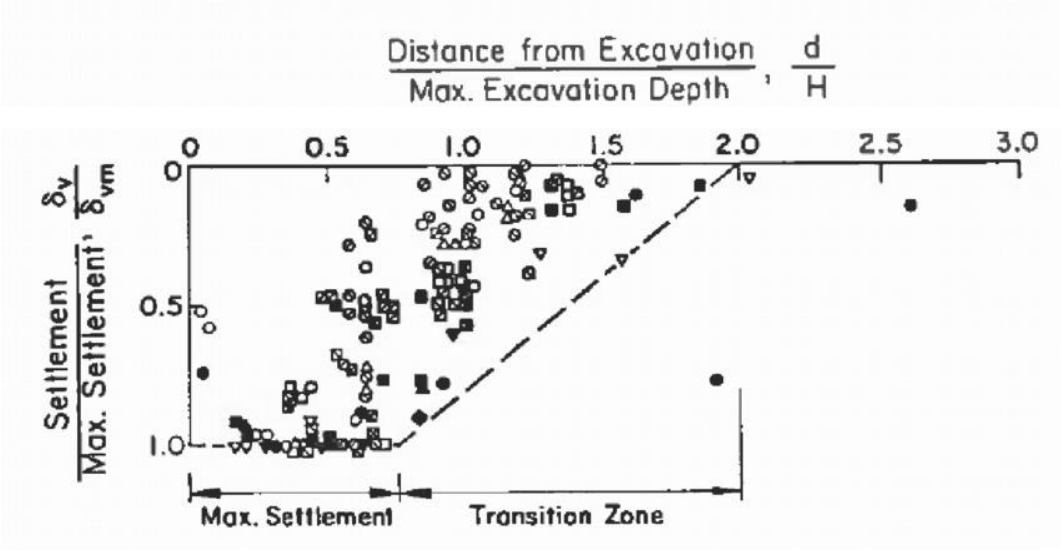

Figure 3-4 Ground settlement relative to the maximum ground settlement (Clough et al., 1990)

These are all categorized data. However, in order to come to a design Clough and O'Rourke (1990) suggested the use of dimensionless settlement envelopes. The recommended envelopes are depicted in Figure 3-5 .

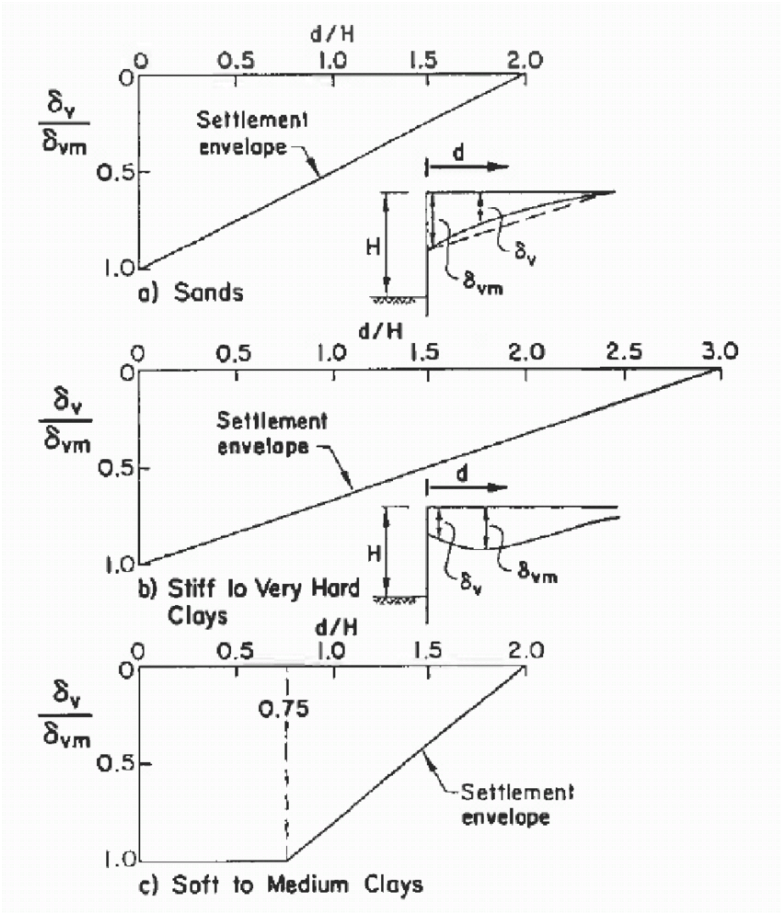

Figure 3-5 Dimensionless settlement envelopes suggested by Clough et al. (1990)

3.1.3 Dhanjal, Thurlow and Bailey

Over the past different prediction have been made for settlement. One of those is presented by Dhanjal et al. (2001). In order to make a settlement prediction for the construction of the Copenhagen metro a new settlement envelope has been developed. Dhanjal et al. (2001) stated that the surface level settlement through is a scaled version of the lateral displacement of the retaining wall. The ratio between the two is in most cases between 0.6 and 0.8. The ground conditions in Copenhagen consist of made ground and glacial till overlying Copenhagen limestone. The glacial till consists of overconsolidated sandy clay or clayey sand with bands of water bearing meltwater sands and gravels (Netzel, 2009). The chosen design settlement curve is shown in Figure 3-6.

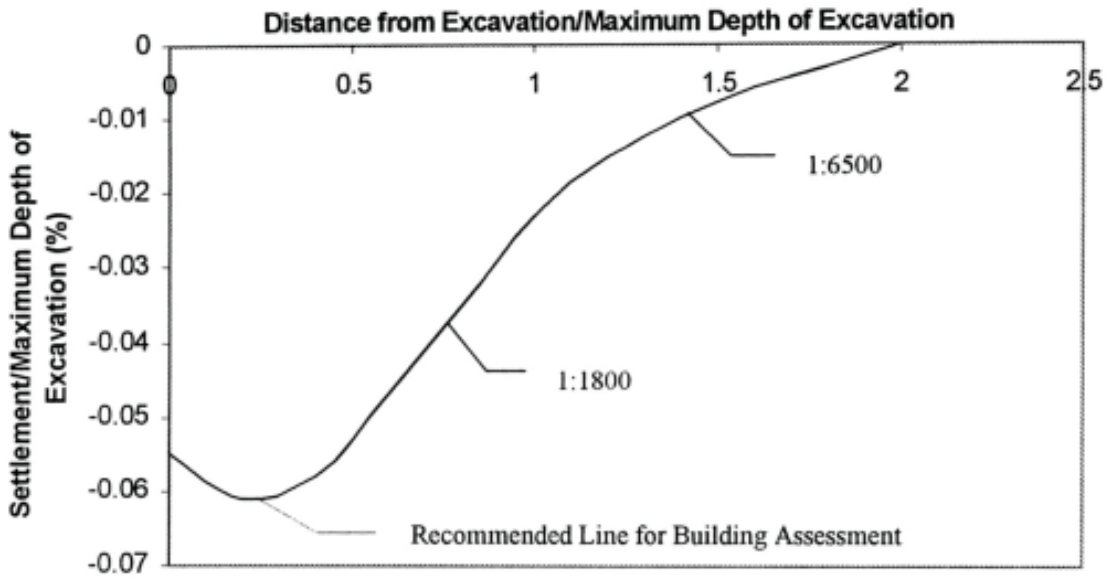

Figure 3-6 Design settlement curve adjacent to the building pit in Copenhagen by Dhanjal et al. (2001)

3.1.4 Hashash, Whittle

Hashash et al. (1996) carried out extensive numerical parametric studies to develop charts for estimating maximum lateral wall movements and maximum ground movements for deep excavations in soft soils as functions of the excavation depth, support conditions, the wall length and the stress history of the soil (Netzel, 2009). The focus was mainly on braced diaphragm walls in deep soft clay deposit. This study is used to make a design of the construction of underground highways in Boston. This non-linear approach should give a more precise result due to the inclusion of non-linear stiffness properties at small shear strains and anisotropic stress-strength behaviour. However, this non-linear approach also has its limitations according to Whittle et al. (1993). The use of laboratory test to analyse soil behaviour is still an essential aspect of predicting soil deformation.

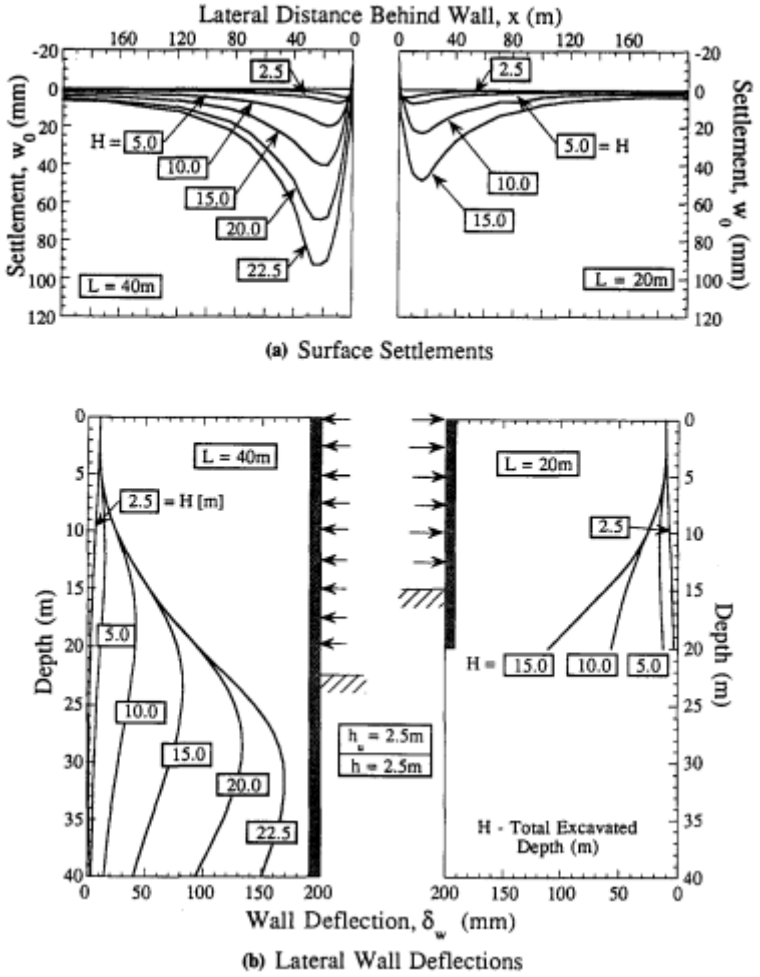

Figure 3-7 Effect of wall length on lateral deflections and surface settlements (Hashash et al. 1996)

3.1.5 Hsieh and Ou

Hsieh and Ou (1998) also stated that the settlement through follows the deflected shape of the retaining wall. In the case of a strutted retaining wall the maximum deflection occurs a relatively large distance away of the retaining wall. Hsieh and Ou presented a normalized settlement profile. The base of this profile are 10 Taipei cases. The result found is that the maximum settlement occurs a distance halve the excavation depth away from the excavation.

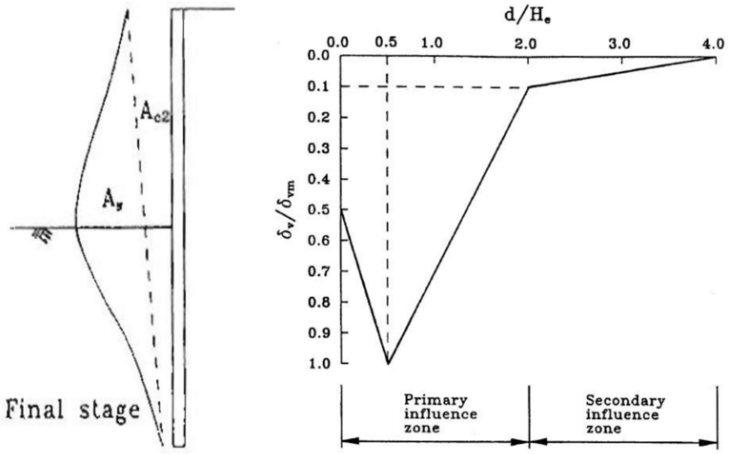

Figure 3-8 Ground settlement curve according to Hsieh and Ou (1998)

3.2 BUILDING RESPONSE

The increasing use of building pits in urban areas has raised increasing concerns about its effect. Firstly, concerns about the soil displacements are raised. Often these soil displacements imply effect on existing buildings adjacent to the excavation. Which has raised even more public concerns. This has an even more effect on people's lives and property. These displacements could cause damages to the adjacent buildings. Which could cause the structure to lose its economic and/or historic value. These effect on the adjacent building could also imply third party impact, construction delay and substantial increase of project cost (Son-Cording, 2005).

It has become more necessary to set a detailed assessment of the possible impacts of certain activities. By this means the activities can be rethought and the impact can be minimized by taking additional or aberrant measures to mitigate or minimize the problems. In order to assess potential damage to adjacent buildings Son and Cording (2005) have set a simplified road map on the steps to be taken to assess and estimate potential building damage. The following was stated:

"In general, building damage estimation is performed with the following steps:

1. *Estimation of free-field ground movement;*
2. *Consideration of effect of building stiffness on free-field ground movement, defined as the movement for the ground if no building were present;*
3. *Estimation of building distortion based on soil–structure interaction;*
4. *And estimation of damage level."*

3.2.1 Limiting Tensile Strain Method (LTSM)

A popular method to assess building deformation due to settlements is the limiting tensile strain method (LTSM). Studies performed by Burland et al. (1974) and Boscardin et al. (1989) form the basis of the method. The method is based on the development of strains in the element due to ground deformations. Whit these strains displacements and damages can be assessed. The level of expected tensile strains is determining the degree and amount of damage. The method is quite popular in practical engineering for settlement risk assessment in the design stage of excavation works in urban surrounding (Netzel, 2009). The Limiting Tensile Strain Method also describes 4 steps to come to a damage prediction and doesn't differ much from the steps described by Son et al. (2005). The steps described by the Limiting Tensile strain method are depicted in the figure below.

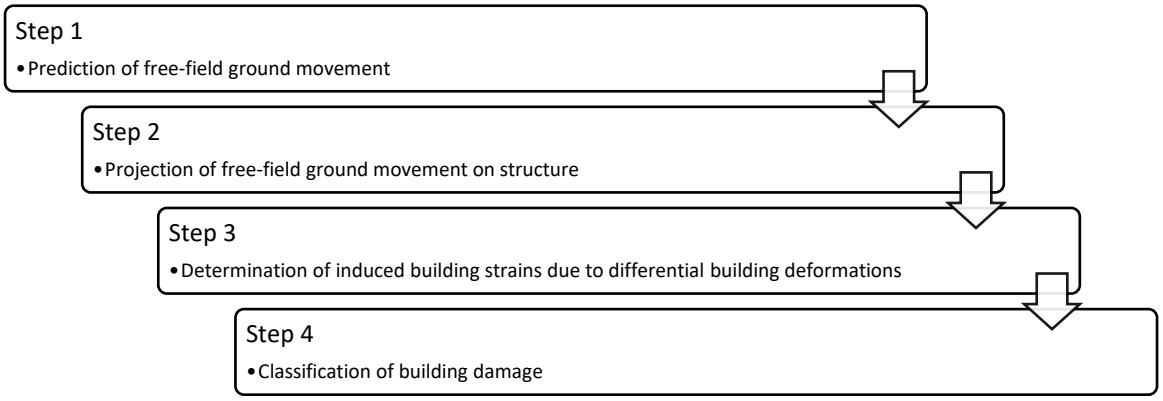

Figure 3-9 Steps of the Limiting Tensile Strain Method

Step 1: Prediction of free-field ground movement

The free-field ground movements are determined using either analytical or numerical methods. The free-field ground movements are often described as the green field ground movements. These

movements are the ground movements without any influence of present structures. This means that the results are on the basis that the soil is decoupled from the present structures. The relevant area is called the influence area and can be described as the area where the excavation induced settlement is larger than 1 mm. The differential settlement outside the influence area is regarded as irrelevant and is expected not to cause any damage to the above laying structures.

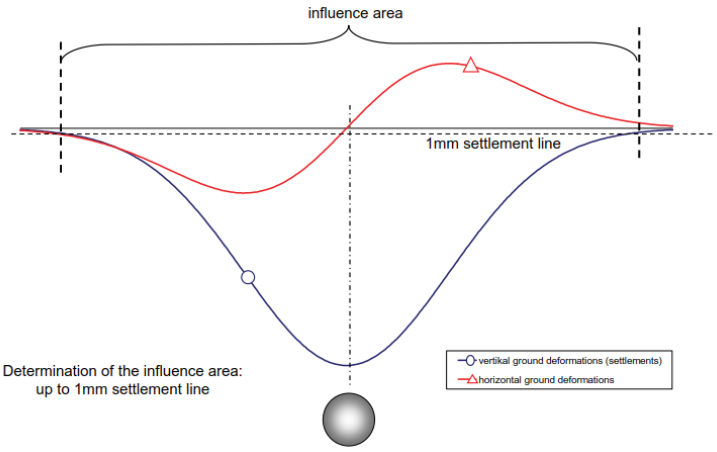

Figure 3-10 Determination of the influence area due to TBM-tunnelling (Netzel, 2009)

Step 2: Projection of free-field ground movement on the structure

In this step the previously determined free-field deformation is projected on the existing buildings. Again, the example of the TBM-tunnelling is used.

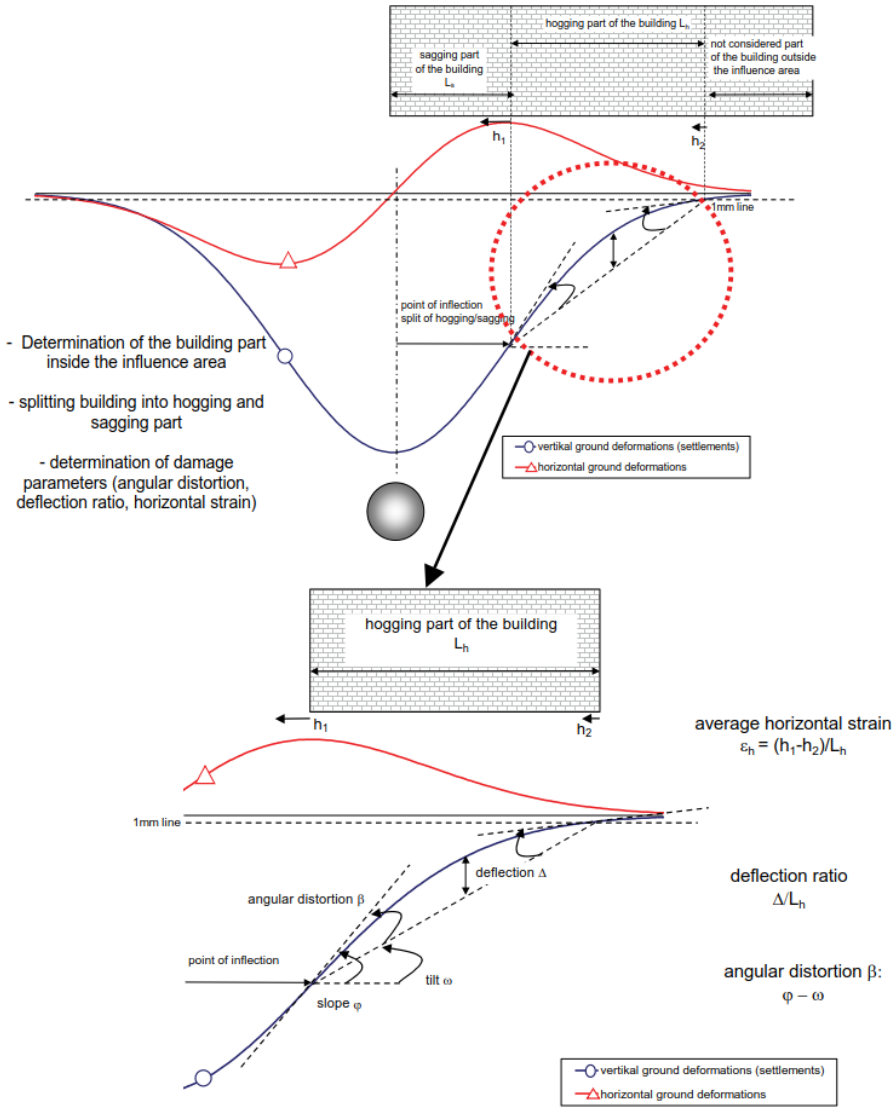

Figure 3-11 Projection of the green field movement on the structure (Netzel, 2009)

Firstly, the part of the building inside the influence area is determined. Then the hogging and sagging parts of the building are determined. This is done by taken the vertical settlement curve and pointing out the point of inflection. This point forms the boundary between the hogging zone and the sagging zone.

Also, the differential horizontal free-field movement is projected on to the building. This is done by taking the average horizontal strain and inducing the strain to the building. This strain is depicted as ε_h in Figure 3-11.

Step 3: Determination of induced building strains

The building is modelled as a weightless, rectangular, isotropic elastic beam of length L, Height H and material parameter E/G. the parameter E/G is the ratio between the Young's Modulus and the Shear Modulus. The material parameter E/G accounts for the expected structural behaviour of a (framed) structure (Netzel, 2009). Burland et al. (1974) suggested an E/G value of 2.6 for a massive wall. This value does also depend on the Poisson's ratio (v). The relation between the different values is described by the following formula:

$$E = \frac{G}{2(1+v)}$$

The strains induced to the structure are determined using analytical beam equations. The structure is modelled as a simply supported beam. This simply supported beam is assumed to be loaded by a fictious point load. This load should give similar deflections and angular distortions as imposed by the ground displacement resulting from step 2. A visualization of the this fictious beam model is depicted in Figure 3-12.

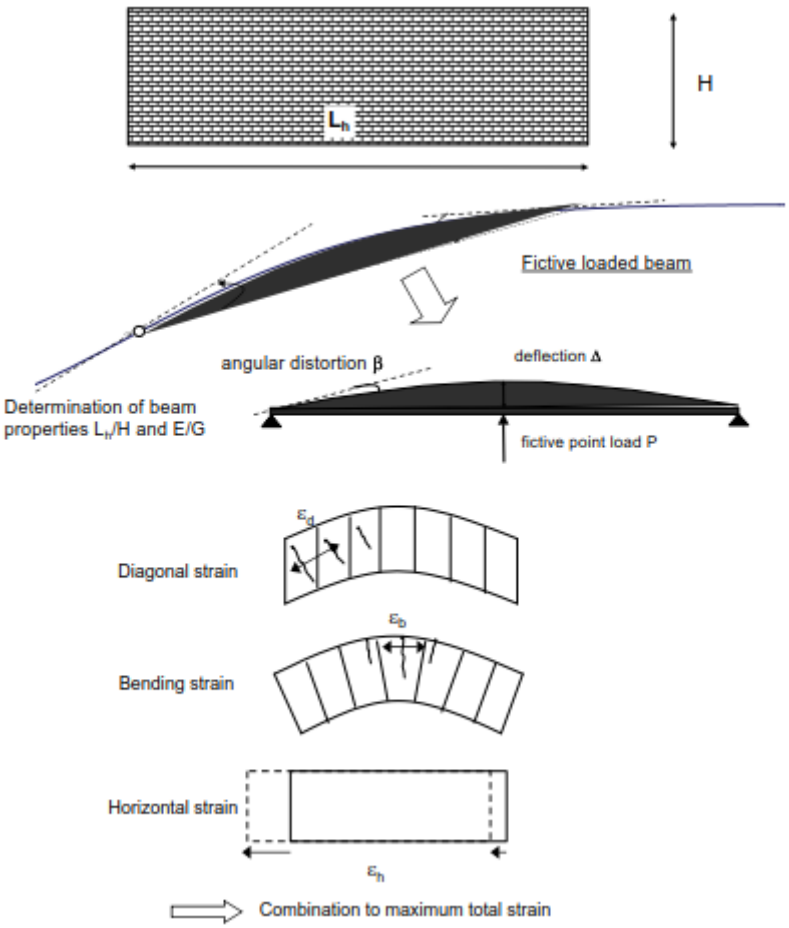

Figure 3-12 Fictious beam model (Netzel, 2019)

The beam equations are used to determine mainly the bending and shear deformations. However, it matters which driving parameter is chosen. Usually, the deflection ratio or the angular distortion is chosen as the driving parameter. Burland et al. (1974) has developed the following equations with the deflection ratio as the driving parameter. The equations for the maximum bending strain ($\varepsilon_{b,max}$) and the maximum diagonal strain ($\varepsilon_{d,max}$) are both based the Timoshenko's beam equations (1957):

$$\varepsilon_{b,max} = \frac{\frac{\Delta}{L}}{\frac{L}{12*t} + \frac{3*I}{2*t*L*H}*\frac{E}{G}}$$

$$\varepsilon_{d,max} = \frac{\frac{\Delta}{L}}{1 + \frac{H*L^2}{18*I}*\frac{G}{E}}$$

In which:

L Length of the beam i.e., the considered part of the building
I Moment of inertia of the beam
E Young's modulus of the beam
G Shear modulus of the beam
t furthest distance from the neutral axis to the edge of the beam in tension (if the neutral axis is in the middle of the beam t = H/2; if the neutral axis is at the bottom edge of the beam t = H)

An essential observation made by Burland et al. (1974) is that the building rather sensitive to damage in a hogging mode deformation in comparison to a sagging mode deformation. This was observed by analysing empirical data. This difference in sensitivity can be accounted for by changing the level of the neutral axis as suggested by Burland et al. (1974).

Boscardin et al. (1989) proposed the usage of angular distortion (β) to determine the influence of the vertical displacement on the building. The result was a relationship between the angular distortion and the deflection ratio for a simply supported beam, centrally loaded with a point load and the neutral axis at the lower edge of the beam (assumed for the hogging zone):

$$\beta = 3 * \frac{\Delta}{L} * \left(\frac{1 + 4 * \left(\frac{E}{G}\right) * \left(\frac{H}{L}\right)^2}{1 + 6 * \left(\frac{E}{G}\right) * \left(\frac{H}{L}\right)^2} \right)$$

The derivation of the maximum total strain is done by distinguishing the highest value of the combination of the maximum bending strain with the average horizontal strain and the combination of the maximum diagonal strain with the average horizontal strain. This highest value is regarded as the dominant tensile strain imposed on the building.

The suggestion to determine ε_{bt} by superposition is done by Boscardin et al. (1989) for the case of the hogging zone. Given that the neutral axis is assumed to be at the bottom of the structure. This superposition is presented by the following formula:

$$\varepsilon_{bt} = \varepsilon_h + \varepsilon_b$$

In the case of a horizontal strain being transferred at the neutral axis, a horizontal strain will occur over the height of the structure. The combined maximum strain (ε_{bt}) will then occur at the top fibre for a structure in the hogging zone.

The maximum diagonal strain is determined quite differently. As the diagonal strain and horizontal strains act in divergent directions. However, it is possible to project the strains onto the maximum principal stress (ε_{dt}) by the formula presented by Timoshenko et al. (1971):

$$\varepsilon_{dt} = 0.5 * \varepsilon_h + \sqrt{0.25 * \varepsilon_h^2 + \varepsilon_d^2}$$

Step 4: Classification of building damage

The possible or potential damage to a structure can be related to the total strain derived in step 3. A numerous number of large-scale tests on masonry structures was carried out and analysed by Burland et al (1974). The results showed that the tensile strain in structures is the driving parameter for the formation of cracking in masonry structures. This study formed the basis for Burland et al. (1977) to formulate a system to classify damage to masonry structures only to be slightly changed by BRE (1981), (1990). The severity of the damage is classified based on the ease of repair. This system is limited for standard domestic buildings and office buildings. Boscardin et al. (1989) contributed to the system by

relating the strains directly to the damage. Further description and classifications are described in Table 3-1.

Table 3-1 Damage classification in LTSM (according BRE (1981), (1990) and Boscardin et al. (1989))

Category of damage	Damage class	Description of typical damage and ease of repair	Approximate crack width (mm)	Limiting tensile strain levels (Boscardin et al. (1989)) (%)
Aesthetic damage	0 - Negligible	Hairline cracks of less than about 0,1mm width	Up to 0.1mm	0 - 0.05
	1 - Very slight	Fine cracks which can easily be treated during normal decoration. Perhaps isolated slight fracturing in building. Cracks in external brickwork visible on close inspection.	Up to 1mm	0.05 - 0.075
	2 - Slight	Cracks easily filled. Redecoration probably required. Several slight fractures showing inside of building. Cracks are visible externally and some repainting may be required externally to ensure water tightness. Doors and windows may stick slightly	Up to 5mm	0.075 - 0.15
Functional damage, affecting Serviceability	3 - Moderate	The cracks require some opening and can be patched by a mason. Recurrent cracks can be masked by suitable linings. Repainting of external brickwork and possibly a small amount of brickwork to be replaced. Doors and windows sticking. Service pipes may fracture. Weather-tightness often impaired.	5 to 15mm or several cracks >3mm	0.15 - 0.3
	4 - Severe	Extensive repair work involving breaking out and replacing sections of walls, especially over doors and windows. Windows and door frames distorted, floors sloping noticeably. Walls leaning or bulging noticeably, some loss of bearing in beams. Service pipes disrupted.	15 to 25mm but also depends on number of cracks	>0.3
Structural damage, affecting stability	5 - Very severe	This requires a major repair involving partial or complete rebuilding. Beams loose bearing, walls lean badly and require shorting. Windows broken with distortion. Danger of instability.	Usually >25mm, but depends on number of cracks	

Several remarks must be noted when using this system:

1. There is no simple relationship between serviceability and degree of visible damage
2. It must be emphasized that in assessing the degree of damage, account must be taken of both the location and market value of the building.
3. Crack width is one factor in assessment and should not be used on its own as a direct measure of damage.
4. Boscardin et al. (1989) described the damage corresponding to the tensile strain in the range 0,15 – 0,3% as 'moderate to severe'. However, none of the cases quoted by them exhibit severe damage for this range of strains.

Conclusion

The limiting tensile strain method is simple, though quite effective at assessing building deformations and damages. However, the method is quite conservative depending on modelling choices and design approach. Giardina (2013) named a set of limitations of the LTSM.

This is firstly due to its assumption of a fully decoupled reality in which the greenfield ground movements are imposed on to a separate structure, neglecting any interaction.

The nonlinear behaviour of structural elements is neglected, since the structure is modelled as a weightless, rectangular, isotropic elastic beam. This is especially risky when assessing deformations of a masonry building due to the extreme nonlinear behaviour of masonry structures.

Another limitation of the LTSM is the fact that a three-dimensional problem is brought back to a two-dimensional model. This off coarse neglects any 3D effects caused by the building being unaligned or any asymmetrical properties of the structure.

Since in the limiting tensile strain approach the calculated displacements are applied directly to the beam model, the interaction effect provided by the foundation is neglected. This is in principle a conservative assumption for vertical displacements, but for horizontal displacements it can lead to an underestimation of the damage if the building is located in the sagging zone of the tunnelling-induced trough (Netzel, 2009).

The approach also simplifies structural imperfections. Perforations, such as doors and windows are taken into account by reducing the equivalent stiffnesses of the structure. However, the actual location of a perforation in a wall can have significant implications to is behaviour.

3.2.2 Relative stiffness method

An alternative to the uncoupled Limiting Tensile Strain Method was presented by Potts and Addenbrooke (1997). A wide parametric study was conducted using two-dimensional parametric analysis. This allowed for the inclusion of the building's stiffness into the design approach. This should give hypothetically a more realistic representation of the situation and therefore deliver more better results. However, the analysis looked at the influence of the building stiffness onto its behaviour. The weight of the building has been neglected by modelling the building as a weightless elastic beam.

The parametric study analysed the results of over 100 two-dimensional (2D) plain strain numerical models. In which, the geometry and stiffness were altered. The soil has been modelled as linear elastic. The stiffness of the building is related to the stiffness of the soil. To determine the stiffness of the structure the relative stiffness parameters are used. These are represented by ρ^* for the relative bending stiffness and α^* for the relative axial stiffness:

$$\rho^* = \frac{EI}{E_s\left(\frac{B}{2}\right)^4}, \qquad \alpha^* = \frac{EA}{E_s\left(\frac{B}{2}\right)}$$

In which:

E	=	Young's modulus of the structure
I	=	Second moment of inertia of the structure
A	=	Cross-sectional area of the structure
E_s	=	Secant stiffness of the soil at 0.1% axial strain from a triaxial compression test taken from a depth z/2
B	=	Width of the structure

The analysis resulted in a settlement profile and horizontal displacement profile. The assumption is that these are the driving parameters concerning building distortion. These results are then used to determine the building distortion parameters: a sagging deflection ratio (DR_{sag}) with a respective compressive horizontal strain (ε_{hc}) for the building, and a hogging deflection ratio (DR_{hog}) with a respective tensile horizontal strain (ε_{ht}). Often, the allowed tensile strain is limited.

The effect of the building on the soil deformation has been compared to the greenfield settlements. The degree to which the presence of a building influences the ground movements is expressed in modification factor (M), given the relative stiffness parameters and the building size (B) and the building location (e). Often, mentioned as relative position (e/B). The modification factor for the deflection ratios is defined by the following equations:

$$M^{DR_{hog}} = \frac{DR_{hog}}{DR_{hog}^{g}}, \qquad M^{DR_{sag}} = \frac{DR_{sag}}{DR_{sag}^{g}}$$

The modification factor for the horizontal strains is defined by the following equations:

$$M^{\varepsilon_{ht}} = \frac{\varepsilon_{ht}}{\varepsilon_{ht}^{g}}, \qquad M^{\varepsilon_{hc}} = \frac{\varepsilon_{hc}}{\varepsilon_{hc}^{g}}$$

The super script "g" denotes the values obtained from the green field analysis. The results found by Potts and Addenbrooke (1997) are translated into a relation presented in Figure 3-13. The modification factors are plotted against the relative stiffness parameter for a given relative position of a structure.

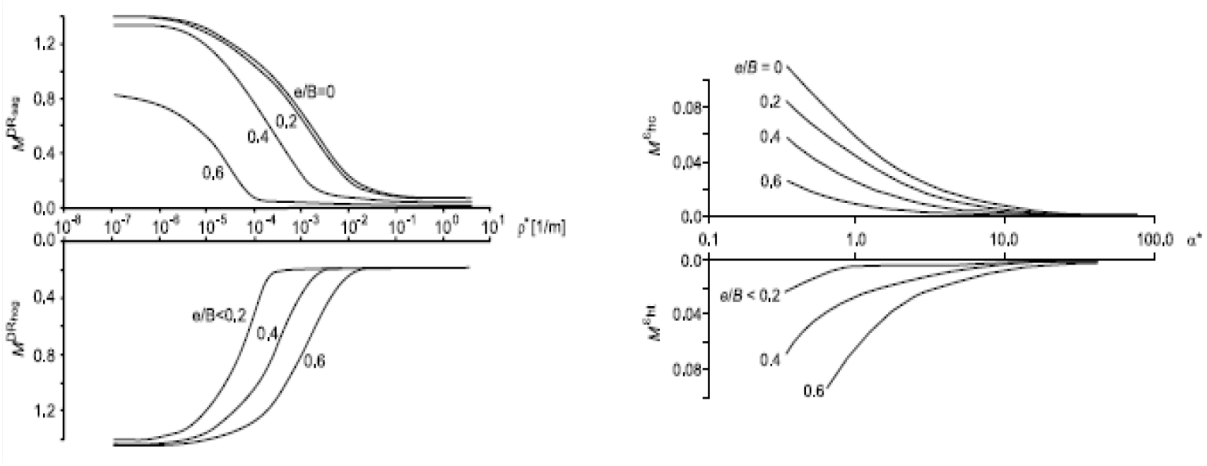

Figure 3-13 Modification factors (Potts & Addenbrooke, 1997)

The Relative stiffness method can be brought back to set of 6 steps to come to a damage prediction. The steps described by the Relative stiffness method are depicted in the figure below.

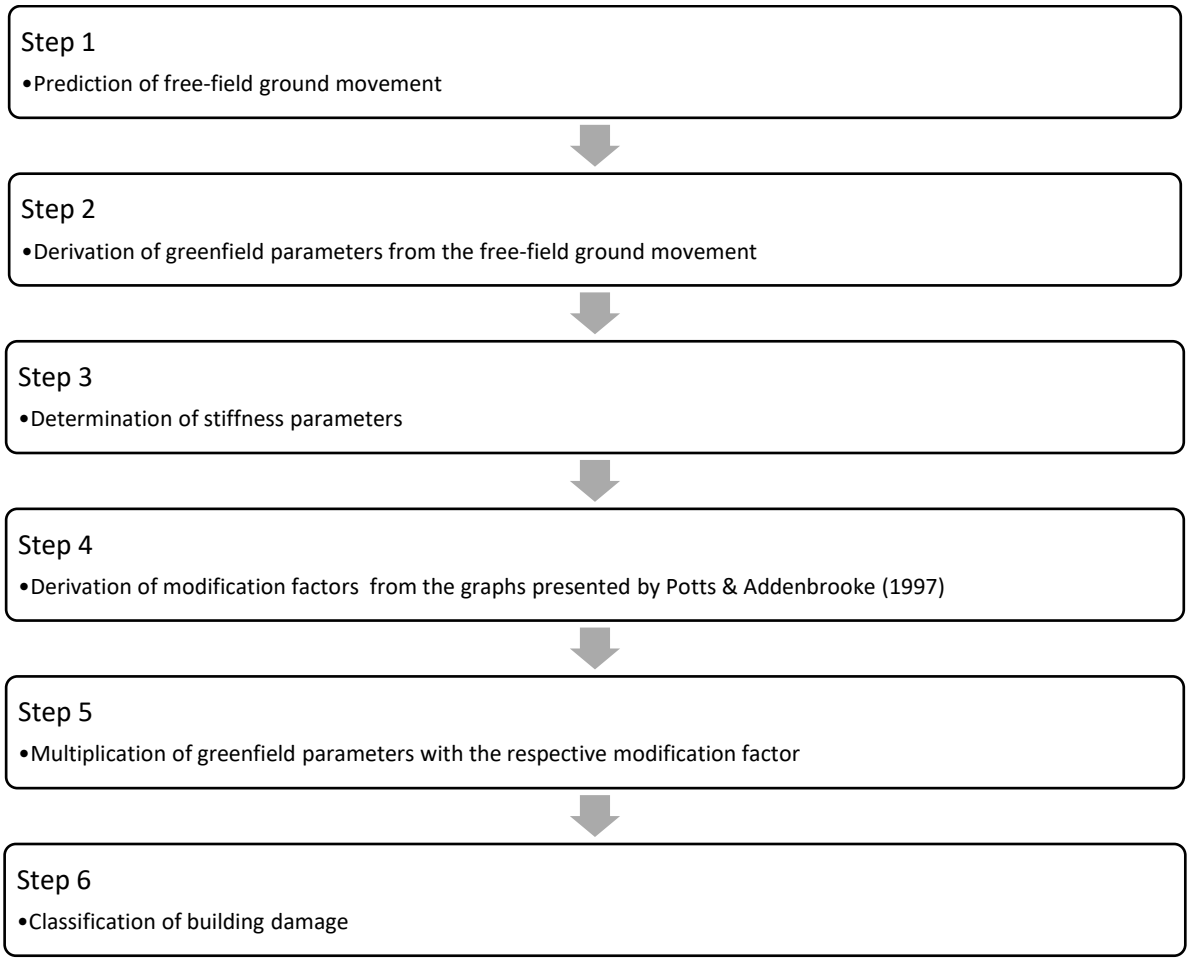

Figure 3-14 Steps of the Relative stiffness method

Conclusion

The relative stiffness method aimed to deliver a better alternative to the rather conservative LTSM. At first glance it predicts building deformation more accurate. On average the results are satisfying. This can differ between individual cases drastically. The method was found to be rather sensitive to difference in design approach. The approach also doesn't account for the complicated interaction between soil and structure (the foundation in particular). The study done by Potts & Addenbrooke (1997) looked solely at settlements induced by tunnelling.

3.2.3 Relative stiffness method as proposed by Goh (2010)

Franzius (2003) has done extensive research analysing the relative stiffness method by varying different parameters. The study focussed on varying the parameters B (building size), e (eccentricity) and z_0 (tunnel depth) individually. The study showed that the parameters B (building size) and z_0 (tunnel depth) can provide a significant scatter in results and consequently showing a large dependency on these parameters. The results are still on the conservative end of the spectrum and rarely overestimate building deformations. Thus, showing to be a reliable method to assess building deformations and subsequently possible damages.

Franzius (2003) proposed a slightly different approach. Based on the obtained result it was proposed to reduce the influence of the building size (B) and to increase the influence of tunnel depth (z_0). Franzius (2003) came up with the following improvements to the relative stiffness parameters:

$$\rho^*_{m1} = \frac{EI}{z_0^2 E_s \left(\frac{B}{2}\right)^2}, \qquad \alpha^*_{m1} = \frac{EA}{z_0 E_s \left(\frac{B}{2}\right)}$$

A different modification was proposed by Goh (2010) to enable the use of the relative stiffness method for deformations induced by deep excavations. These modification factors were obtained by modelling a weightless beam next to an excavation and varying the length, location and stiffness of the beam. The weightless beam represents a building with certain dimensions and stiffness. The formulae proposed by Potts and Addenbrooke (1997) were modified into:

$$\rho^*_{exc} = \frac{EI}{E_s L^3}, \qquad \alpha^*_{exc} = \frac{EA}{E_s B}$$

Where L represents the length of the building in either hogging or sagging mode. The design curves to determine the modification factors as proposed by Goh (2010) are presented in Figure 3-15.

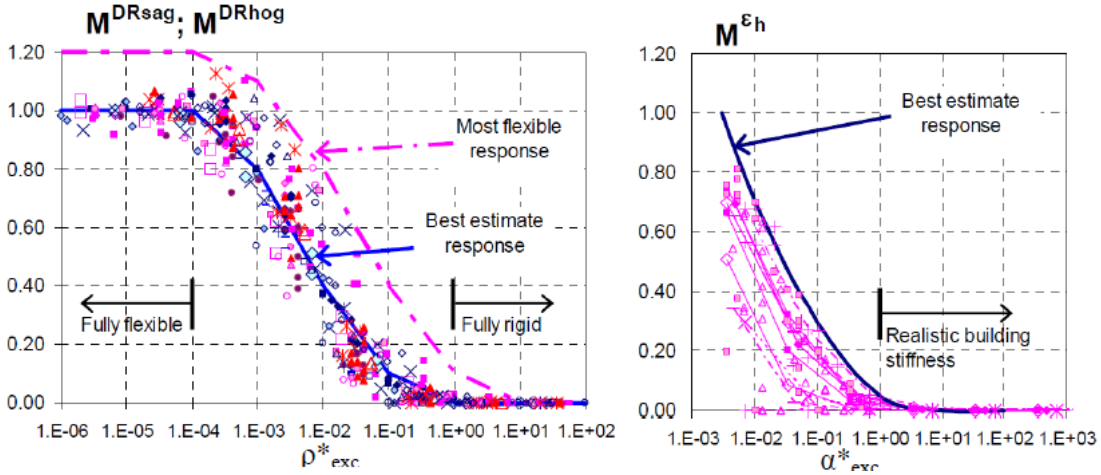

Figure 3-15 Design curves for modification factors for buildings as proposed by Goh (2010)

Conclusion

In general, this approach gives a better estimation of the building deformations. Looking closer to the results it becomes clear that the proposed method reduces the scatter when plotting the relative stiffness parameters against the corresponding sagging modification graphs. A slight increase in scatter is the case when plotting those stiffness parameters against the corresponding hogging modification graphs. Building damage is predominantly caused by the hogging deformation of the structure. So, it is quite questionable whether these proposed formulae are an overall improvement in predicting building damages.

The adjustments to the relative stiffness formulae by Goh (2010) have resulted in both parameters becoming dimensional, which is not ideal:

$$\rho^*_{exc} = \frac{EI}{E_s L^3}, \qquad \alpha^*_{exc} = \frac{EA}{E_s B}$$

3.3 SOIL-STRUCTURE INTERACTION

Netzel (2009) conducted a study in which building damage prediction was assessed using both the LTSM approach and numerical models. The aim was to get a better understanding effect of soil-structure interaction on building damage for the case of tunnelling induced ground movements. This was done by analysing the results of parametric numerical studies.

The study looked at the influence of different configurations and combinations of soil stiffness., interface properties and type, geometry and location of the structure on the expected building damage. The results were compared with the results using of the modified LTSM in order to assess the influence of these parameters (Netzel, 2009).

The study showed a clear relation between soil stiffness and damage sensitivity, with the same imposed green-field settlement. The damage sensitivity increases with an increase in soil stiffness. This relation is the result of the increase of mobilization of compatibility forces. As a result, the redistribution of building loads leads to an increase of tensile strains and building damage. The relation is schematized by Netzel (2009) in Figure 3-16 for the vertical interaction in the sagging zone of the settlement.

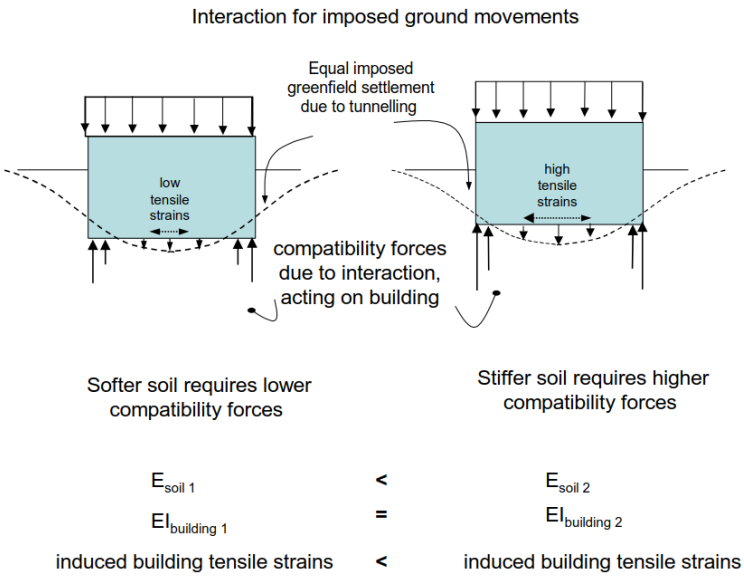

Figure 3-16 Schematic interaction effect depending of the soil stiffness (Netzel, 2009)

3.3.1 Interface

Netzel (2009) looked at the effect of the inclusion of an interface on the building deformation and damage. This was done by looking at cases with a rough interface and cases with a smooth interface. Also, a distinction was made between the effects when the building is situated in the hogging zone and when the building is in the hogging zone.

Hogging zone

A rough interface was found to have a significant impact on the mobilization of horizontal shear stresses at the bottom edge of the building. These horizontal shear stresses induce horizontal tensile strains in the building when situated in the hogging zone and compressive stresses when situated in the sagging zone. This leads to an increase in damage for the hogging zone. On the other hand, a decrease of building damage was found for the building in the sagging zone. The details of the connection between soil and structure are supposed to model the interface properties.

On the other hand, a smooth interface doesn't allow for any significant transfer of shear stress between building and soil. In contrary to the cases with a rough interface, a smooth interface results in significantly smaller deformation and damage in the hogging zone. This is due to the absent transfer of horizontal strains from the soil to the bottom edge of the building. The opposite holds for the sagging zone. The differential horizontal ground movements would lead to compressive strains at the bottom of the structure. The smooth interface doesn't allow for the friction transfer to occur.

Comparing the numerical models analysing the effect of an interface on building damage with a LTSM damage prediction has led to interesting results and hard conclusions. In the hogging zone, the influence of horizontal differential ground movements is of importance for the damage profile. If slip between the soil and the building is an unrealistic representation of the case, the horizontal interaction has to be taken into account for a damage prediction in the hogging zone. In the Neglecting the presence of differential horizontal greenfield ground movements using the LTSM is incomplete and provides an unsafe damage prediction. Neglecting of horizontal ground movements and horizontal interaction for a damage prediction is only considered acceptable if detailed information is available which confirms the existence of an effective slipping layer between building and soil, which verifies the assumption of a smooth interface (Netzel, 2009).

When the assumption of a smooth interface is shown to be a viable representation, the LTSM for full differential vertical movement transfer has shown to be a rather conservative approach to assess possible damages is almost all situations. The introduction of an interface has shown to be quite beneficial, because of the reduction of vertical movements.

Sagging zone

In the sagging zone, the differential horizontal ground movement induce a different phenomenon. As opposed to the hogging zone, compression forces are induced at the bottom of the building. This implicates important effect on damage profiles. Significantly less damage is noticed in the case of a rough interface than of a smooth interface. The vertical movement of the structure induces tensile strains at the bottom of the building. The horizontal movement of the soil induces compression at the bottom of the building through the interface. A rough interface allows for a more efficient transfer of these compressive strains to the building. The differential horizontal ground movement in subsequently counteracting the tensile strains induced by the differential vertical ground movement.

A rough interface could lead to a reduction of the tensile strains in the sagging zone. Including a rough interface could therefore lead to unsafe damage estimation. Especially, when a when the presence of a rough interface isn't demonstratable. Netzel (2009) therefore recommended to neglect the beneficial horizontal compression transferred to the building due to differential horizontal strains for tunnelling induced sagging cases.

3.3.2 Soil-pile interaction

The foundation of a building plays an important role in its reaction to soil deformations. Buildings with a shallow foundation react different to induced settlements than building with a piled foundation. The characteristics of the foundation is of great importance when assigning relative stiffnesses and interface characteristics. Korff (2012) has summed up several effects a deep excavation can have on the soil, the interaction between the soil and the pile and the interaction between the pile and the building of buildings inside the influence zone. The settlement of the pile head is composed of the following effects:

1. Reduction of pile capacity due to lower stress levels.
2. Settlement of the pile tip due to soil displacement below the base of the pile.
3. Development of negative (or positive) skin friction due to relative movements of the soil and the pile shaft.
4. Redistribution of pile load over the piles under the building slab, the building wall or a foundation cap or beam.

The lowering of stress levels is a direct result of the loosening of the soil around the pile tip. Depending to which degree the pile has been loaded, with respect to its capacity, this can have serious implications for the pile loads. Additional positive skin friction is mobilised and the resistance at the tip of the pile is reduces leading to an altering load-displacement curve for the pile. This effect becomes more significant the closer a pile is located to the excavation.

The settlement of the soil below the pile tip allows the pile itself to be vertically displaced. This is especially the case for piles mobilising significant toe resistance and therefore the stability relies largely on the toe resistance/stability of the pile. Aye et al. (2006) developed an analytical method to estimate vertical soil displacements at a specific location at a specific depth next to an unsupported deep excavation. Korff (2012) developed and proposed an analytical method that estimates the vertical soil displacements next to a supported/strutted deep excavation. The analytical model proposed by Korff (2012) is shown in Figure 3-17.

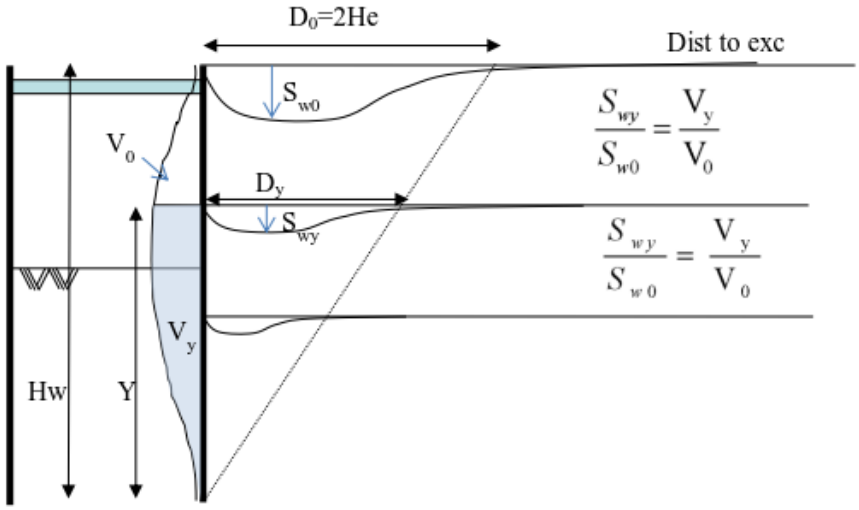

Figure 3-17 Influence area for vertical soil displacements as proposed by Korff (2012)

Soil displacements relative to the pile can affect the forces. The effects depend largely of the magnitude of the mobilised positive and/or negative skin friction and on whether it's a friction pile or an end-bearing pile. The initial factor of safety of the pile plays also an important role in the displacements afterwards. Piles with an initial low factor of safety tend to settle more than piles with a high factor of safety.

During different tunnelling stapes or excavation steps the piles under the building slab, the building wall or a foundation cap or beam are subjugated to displacements. This is due to the differential settlement of the soil leading to different loads on a pile via skin friction. Since piles are often connected through a structural element. The stiffness of this element accounts for redistribution of loads and displacements. A coupled analysis can often offer a solution to assess the effect of the load redistribution.

Piles inside the influence zone also deform horizontally. The piles are subjugated to differential horizontal settlements causing bending of the pile. The flexibility of the timber piles present under typical Amsterdam masonry buildings allows the piles to follow the horizontal movement of the soil almost completely. The horizontal movement of piles is limited by the overall interaction between the pile through a structural element interconnecting the pile heads.

3.4 Finite Element Method

The use of finite element analysis has become widely accepted and used by engineers. Finite Element Analysis allows engineers to bring complex matter back to a rather simplified model in order to be able to make calculations and predictions on the behaviour of an element or a combination of elements. The results allow for strength and stability calculations and other relevant engineering problems. The use of Finite Element Method has become time efficient in most cases and gives accurate results. In the past several analytical methods were to be used to obtain the aimed results, now a rather simplistic model can give these sought results.

The Finite Element Method divides the construction or components into a limited number of elements. This limited amount of element is actual a finite number of elements, hence the name Finite Element Method. These elements are then linked with each other through nodes. Several characteristics are assigned to these links. These characteristics depend on the element. The coupled nodes should allow for joint displacements.

Finite Element Method Programs are increasingly used for the design of building pits. It is regularly the case that the strength of a retaining structure isn't the governing factor of the design. Often, the governing elements are deformations of the retaining structure and especially the surroundings. These deformations are modelled by Finite Element Method Programs more precise compared to the commonly used traditional spring models. This results in more reliable checks on the serviceability. Traditional spring models are suitable for determining bending moments or anchor/strut forces than predicting deformations.

In the Netherlands PLAXIS is often used as a software to conduct numerical analyses for the assessment of geotechnical problems. Most early work in engineering performed using numerical analysis is done two-dimensional, assuming plane strain condition (Pickhaver, 2006). The preparation and use pf two-dimensional numerical analysis is less time consuming than full three-dimensional numerical modelling. However, in most cases bringing back a three-dimensional problem to a two-dimensional model requires simplifications in both geometries and properties.

PLAXIS 2D offers the ability to construct a plain strain model or using axisymmetric. A plain strain model is often used for geometries with a (nearly) uniform cross-section with a specific length perpendicular to the cross-section. Strains and displacements are assumed to be zero perpendicular to the cross-section.

Axisymmetric models are often used to evaluate geometries which are circular in shape. Stress state and deformation is assumed to be constant in any radial direction.

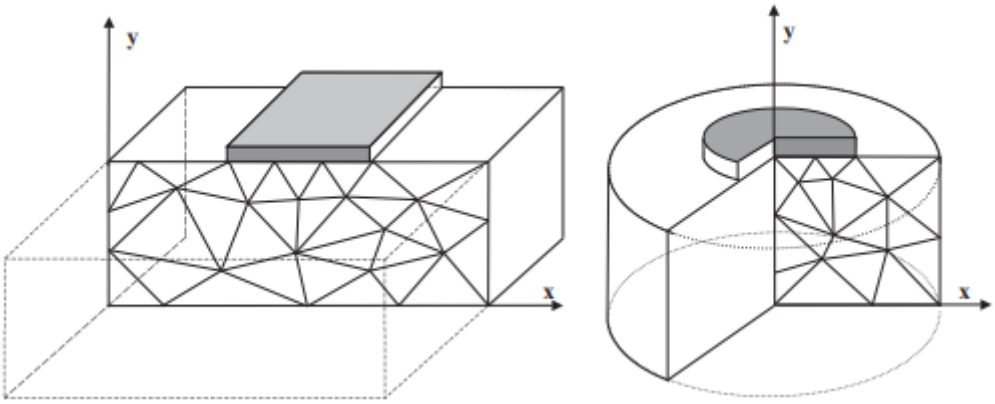

Figure 3-18 Example of a plane strain (left) and axisymmetric problem (right) (Plaxis 2D Reference Manual)

There is also a wide variety of soil models available assign to the soils in PLAXIS. In general, there are linear elastic, plastic, elastoplastic cap and nonlinear elasto-plastic cap soil models. It is generally accepted that simple linear elastic-plastic models lead to the prediction of profiles that are too wide and shallow as they cannot correctly account for the nonlinear and inelastic soil behaviour which has been shown to occur at small strains and is an important feature of soil-structure interaction (Calabresi et al., 1999). However, elastic soil models can give a rough first estimate for characteristic values.

Pickhaver (2006) has stated that over the years the necessity of modelling soil nonlinearity at small (pre-failure) strains, which occur in overconsolidated clays has become clear. Negro and de Queiroz (2000) concluded that maximum surface settlements predicted in finite element analyses were close to the measured field value in 71% of cases but that over half of the analyses gave poor predictions of overall soil movement profiles. According to the authors this was due to oversimplification of soil constitutive models and the use of a nonlinear pre-yield soil model to overcome this problem was recommended. Pickhaver (2009) stated that this nonlinear pre-yield model combined with a Mohr-Coulomb failure criterion and plastic potential was used by Addenbrooke et al. (1997) and compared with a linear elastic model to conclude that modelling nonlinear pre-failure stiffness is required to predict reasonable surface settlements. The same model has been used in other reported numerical analyses including the works of Potts and Addenbrooke (1997) and Franzius (2004).

The PLAXIS manual for material models suggests the use of Hardening Soil small strain soil models for assessing deep excavations. It is the best standard model in PLAXIS for this application.

3.5 The Vijzelgracht Station Case

The Vijzelgracht Station is part of the Amsterdam North-South Metro line project. This project intended the realisation of a 9.5 km metro line between the north and south of Amsterdam. 3.6 km of the trajectory is built underground. A total of 5 underground stations were built along the line. Three of them were constructed with the cut and cover method. Depths of approximately 35m with respect to surface level where reached. Between these station two bored tunnels are constructed with a diameter of 5.82 m. One for each railway track. The bored section is 3.1 km long and is situated between Amsterdam Central Station and Amsterdam RAI.

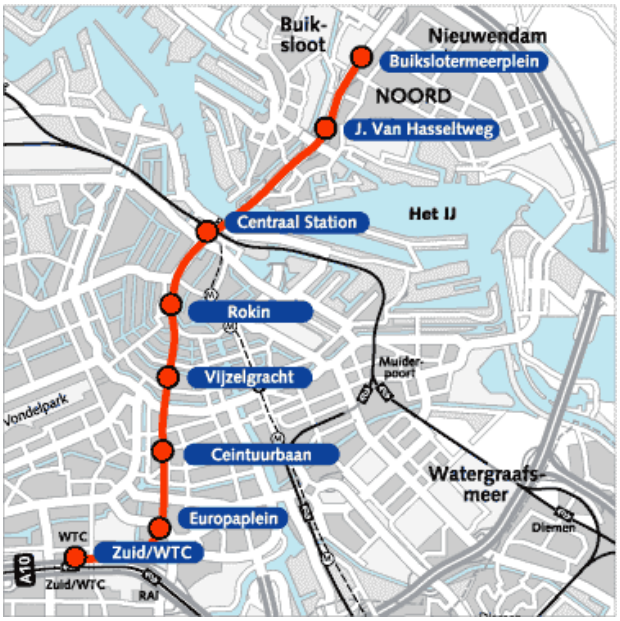

Figure 3-19 North-South line trajectory (http://www.sgaschaken.nl/)

This has been a challenging project due to the sensitive historical centre of the city where the tunnel and the stations were constructed. The tunnel came very closely to the existing sensitive monumental buildings. And at some parts the tunnel is constructed beneath the existing buildings. The trajectory follows mostly the street pattern but deviates at some points. One of the biggest challenges during the project has been damage control.

The construction of the metro line has been intensely monitored. Not only the tunnel but also the construction of the three deep laying underground stations have been monitored. Especially the effects on the surrounding building have been particularly interesting. In order to subsurface monitoring is carried out during the project. For a more precise picture two different cross-sections have been regarded of the Vijzelgracht Station. The location of the cross-section is depicted in Figure 3-20.

Figure 3-20 Locations of cross sections with subsurface monitoring (Data Set Vijzelgracht Station)

3.5.1 Geometry

The Vijzelgracht Station is 250 meters long and 22 meters wide. The excavation reaches a maximum depth of NAP 29.5 meters. The top-down constructed station has diaphragm walls of 1.2 meters thick and reach a depth of NAP -44.5 meters. Adjacent buildings are as close as 3.2 meters from the excavation.

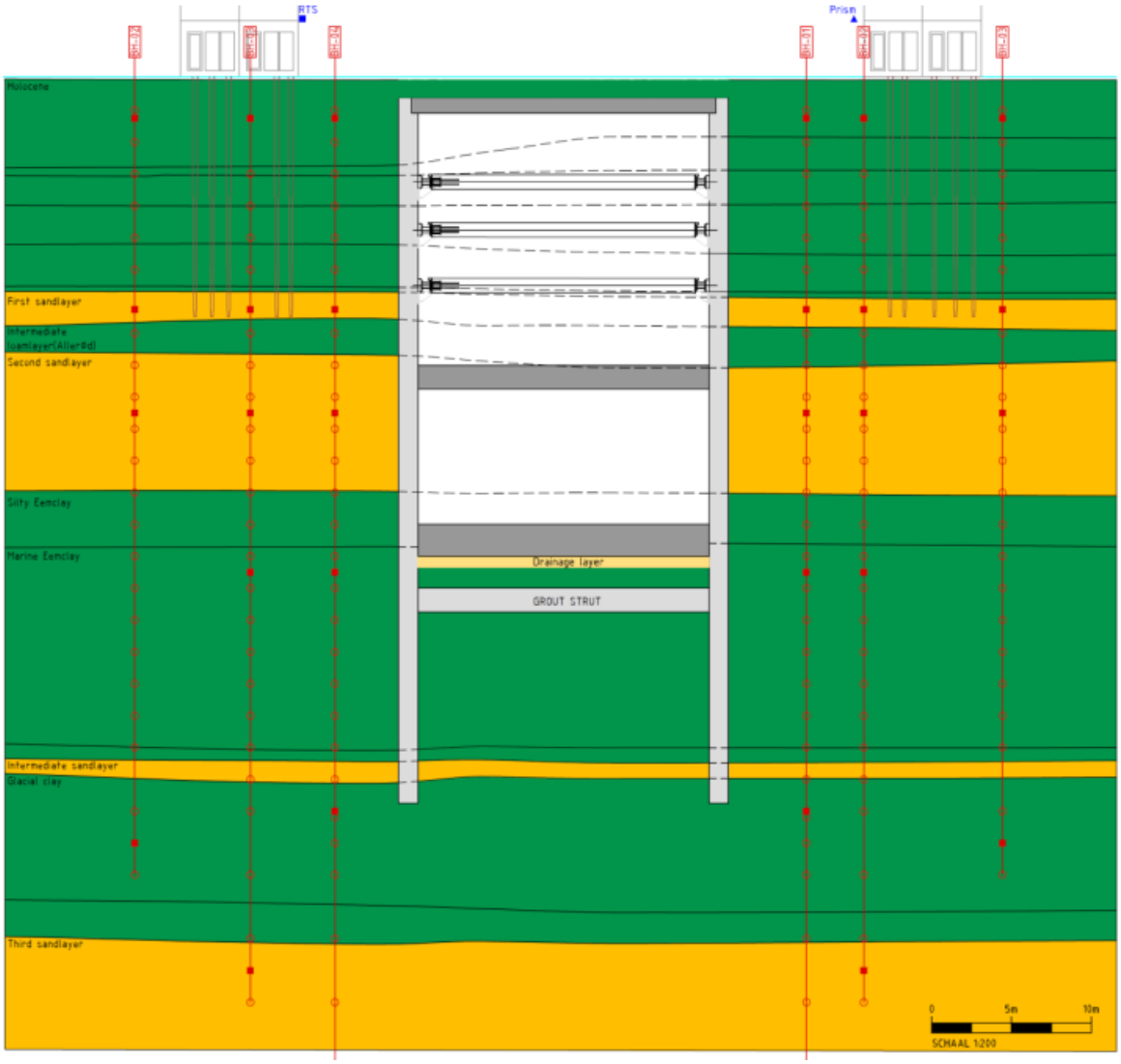

Figure 3-21 Cross-section 12270 of the Vijzelgracht station. (Data Set Vijzelgracht Station)

3.5.2 Geotechnical parameters

The soil profile over the length of the excavation is found to by uniform. Two cross-sections have been considered. Globally, the typical Amsterdam soil profile is found. The soil profile is built up off a man-made top layer, a Holocene clay layer and a peat layer until the first sand layer is reached at approximately NAP -11.0 m. Below the first sand layer lies the Alleröd layer. This is a sandy silt stratum. The following layer is the second sand layer at NAP -16.0 m with a thickness of 8-9 meters. The second sand layer lies on top of the Eem Clay layer. This layer has a thickness of approximately 16 meters.

Table 3-2 Soil profiles of the two cross-sections of the Vijzelgracht Station (Data Set Vijzelgracht Station)

	Cross-section 12197 (Top approximately m to NAP)	Cross-section 12270 (Top approximately m to NAP)
Man-Made Fill	+ 1.3	+1.0
Peat	Between -2.5 and -3.5	Between -3.0 and -5.0
Old Seaclay	Between -4.5 and -5.0	-5.0
Wad deposit, with sand	-6.7	-7.0
Hydrobia clay	-9.0	Between -10.0 and -10.5
Peat	-12.0	-11.3
First sand layer	-12.5	-11.5
Alleröd	Between -13.7 and -15	Between -14.0 and -14.3
Second sand layer	Between -16.5 and -17	Between -16.0 and -17.0
Marine silty Eemclay	Between -25.3 and -25.7	Between -20.5 and -21.0
Marine Eemclay (zone 1)	Between -28.3 and -28.7	Between -23.0 and -24.0
Marine Eemclay (zone 4)	Between -40.0 and -41.0	-
Harting layer	-40.7	-40.7
Intermediate sand layer	-41.3	-41.3
Glacial Drenthe Clay	-42.5	Between -42.5 and -43.0
Glacial Warven Clay	-50.0	-50.0
Third sand layer	-52.5	-52.0

The phreatic level in Amsterdam can be found be found around -0,4 m NAP. However, the phreatic level differs per location and over depth per layer. An overview of the relevant piezometric heads is presented in Table 3-3.

Table 3-3 Phreatic and piezometric level at the Vijzelgracht Station (Data Set Vijzelgracht Station)

	Minimal piezometric head (m NAP) -5% Percentile-	Average piezometric head (m NAP)	Maximal piezometric head (m NAP) -5% Percentile-
Phreatic layer	-0.69	-0.25	+0.19
First sand layer	-2.60	-2.35	-2.10
Second sand layer	-2.69	-2.47	-2.24
Intermediate sand layer		-2.67	
Third sand layer	-2.87	-2.45	-2.02

3.5.3 Building pit characteristics

This paragraph aims to lay down the relevant characteristics of the structural elements of the building pit. The characteristics of the diaphragm wall and supports are given.

Diaphragm wall

The characteristics of the diaphragm wall are presented in Table 3-4.

Table 3-4 Diaphragm wall parameters (Data Set Vijzelgracht Station)

Diaphragm wall			
Top level		-0.2	m NAP
Bottom level		-45.0	m NAP
Width		1200	mm
Tolerance internal		250	mm
Tolerance external		200	mm
Strength Class		B25	-
E'_b		10000	N/mm^2
EA	**Average**	$1.2x10^7$	kN/m
	Upper	$1.8x10^7$	
	Lower	$9.60x10^6$	
EI	**Average**	$1.44x10^6$	kNm^2/m
	Upper	$2.16x10^6$	
	Lower	$1.152x10^6$	
Volumetric weight		23	kN/m^3

Struts

The characteristics of the steel struts are presented in Table 3-5.

Table 3-5 Characteristics of the steel struts (Data Set Vijzelgracht Station)

Struts		
Minimum quality	Fe 360B	
Yield stress	240	N/mm^2
Elasticity modulus	210	GPa

The positioning of struts is different over the two cross-sections. The level and cross-sectional properties are presented in Table 3-6 and

Table 3-7.

Table 3-6 Properties of the struts at cross-section 12270 (Data Set Vijzelgracht Station)

Heart level [m NAP]	**Diameter x wall thickness [mm]**	**A [mm^2]**	**EA [kN]**	**Centre-to-centre distance [m]**	**Prestressing force**			
					Per meter [kN/m]	**Total [kN]**	**SLS design [kN/m]**	**ULS design [kN/m]**
-5	1067 x 20	65752	13807836	5.000	1000	4997	1150	5747
-9	806 x 22	54159	11373331	4.904	1500	7355	1600	7846
-13	1067 x 20	65752	13807836	4.904	1500	7355	1600	7846

Table 3-7 Properties of the struts at cross-section 12197 (Data Set Vijzelgracht Station)

Heart level [m NAP]	Diameter x wall thickness [mm]	A [mm^2]	EA [kN]	Centre-to-centre distance [m]	Prestressing force			
					Per meter [kN/m]	Total [kN]	SLS design [kN/m]	ULS design [kN/m]
-5	806 x 22	54159	11373331	4.990	1000	4992	1150	5741
-8.5	1067 x 20	65752	13807836	4.992	1500	7488	1600	7987
-12	1067 x 20	65752	13807836	4.992	1500	7488	1600	7987

Roofs and floors

The roof and the floors also have a supporting function. Both are concrete elements and fulfil a strutting function between the diaphragm walls on both sides. The construction of both elements is carried out in concrete strength class B35. Further details about the roof and floors are presented in Table 3-8 and Table 3-9.

Table 3-8 Cross-sectional properties of the floors and roof of cross-section 12270 (Data Set Vijzelgracht Station)

Top level in cross-section 12270 [m NAP]	Thickness [mm]	E [N/mm^2]
-0.200	1000	10000
-17.000	1500	10000
-27.000	2000	10000

Table 3-9 Cross-sectional properties of the floors and roof of cross-section 12197 (Data Set Vijzelgracht Station)

Top level in cross-section 12197 [m NAP]	Thickness [mm]	E [N/mm^2]
-0.200	1000	10000
-18.250	1500	10000
Between -27.130 and -27.825	2500	10000

Grout strut

Below the floor a grout strut will be constructed to help support the retaining walls. This grout strut consists of grout columns and are installed from the surface. The grout strut does not have uniform cross-section. Some openings have been left deliberately and also the thickness of the strut varies between 2.5 m at the edges close to the diaphragm walls to 1.5 meters at the middle of the cross-section. A schematization of the grout strut at cross-section 12197 is depicted in Figure 3-22.

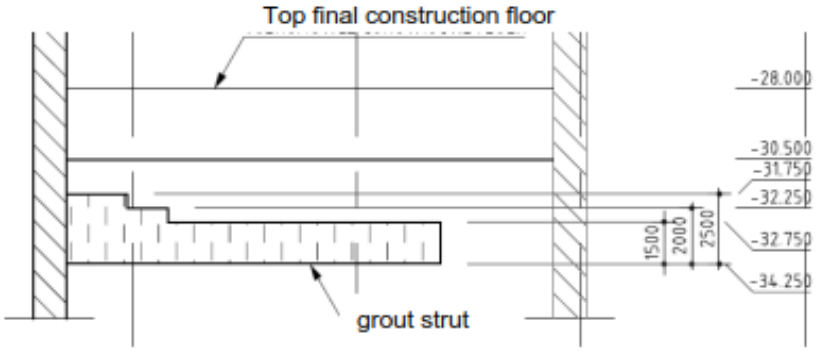

Figure 3-22 Schematization of the grout strut (Data Set Vijzelgracht Station)

The characteristics of the grout strut are presented in Table 3-10.

Table 3-10 Properties of the grout strut (Data Set Vijzelgracht Station)

	Compressive strength [MPa]	Tensile strength [MPa]	Elasticity modulus [MPa]	Poisson's ratio [-]	Volumetric weight [kN/m^3]
Average values PIP (Van der Stoel 2003)	12.6	0.86	2800	0.3	17.1
Selected test results grout strut (Delfgaauw et al, 2009)	12.6		4000		17.1
Average test results grout strut (Delfgaauw et al, 2009)	6-9		1920-2880 (E/UCS is 320)		15-16

3.5.4 Construction phases

The whole construction process of the Vijzelgracht station can be drawn back to 7 main stages:

1. Preparations, construction of the diaphragm walls, construction of the roof and pumping test, inclusive of excavation to NAP -3.5m
2. Excavation to NAP –6.5m. -5.9
3. Excavation to NAP –10.5m. -9.9
4. Excavation to NAP –15.6m. -13.9 and -16.9
5. Excavation to NAP –19.6m. -18.8 and -22.9
6. Excavation to NAP –31.2m. -30
7. TBM passing through.

3.6 PLAXIS MODEL

PLAXIS is used to model the Vijzelgracht Station Case. The model parameters and settings are presented in this section.

3.6.1 Model parameters

A plain strain model is used. The elements consist of 15-nodes. The Hardening Soil model with small-strain is used for the modelling of soil. This soil model is slightly more sophisticated than the conventional Hardening Soil model, because this model additionally accounts for the increased stiffness at small strains.

3.6.2 Soil layers

Table 3-11 shows the characteristic soil parameters per soil layer. The parameters are taken from Haryono (2013).

Table 3-11 Characteristic soil parameters per soil layer

	Top [m NAP]	γ_dry [kN/m³]	γ_wet [kN/m³]	e [-]	c' [-]	ϕ' [°]	ψ [°]	E_{50}^{ref}	k_v [m/s]	v [-]	K_0 [-]
Man-Made Fill	+1.3	10.0	15.0	1.37		25		[kPa]	1.0E-06	0.15	0.50
Peat	-3.0	2.5	10.5	7.78	5	19		10000	1.0E-08	0.35	0.65
Old Seaclay	-5.0	11.0	16.5	1.35	7	25		1000	1.5E-09	0.33	0.50
Wad deposit, with sand	-6.7	13.3	17.9	0.97	2	27		9000	1.0E-07	0.30	0.40
Hydrobia clay	-9.0	9.0	15.2	1.73	8	27		12000	1.0E-09	0.30	0.59
First sand layer	-12.5	16.8	19.8	0.52		33	3	9000	1.5E-04	0.25	0.40
Alleröd	-14.0	14.4	18.5	0.81	3	28		40000	3.0E-05	0.30	0.40
Second sand layer	-17.0	15.9	19.0	0.64		33	3	17000	1.0E-04	0.25	0.40
Marine silty Eemclay	-25.5	14.6	18.4	0.79		27		35000	2.4E-06	0.30	0.40
Marine Eemclay (zone 1)	-28.5	13.1	17.9	0.99	15	29		30000	2.0E-09	0.33	0.68
Marine Eemclay (zone 4)	-40.0	11.2	16.6	1.32	10	28		11000	2.0E-09	0.33	0.68
Harting layer	-40.7	8.3	14.5	1.91	10	28		8000	6.0E-09	0.33	0.57
Intermediate sand layer	-41.3	16.0	19.4	0.64		30		10000	1.0E-05	0.30	0.40
Glacial Drenthe Clay	-42.5	15.9	19.7	0.64	15	29		25000	1.0E-09	0.33	0.54
Glacial Warven Clay	-50.0	14.0	18.5	0.86	5	26		15000	1.0E-07	0.33	0.54
Third sand layer	-52.5	17	19.6	0.55		33	3	15000	1.0E-04	0.25	0.40

The use of the Hardening Soil small strain model requires additional input for stiffness parameters. The additional stiffness parameters are presented in Table 3-12.

Table 3-12 Additional stiffness parameters per soil layer

	Top of the layer [m NAP]	E_{50}^{ref} [kPa]	E_{oed}^{ref} [kPa]	E_{ur}^{ref} [kPa]
Man-Made Fill	+1.3	10000	8000	30000
Peat	-3.0	1000	1000	5000
Old Seaclay	-5.0	9000	3000	25000
Wad deposit, with sand	-6.7	12000	5000	33000
Wad deposit, Hydrobia clay	-9.0	9000	3000	25000
First sand layer	-12.5	40000	30000	200000
Alleröd	-14.0	17000	13000	45000
Second sand layer	-17.0	35000	35000	190000
Marine silty Eemclay	-25.5	30000	20000	120000
Marine Eemclay (zone 1)	-28.5	11000	4000	50000
Marine Eemclay (zone 4)	-40.0	8000	3000	45000
Harting layer	-40.7	10000	2000	46000
Intermediate sand layer	-41.3	25000	15000	140000
Glacial Drenthe Clay	-42.5	15000	5000	75000
Glacial Warven Clay	-50.0	15000	4000	58000
Third sand layer	-52.5	35000	40000	200000

3.6.3 Geometry

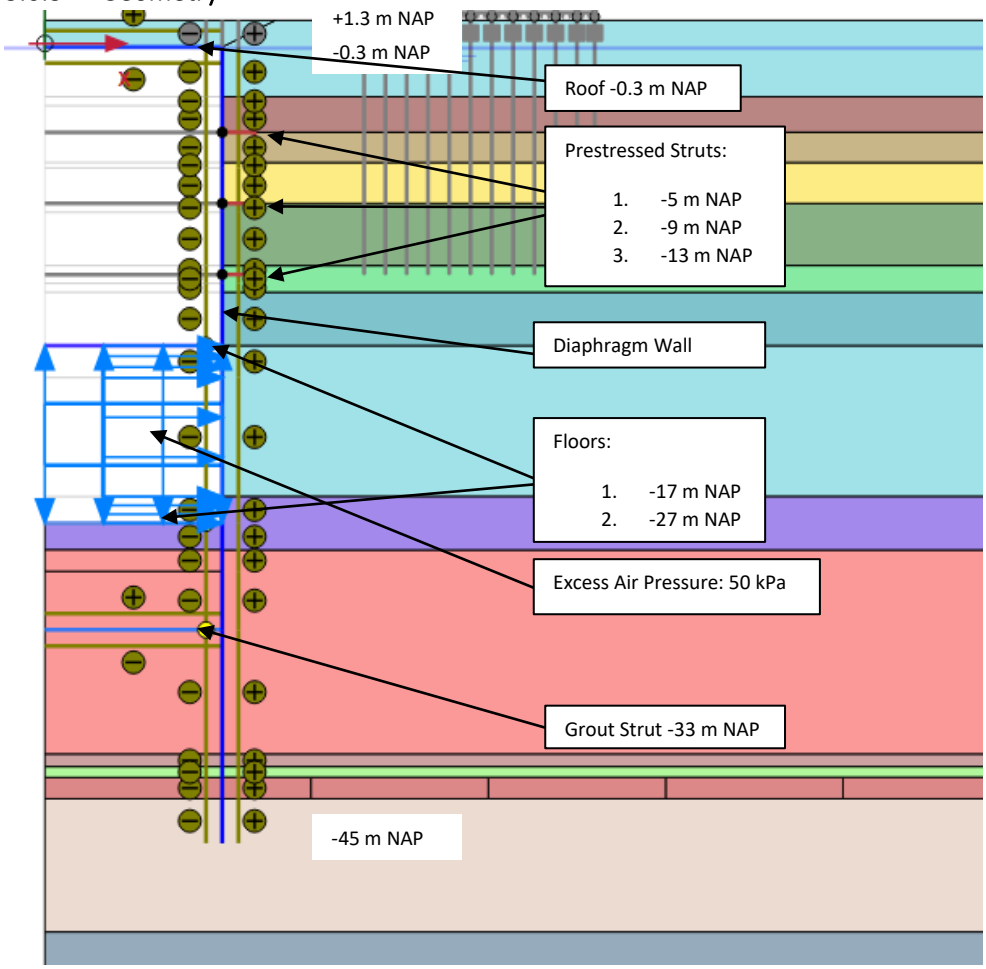

Figure 3-23 PLAXIS model of the deep excavation

The modelled deep excavation has a width of 20 meter and is assumed to be symmetrical around the middle of the deep excavation. A diaphragm wall forms the retaining wall of the deep excavation. The retaining wall is modelled as a plate. The retaining wall is supported by the roof, three row of steel struts, two floors and a grout strut respectively. These structural elements are depicted in Figure 3-23. The parameters used for the retaining wall are based on Table 3-4 and are presented in Table 3-13.

Table 3-13 Retaining wall parameters

Diaphragm wall		
Top level	-0.2	m NAP
Bottom level	-45.0	m NAP
Width	1200	mm
v	0.15	-
E	10000	N/mm^2
EA	$12x10^6$	kN/m
EI	$1.44x10^6$	kN/m
Volumetric weight	23	kN/m^3

The roof, floors and grout struts are modelled as plates and the parameters are presented in Table 3-8. The parameters are based on the parameters presented in Table 3-8, Table 3-9 and Table 3-10.

Table 3-14 Cross-sectional properties of the grout strut, floors and roof.

Element	Thickness [mm]	E [N/mm^2]
Roof at -0.3 m NAP	1000	10000
Floor at -17.0 m NAP	1500	10000
Floor at -27.0 m NAP	2000	10000
Grout strut at -33 m NAP	1500	4000

The steel struts are modelled as anchors. The parameters for the steel struts are taken from Table 3-6 and are presented in Table 3-15

Table 3-15 Properties of the steel struts

Heart level [m NAP]	A [mm^2]	EA [kN]	Centre-to-centre distance [m]	Prestressing force per meter [kN/m]
-5	65752	13807836	5.000	1000
-9	54159	11373331	4.904	1500
-13	65752	13807836	4.904	1500

3.6.4 Excavation steps

The construction of the Vijzelgracht station is divided in 17 phases. An overview of the construction phases is presented below:

0. Initial Phase
1. Placement of the Diaphragm Walls
2. Placement of the Grout Strut
3. Excavation to -3 m NAP
4. Excavation to -3.5 m NAP and placement of the Roof
5. Backfilling of the sand on top of the roof
6. Excavation to -7 m NAP
7. Placement of the 1st Steel Strut row and applying 1000 kN/m prestress
8. Excavation to -9.5 m NAP
9. Placement of the 2nd Steel Strut row and applying 1500 kN/m prestress
10. Excavation to -13.5 m NAP
11. Placement of the 3rd Steel Strut row and applying 1500 kN/m prestress
12. Excavation to -18.8 m NAP
13. Placement of the 1st Floor -17 m NAP
14. Excavation to -29.7 m NAP and simultaneously applying excess air pressure
15. Realisation of the drainage layer
16. Placement of the 2nd Floor -27 m NAP

Further information about the excavation phases is presented in Appendix B

PLAXIS input

3.6.5 Loads

During the last excavation step (phase 14) excess air pressure is used in order to support the diaphragm wall. The air pressure is applied in the tunnel exit section section (between -17 m NAP and -27 m NAP).

3.6.6 Mesh

The mesh is automatically generated by PLAXIS FEA. A medium element size (approximately 8 m) is generated in combination with enhanced mesh refinement. Closer to the excavation elements are smaller and closer to surface level, due to the need for more accurate results. Locally, the mech is either halved or multiplied by 0.25 for more accurate results. The incorporated façade is assigned to have a denser mesh. The mesh size in the façade is set to be roughly 0.5 m.

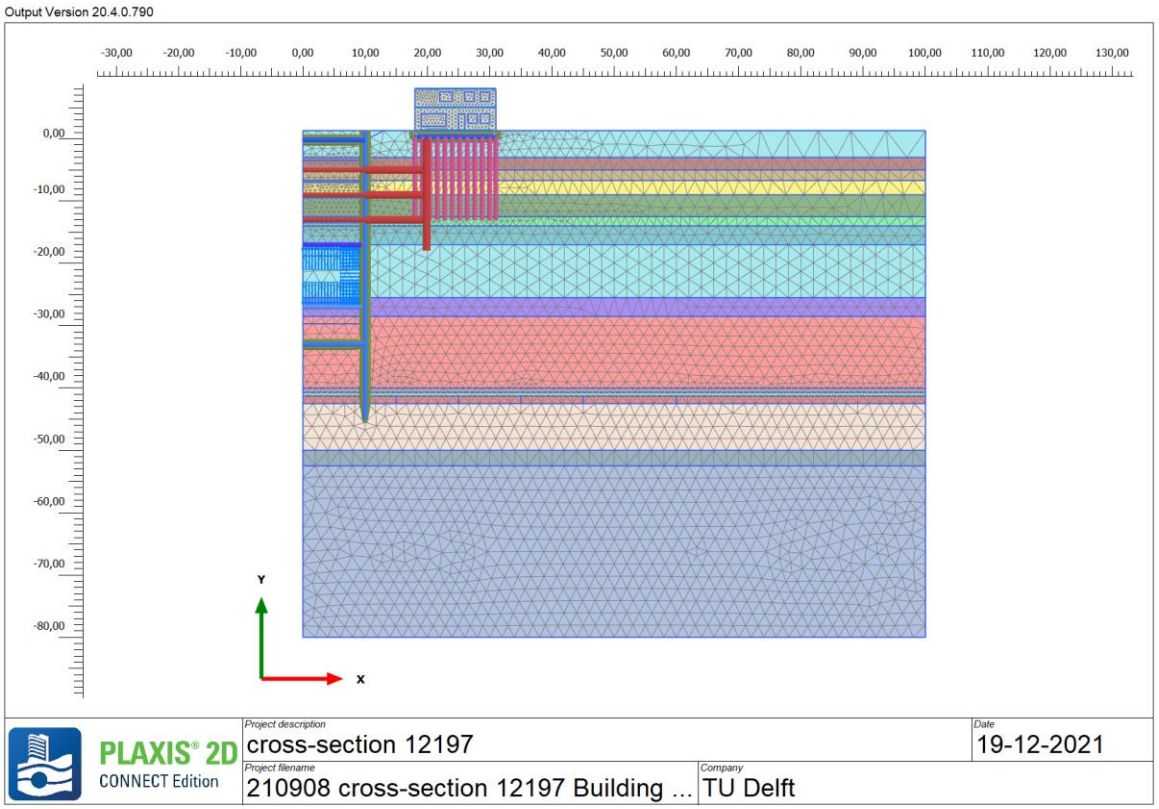

4 PILE DISPLACEMENT ANALYSIS

Building deformations are dependent on the deformation of the soil underneath its foundation. The construction of a deep excavation leads to deformations in the adjacent soil. This has implications for the structures underneath and on top of the soil, which could lead to potential damages. Although the construction of deep excavations is a three-dimensional problem, in the case of a long excavation the problem can be reduced to a two-dimensional problem for large parts of the excavation. A summary of the methods to predict soil deformation and subsequently building deformation are discussed in Section 3. This chapter will use these methods to compare monitoring data with numerical and analytical soil settlements results. The construction of the Vijzelgracht Station will be the case studied. The second part of this chapter focusses on the analysis of the important parameters of the foundation of a typical old Amsterdam building. These are the buildings predominantly present in the area around the deep excavation.

The Vijzelgracht Station case will be used to compare different models to identify the important parameters of a building foundation in its deformation induced by a deep excavation. In turn, this helps to distinguish relevant parameters which could be used for the modelling of a 2D numerical model of a building next to a deep excavation. The results will enable numerical models of the buildings to be more realistic and give better overall representation of the situation.

The monitoring data of the surface settlements is visualized in Section 4.2. The measured data is used to evaluate the free-field numerical model. This numerical model forms the basis for the pile settlement analysis in which structural elements will be introduced. The building pit will be modelled using PLAXIS. Embedded beam rows will be introduced to depict the wooden pile foundation of a typical Amsterdam building. Several parameters of these piles will be varied to perform a sensitivity analysis in Section 4.3 to determine the relevant parameters for modelling such a foundation. This information is desirable for the introduction of a full building in numerical model.

4.1 ANALYTIC ASSESSMENT OF SOIL SETTLEMENTS

The settlements adjacent to the building pit are assessed analytically parallel to the measured settlements. The overall shape of the settlement profile is based on the result presented by Hsieh & Ou (1998) (Section 3.1.5). In which the maximum settlement ($\delta_{v,max}$) occurs a distance (d) halve the excavation depth (H) away from the excavation. Next to the retaining wall the settlement (δ_v) is halve the maximum settlement. At a distance double the excavation depth the settlement becomes negligible. The value for the maximum settlement is taken form Dhanjal Thurlow &Bailey (2001) (Section 3.1.3). They found a maximum settlement of 0,06 % of the excavation depth to be a good estimate. The settlement curve used for the assessment is presented in Figure 4-1.

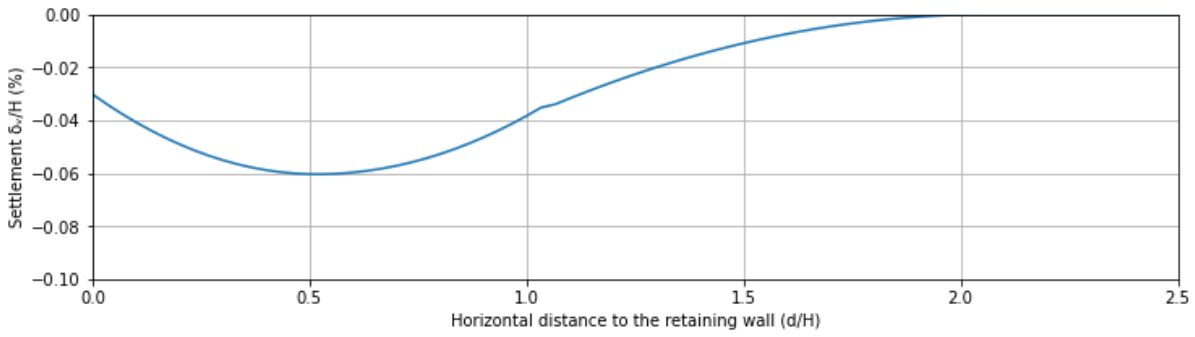

Figure 4-1 Settlement curve used for the assessment

The settlements at foundation level are also important. These will be assessed using the relation presented in Section 3.3.2 and developed by Korff (2013). The influence are decreases linearly of the length of the length of the retaining wall. The deformations at a specific depth follow the shape of the surface settlements and depend on the ratio between the displaced volume of the retaining wall beneath the specified level and the total displaced volume of the retaining wall.

The foundation layer (1st sand layer) is located at a depth of roughly -12.5 m NAP. Halve a meter below this level is the depth at which most old buildings are assumed to be founded (-13 m NAP). This results in a depth of +1.3- -13.0 = 14.3 m. The total length of the retaining wall equals +1.3- -45 = 46.3 m. Since, the influence area is assumed to be 2 times the excavation depth ($2H$). This results into an influence area at foundation level of $\frac{46.3-14.3}{46.3} * 2H \approx 1.38H$.

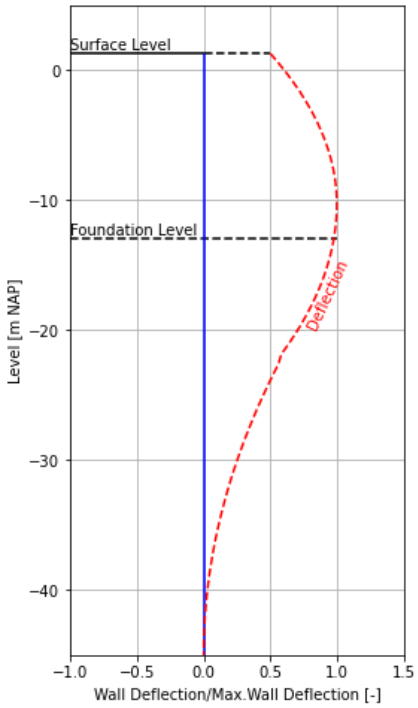

Figure 4-2 Wall deflection relative to the maximum deflection

The settlement curve is usually assumed to have a similar shape to the deflection of the retaining wall. Therefore, the settlement curve is used to form a general approximation for the deflection of the retaining wall. The assumed wall deflection is presented in Figure 4-2. The deflection of the retaining wall is then used to determine the maximum settlement at foundation level. The deflected area below the retaining wall is roughly halve the total deflected area. Based on the relation presented in Section 3.3.2, the following applies:

$$\frac{S_{wy}}{S_{w0}} = \frac{V_y}{V_0} = \frac{0.5}{1} \rightarrow S_{w,foundation\ level} = \frac{1}{2} S_{w0}$$

Which means that the maximum settlement at foundation level is halve the maximum settlement at surface level. The settlement curve for at surface level and at foundation level are presented in Figure 4-3.

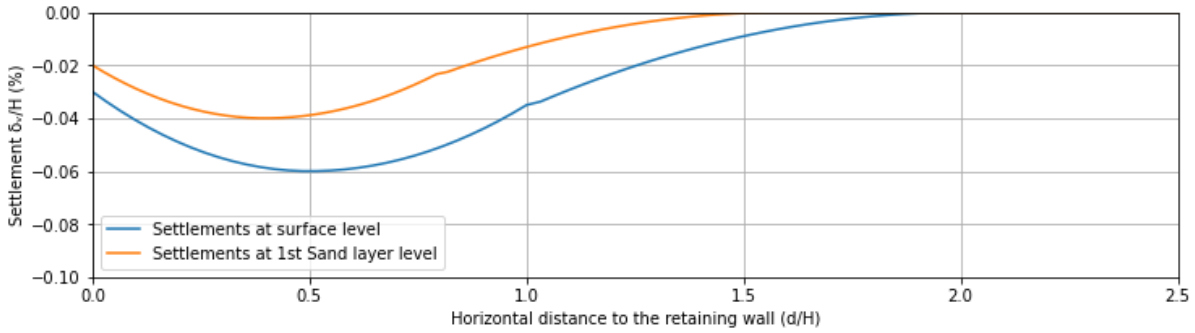

Figure 4-3 Settlement curve used for the assessment

4.2 Free-field Soil Settlements

The settlement data of the Fokke Simonszstraat, the Lijnbaansgracht and the Noorderstraat are compared. The data of the Fokke Simonszstraat shows significant responses to the activities in the building pit. The settlement data of the Fokke Simonszstraat have been filtered by taking out the uniform settlement of the surface. This is done by taking out the settlement of the furthest points from the excavation. These points are further from the excavation than two times the excavation depth. These points are assumed to be uninfluenced by the excavational activities. The figure below shows the settlement data of four specified points. The distance perpendicular to the excavation is presented in the table.

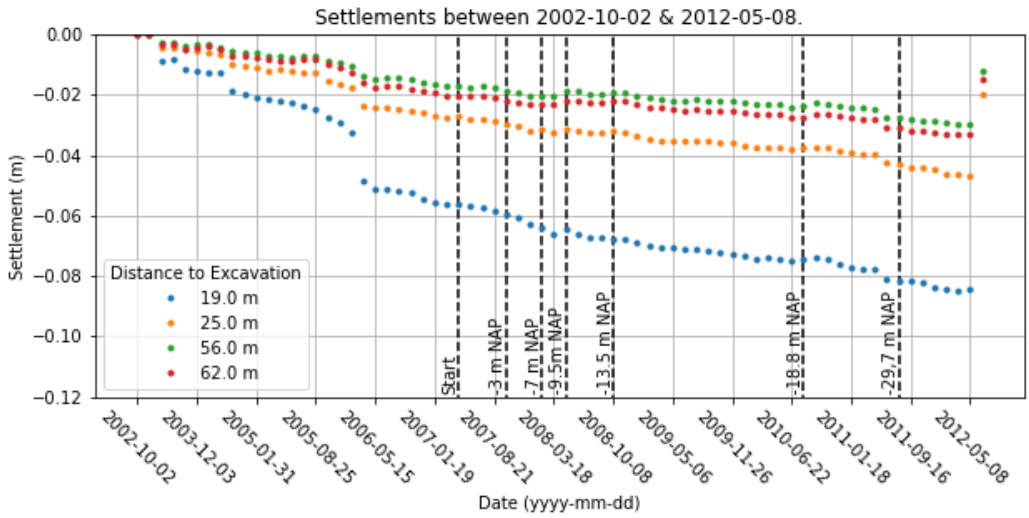

Figure 4-4 Settlements of specific locations over time at the Fokke Simonszstraat

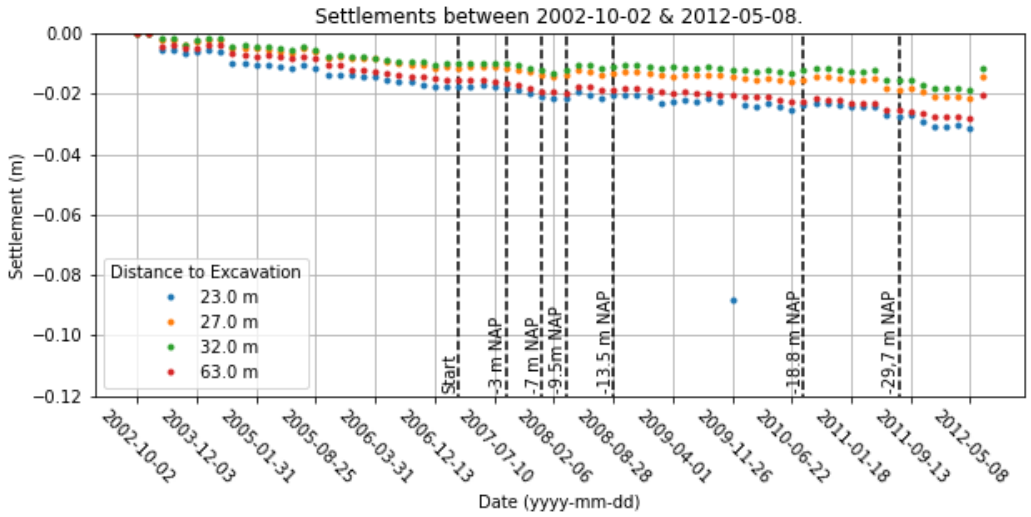

Figure 4-5 Settlements of specific locations over time at the Lijnbaansgracht

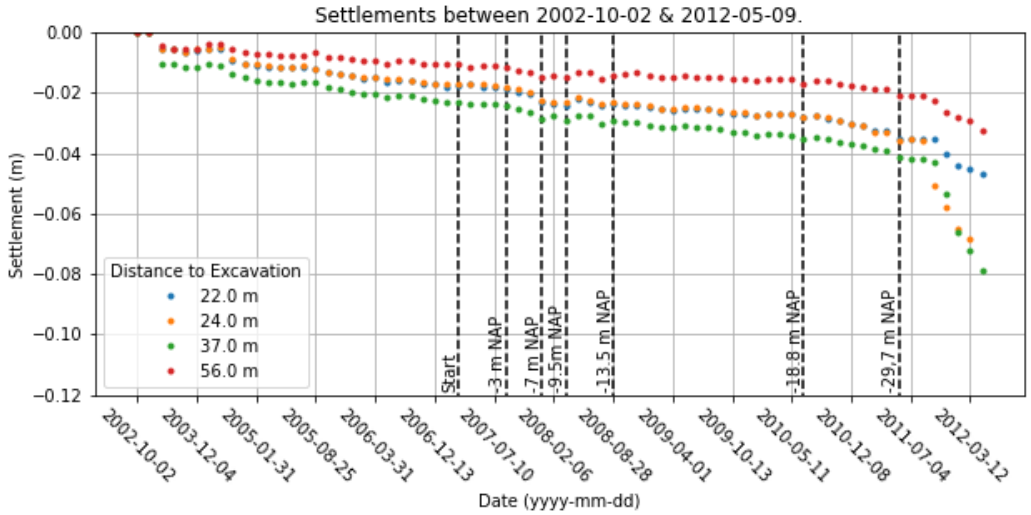

Figure 4-6 Settlements of specific locations over time at the Noorderstraat

This report includes the analysis of green-field settlement of the excavation steps described in Section 3.5 (-3m, -7m, -9.5m, -13.5m, -18.8m, -29.7m NAP). In the following paragraphs the PLAXIS results are put next to the settlement data of the Fokke Simonszstraat.

The installation of diaphragm walls is very sophisticated to model and a subject on its own. Therefore, the analysis is done by modelling only the excavation (excluding the installation of diaphragm walls). This is done by resetting the deformations to zero after the installation of the diaphragm walls. The installation of the grout strut is still included since it is installed almost simultaneously to the start of the first excavation works.

4.2.1 Excavation to -3 m NAP

The PLAXIS result of the first excavation is plotted, excluding the installation of the diaphragm walls. The result is shown in the figure below.

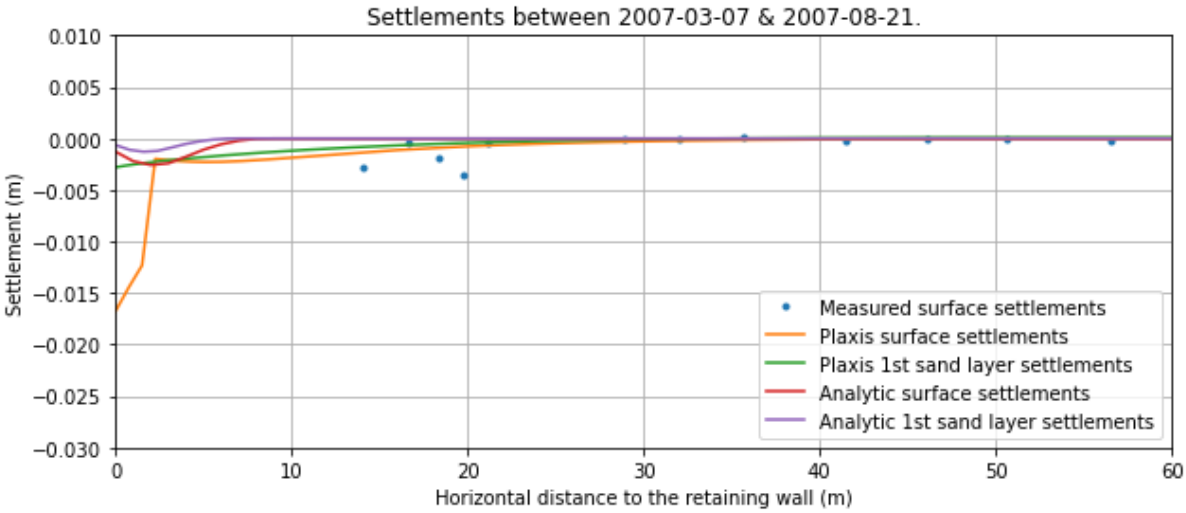

Figure 4-7 Settlements after the building pit is excavated to -3 m NAP

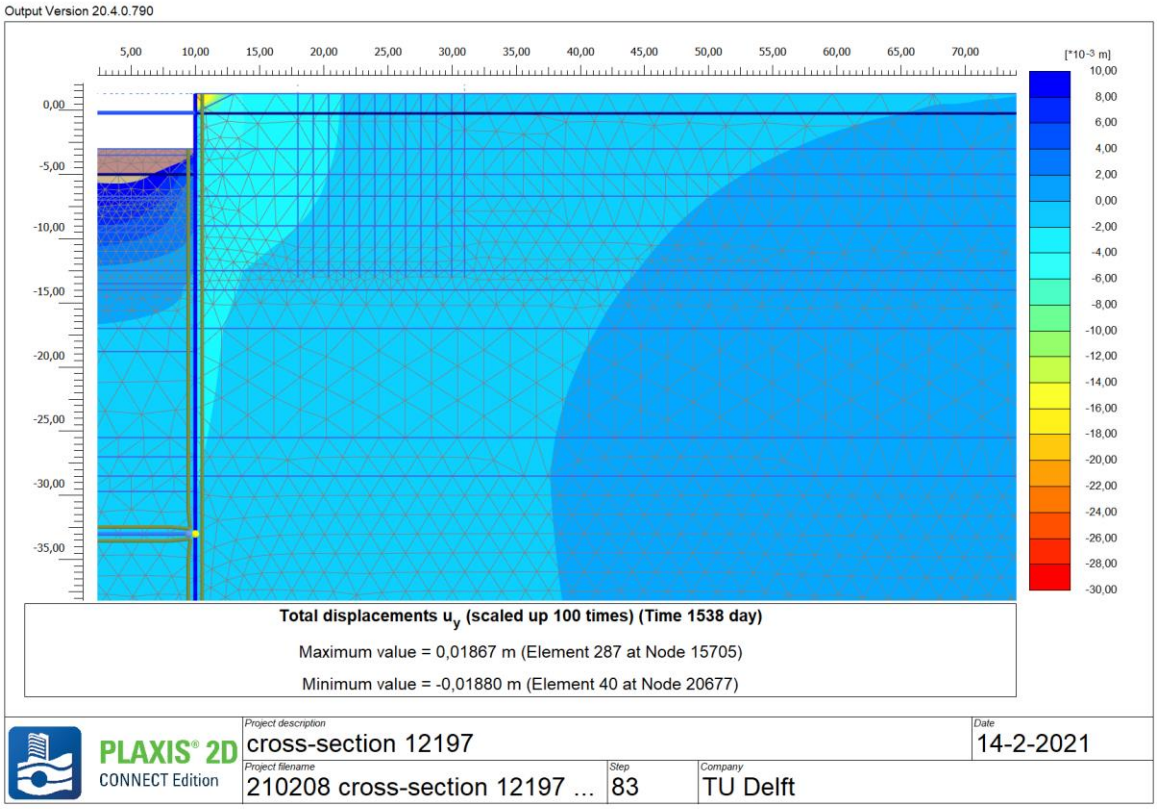

Figure 4-8 Vertical ground deformation after the building pit is excavated to -3 m NAP.

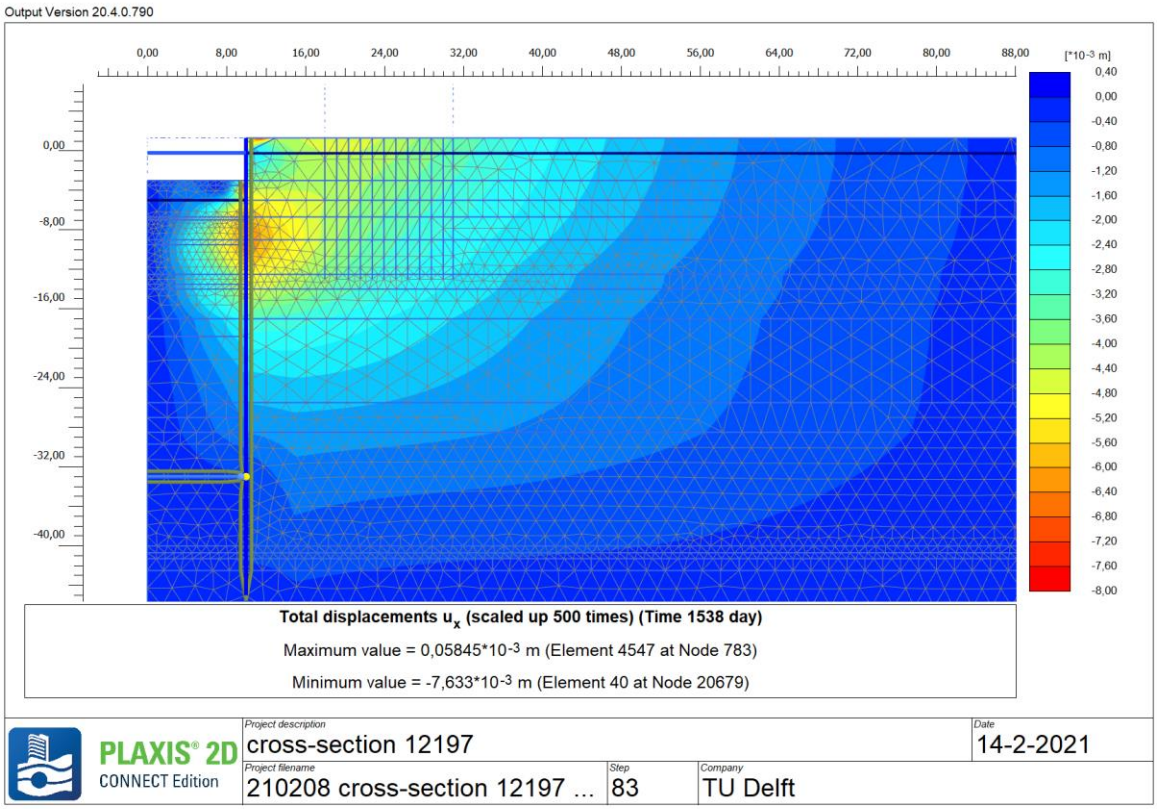

Figure 4-9 Horizontal ground deformation after the building pit is excavated to -3 m NAP.

4.2.2 Excavation to -7 m NAP

The PLAXIS result of the second excavation is plotted, excluding the installation of the diaphragm walls. The result is shown in the figure below.

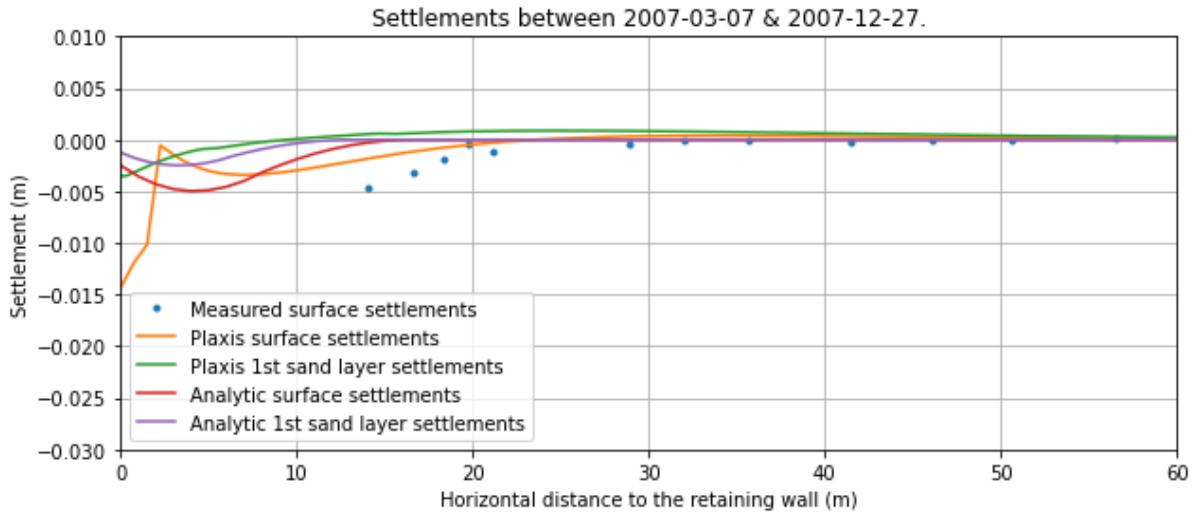

Figure 4-10 Settlements after the building pit is excavated to -7 m NAP.

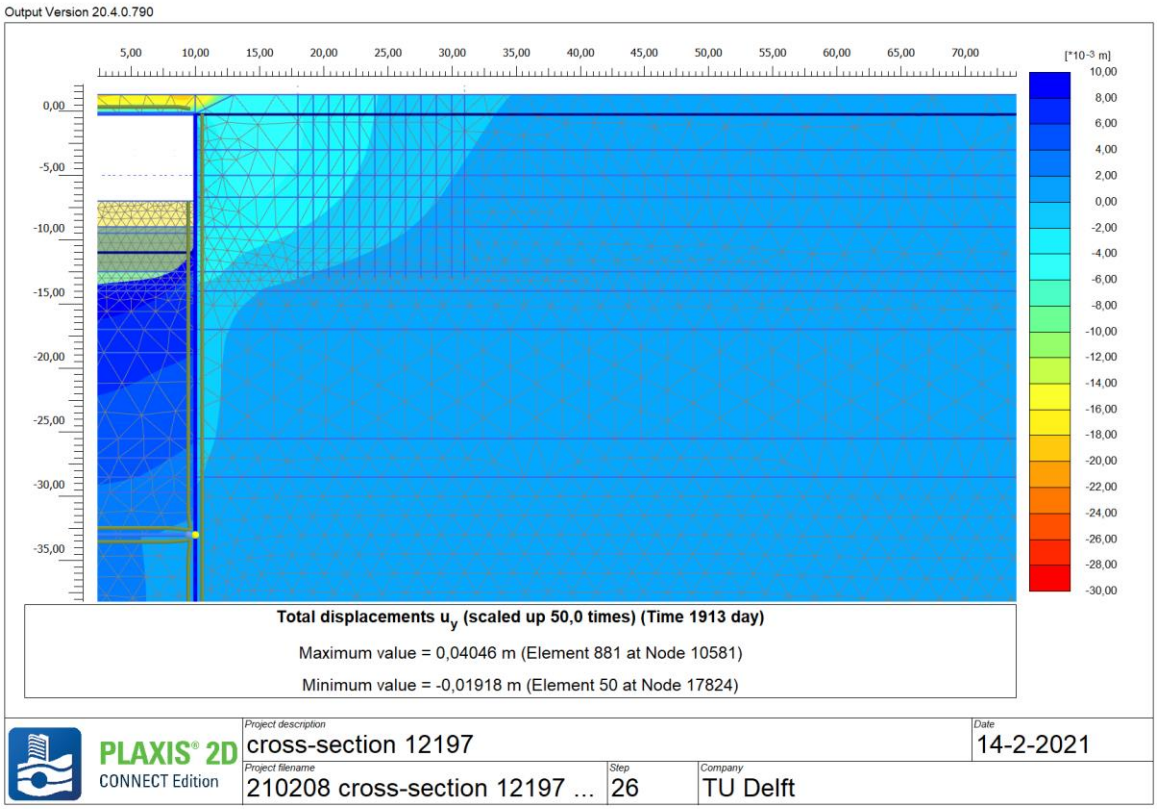

Figure 4-11 Vertical ground deformation after the building pit is excavated to -7 m NAP.

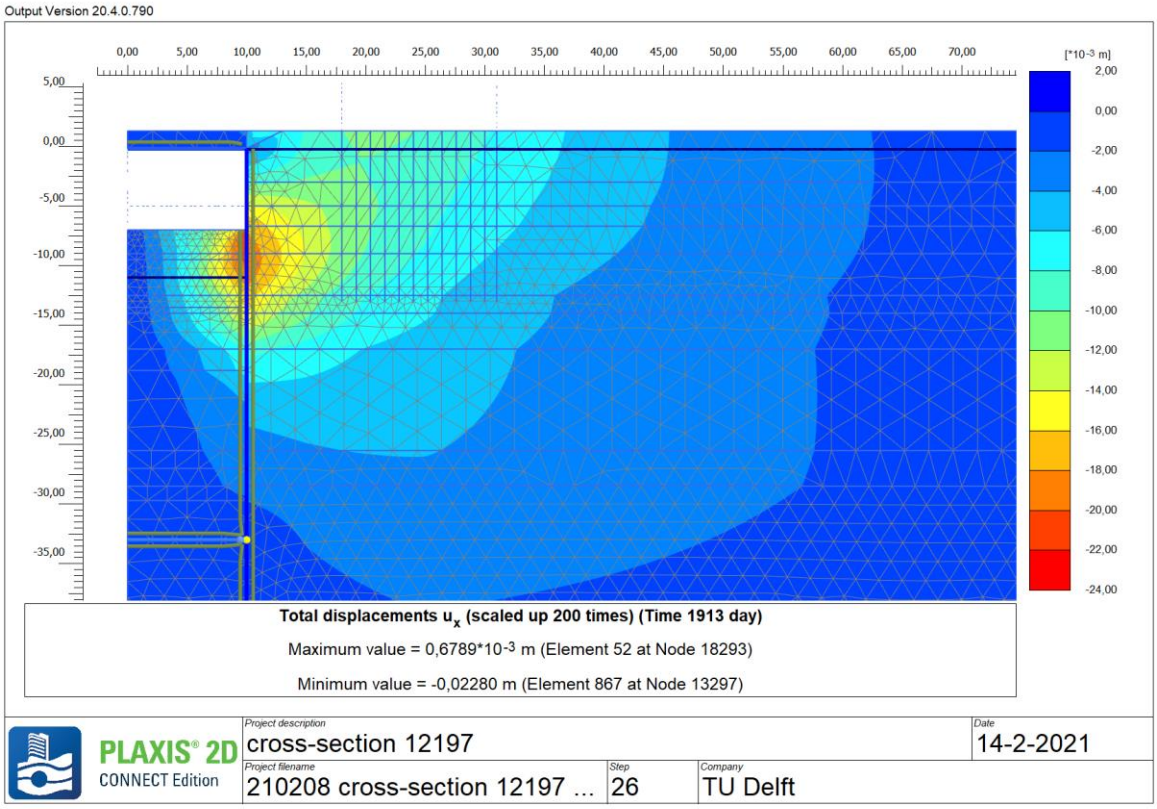

Figure 4-12 Horizontal ground deformation after the building pit is excavated to -7 m NAP.

4.2.3 Excavation to -9.5 m NAP

The PLAXIS result of the third excavation is plotted, excluding the installation of the diaphragm walls. The result is shown in the figure below.

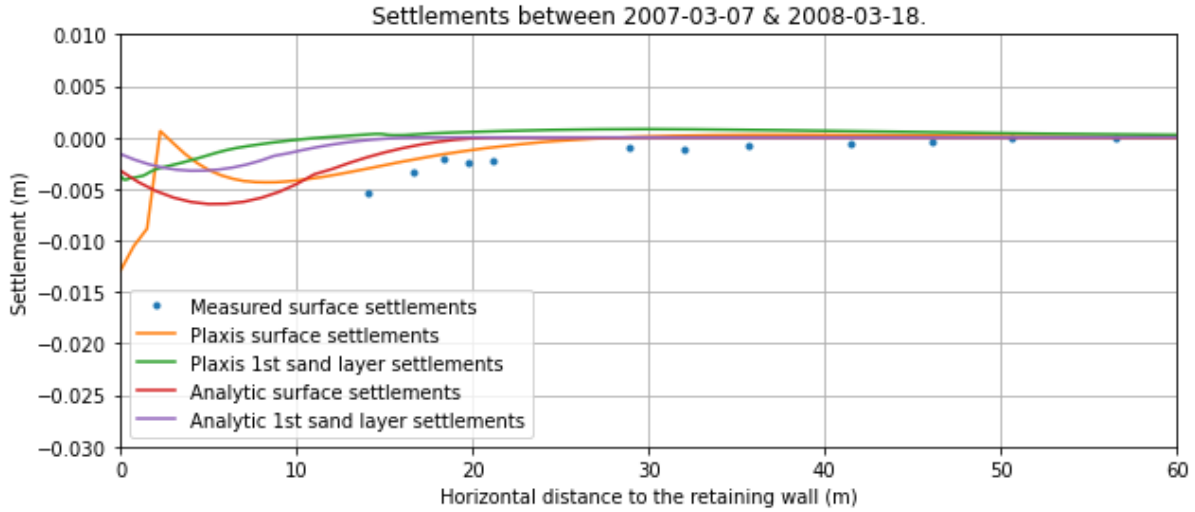

Figure 4-13 Settlements after the building pit is excavated to -9.5 m NAP.

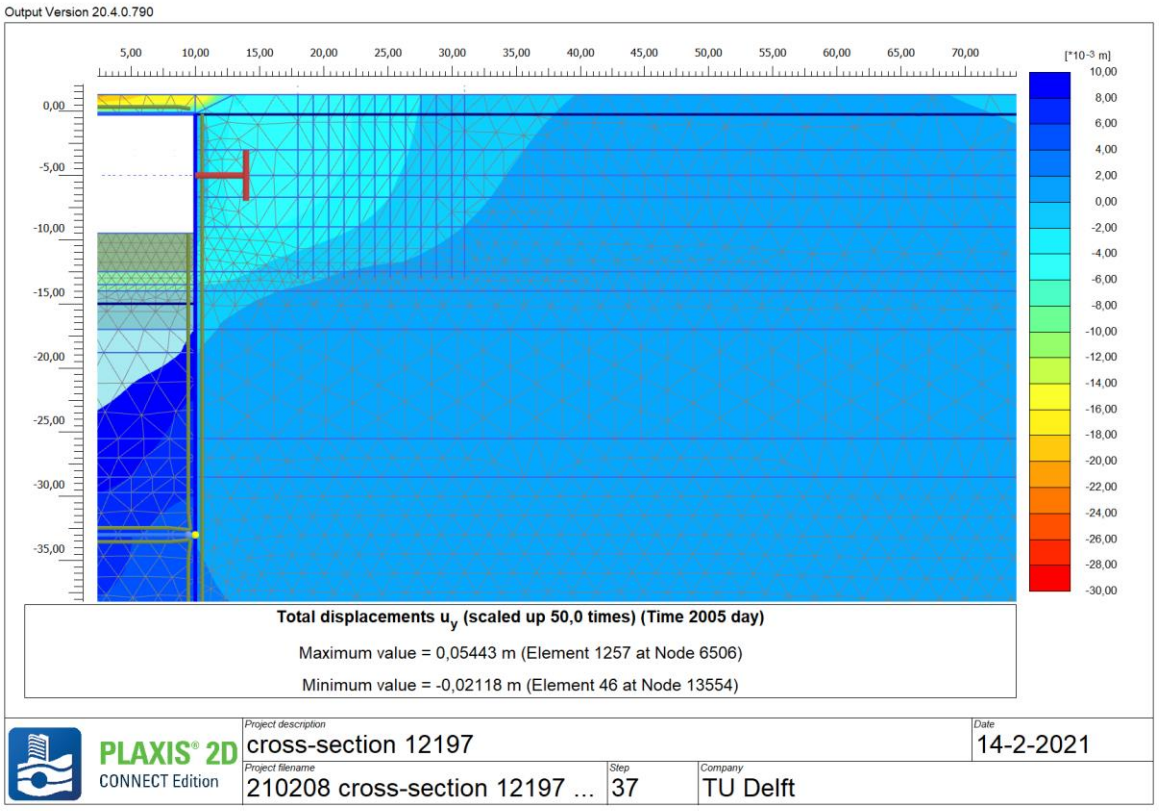

Figure 4-14 Vertical ground deformation after the building pit is excavated to -9.5 m NAP.

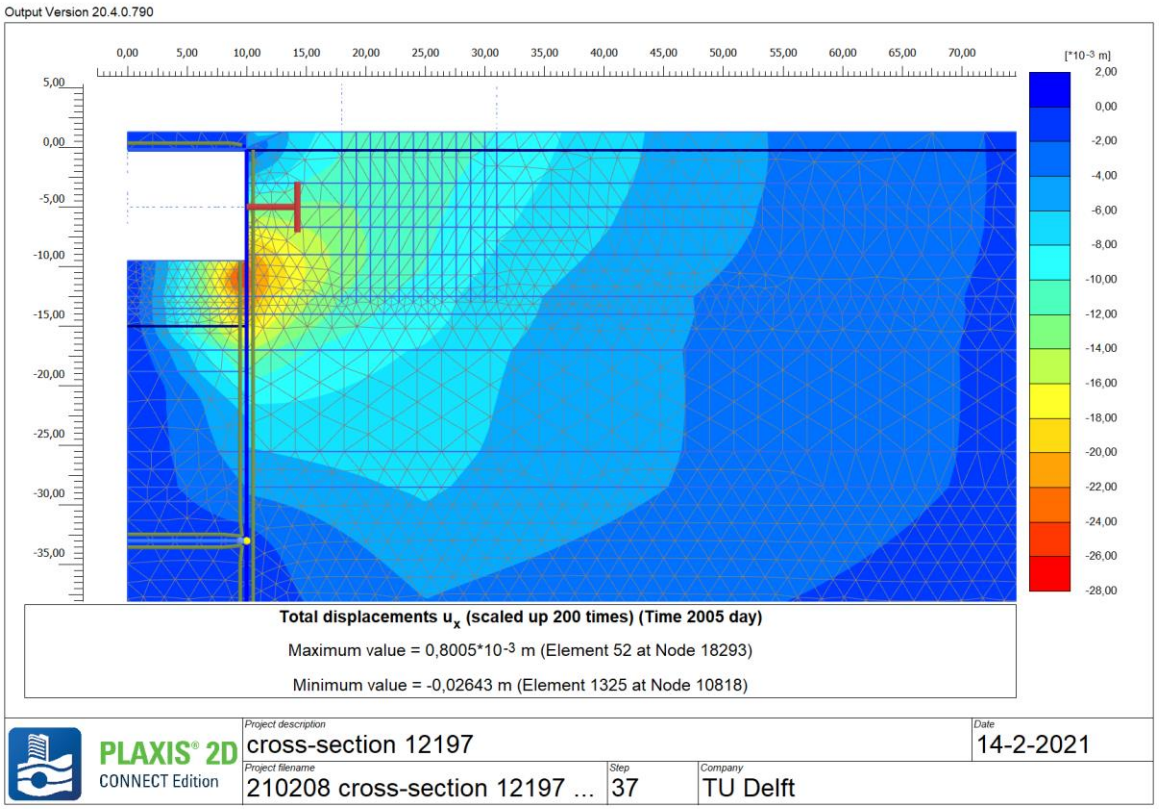

Figure 4-15 Horizontal ground deformation after the building pit is excavated to -9.5 m NAP.

4.2.4 Excavation to -13.5 m NAP

The PLAXIS result of the fourth excavation is plotted, excluding the installation of the diaphragm walls. The result is shown in the figure below.

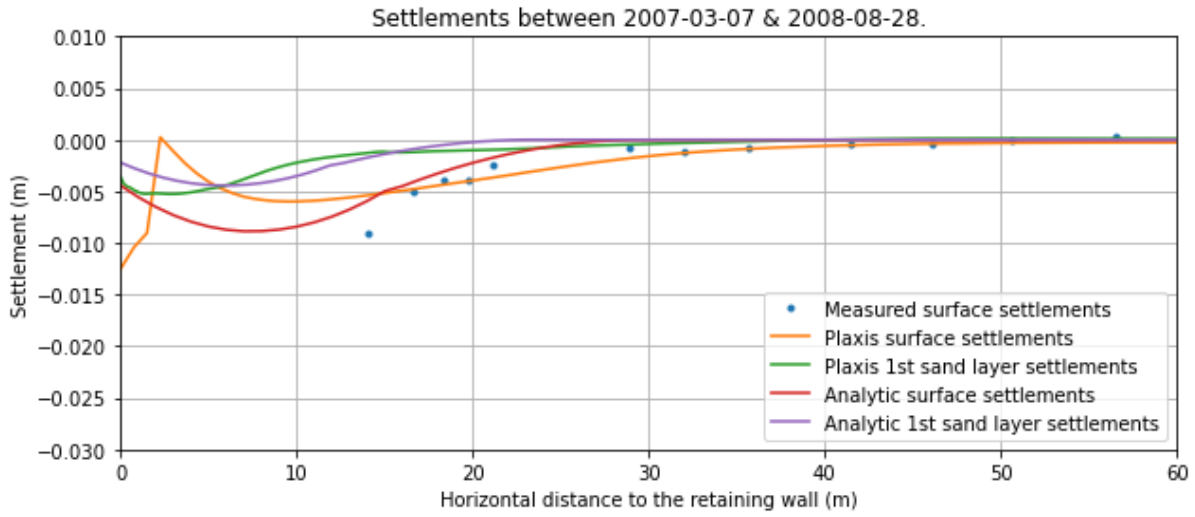

Figure 4-16 Settlements after the building pit is excavated to -13.5 m NAP.

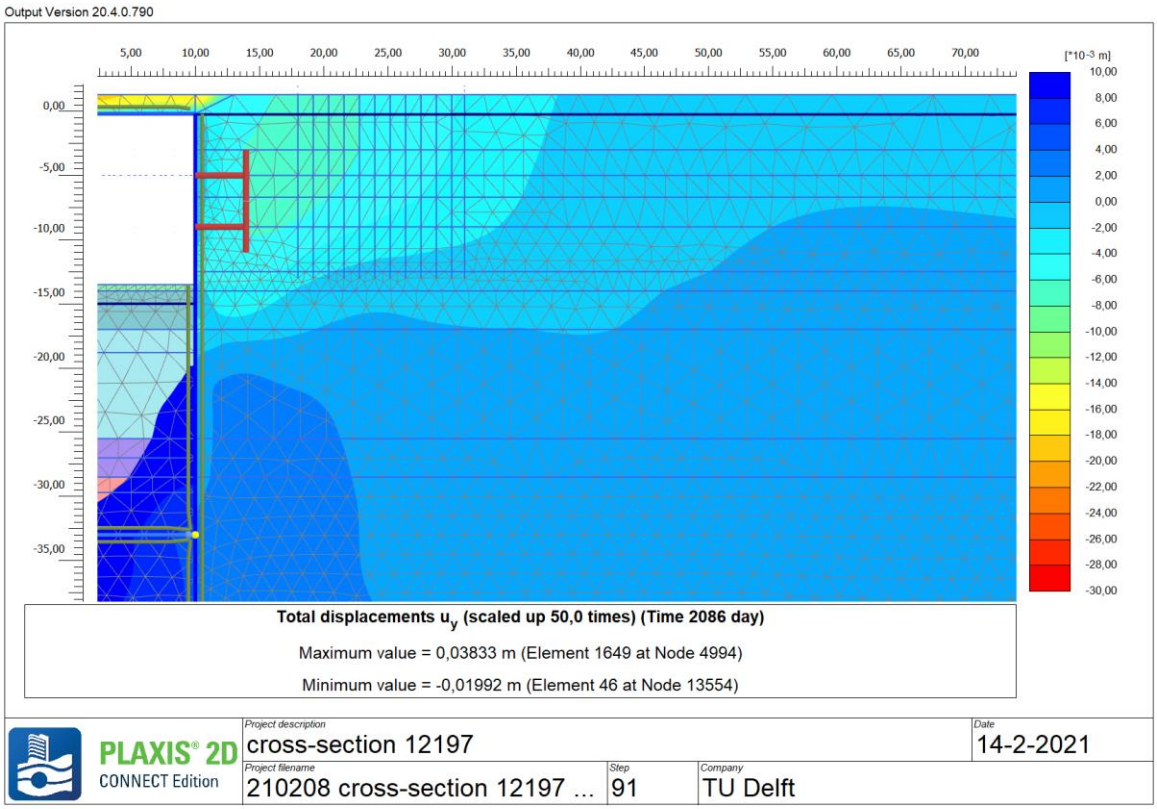

Figure 4-17 Vertical ground deformation after the building pit is excavated to -13.5 m NAP.

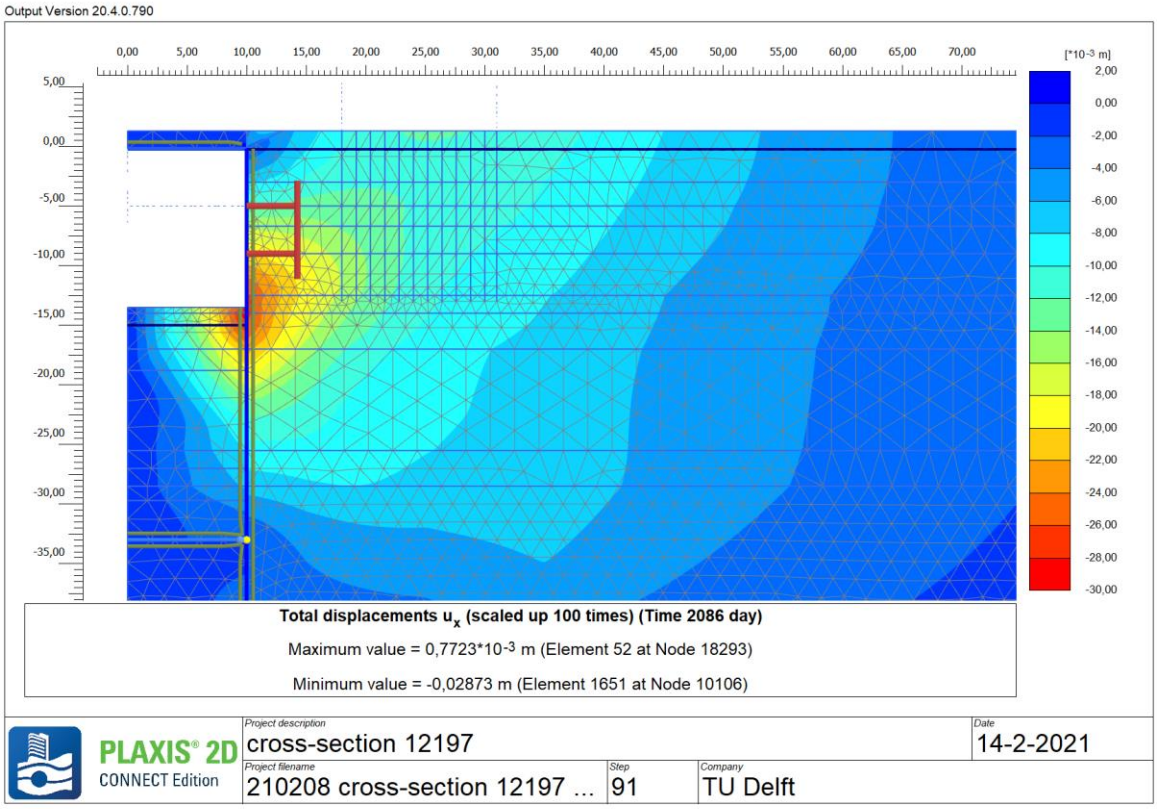

Figure 4-18 Horizontal ground deformation after the building pit is excavated to -13.5 m NAP.

4.2.5 Excavation to -18.8 m NAP

The PLAXIS result of the fifth excavation is plotted, excluding the installation of the diaphragm walls. The result is shown in the figure below.

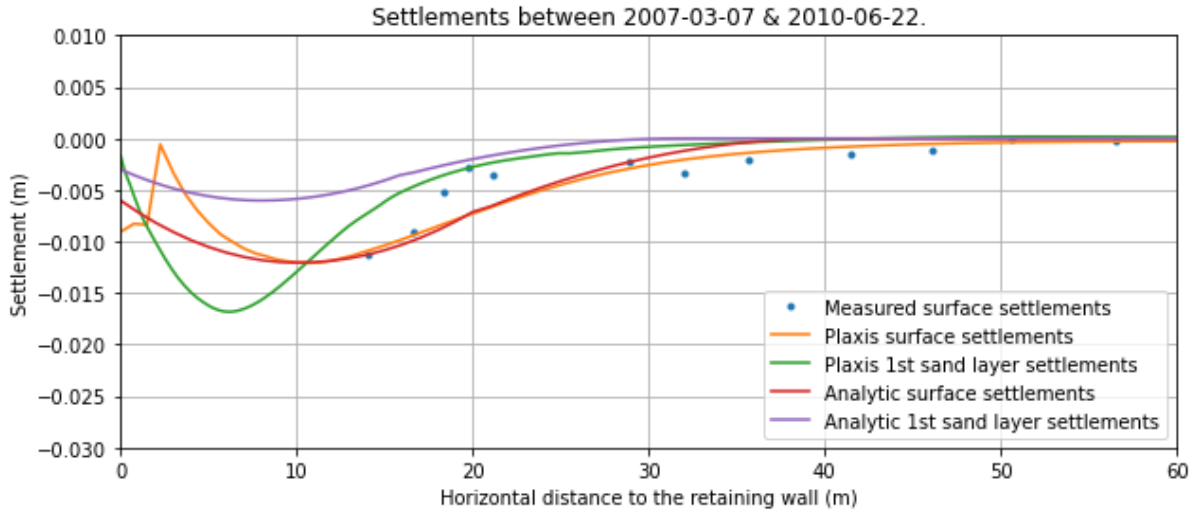

Figure 4-19 Settlements after the building pit is excavated to -18.8 m NAP.

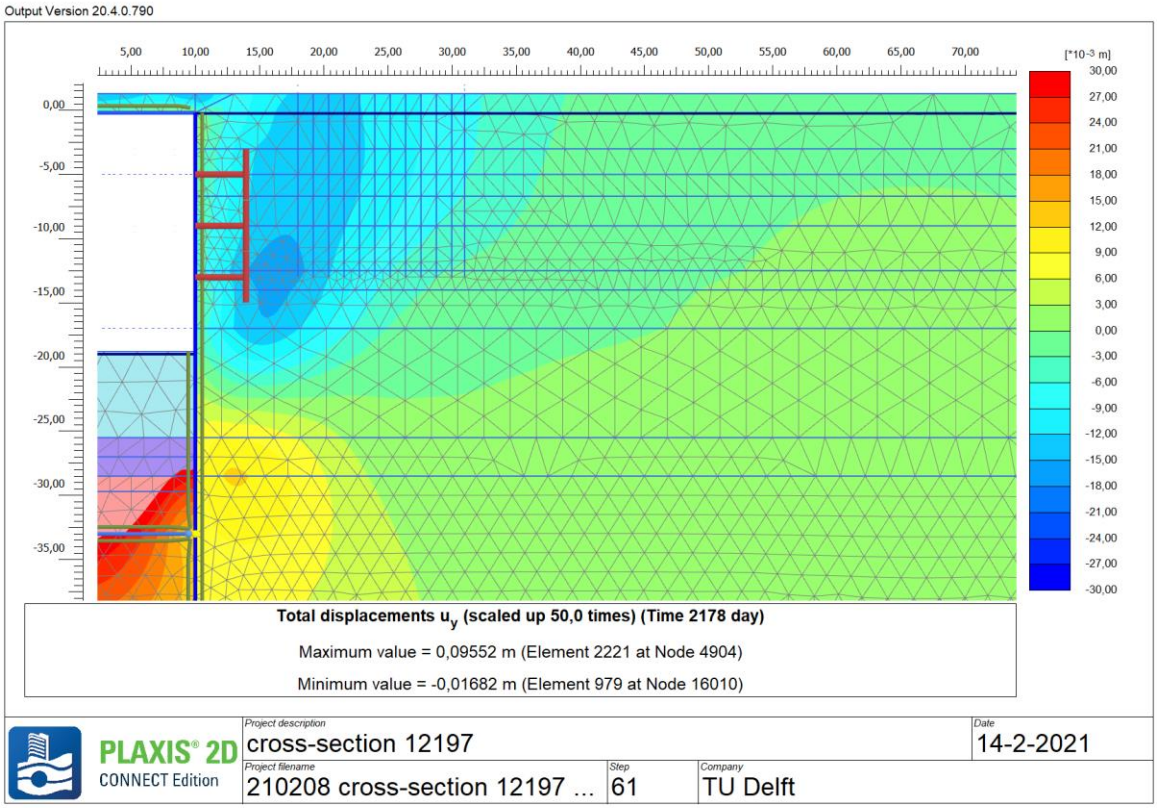

Figure 4-20 Vertical ground deformation after the building pit is excavated to -18.8 m NAP.

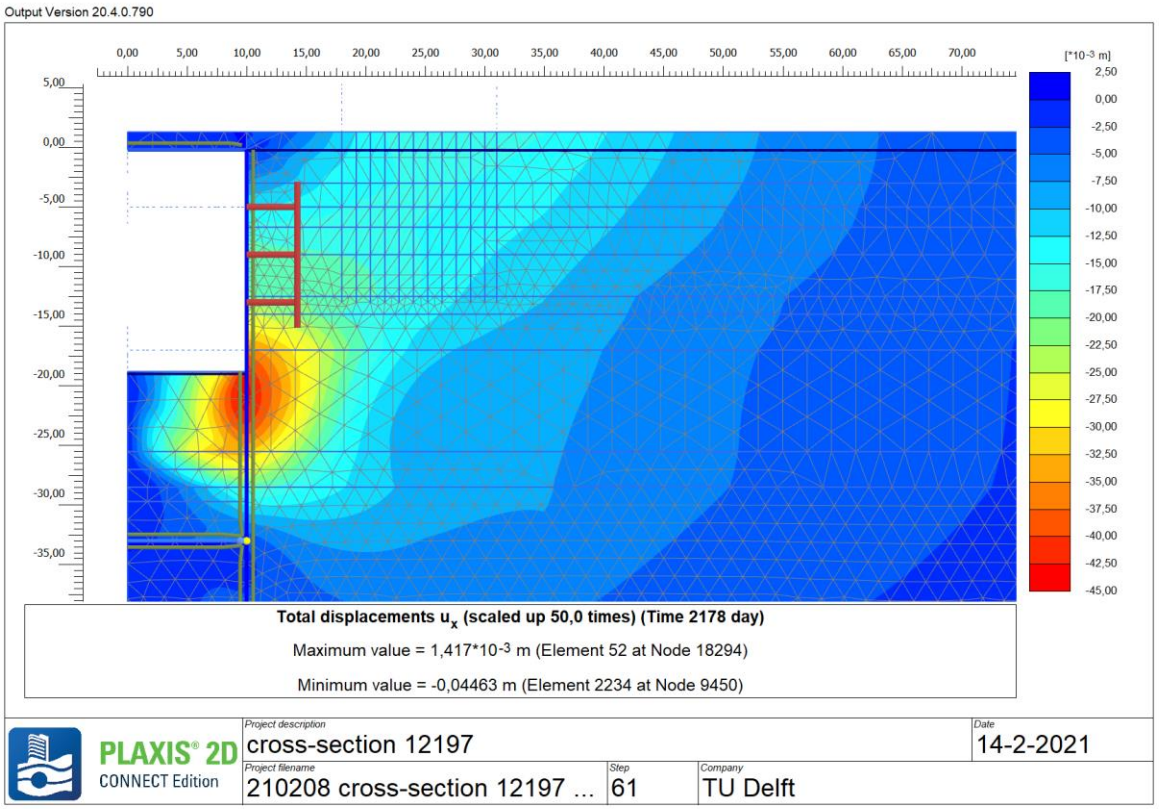

Figure 4-21 Horizontal ground deformation after the building pit is excavated to -18.8 m NAP.

4.2.6 Excavation to -29.7 m NAP

The PLAXIS result of the sixth excavation is plotted, excluding the installation of the diaphragm walls. The result is shown in the figure below.

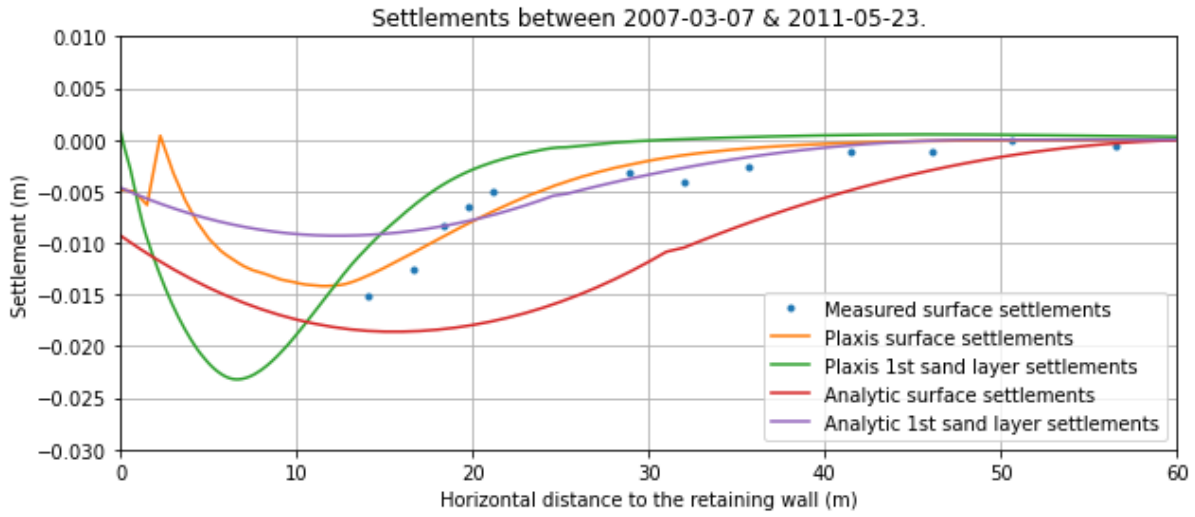

Figure 4-22 Settlements after the building pit is excavated to -29.7 m NAP.

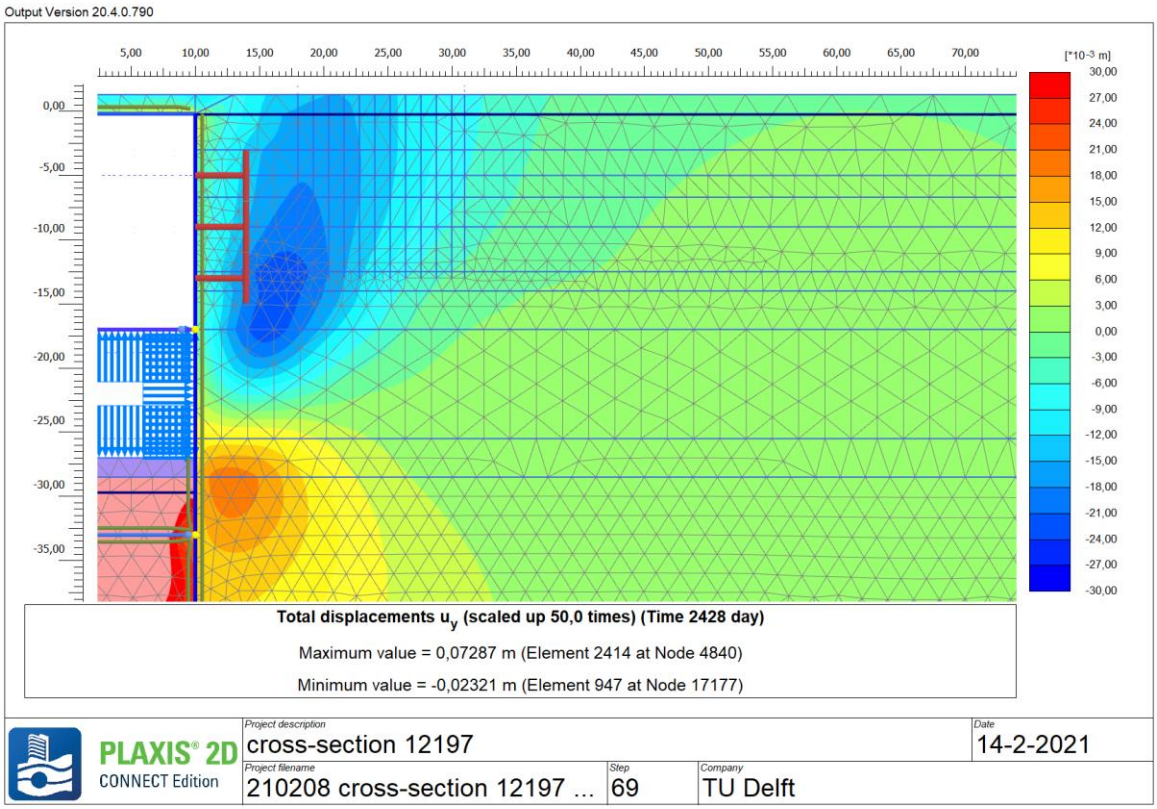

Figure 4-23 Vertical ground deformation after the building pit is excavated to -29.7 m NAP.

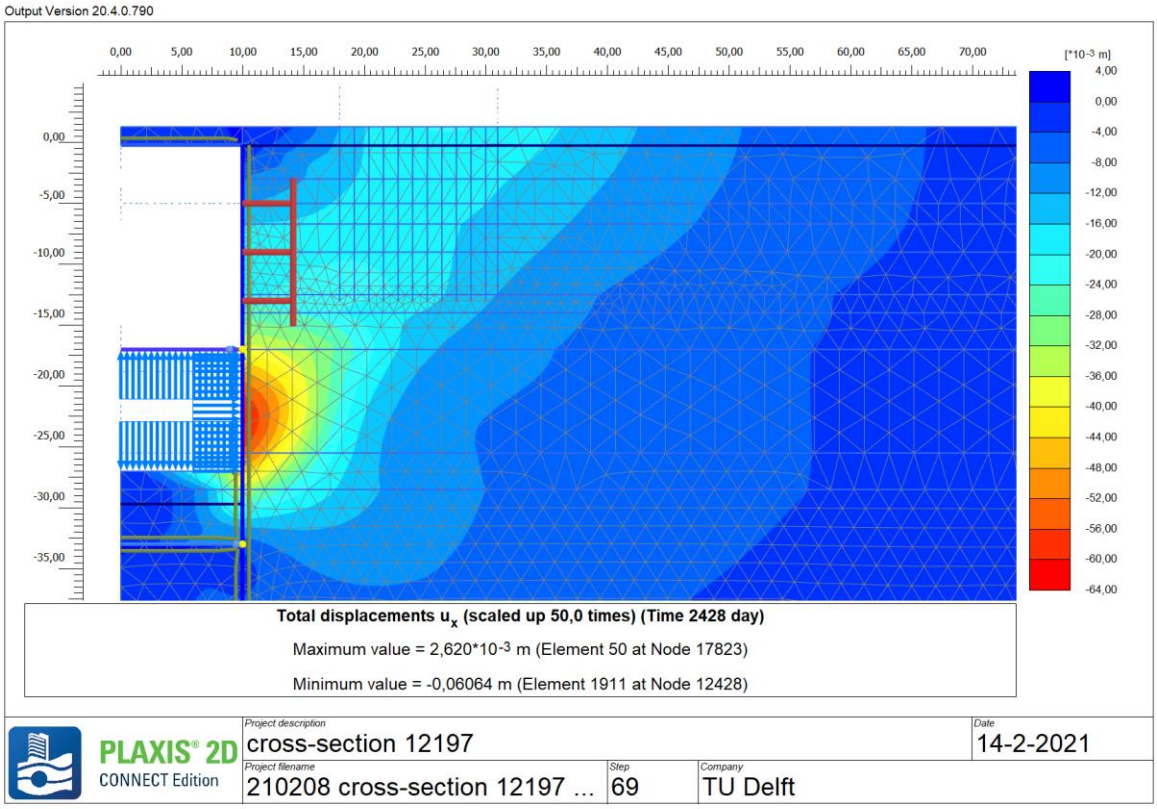

Figure 4-24 Horizontal ground deformation after the building pit is excavated to -29.7 m NAP.

4.2.7 Conclusions

In this section the measured settlements are presented along with the computed settlements using numerical an analytical calculations. The surface settlements following the different methods show varying results in terms of comparability.

During the first few excavation steps (-3 m NAP, -7 m NAP, -9.5 m NAP) the influence area is larger than the assumed influence area in the analytic assessment. Generally, the influence area is assumed to be between 1.5 and 3 times the excavation depth. The influence area at surface level in the numerical model was equal to roughly 4 times the excavation depth. The numerical results have an influence area which is consistent with the measurements. However, the numerical results show a slight underestimation of the surface settlements during these phases. The magnitude of the settlement is in line with the analytic results.

Later excavation steps have shown that the surface settlements are coming together. The numerical results have consistently shown an influence area that is comparable with the measurement data. During step 5 (-18.8 m NAP) of the excavation steps the numerical and analytic results for surface settlement are similar and both concur well with the measurement data available.

The last excavation step showed an overestimation of the surface settlement in the analytic calculations. Both the magnitude of the settlements and the influence area are overestimated. The numerical results of the surface settlements on the other hand are still in agreement with the measurement data.

The numerical results show sufficient resemblance to the measurement data. The analytic calculations fit in term of magnitude the numerical results. Depending on the excavation step the analytic results could either fit the measurements quite well or not that much. Up until the excavation reaches -13.5 m NAP the analytic calculation of the settlement of the first sand layer are in line with the numerical results. Afterward, the analytic calculations underestimate the settlements severely due to the increased deformations of the deeper soil layers. The numerical models are assumed to be representative for the measured data and therefore the real-life situation. The analytic results are assumed to be representative when these are in line with both the numerical results and measurement data.

4.3 Pile Settlement Analysis

Before including the buildings into the numerical model, the foundation piles are included separately into the numerical model. This enables the analysis where structural properties of the piles are of importance for its deformation and displacement during an excavation. The influence of structural properties, such as the diameter of the pile, the stiffness of the pile and the pile load, are analysed by varying the parameters. Also, the influence of the distance of the pile to the excavation on the displacements is analysed by assessing the deformations and the skin friction.

4.3.1 Pile Diameter

A typical old Amsterdam foundation pile is round, tapered and wooden, often pine wood. The tip is in most cases around 110 mm in diameter and the head is on average around 220 mm in diameter. In PLAXIS these piles are modelled as embedded beam rows in a 2D plane. This means that the piles need to be brought back to a line element with one uniform diameter. Before choosing directly a specific pile diameter for the building models, the relevance of the diameter is assessed in the following. The influence of the soil displacements on the displacements of the piles is assessed. This is done by constructing a model with uncoupled piles and varying the diameter:

- 110 mm (this is the minimum value)
- 180 mm (this is a widely used average)
- 220 mm (this is the maximum value)

The piles are typically founded in the first sand layer (-13 m NAP). The analysed piles are placed at 8 m from the diaphragm walls. The piles are modelled as massive circular beams with a set diameter. The piles are supporting the walls in sets of two. The couples are spaced out of plane approximately 8 m. Therefore, the spacing is divided between the coupled piles (4 m). The piles have a Young's modulus of $E = 6000 \frac{N}{mm^2}$ and a specific density of $\gamma = 4.6 \frac{kN}{m^3}$. The pile is not loaded, which means that no external force is exerted on the pile. The axial skin resistance is set to be dependent on the soil layer. The lateral resistance is assumed to be unlimited, as failure through bending is very unlikely. The base resistance is assumed to be 100 kN. A study was conducted by loading old timber piles in Amsterdam and the average base resistance was found to be roughly 100 kN (Korff M. , 2009). Default interface stiffness factors are used. The default values are derived using the following formulae:

$$ISF_{RS} = ISF_{RN} = 2.5\left(\frac{L_{spacing}}{D_{eq}}\right)^{-0.75}$$

$$ISF_{KF} = 25\left(\frac{L_{spacing}}{D_{eq}}\right)^{-0.75}$$

In which:

$L_{spacing}$ = Out-of-plane spacing between the embedded beams [m]

D_{eq} = Equivalent diameter of the embedded beam [m]

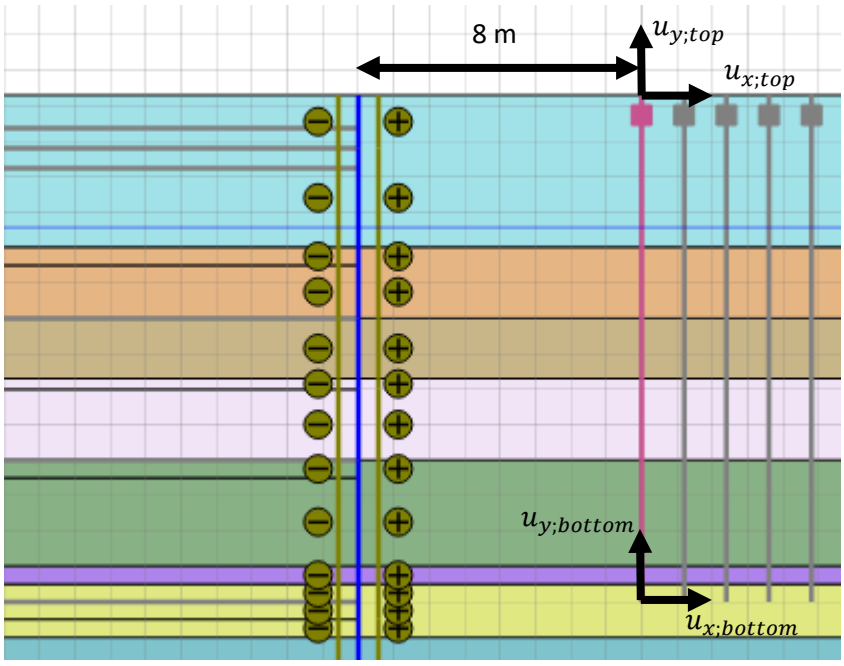

Figure 4-25 Schematization of the model with the axes for displacement displayed.

The horizontal and vertical displacements of the top and bottom of the piles are calculated and the results are represented in Table 4-1, Table 4-2 and Table 4-3 for the diameters of 110 mm, 180 mm and 220 mm respectively.

Table 4-1 Results of foundation pile with diameter 110 mm

Excavation step	$U_{x;top}$ (mm)	$U_{y;top}$ (mm)	$U_{x;bottom}$ (mm)	$U_{y;bottom}$ (mm)	Δu_y (mm)
-3	-4,71	-2,17	-3,74	-1,66	-0,52
-7	-10,16	-2,41	-8,73	-0,98	-1,43
-9,5	-10,14	-3,37	-11,59	-1,71	-1,66
-13,5	-10,08	-5,16	-15,15	-3,93	-1,23
-18,8	-11,21	-13,30	-18,36	-14,83	1,53
-29,7	-12,33	-16,99	-21,01	-19,37	2,38

Table 4-2 Results of foundation pile with diameter 180 mm

Excavation step	$U_{x;top}$ (mm)	$U_{y;top}$ (mm)	$U_{x;bottom}$ (mm)	$U_{y;bottom}$ (mm)	Δu_y (mm)
-3	-4,80	-1,96	-3,74	-1,65	-0,32
-7	-10,32	-1,83	-8,69	-0,95	-0,89
-9,5	-10,36	-2,67	-11,56	-1,59	-1,07
-13,5	-10,33	-4,59	-15,18	-3,80	-0,79
-18,8	-11,36	-13,70	-11,72	-13,42	-0,28
-29,7	-12,55	-17,90	-21,10	-19,17	1,27

Table 4-3 Results of foundation pile with diameter 220 mm

Excavation step	$U_{x;top}$ (mm)	$U_{y;top}$ (mm)	$U_{x;bottom}$ (mm)	$U_{y;bottom}$ (mm)	Δu_y (mm)
-3	-4,78	-1,90	-3,73	-1,64	-0,25
-7	-10,33	-1,63	-8,67	-0,92	-0,71
-9,5	-10,39	-2,41	-11,55	-1,55	-0,86
-13,5	-10,38	-4,39	-15,18	-3,76	-0,63
-18,8	-11,42	-13,85	-18,45	-14,49	0,64
-29,7	-12,59	-18,21	-21,12	-19,19	0,98

4.3.1.1 *Vertical displacement*

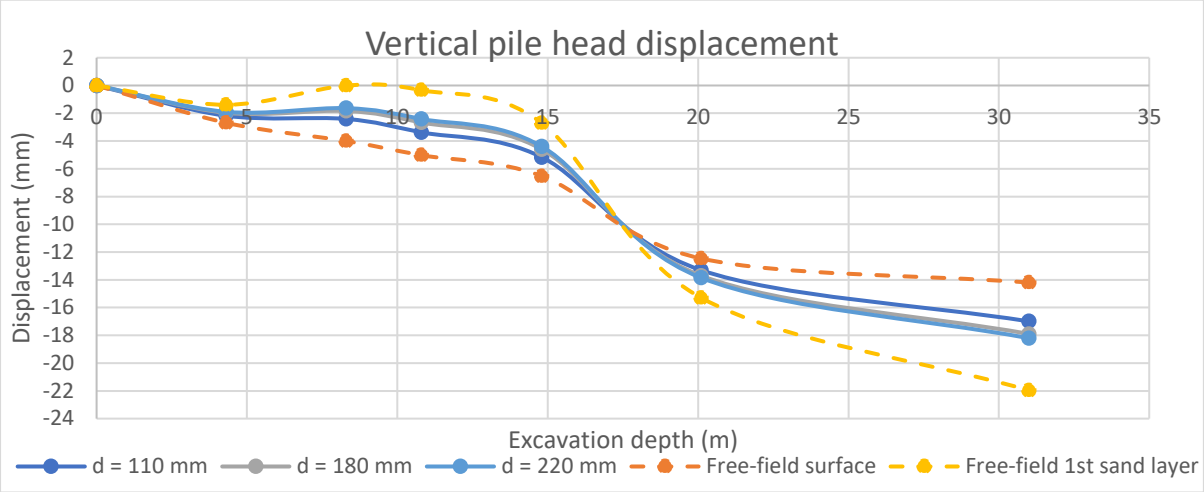

Figure 4-26 Vertical displacement of the top of the pile

The displacements of the piles have been plotted together with the free-field displacements. Figure 4-26 shows the vertical displacements of the pile head for the three chosen diameters together with the free-field displacements of the nodes in the same location as the pile tip (-13 m NAP). The horizontal axis represents the excavation depth and the vertical axis represents the vertical displacements of the pile heads.

There is some difference of response between the pile responses and the free-field displacements. Initially, the difference increases with the excavation depth. After the excavation to -13.5 m NAP the difference becomes smaller. This is due to the settlements of the deeper soil layers. These layers now act as an active force on the piles by dragging them and inducing negative skin friction on the piles. The upper soil layers now exert positive skin friction on the piles, which is contrary to the shallower excavation cases. This mechanism is schematized and shown in Figure 4-27. In the left figure a shallow excavation is depicted. The shallow excavation induces soil settlements in the upper soil layers. The dotted lines show the influence area. The pile sections inside this influence undergo negative skin friction due to the soil settlements in this area. This results in positive skin friction in the deeper part of the foundation piles to counter-act the negative skin friction shown in the figure. The right figure shows a deeper braced excavation. The larger stiffness induced by the struts allow for less horizontal deformation at the level of the struts. The unbraced lower section of the wall deforms more than the upper section. As a result, the local deeper soil sections deform more than the upper sections (depicted by the size of the settlement arrow). This greater soil settlement induces a larger vertical friction on the pile, resulting in negative skin friction. Due to the upper section deforming less the piles present in this area undergo resistance in the form of positive skin friction, counter-acting the larger movement in the deeper section of the pile foundation.

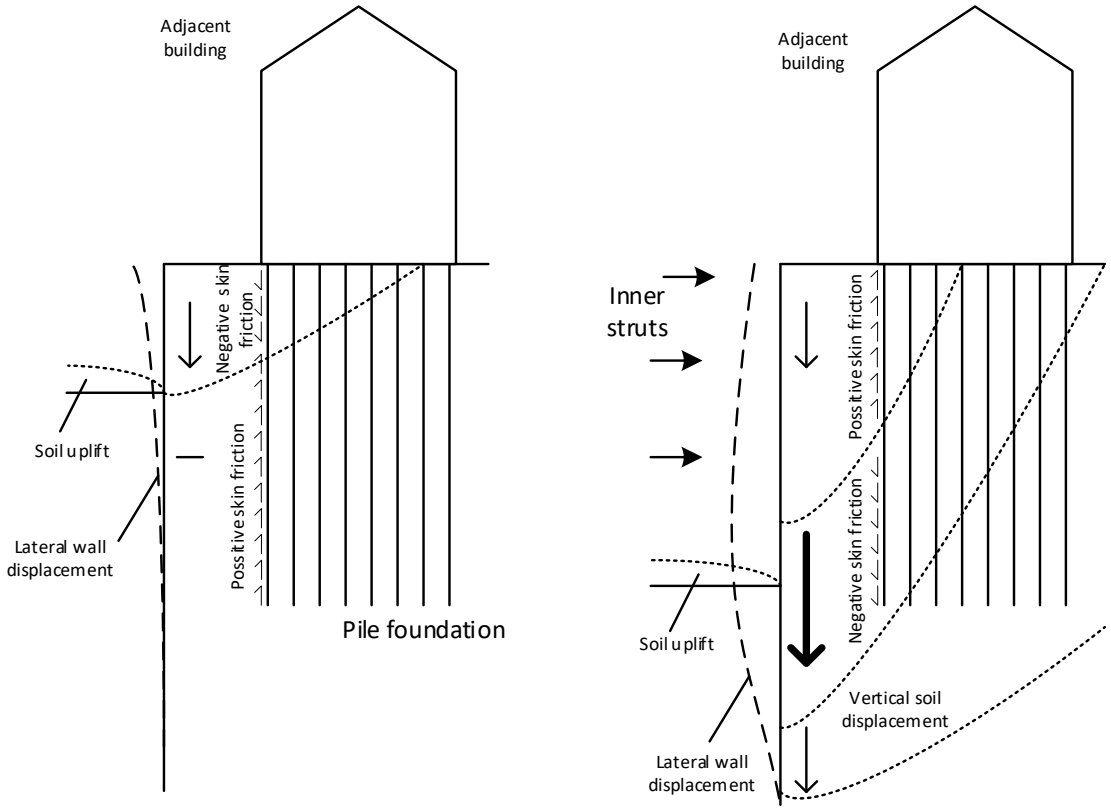

Figure 4-27 Soil settlements and activated skin friction.

The pile diameter has a minor influence on the vertical displacement of the pile head. The head of the pile with a diameter of 110 shows a to be more responsive to the induced soil deformations and follows the free-field trend more, whereas the other piles react stiffer. However, the difference between the pile responses is relatively small (+/- 1 mm) compared to the difference between the piles and the free-field deformations (+/- 4 mm).

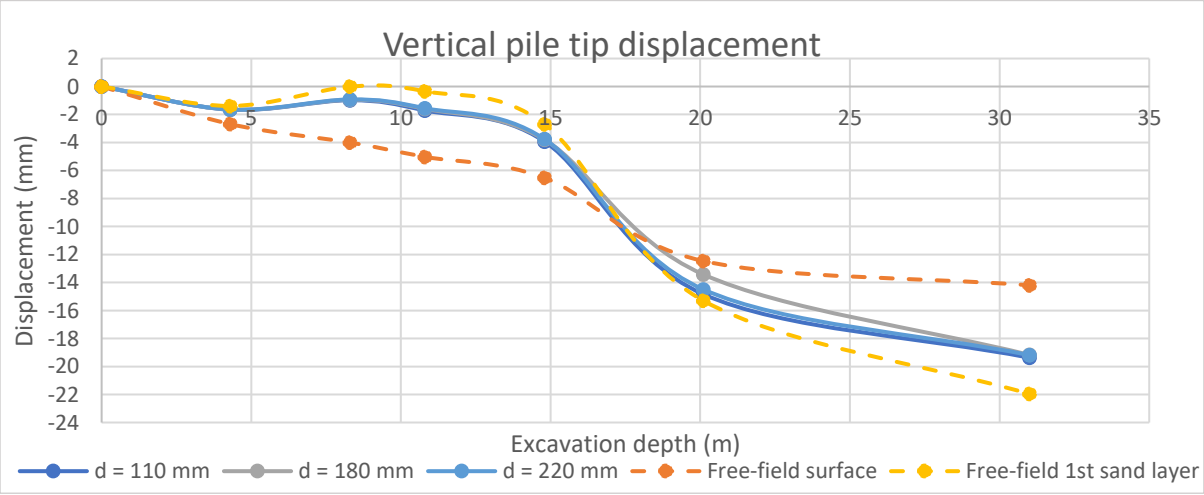

Figure 4-28 Vertical displacement of the tip of the pile

Figure 4-28 shows the vertical displacements of the pile tip for the three chosen diameters together with the free-field displacements of the exact point in the model. The horizontal axis represents the excavation depth and the vertical axis represents the vertical displacements of the pile toes.

The results show some small deviations of the pile tip displacement from the free-field settlements. The deviation tends to increase with excavation depth. The difference reaches up to 3 mm. Which is roughly 15% of the expected free-field settlements.

The difference in displacement between the different diameter is less apparent at the tip of the pile. The tip of the piles shows a stiffer response and the diameter of the pile doesn't seem to have any significant influence on the pile toe displacement. The piles displace independently from their respective diameter.

4.3.1.2 Horizontal displacement

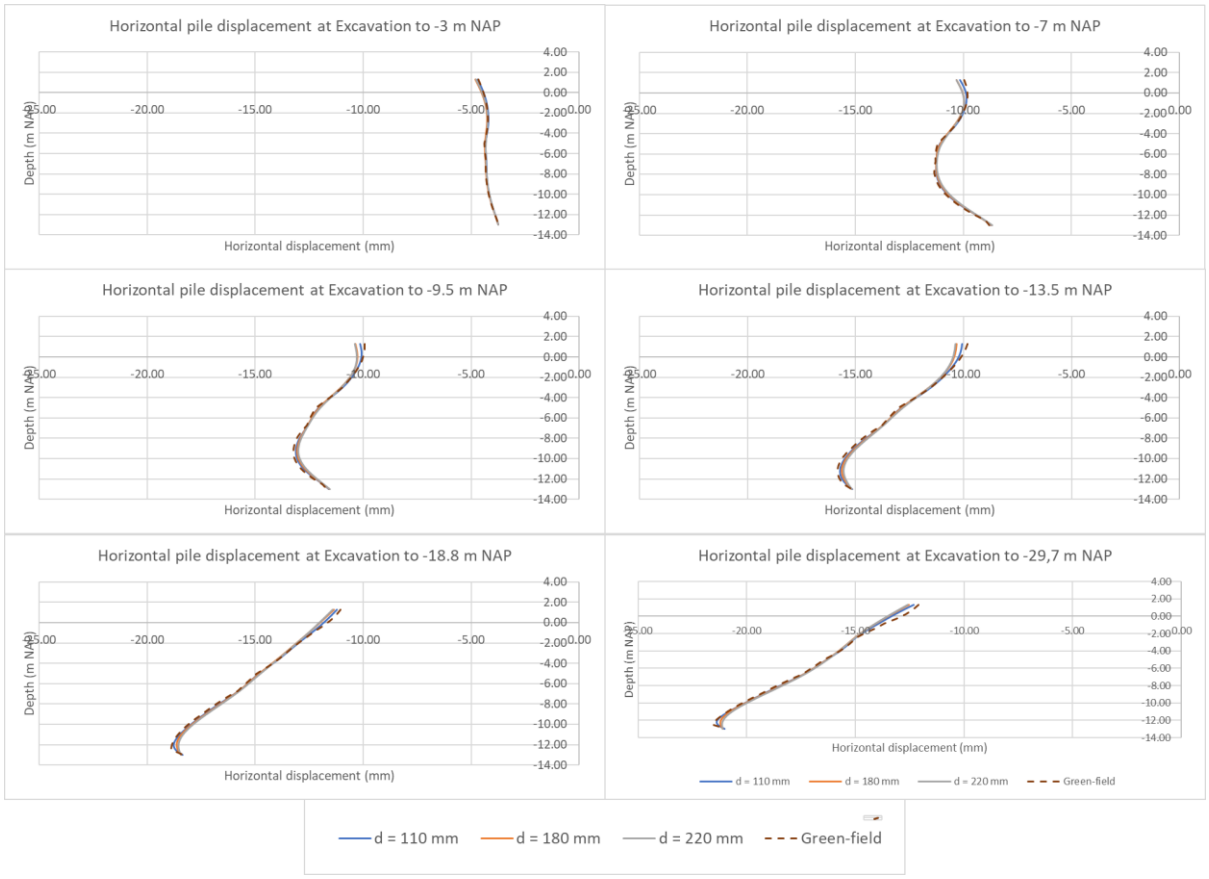

Figure 4-29 Horizontal displacements of the foundation piles with different diameters relative to their position at the start of the excavatory works

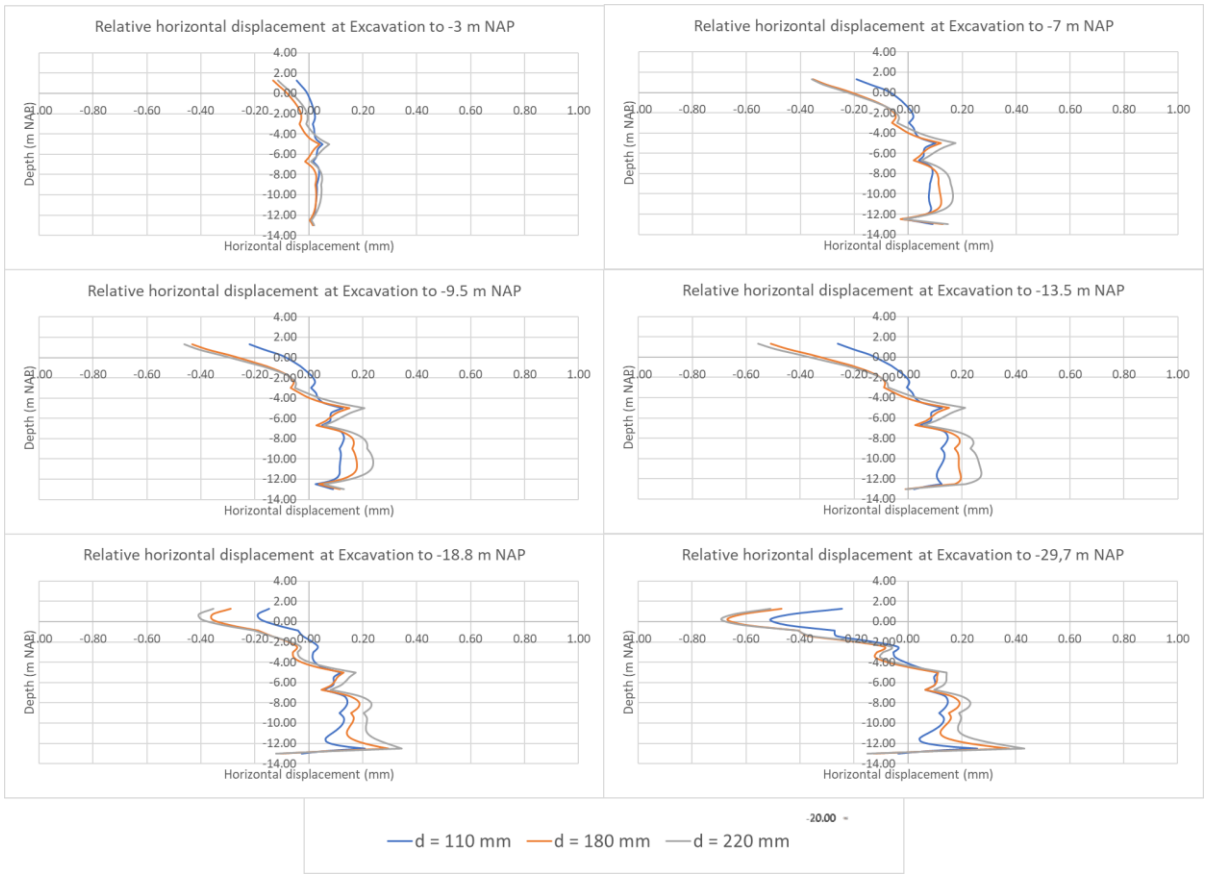

Figure 4-30 Relative horizontal displacements of the foundation piles with different diameters

Figure 4-29 shows the horizontal displacements of the piles the three chosen diameters together with the free-field displacements of the nodes in the same location as the piles. Figure 4-30 shows the horizontal displacements of the piles the three chosen diameters relative to the free-field soil deformations. The horizontal axis represents horizontal displacements and the vertical axis represents the vertical location of the pile increment.

The results show that the soil displacements are dominant. This is mainly due to the piles being relatively flexible, even for the piles with a bigger diameter. During the first few excavation phases the piles deform almost uniformly, independent of diameter. The upper part of the pile shows some small deviations, but this does not exceed 1 mm in deviation compared to the free-field deformations. During the later phases the differences become more significant. Especially, during the excavation phases to -18.8 m NAP and -29.7 m NAP. Overall, some deviations between the different pile diameters are visible. But these deviations are less than halve a millimetre, which is almost negligible in terms of deformations.

4.3.1.3 *Vertical Skin Friction*

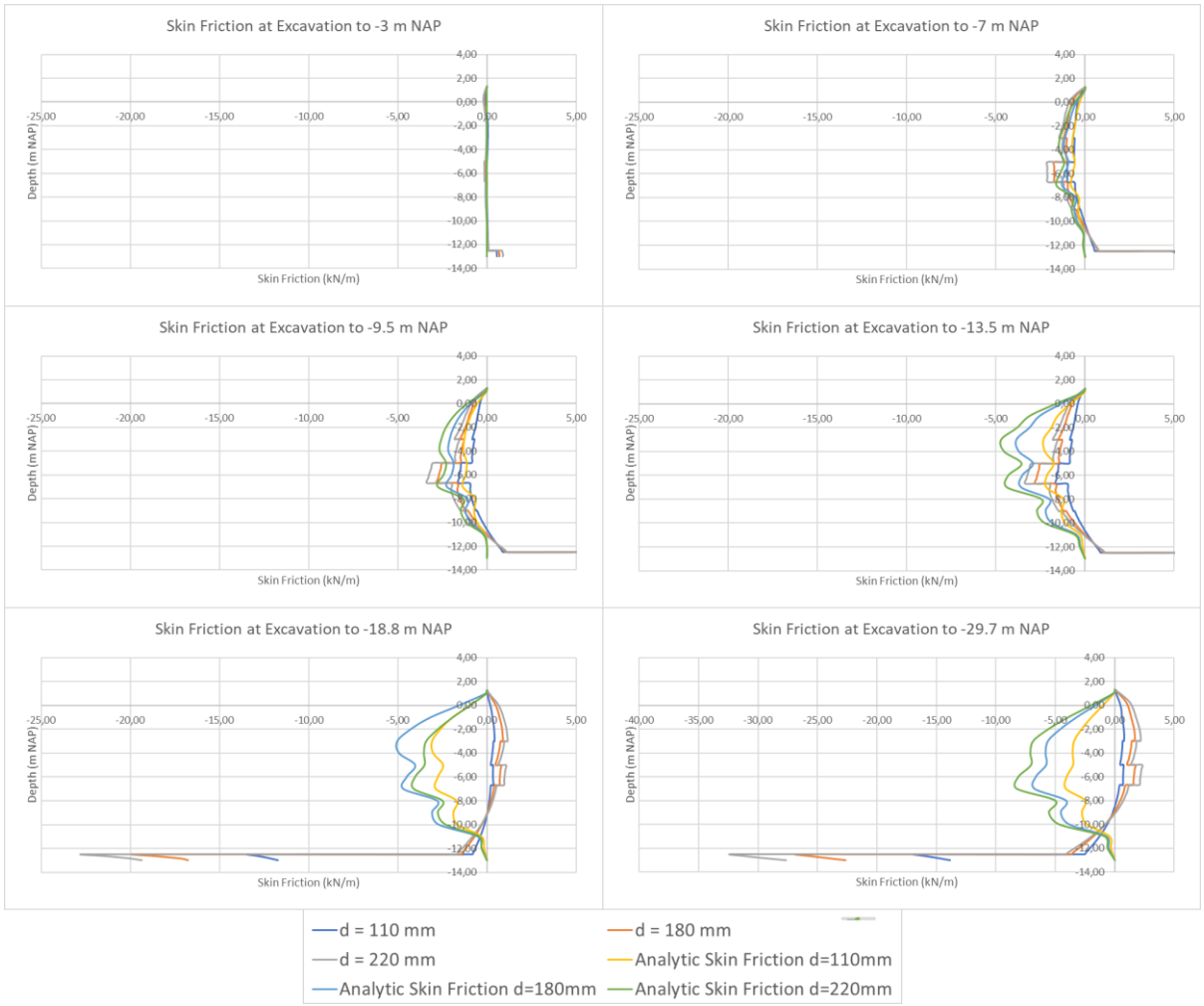

Figure 4-31 Vertical skin friction on the foundation piles with different diameters

Figure 4-31 shows the vertical skin friction acting on the piles for the three chosen diameters together with the expected skin friction following analytic calculations. The horizontal axis represents the skin friction per meter and the vertical axis represents the vertical location of the pile increment. A negative value indicates downward friction (negative skin friction) and a positive value indicates upward friction (positive skin friction).

The results show an interesting development over the excavation steps. The settlements of the upper soil layers are clearly visible after the first excavation step. The settlements induce negative skin friction on the upper section of the pile. The mechanism described in Figure 4-27 becomes visible after the excavation phase to -18.8 m NAP. Soil around the lower section of the pile settles more than the soil in upper layers, inducing a higher downward skin friction and moving the pile increments to a higher rate than the upper soil layers. Meaning that the upper section acts negatively and as positive skin friction on the pile. This mechanism is visible during the later excavation steps in Figure 4-31.

The numerical results show that the lower soil layers counter act the upper soil layers. This is not visible in the analytic results. For the analytic results it was assumed that the piles are end bearing and the pile tip is fixated. The pile tip moves solely with the underlying soil layer and no differential movement is accounted for. Realistically some movement between the pile tip and surrounding soil should occur. In a later stage this could be included using the modulus of subgrade reaction.

4.3.2 Pile Stiffness

To determine the influence of the Young's modulus on the pile displacement one characteristic diameter is chosen for the piles. The average value of 180 mm is chosen. These piles get a different young's modulus assigned to try to determine the influence. In PLAXIS these piles are again modelled as embedded beam rows in a 2D plane. This is done by constructing 3 models with different pile diameters: The literature provides a variety of literature concerning the young's modulus for old timber piles. Old Timber piles behave very different from new piles that's why this is interesting to assess. New pine wood piles have a Young's modulus of 15000 MPa. Older piles have a lower Young's modulus after degrading of timber over time. A Young's modulus of 6000 MPa is found for aged Pine wood and often the Young's modulus is even lower reaching a value of 3000 MPa:

- 15000 MPa (new stiff pile)
- 6000 MPa (aged Pine wood)
- 3000 MPa (low value found for aged Scot's pine wood)

The piles are typically founded in the first sand layer (-13 m NAP). The analysed piles are placed at 8 m from the diaphragm walls. The piles are modelled as massive circular beams with a set diameter. The piles are supporting the walls in sets of two. The couples are spaced out of plane approximately 8 m. Therefore, the spacing is divided between the coupled piles (4 m). The piles have a diameter of 180 mm and a specific density of $\gamma = 4.6 \frac{kN}{m^3}$. The pile is not loaded, which means that no external force is exerted on the pile. The axial skin resistance is set to be dependent on the soil layer. The lateral resistance is assumed to be unlimited, as failure through bending is very unlikely. The base resistance is assumed to be 100 kN.

The horizontal and vertical displacements of the top and tip of the piles are calculated and the results are represented in Table 4-1, Table 4-2 and Table 4-3 for the diameters of 3000 MPa, 6000 MPa and 15000 MPa respectively.

Table 4-4 Results of foundation pile with a Young's modulus of 3000 MPa

Excavation step	$U_{x;top}$ (mm)	$U_{y;top}$ (mm)	$U_{x;bottom}$ (mm)	$U_{y;bottom}$ (mm)	Δu_y (mm)
-3	-4,73	-2,12	-3,73	-1,60	-0,52
-7	-10,22	-2,27	-8,70	-0,79	-1,48
-9,5	-10,23	-3,18	-11,57	-1,40	-1,78
-13,5	-10,19	-4,99	-15,16	-3,65	-1,34
-18,8	-11,31	-13,42	-18,40	-14,75	1,33
-29,7	-12,44	-17,46	-21,06	-19,81	2,36

Table 4-5 Results of foundation pile with a Young's modulus of 6000 MPa

Excavation step	$U_{x;top}$ (mm)	$U_{y;top}$ (mm)	$U_{x;bottom}$ (mm)	$U_{y;bottom}$ (mm)	Δu_y (mm)
-3	-4,80	-1,96	-3,74	-1,65	-0,32
-7	-10,32	-1,83	-8,69	-0,95	-0,89
-9,5	-10,36	-2,67	-11,56	-1,59	-1,07
-13,5	-10,33	-4,59	-15,18	-3,80	-0,79
-18,8	-11,36	-13,70	-18,43	-14,54	0,84
-29,7	-12,55	-17,90	-21,10	-19,17	1,27

Table 4-6 Results of foundation pile with a Young's modulus of 15000 MPa

Excavation step	$U_{x;top}$ (mm)	$U_{y;top}$ (mm)	$U_{x;bottom}$ (mm)	$U_{y;bottom}$ (mm)	Δu_y (mm)
-3	-4,78	-1,84	-3,74	-1,69	-0,15
-7	-10,33	-1,48	-8,68	-1,08	-0,40
-9,5	-10,38	-2,26	-11,56	-1,78	-0,48
-13,5	-10,35	-4,28	-15,19	-3,93	-0,35
-18,8	-11,38	-13,99	-18,46	-14,38	0,39
-29,7	-12,54	-18,23	-21,14	-18,77	0,54

4.3.2.1 Vertical displacement

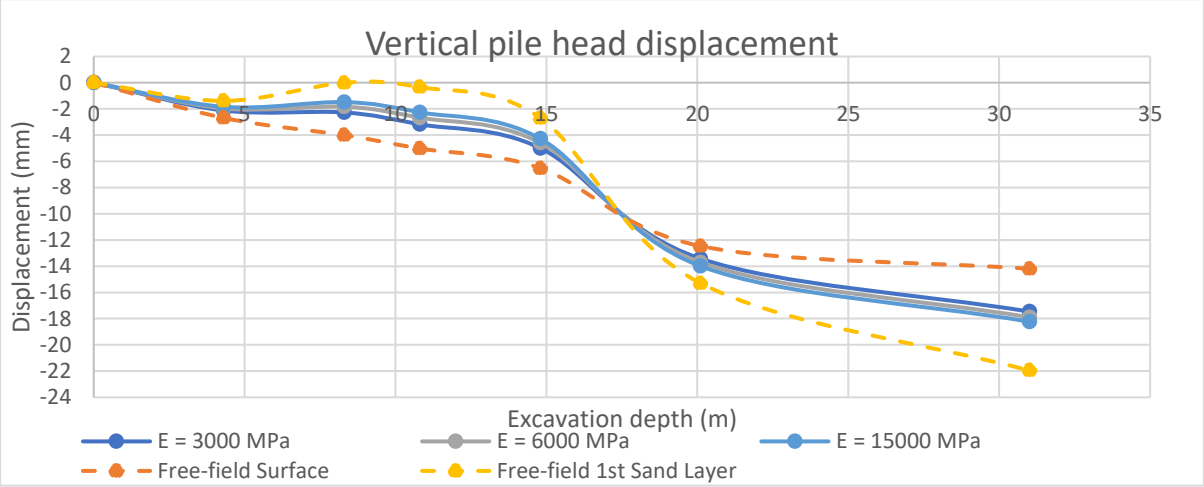

Figure 4-32 Vertical displacement of the top of the pile

The displacements of the pile have been plotted together with the greenfield displacements. Figure 4-32 shows the vertical displacements of the pile head for the three chosen Young's moduli together with the free-field displacements of the node in the same location as the pile tip. The horizontal axis represents the excavation depth and the vertical axis represents the vertical displacements of the pile heads.

The results show a clear difference between the different piles and the free-field displacements. However, the head of the pile with stiffness of 3000 MPa shows a more responsive behaviour of the pile to the induced soil deformation. Nevertheless, the difference between the piles is roughly a quarter (+/- 1mm) of the difference between the piles and the free-field deformations (+/- 4 mm).

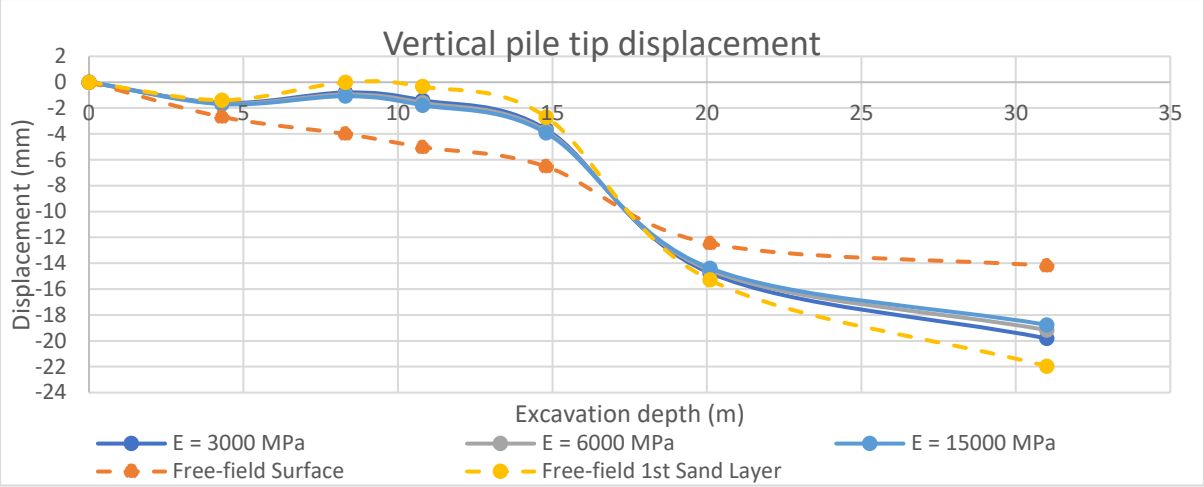

Figure 4-33 Vertical displacement of the tip of the pile

Figure 4-33 shows the vertical displacements of the pile tip for the three chosen Young's moduli together with the free-field displacements of the exact point in the model. The horizontal axis represents the excavation depth and the vertical axis represents the vertical displacements of the pile toes.

The results show a clear deviation of the pile tip displacement from the free-field settlements. The deviation tends to increase with excavation depth. At the excavation to -29.7 m NAP the difference reaches about 4 mm, which is roughly 20% less than the expected free-field settlements.

The difference in displacement between the different stiffnesses is also apparent at the tip of the pile. Overall, the tip of the piles show a similar response to compared to the pile head. In the final excavation step the difference between the new and the old pile became roughly 2 mm.

4.3.2.2 *Horizontal displacement*

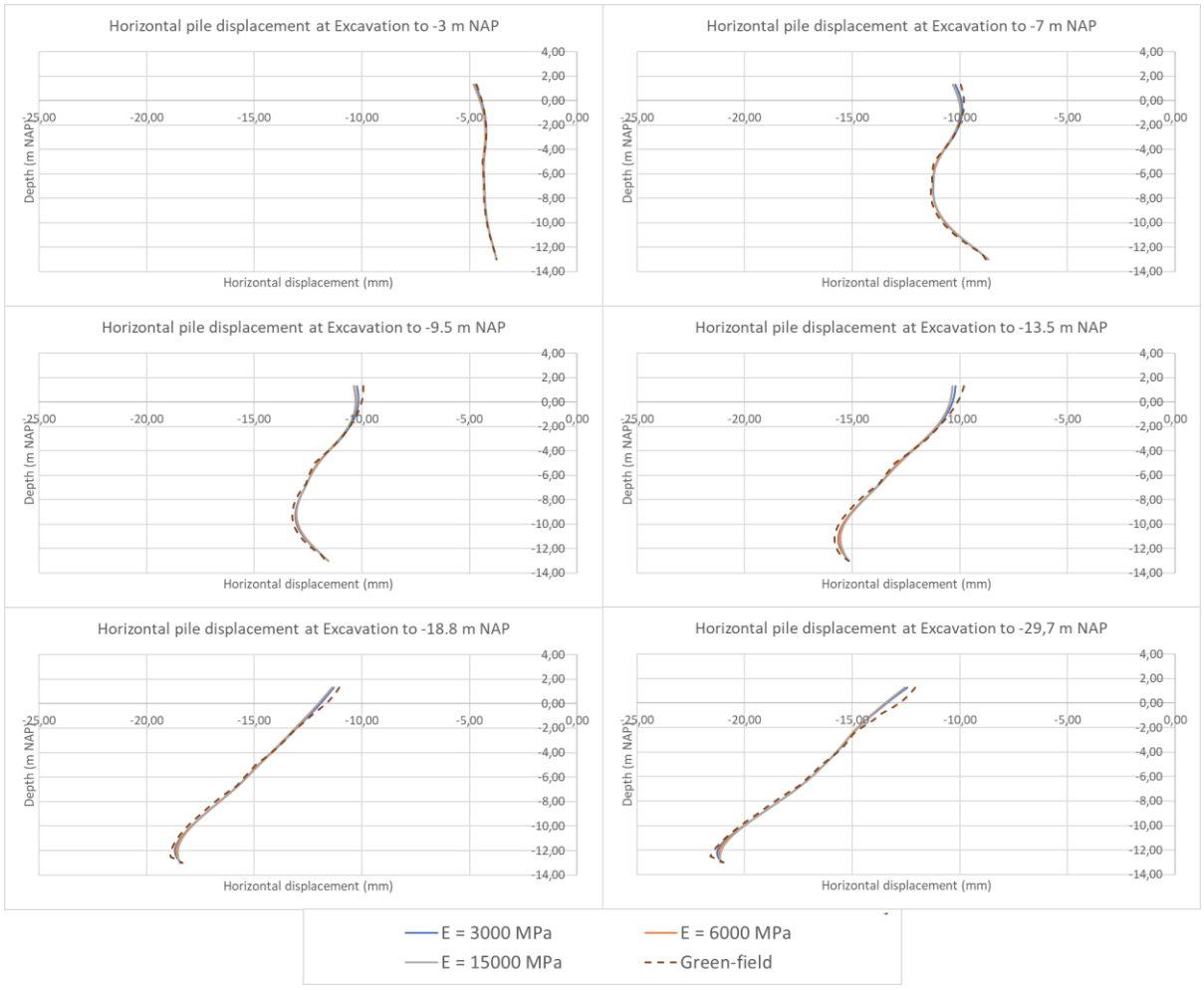

Figure 4-34 Horizontal displacements of the foundation piles with different stiffnesses relative to their position at the start of the excavatory works

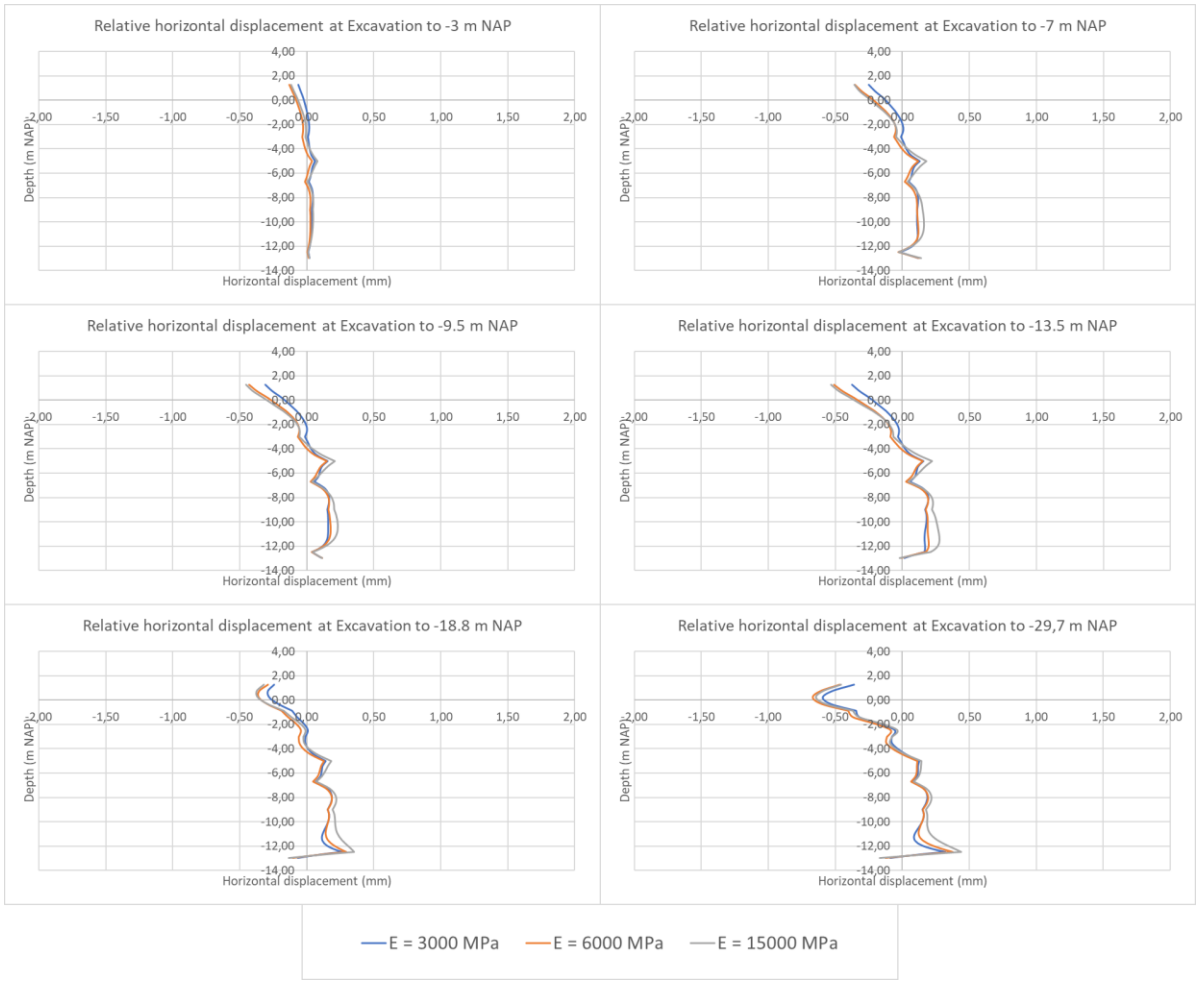

Figure 4-35 Relative horizontal displacements of the foundation piles with different stiffnesses

Figure 4-34 shows the horizontal displacements of the piles for the three chosen stiffnesses together with the free-field displacements of the nodes in the same location as the piles. Figure 4-35 shows the horizontal displacements of for the piles the three chosen stiffnesses relative to the free-field soil deformations. The horizontal axis represents horizontal displacements and the vertical axis represents the vertical location of the pile increment.

The results show that the soil displacements are dominant. A higher pile stiffness does not seem to influence the horizontal displacements significantly. During the first few excavation phases the pile heads deform roughly 0.5 mm more towards the excavation compared to the free-field deformations. The difference between the stiffest and least stiff pile is negligible. During the later phases the differences become more spread out over the length of the pile. But these remain below 1 mm, making the relative horizontal displacement negligible.

4.3.2.3 *Vertical Skin Friction*

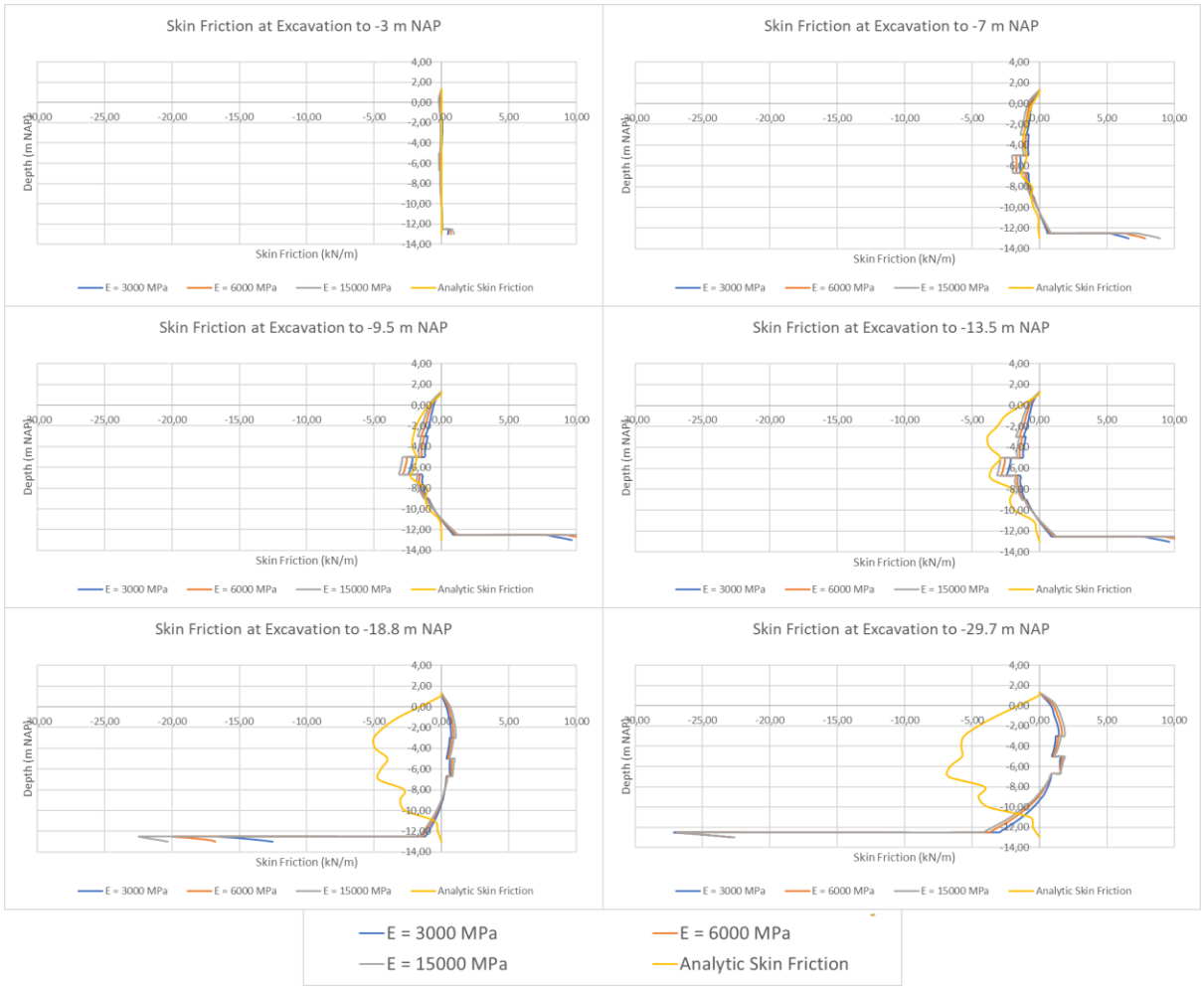

Figure 4-36 Vertical skin friction on the foundation piles with different stiffnesses

Figure 4-36 shows the vertical skin friction acting on the piles for the three chosen stiffnesses together with the expected skin friction following analytic calculations for a 180 mm diameter pile. The horizontal axis represents the skin friction per meter and the vertical axis represents the vertical location of the pile increment. A negative value indicates downward friction (negative skin friction) and a positive value indicates upward friction (positive skin friction).

Generally, the differences between the numerical results and the analytic results are the same as described in paragraph 4.3.1.3. The skin friction for the different stiffnesses is different. Minor differences between the piles with stiffnesses of 3000 MPa and 6000 MPa are observed. In contrary, the stiffest pile (15000 MPa) seams to attract more skin friction. The stiffness of the pile allows for less strain. This causes the soil displacements to be relatively larger inducing a higher skin friction on the pile. As the skin friction is dependent on the relative soil displacement, for relative displacements smaller than 10 mm. During the first 3 excavation phases this pile also tends to undergo the same skin friction as the calculated values (infinitely stiff). Deviations from the analytic values start to occur after these steps, as the values tend to become higher than calculated and the overall shape differs.

4.3.3 Pile Load

It is very interesting to assess the effect initial pile loading has on its deformation during the excavation steps. Literature suggests that the initial loading of the pile influences its behaviour significantly. To assess the magnitude for this case 4 different loading cases are analysed. Firstly, the unloaded uncoupled pile is the starting point and the point of reference. Additional cases are investigated using an additional axial load on the pile of respectively 50 kN, 100 kN and 200 kN. In summary the following models are analysed:

- Self-weight of the pile
- Self-weight + 50 kN
- Self-weight + 100 kN
- Self-weight + 200 kN

The piles are typically founded in the first sand layer (-13 m NAP). The analysed piles are placed at 8 m from the diaphragm walls. The piles are modelled as massive circular beams with a set diameter. The piles are supporting the walls in sets of two. The couples are spaced out of plane approximately 8 m. Therefore, the spacing is divided between the coupled piles (4 m). The piles have a Young's modulus of $E = 6000 \frac{N}{mm^2}$ and a specific density of $\gamma = 4.6 \frac{kN}{m^3}$. The piles have a diameter of 180 mm. The axial skin resistance is set to be dependent on the soil layer. The lateral resistance is assumed to be unlimited, as failure through bending is very unlikely. The base resistance is assumed to be 100 kN.

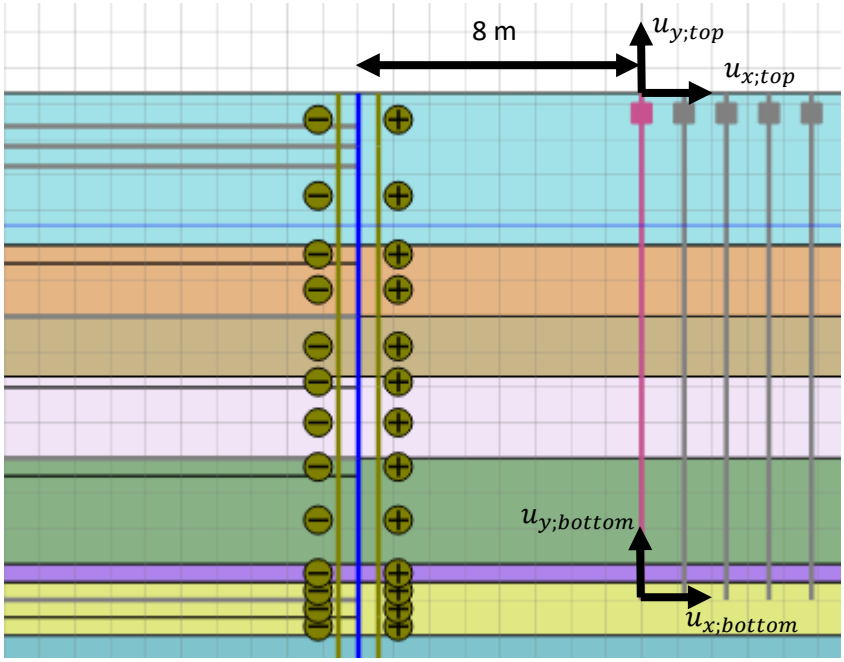

Figure-4-37 Schematization of the model with the axes for displacement displayed.

The horizontal and vertical displacements of the top and bottom of the piles are calculated and the results are represented in Table 4-7, Table 4-8 and Table 4-9 for the diameters of the additional axial load of 50 kN, 100 kN and 200 kN respectively.

Table 4-7 Results of foundation pile with an additional axial load of 50 kN

Excavation step	$U_{x;top}$ (mm)	$U_{y;top}$ (mm)	$U_{x;bottom}$ (mm)	$U_{y;bottom}$ (mm)	Δu_y (mm)
-3	-4,76	-2,13	-3,74	-1,83	-0,31
-7	-10,30	-2,37	-8,75	-1,44	-0,93
-9,5	-10,39	-3,31	-11,67	-2,20	-1,10
-13,5	-10,32	-5,51	-15,49	-4,78	-0,73
-18,8	-11,16	-15,36	-19,04	-16,27	0,91
-29,7	-11,96	-20,40	-21,88	-22,06	1,67

Table 4-8 Results of foundation pile with an additional axial load of 100 kN

Excavation step	$U_{x;top}$ (mm)	$U_{y;top}$ (mm)	$U_{x;bottom}$ (mm)	$U_{y;bottom}$ (mm)	Δu_y (mm)
-3	-4,77	-2,19	-3,75	-1,88	-0,31
-7	-10,32	-2,55	-8,85	-1,61	-0,94
-9,5	-10,40	-3,57	-11,83	-2,45	-1,12
-13,5	-10,29	-6,06	-15,87	-5,40	-0,66
-18,8	-10,72	-16,53	-19,81	-17,33	0,80
-29,7	-11,27	-21,74	-22,80	-23,25	1,51

Table 4-9 Results of foundation pile with an additional axial load of 200 kN

Excavation step	$U_{x;top}$ (mm)	$U_{y;top}$ (mm)	$U_{x;bottom}$ (mm)	$U_{y;bottom}$ (mm)	Δu_y (mm)
-3	-4,99	-2,35	-3,84	-2,04	-0,30
-7	-10,47	-2,96	-9,13	-2,07	-0,89
-9,5	-10,50	-4,29	-12,40	-3,28	-1,01
-13,5	-10,13	-7,41	-13,52	-4,45	-2,96
-18,8	-9,74	-19,41	-21,71	-19,78	0,37
-29,7	-9,90	-25,54	-24,94	-26,14	0,60

4.3.3.1 *Vertical displacement*

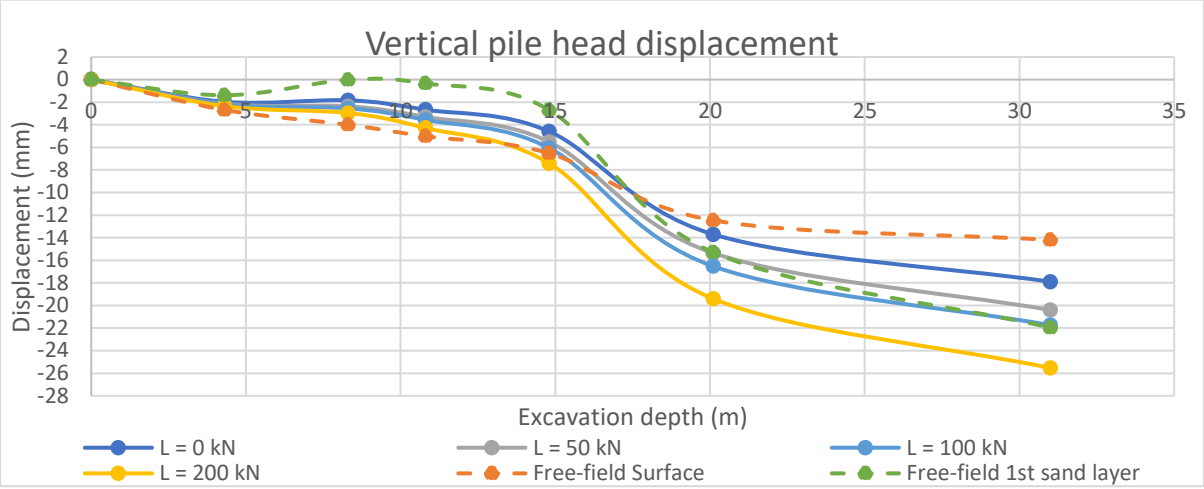

Figure 4-38 Vertical displacement of the top of the pile

The displacements of the piles have been plotted together with the greenfield displacements. Figure 4-38 shows the vertical displacements of the pile heads for 4 different load cases together with the free-field displacements of the nodes on the same location as the pile heads. The horizontal axis represents the excavation depth and the vertical axis represents the vertical displacements of the pile heads.

The results show a significant influence of initial load on the vertical displacement of the pile head. The additional load forces the pile to settle to a larger extent than the free-field displacements. The difference between pile settlement and free-field settlement reaches up to roughly 10 mm in this case. During the first few excavation steps the pile heads deform less than the projected free-field settlements. However, during the excavation to -9.5 m NAP an infliction point is reached where the rate of change decreases for the free-field settlements and increases for the heads. At this stage the piles start to deform more than the projected free-field settlements. At this stage the difference reaches 10 mm, which is almost an 80 % increase in deformation compared to the free-field settlements. Interestingly, the pile with a load of 200 kN deformed more than the free-field settlements during all excavation steps.

The load shows to have a big influence on the pile behaviour. The deformations increase with increasing load. The difference reaches up to 10 mm between the pile with no additional load and an additional load of 200 kN. This range of deformation could have significant implications for the strength and stability of a structure.

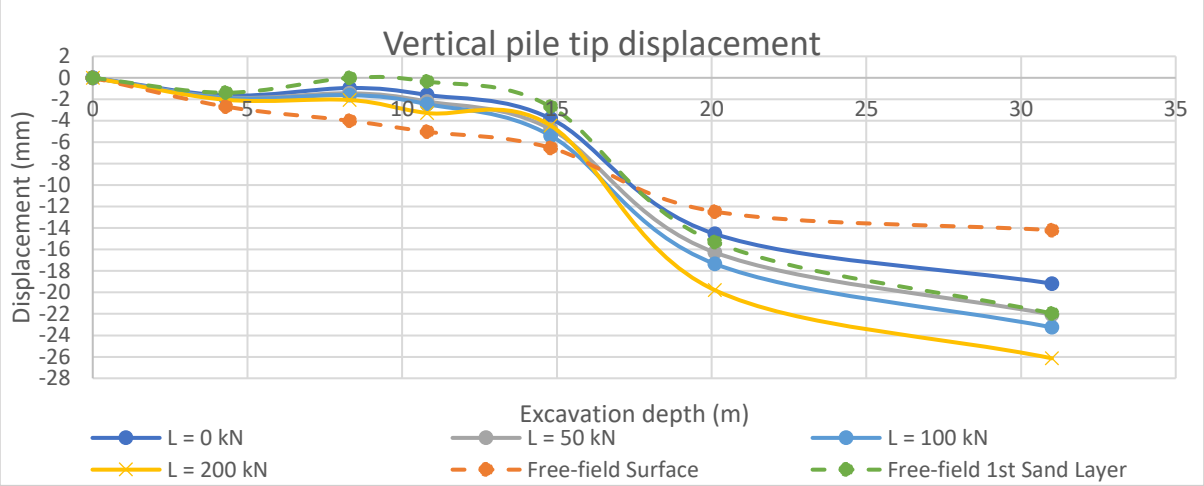

Figure 4-39 Vertical displacement of the tip of the pile

The displacements of the piles have been plotted together with the greenfield displacements. Figure 4-39 shows the vertical displacements of the pile tip for 4 different load cases together with the free-field displacements of the nodes on the same location as the pile heads. The horizontal axis represents the excavation depth and the vertical axis represents the vertical displacements of the pile heads.

The results again show a significant influence of the initial load on the vertical displacement of the pile. The additional load forces the pile tip to settle to a larger extent than the free-field displacements. The difference between pile settlement and free-field settlement reaches up to 4 mm. This is the stage at which the difference reaches 4 mm, which is almost a 20 % less deformation than the free-field settlements. Interestingly, again the pile with a load of 200 kN deformed more than the free-field settlements during all excavation steps. The same can now be stated for the piles with an additional load of 100 kN.

The results show a large dependency of vertical pile tip displacement on the initial load. The deformations increase with increasing load for the investigated cases. The difference reaches up to 7 mm between no additional load and an additional load of 200 kN.

4.3.3.2 *Horizontal displacement*

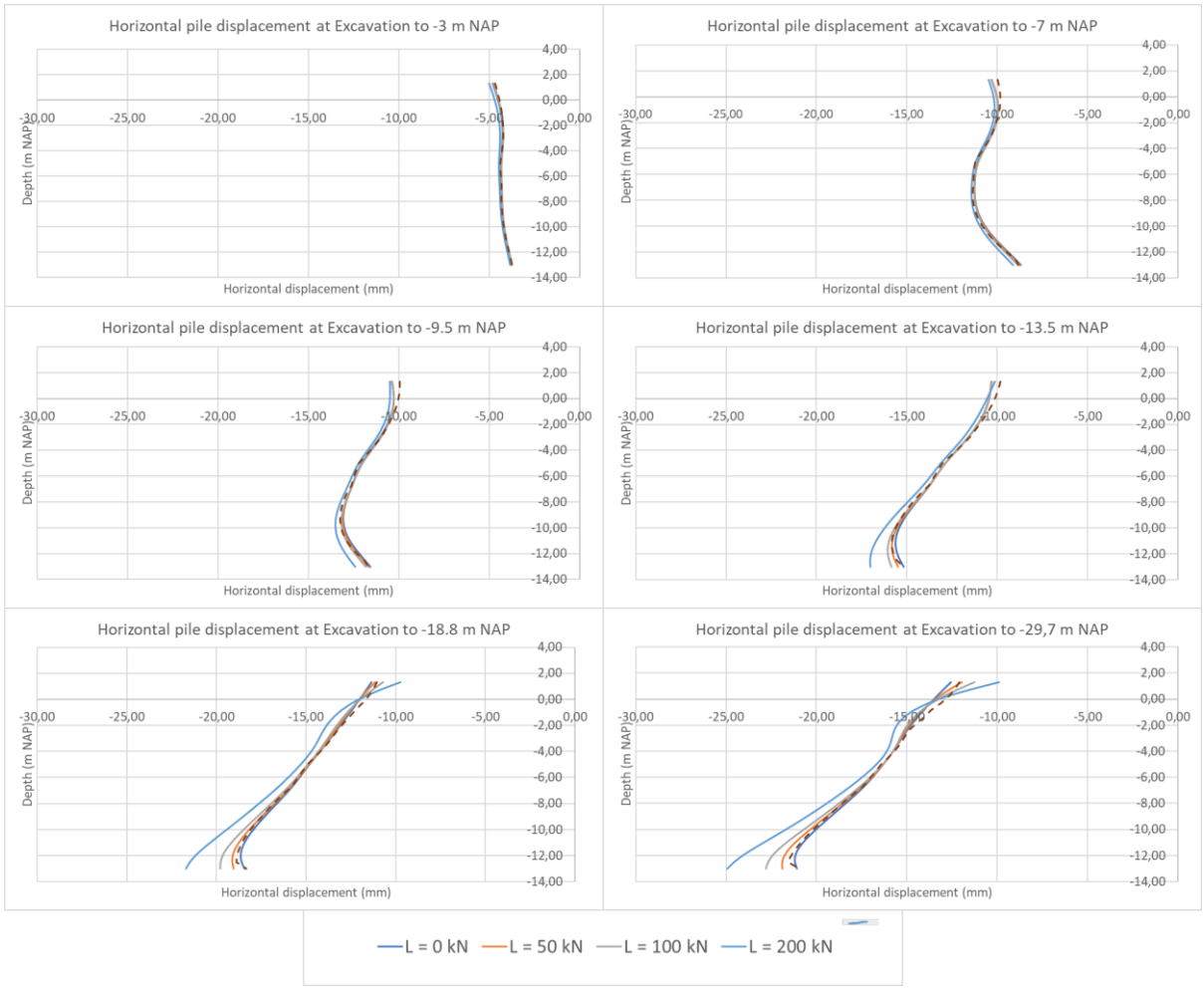

Figure 4-40 Horizontal displacements of the foundation piles with different loads relative to their position at the start of the excavatory works

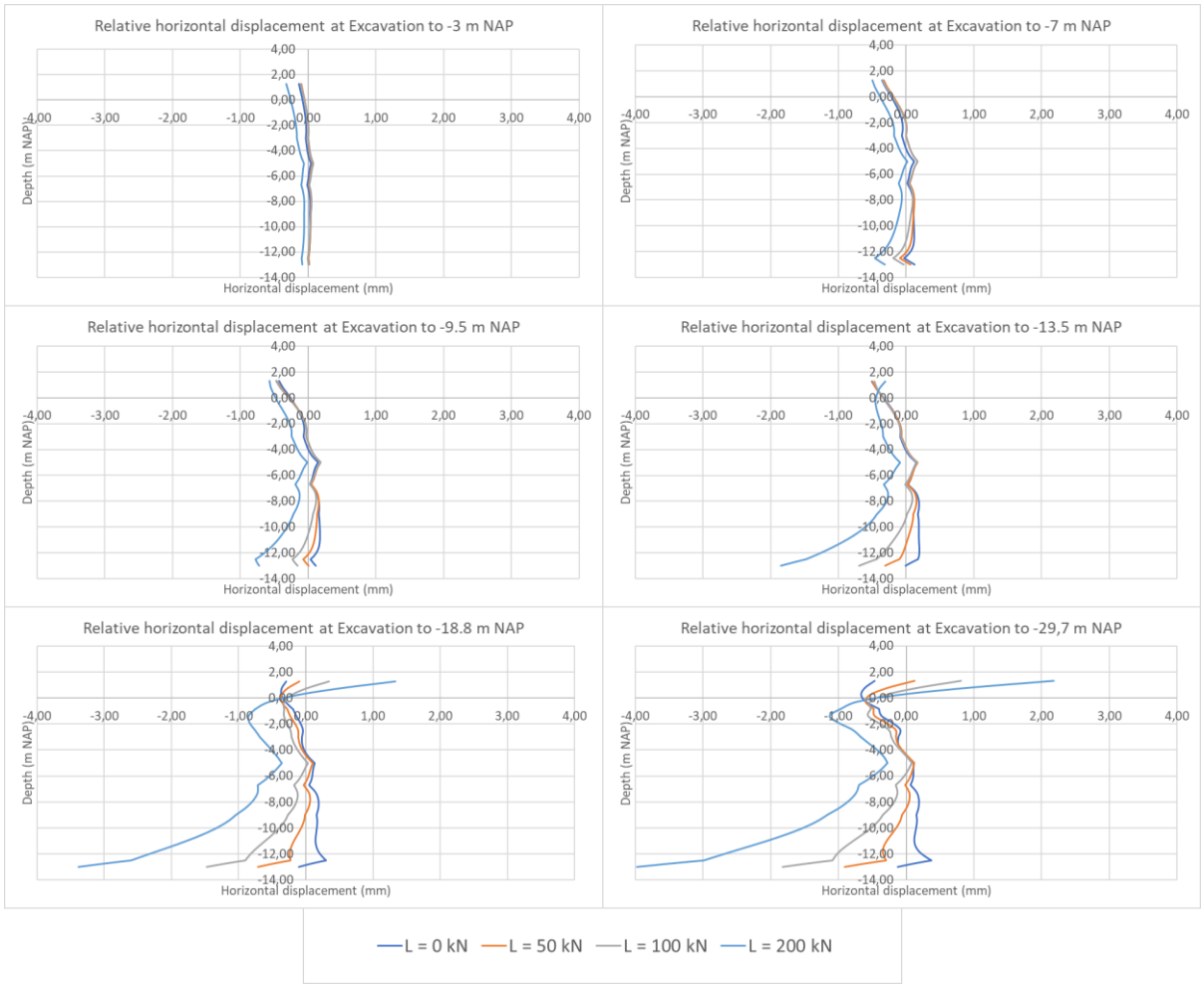

Figure 4-41 Relative horizontal displacements of the foundation piles with different loads

Figure 4-40 shows the horizontal displacements of the piles the four chosen load cases together with the free-field displacements of the nodes in the same location as the piles. Figure 4-41 shows the horizontal displacements of for the piles the four chosen load cases relative to the free-field soil deformations. The horizontal axis represents horizontal displacements and the vertical axis represents the vertical location of the pile increment.

The results show a clear influence of the additional load on the overall pile displacements when compared with the free-field soil displacements. During the first few excavation phases this is especially visible at the upper sections of the pile. The horizontal pile head displacement becomes less with increasing initial load. The deeper section of the piles tend to follow the green field displacements initially. However, deviation start to become more visible with increasing excavation depth. During the excavation to -9.5 m NAP the pile tip starts to displace differently from the free-field displacements. At this stage the difference becomes roughly 1 mm for the pile with the highest load. The deviations continues to increase with increasing excavation depth. At the final excavation step (-29.7 m NAP) the pile tip displaces roughly 4 mm more than the projected free-field soil displacements, while the pile head still deforms 2 mm with respect to the projected free-field displacements. The displacement of the pile tip equates to roughly an increase of 15%.

The results also show the difference in reaction between the different pile loads. During the first few excavation phases there is a difference in horizontal displacement visible of the pile head. The difference doesn't exceed 1mm. The larger load on the pile seems to have a reducing effect on the

horizontal displacement of the pile head. In the later excavation phases the pile tip shows a larger displacement for an increased load. The difference between pile tip displacements reaches roughly 4 mm. This larger displacement of the pile tip could be due to the loosening of the soil around the pile tip. The pile tip is subsequently less fixated at the tip, allowing the pile tip to deform horizontally to a larger extent, due to the reduced horizontal constraint. This larger horizontal displacement at the pile tip is also a result of the external force now enables a second order effect due the load now being eccentric and therefor enabling a slight rotary movement of the pile. Due to these piles being largely end-bearing the increased load leads to less stability. The piles searches to restabilize by relaxation/straightening at the pile tip, until a new equilibrium (vertical and horizontal) is reached. This is shown by the reduced curvature of the lower section of the pile loaded by 200 kN and 100 kN in Figure 4-41.

4.3.3.3 Vertical Skin Friction

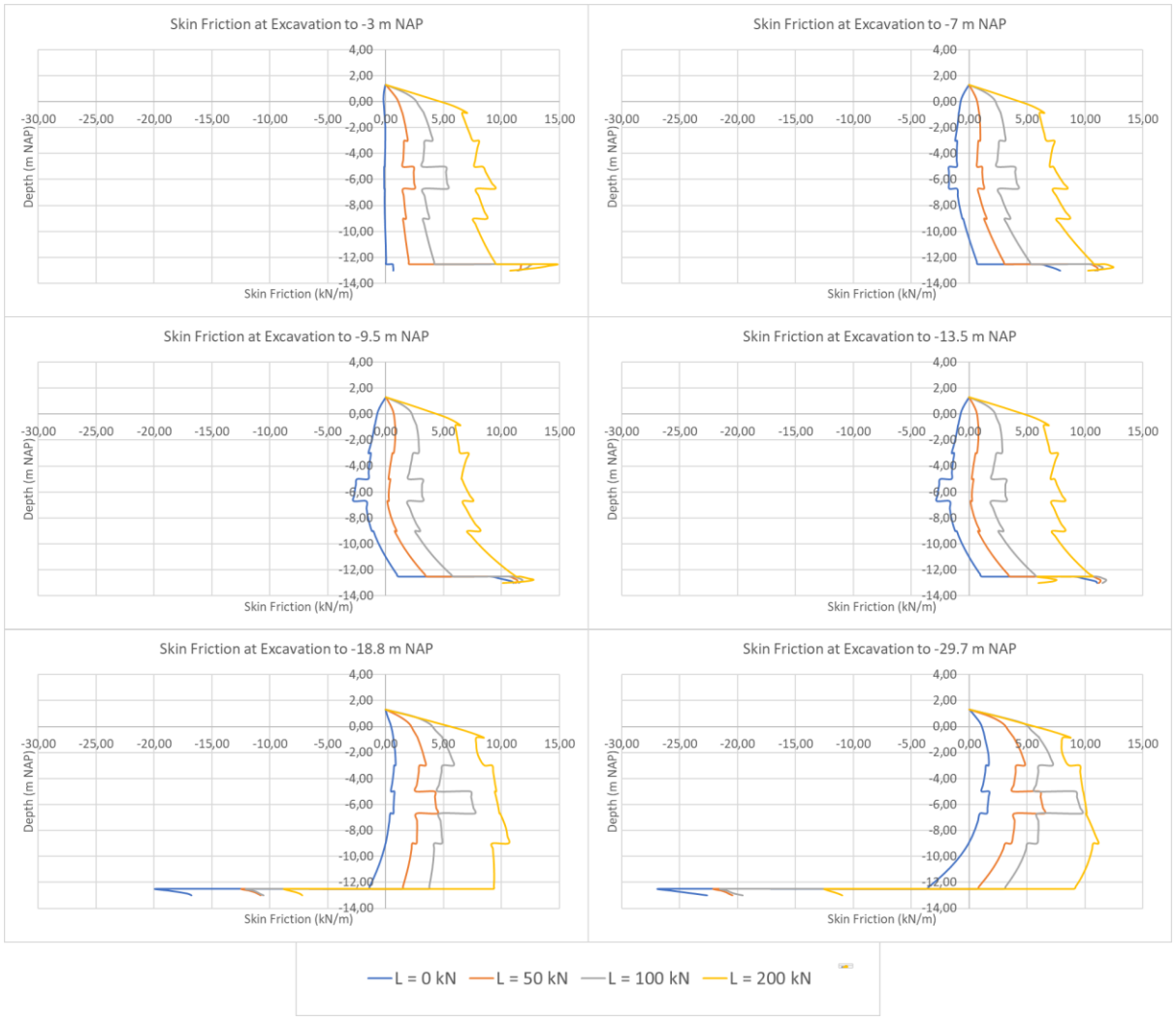

Figure 4-42 Vertical skin friction on the foundation piles with different loads

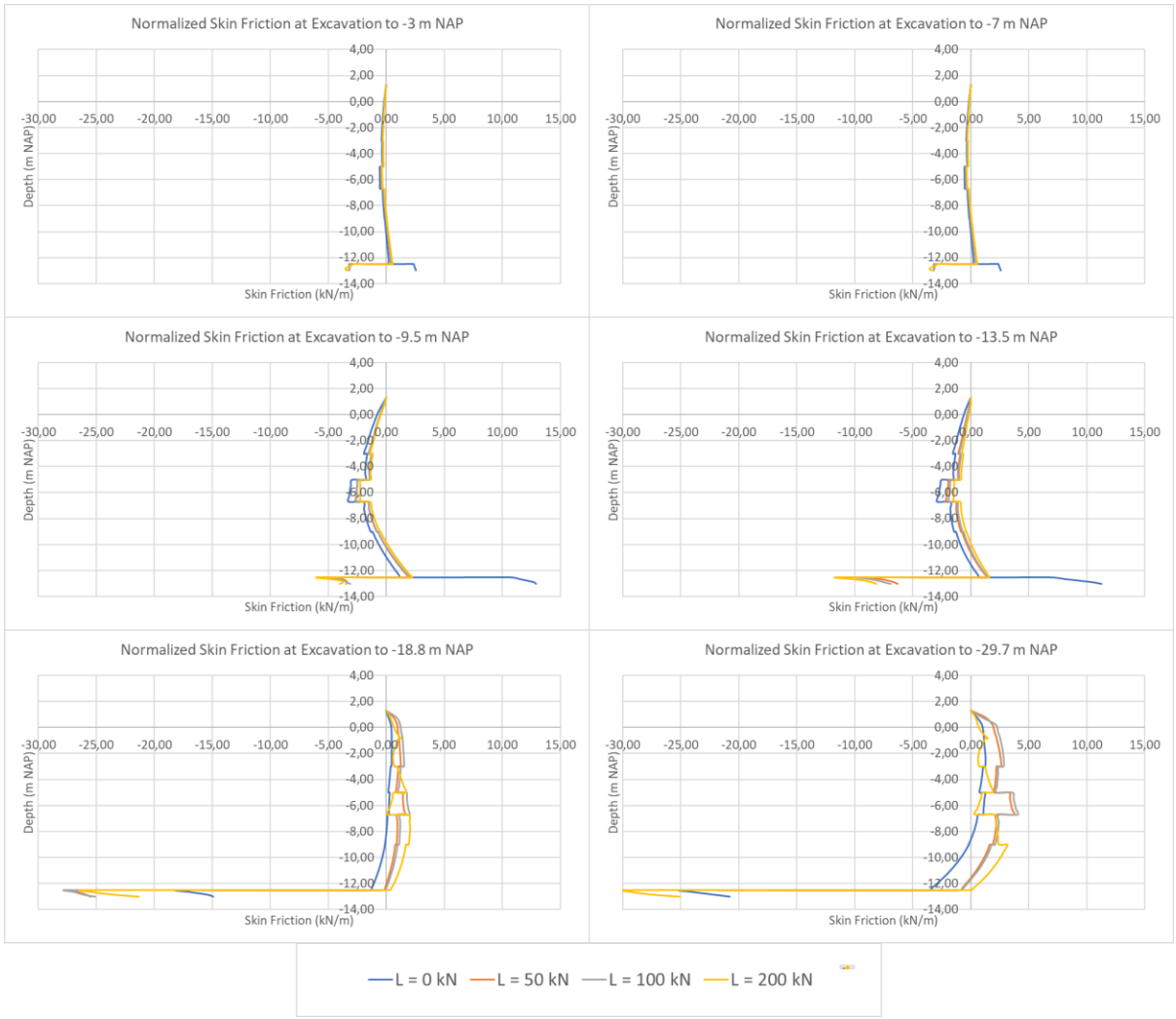

Figure 4-43 Normalized vertical skin friction on the foundation piles with varying load

Figure 4-42 shows the vertical skin friction acting on the piles for the four described load cases. The horizontal axis represents the skin friction per meter and the vertical axis represents the vertical location of the pile increment. A negative value indicates downward friction (negative skin friction) and a positive value indicates upward friction (positive skin friction).

The higher the force exerted on the pile the larger the mobilised skin friction becomes as the resistance of a pile is composed of the combination of skin friction and the base resistance. A larger load will mobilise more skin friction as the due to the pile deforming more. it's interesting to see with increasing load the mobilised negative skin friction reduces. This is due to the needed positive skin friction for the pile to bear the additional load.

In order to assess the exact effect of the presence of the load on the skin friction of the piles, a normalization is performed. The initial skin friction on the pile is subtracted and only the effect of the additional excavation is left. Figure 4-42 shows the normalized vertical skin friction acting on the piles for the four described load cases. With increase in load, less negative skin friction is developed. This is to be expected when looking at the vertical displacements of the piles. Increase in load leads to increase in downward displacement of the pile. This downward movement of the pile does counteract the mobilisation of negative skin friction.

4.3.4 Pile Distance to Excavation

Three different location of piles are analysed. To do so, a building is selected to analyse different piles at different distances from the excavation without the piles being coupled. A typical old Amsterdam building facing the excavation is selected for the analysis. This is a 3-story masonry building.

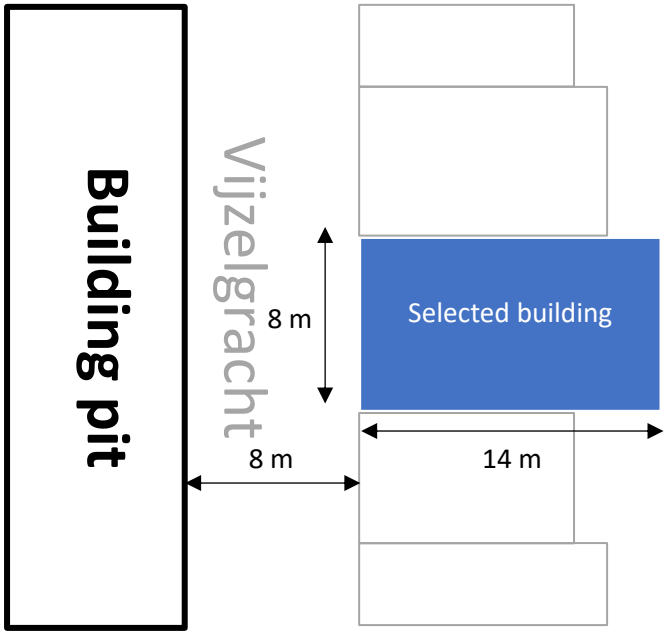

Figure 4-44 Top view of chosen building

With this geometry in mind the piles are placed at left middle and right. The piles are placed at 8m, 14m and 20 m from the excavation. Again, the piles are typically founded in the first sand layer (-13 m NAP). The piles are modelled as massive circular beams with a set diameter. The piles are supporting the walls in sets of two. The couples are spaced out of plane approximately 8 m. Therefore, the spacing is divided between the coupled piles (4 m). The piles are assigned a diameter of 180 mm, a Young's modulus of $E = 6000\ \frac{N}{mm^2}$ and a specific density of $\gamma = 4.6\ \frac{kN}{m^3}$. The pile is not loaded, which means that no external force is exerted on the pile. The axial skin resistance is set to be dependent on the soil layer. The lateral resistance is assumed to be unlimited, as failure through bending is very unlikely. The base resistance is assumed to be 100 kN.

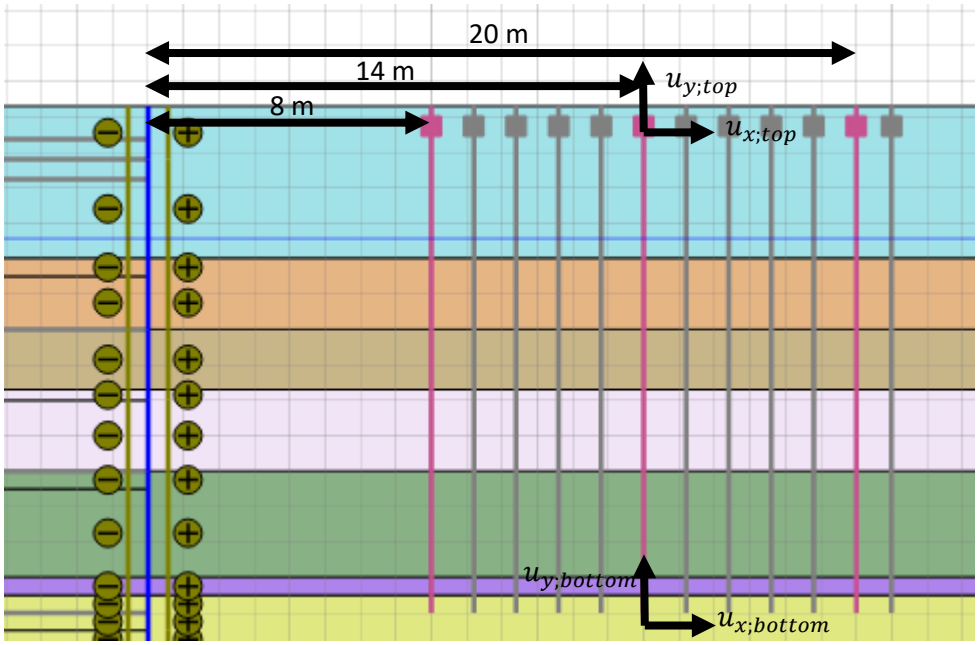

Figure 4-45 Schematization of the model with the axes for displacement displayed

The results are presented in the tables and figures below.

Table 4-10 Results of foundation pile at 8 m distance from the excavation

Excavation step	$U_{x;top}$ (mm)	$U_{y;top}$ (mm)	$U_{x;bottom}$ (mm)	$U_{y;bottom}$ (mm)	Δu_y (mm)
-3	-12,86	-1,02	-3,62	-0,89	-0,13
-7	-22,05	-0,88	-9,66	-0,33	-0,55
-9,5	-22,23	-0,85	-12,96	-0,27	-0,58
-13,5	-22,58	-2,26	-16,95	-1,88	-0,38
-18,8	-23,85	-13,85	-21,17	-14,33	0,48
-29,7	-25,97	-22,77	-24,59	-23,48	0,72

Table 4-11 Results of foundation pile at 14 m distance from the excavation

Excavation step	$U_{x;top}$ (mm)	$U_{y;top}$ (mm)	$U_{x;bottom}$ (mm)	$U_{y;bottom}$ (mm)	Δu_y (mm)
-3	-8,65	-0,33	-3,06	-0,24	-0,09
-7	-15,41	0,72	-6,78	1,17	-0,45
-9,5	-16,50	1,00	-8,65	1,58	-0,57
-13,5	-17,79	0,32	-10,86	0,99	-0,67
-18,8	-22,96	-7,21	-15,99	-6,47	-0,74
-29,7	-27,57	-13,83	-19,60	-13,08	-0,75

Table 4-12 Results of foundation pile at 20 m distance from the excavation

Excavation step	$U_{x;top}$ (mm)	$U_{y;top}$ (mm)	$U_{x;bottom}$ (mm)	$U_{y;bottom}$ (mm)	Δu_y (mm)
-3	-6,07	0,03	-2,50	0,08	-0,05
-7	-10,93	1,46	-5,01	1,65	-0,19
-9,5	-12,13	1,90	-6,26	2,16	-0,26
-13,5	-13,64	1,76	-7,54	2,12	-0,36
-18,8	-19,32	-1,58	-9,99	-0,82	-0,75
-29,7	-24,22	-4,75	-11,87	-3,72	-1,03

4.3.4.1 Vertical displacement

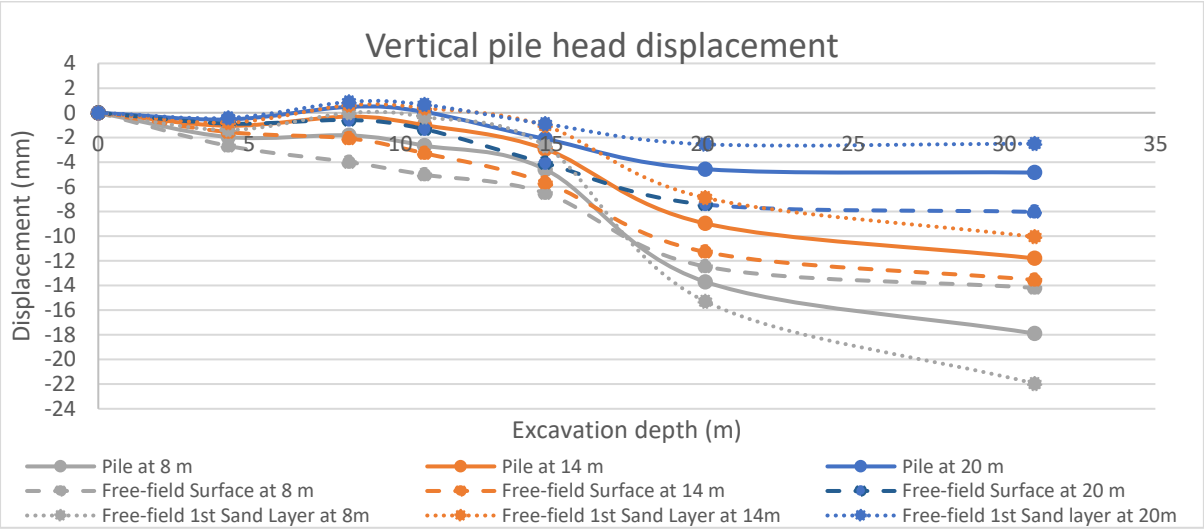

Figure 4-46 Vertical displacement of the head of the piles

The displacements of the piles have been plotted together with the greenfield displacements. Figure 4-46 shows the vertical displacements of the pile heads for three different distances from the excavation together with the free-field displacements of the nodes on the same location as the pile heads. The horizontal axis represents the excavation depth and the vertical axis represents the vertical displacements of the pile heads.

The distance of a pile to the excavation is of great importance on the pile behaviour and displacements as is visible in Figure 4-46. Again, a clear difference between the different piles and the free-field displacements is observed. During the first three excavation phases (to NAP -9.5 m) the difference between the pile displacements and the free-field displacements become larger with closer proximity to the excavation. However, this becomes less afterwards, due to the excavation being braced.

Between the deformations also differences are observed. As the excavation becomes deeper the influenced area adjacent to the excavation also becomes larger, as discussed in 3.3.2. With the approximate triangular influence area in mind (Figure 3-17) the soil deformation varies with distance and with depth, resulting in different effects on the foundation piles present. These effects depend on the excavation depth and the proximity of the pile to the excavation. This means that during an excavation phase the piles of a building are loaded differently, depending on their proximity to the excavation. A clear example for this are the last two excavation steps, at which de surface at 8 m and at 14 m distance the soil deformed almost similar, but the pile heads deformed vastly different. The

pile at a distance of 8 m settled approximately 4 mm more than the free-field deformations, the pile head at 14 m distance settled approximately 2 mm less than the free-field soil deformations. This is the result of different subsurface conditions and deformations. The piles are founded on the first sand layer. This layer settled more than 20mm at a distance of 8m and 10 mm at a distance of 14 m.

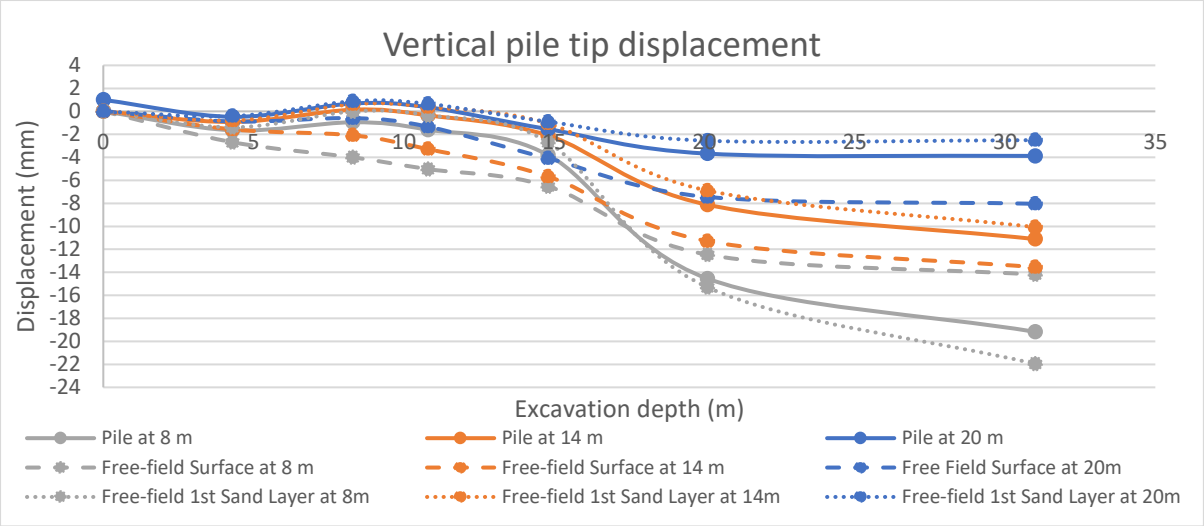

Figure 4-47 Vertical displacement of the tip of the pile

Figure 4-47 shows the vertical displacements of the pile tips for three different distances from the excavation together with the free-field displacements of the exact point in the model. The horizontal axis represents the excavation depth and the vertical axis represents the vertical displacements of the pile toes.

The soil deforms less far from the excavation, leading to different pile responses to these deformations. The pile closer to the excavation (8 m) reacts stiffer than the free-field deformations. At the final excavation stage, the difference between the pile tip and the free-field deformations reaches 3 mm. This means that the pile tip has settled roughly 15% less than the expected green field settlements. The pile tips further from the excavation settle more than the expected green field settlements. This is due to the soil at the pile tip settling less than the soil at the pile head. Therefor the upper soil layers exert negative skin friction on the pile and as a result pushing the pile downwards.

4.3.4.2 *Horizontal displacement*

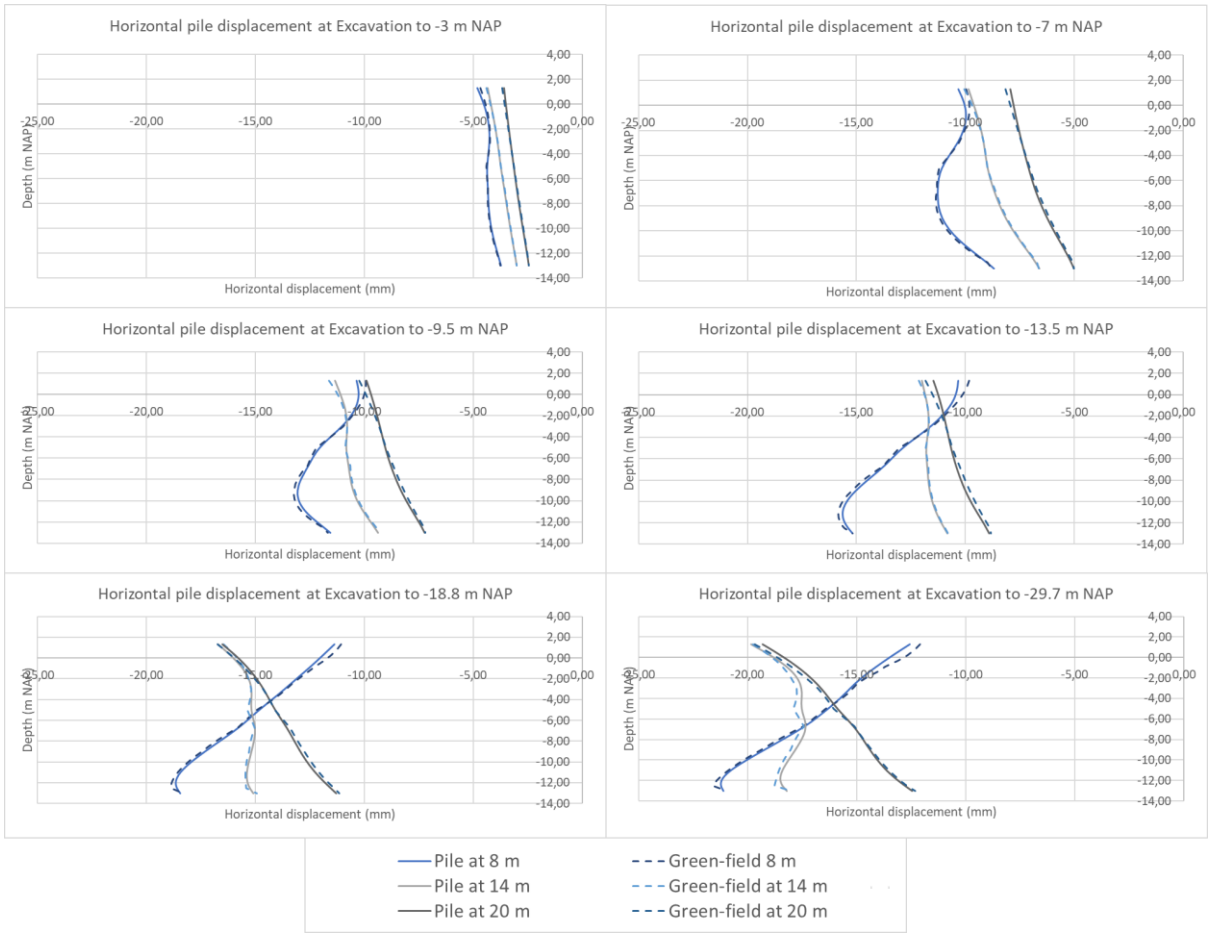

Figure 4-48 Horizontal displacements of the foundation piles with different distances to the excavation relative to their position at the start of the excavatory works

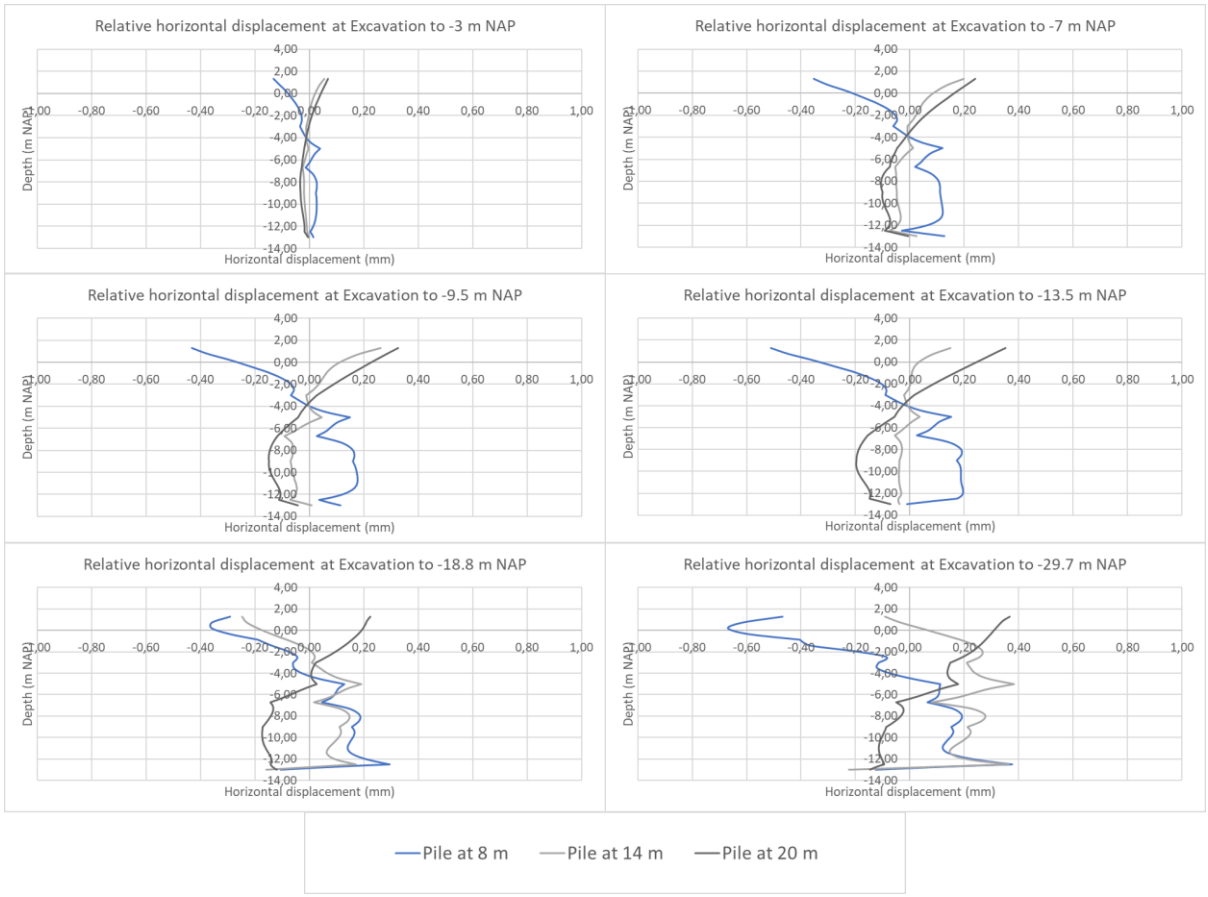

Figure 4-49 Relative horizontal displacements of the foundation piles with different distance to the excavation

Figure 4-48 shows the horizontal displacements of the piles for the three chosen locations together with the free-field displacements of the nodes at the same location as the piles. Figure 4-49 shows the horizontal displacements of for the piles the three chosen stiffnesses relative to the free-field soil deformations. The horizontal axis represents horizontal displacements and the vertical axis represents the vertical location of the pile increment.

The results show no clear influence of the distance of the pile on its overall displacements. The piles all showed a tendency to follow the free-field soil displacements during all excavation phases. In the later excavation stages small deviations are visible between the piles and the projected soil displacements and the pile displacements. the deviations tend to increase with increased overall pile displacements, implying the deviations to be proportional to the overall displacements. The deviations do not exceed 1 mm, showing that the distance of the pile does not influence the tendency of the pile to follow the soil deformations.

4.3.4.3 *Vertical Skin Friction*

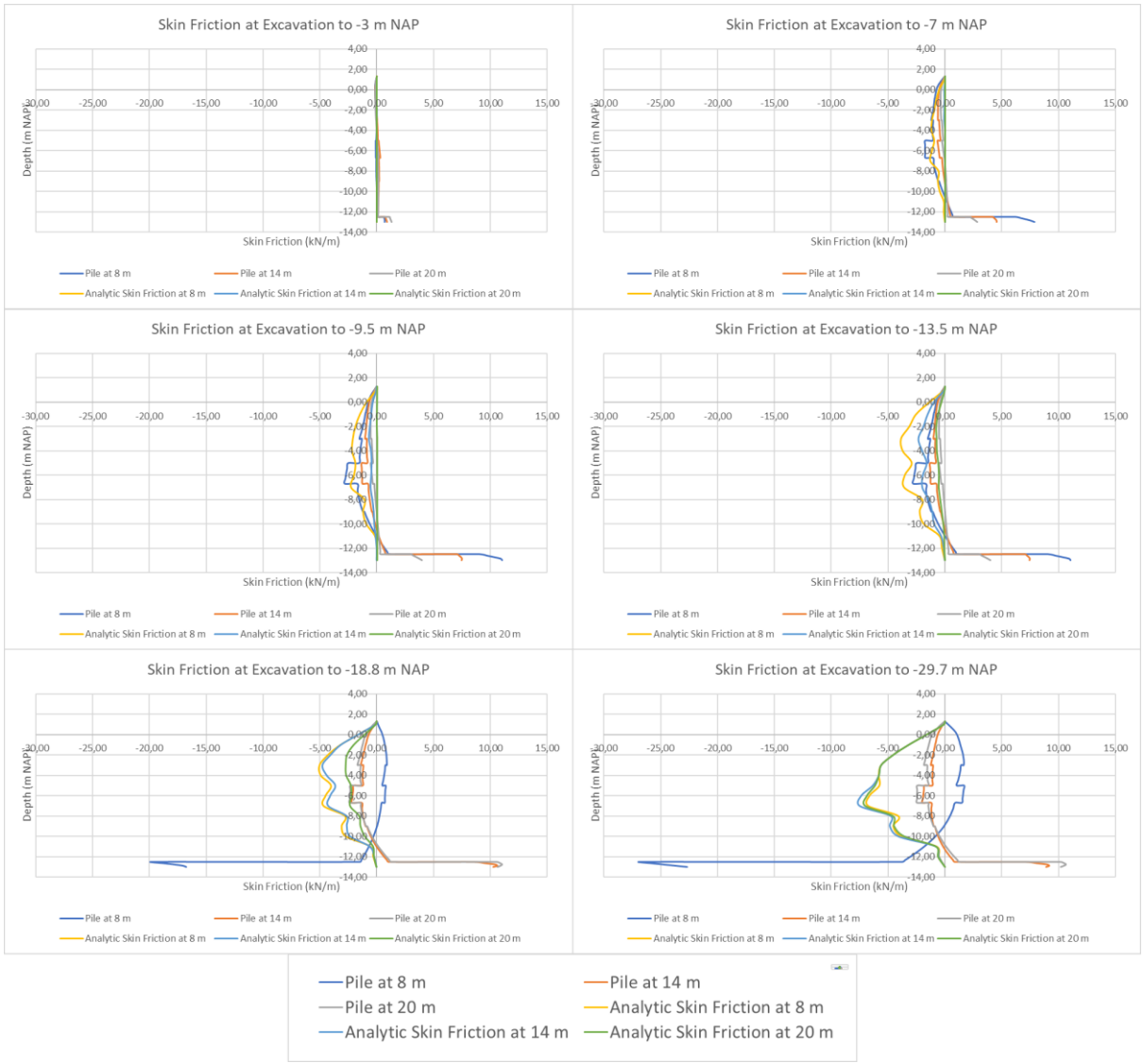

Figure 4-50 Vertical skin friction on the foundation piles with different loads on the pile

Figure 4-50 shows the vertical skin friction acting on the piles for the three chosen distances to the excavation together with the expected skin friction following analytic calculations for piles on the same location. The horizontal axis represents the skin friction per meter and the vertical axis represents the vertical location of the pile increment. A negative value indicates downward friction (negative skin friction) and a positive value indicates upward friction (positive skin friction).

The results show some interesting trends. The analytic results show a slight systematic overestimation of the skin friction. This could be assigned to the assumption that the pile tip is fixated to the surrounding soil layer and moves with the soil around the pile tip.

4.4 CONCLUSIONS

In this chapter the measured settlements are visualized in section 4.2. The measured settlements are compared to the computed settlements using analytic and numerical calculations. The surface settlements of all the different used method show sufficient resemblance to the measured points. This section evaluates whether the used models are representative for the measured data and therefore the real-life situation.

In Section 4.3 the Pile Behaviour Analysis is caried out. Firstly, the influence of the pile diameter and the stiffness are analysed. The pile tip and pile head both show significantly deviant responses to the free-field soil deformations. However, varying the diameter or the stiffness did not lead to significantly different settlements. This difference remained in the range of 1 mm, whereas the settlements relative to the free-field soil settlements reached up to 4 mm. This is a deviation of roughly 20 %.

The initial load on a pile shows to have a big influence on the pile displacements. An increase in load leads to an increase in settlement of the pile. The results further showed that the distance of the pile to the excavation has a large influence on its displacements. The difference between the pile displacements and the free-field displacements become larger with proximity to the excavation as the soil closer to the retaining wall is most disturbed. The deeper soil layer also influence the pile displacements and diminishes with distance to the excavation.

In terms of horizontal displacements, the soil displacements are dominant. Wooden piles are generally flexible which is clearly visible in the results. The piles tended to follow the soil deformation almost completely. The piles do not deviate from the projected free-field soil displacements. The displacements are fairly negligible and are generally smaller than 1mm. A smaller diameter and or stiffness leads to more responsive behaviour of the pile as the flexibility increases with decrease in stiffness and/or diameter. Increasing the load on the piles even showed an increase in horizontal displacements. These displacements reached up to 2 mm at the top and 4 at the bottom of the pile relative to the projected free-field displacements. The results further showed no clear influence of the distance of the pile on its overall displacements as the piles all showed a tendency to follow the free-field soil displacements during all excavation phases.

The shape of the graph of the skin friction was for all cases fairly similar. The difference was visible in the magnitude of the friction as a pile with a larger stiffness attracted more skin friction. This is the result of the larger stiffness leading to less strain and less strain leads to larger relative displacements between the soil and pile shaft. This bigger difference leads to increased skin friction. A bigger pile diameter also leads to an increase in skin friction. A larger diameter results in a larger circumference, which attracts more skin friction. Both the graphs for the diameter and the stiffness seemed to resemble the analytical results for the first few excavation phases. As the deeper soil layers start to settle to a larger rate the shape of the graphs start to differ from the analytical results as this phenomenon is not accounted for in the analytic results. Increasing the load however led to an increase in positive skin friction to carry the additional load. The development of negative skin friction became less with increasing load with increase in excavation depth.

5 THE EFFECT OF STRUCTURAL PRESENCE ON THE SOIL NEXT TO DEEP EXCAVATIONS.

In the past, extensive research is done on the influence of excavations on the structural elements of the excavation itself and adjacent structures. Studies on the effect on the soil adjacent to the excavation are marginal in amount. This would help to understand the differences between coupled and uncoupled in damage prediction and would therefore be beneficiary too this thesis.

This chapter will focus on the effect of the presence of a building on the subsurface during different excavation phases. The soil adjacent to the excavation analysed. The emphasis will be on the difference in vertical and horizontal deformation and the difference in stresses.

The analysis is done by comparing the behaviour of the soil next to a deep excavation including and excluding adjacent structural elements. This will contribute to understand the extent of the presence of a structure influences free-field soil behaviour next to a deep excavation. This is done by comparing three situations which all will be modelled using numerical models in PLAXIS. The three models will be a free-field undisturbed model, a model with loaded piles adjacent to the excavation and a model with a full building next to the excavation. Further information on these models is present in Section 5.2.

5.1 NUMERICAL MODELS

The different models are described in this chapter. Every model has got its own respective section assigned.

5.1.1 Free-field model

A reference model is used by modelling a deep excavation without structures adjacent to the excavation. This will be used as a reference model that describes the undisturbed soil behaviour next to a deep excavation.

5.1.2 Loaded piles model

To verify the effect loaded piles have on the soil a model is used by adding uncoupled piles next to the excavation and putting a vertical load on top of these piles. These piles mimic a pile foundation of a typical old Amsterdam building and the load is proportional to a value expected to be present on the pile supporting a building. The piles are uncoupled in order to assess the effect of the stiffness of the piles and their presence on the overall soil behaviour. A similar case as in 4.3.3 is used.

A typical old Amsterdam building facing the excavation is selected for the analysis. This is a 3-story masonry building.

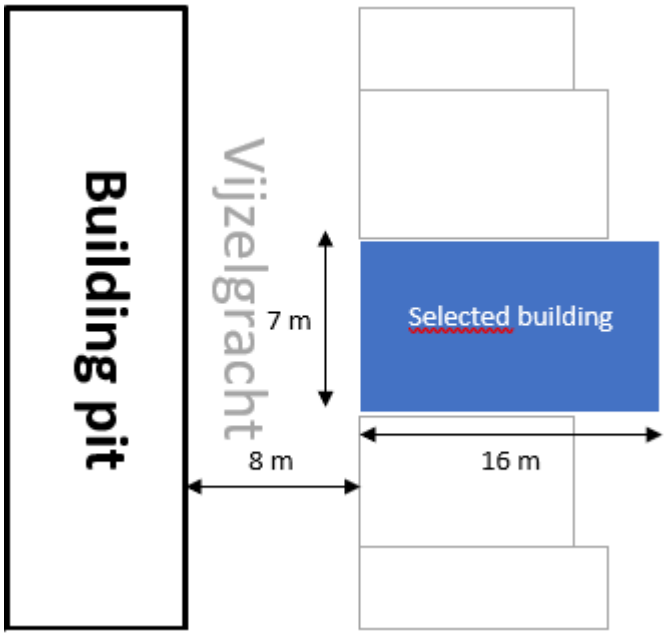

Figure 5-1 Top view of chosen building

The piles are typically founded in the first sand layer (-13 m NAP). The piles are assigned a diameter of 180 mm, a Young's modulus of $E = 6000\ \frac{N}{mm^2}$ and a specific density of $\gamma = 4.6\ \frac{kN}{m^3}$. The piles are also typically spaced 1.5 m apart.

The loads on the piles are composed as follows (with the assumption that only halve the variable load is present):

- Roof:
  - $Q_{p,Roof} = 0.5 \frac{kN}{m^2}$
  - $Q_{v,Roof} = 0.0 \frac{kN}{m^2}$
- Attic:
  - $Q_{p,Attic} = 0.5 \frac{kN}{m^2}$
  - $Q_{v,Attic} = 1.0 \frac{kN}{m^2}$
- Floors:
  - $Q_{p,Floor} = 0.75 \frac{kN}{m^2}$
  - $Q_{v,Floor} = 1.5 \frac{kN}{m^2}$
- Ground floor:
  - $Q_{p,Ground} = 0.75 \frac{kN}{m^2}$
  - $Q_{v,Ground} = 2.0 \frac{kN}{m^2}$
- Wall:
  - $0.22\ m * 5\ m * 20 \frac{kN}{m^3} = 22.0 \frac{kN}{m}$
  - $0.33\ m * 3\ m * 20 \frac{kN}{m^3} = 19.8 \frac{kN}{m}$
- $Q_{p,wall} = 41.8 \frac{kN}{m}$

This results in the following composition of permanent and variable loads:

$$Q_{p,total} = (0.5 + 0.5 + 0.75 + 0.75 + 0.75) * 7 + 41.8 = 22.75 + 41.8 = 64.55 \frac{kN}{m}$$

$$Q_{v,total} = (0.0 + 1.0 + 1.5 + 1.5 + 2.0) * .5 * 7 = 21 \frac{kN}{m}$$

This result in the following load on a pile:

$$F_{pile} = \frac{\left(Q_{p,total} + Q_{v,total}\right)}{2} * 1.2 = 51.3 \frac{kN}{pile}$$

5.1.3 Building model

A typical Amsterdam building is modelled on top of the piles in order assess the full effect of the presence of a building on the overall soil behaviour. The coupled effect of the piles is now also included in the model to assess the impact this has. This will add an additional horizontal constraint to the foundation piles, affecting the piles themselves, the structure and the soil in which the foundation is embedded. For this analysis a continuum model will be used for the masonry. The material parameters are derived from numerical tests in the work by Giardina (Giardina, 2013) for the analysis of masonry structures. The obtained material properties are shown in Table 5-1.

Table 5-1 Material parameters for the continuum masonry model

Parameter	Sign	Value	Unity
Young's Modulus	E_M	3000	MPa
Density	ρ_M	19	kN/m^3
Poisson's Ratio	v_M	0.2	(-)

As these elements normally are modelled individually, combining these different elements are expected to have influence on the soil behaviour, when compared to free-field soil behaviour. Drawing a comparison between the different model will help to get a better understanding of the proportional effect of each of the considered elements. This should show the implications uncoupled 2D modelling has.

5.2 RESULTS

The numerical results of the deformations and stresses for the different models are presented in Appendix C

Numerical results Soil effect. The difference between the models in deformation and stress are presented in order to assess the effect structural presence has on those outputs. The Loaded pile model and the Building model are compared to the free-field model to assess the extent of these elements affecting deformations and stresses.

5.2.1 Uncoupled pile effect

Figure 5-2 shows the vertical soil deformation of the Loaded pile model relative to the Free-field model. Figure 5-4 shows the horizontal soil deformation of the Loaded pile model relative to the Free-field model. The difference is represented by a colour and the magnitude can be derived from the colour bar. The values are derived from calculations performed using PLAXIS FEA. To get a better understanding of the overall development of these influences the results are shown in six intervals. These intervals represent the excavation steps according to chapter 3.5.4. Additionally, these differences in vertical and horizontal displacements are represented relative to the overall free-field situation in Figure 5-3 and Figure 5-5 respectively. This representation helps to show the proportionality of these differences and is the result of dividing the difference between the loaded pile model and the free-field model by the free-field results:

$$relative\ difference\ in\ displacement = \frac{u_{loaded\ pile} - u_{free-field}}{u_{free-field}}$$

5.2.1.1 Vertical displacements

Vertical soil deformation of the Loaded pile model with respect to the Free-field model.

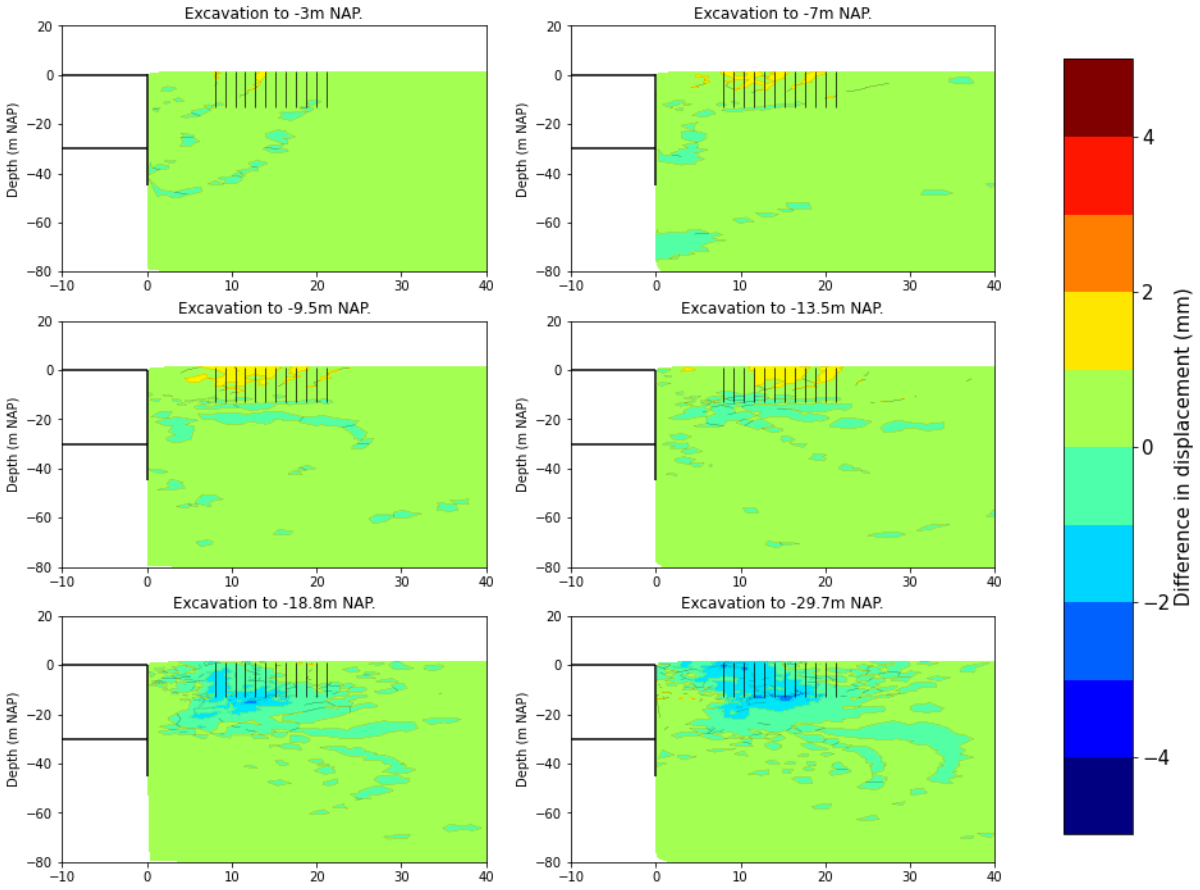

Figure 5-2 Vertical soil deformation of the Loaded pile model relative to the free-field model

Relative vertical soil deformation of the Loaded pile model with respect to the Free-field model.

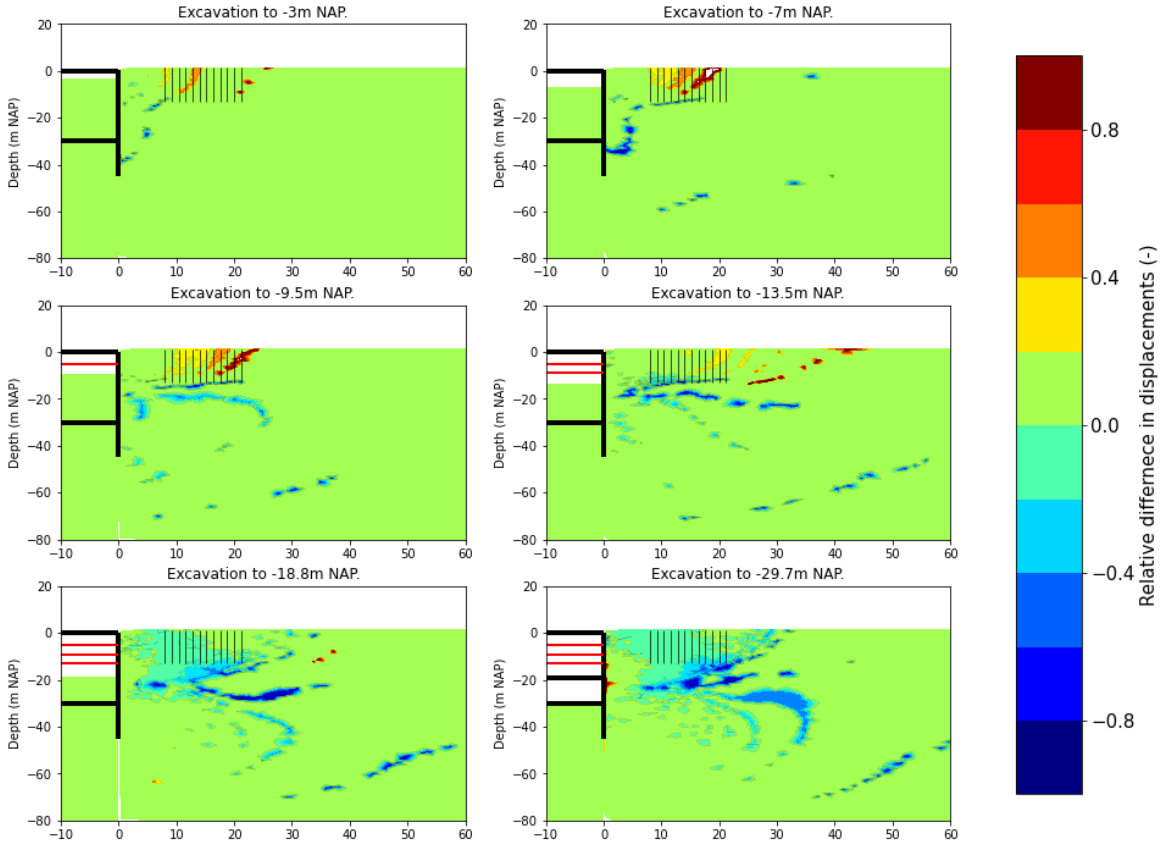

Figure 5-3 Relative vertical soil deformation of the Loaded pile model relative to the free-field model

The results show differences between the Loaded pile model and the Free-field model. In the first few excavation steps the soil around the pile heads deforms less with loaded piles than in the Free-field model. The difference reaches up to 3 mm. This can be ascribed to the upper soil layers settling more than the deeper layers. Since the pile is founded in the 1st sand layer, this layer has a large influence on the deformation of the pile, causing the pile to follow the deformation of the foundation layer. Accordingly, the soil directly surrounding the pile is largely influenced by the pile. This chain effect leads to stiffening of the soil and therefore less settlement at the surface. On the other hand, when the deeper layers deform more than the surface in a free-field situation, the piles will drag the soil along, leading to more settlement at the surface as a result of the settlement of the deeper soil layers. This phenomenon is observed in the last two excavation steps around the piles closest to the excavation. These piles experience negative skin friction discussed in 4.3.1.1 dragging the upper adjacent soil section along, resulting in a larger surface settlement than derived from free-field calculations. The difference reaches up to 4mm. Also, due to the loosening of the soil around the pile tips and the presence of a load on the piles, the piles tend to settle more than in a free-field situation as no sufficient resistance to the load is found otherwise.

5.2.1.2 Horizontal displacements

Horizontal soil deformation of the Loaded pile model with respect to the Free-field model.

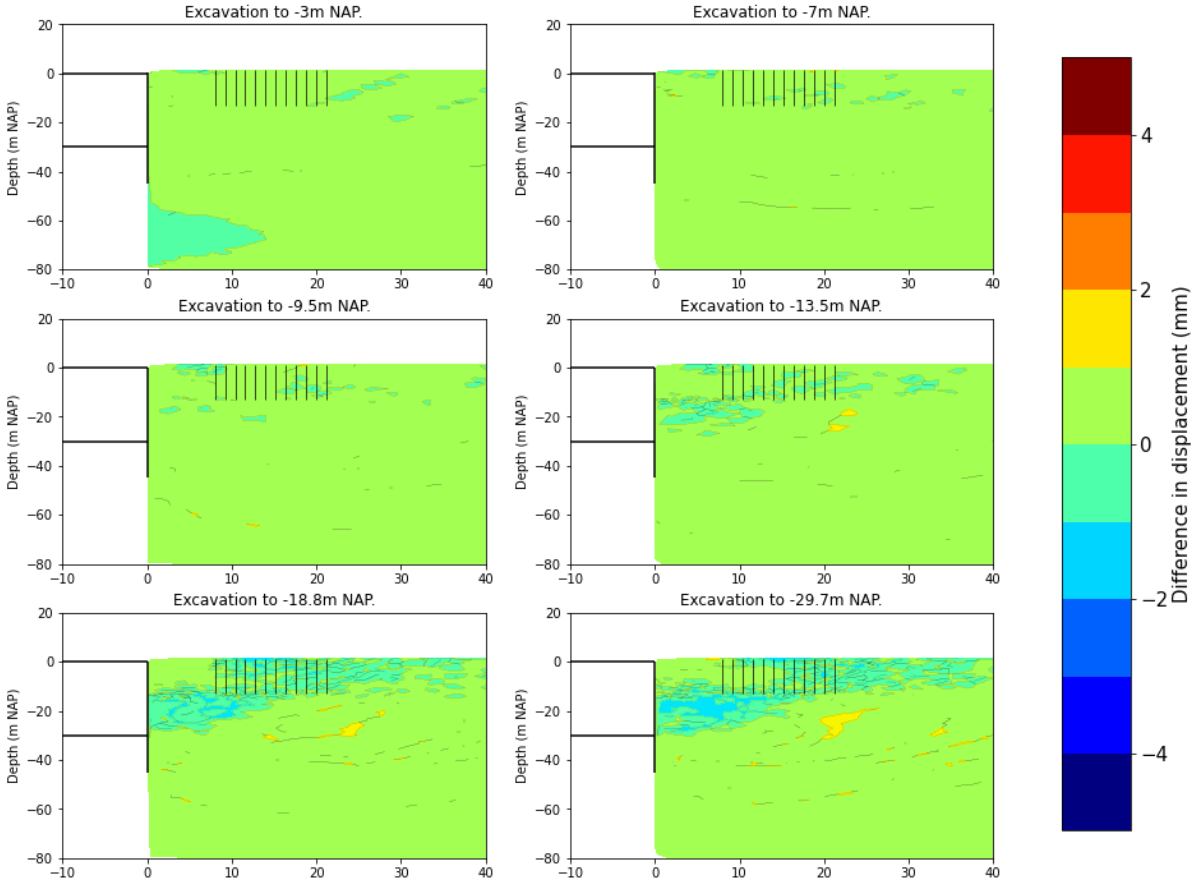

Figure 5-4 Horizontal soil deformation of the Loaded pile model relative to the free-field model

Relative horizontal soil deformation of the Loaded pile model with respect to the Free-field model.

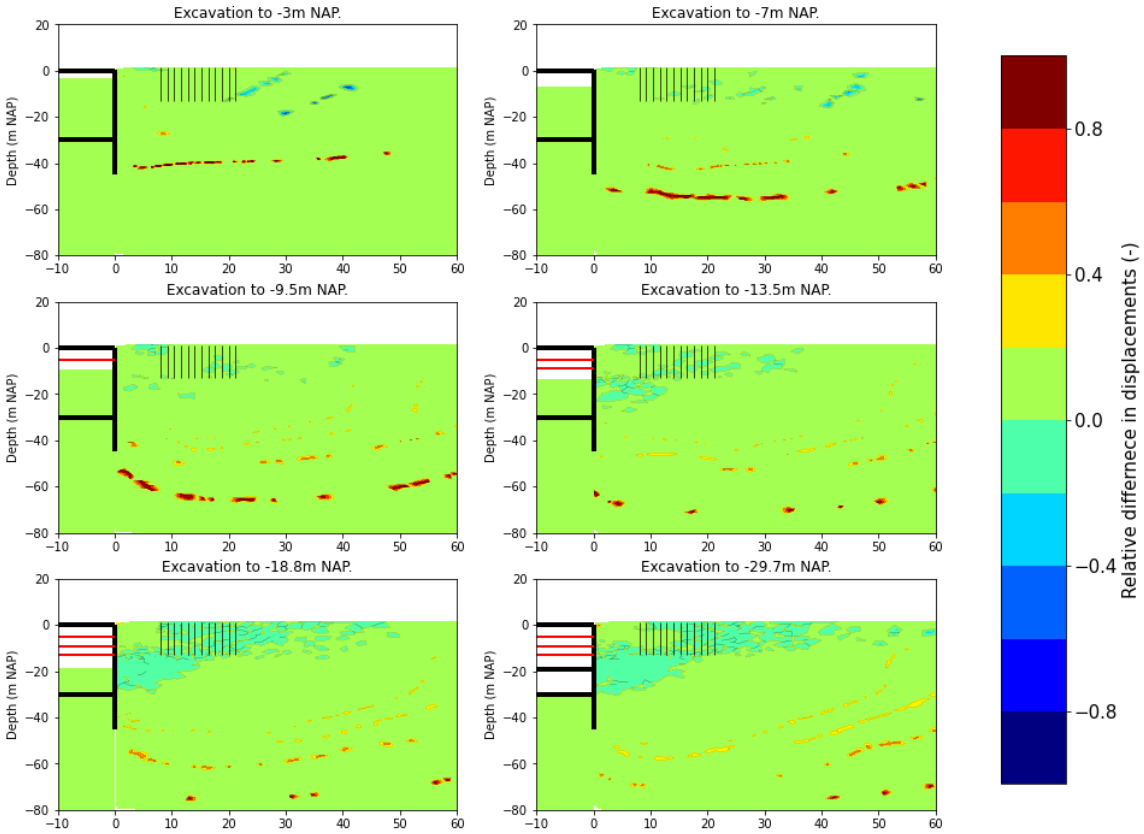

Figure 5-5 Relative horizontal soil deformation of the Loaded pile model relative to the free-field model

The horizontal difference is smaller compared to the vertical differences. This was to be expected, since the piles don't impose any signific ant horizontal constraint. These piles are relatively flexible, which impedes horizontal deformation over its length (vertically). The differences reach up to 2 mm. Interestingly, the deeper soil layers adjacent to the retaining wall deformed more in the uncoupled pile model than in the free-field model. This could be assigned to the increase in stress in the deeper soil layers coming from the load on the piles. The increase in stress vertically leads to an increase in stress horizontally, which is felt by the retaining wall leading to an increased deflection. This deflection then again leads to an extra horizontal deformation of the soil.

5.2.1.3 Effective stress

Figure 5-6 shows the difference in effective stress between the Loaded pile model and the Free-field model for six excavation steps. This difference is represented by a colour and the magnitude can be derived from the colour bar. A net downward pointing stress has a negative value and an upward pointing stress has a positive value. Figure 5-7this difference relative to the stress in the free field situation, according to the following scheme:

$$relative\ difference\ in\ stress = \frac{\varepsilon_{loaded\ pile} - \varepsilon_{free-field}}{\varepsilon_{free-field}}$$

Effective stress of the Loaded pile model with respect to the Free-field model.

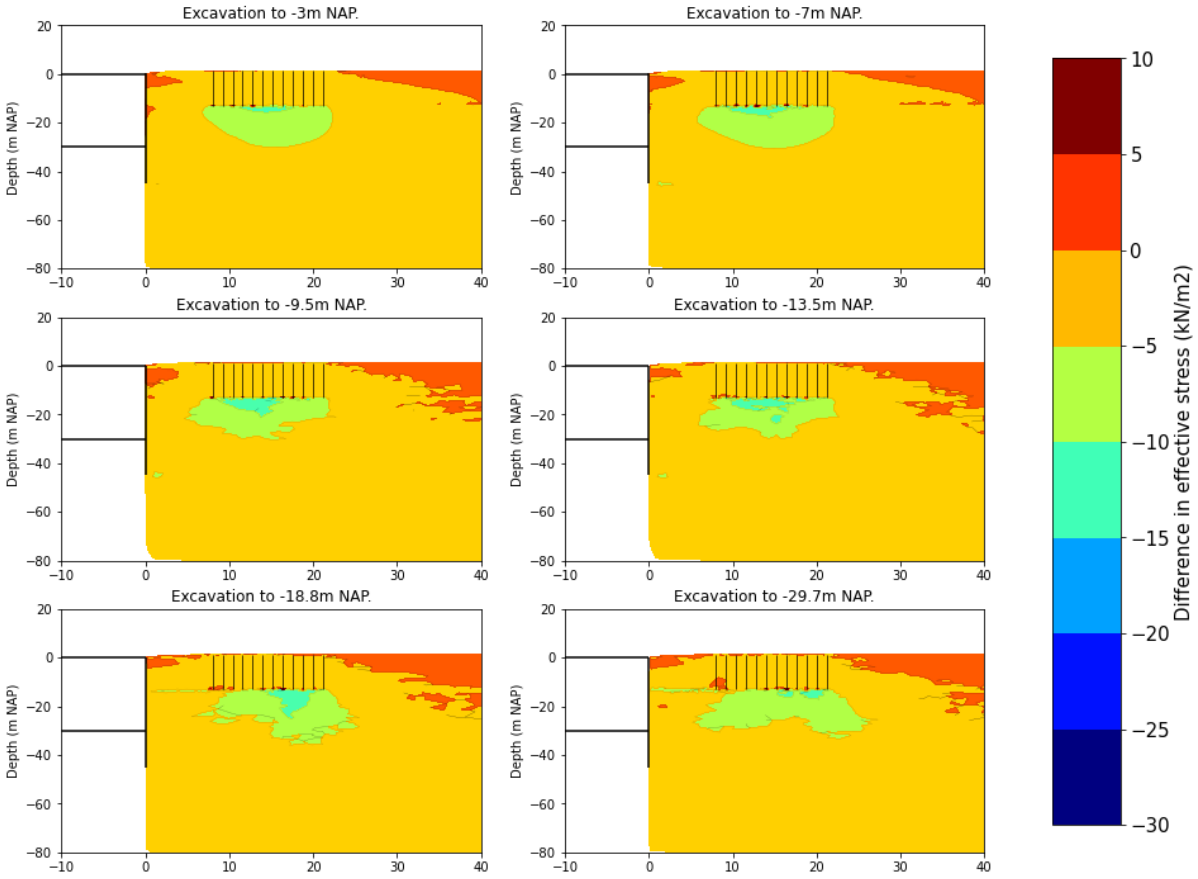

Figure 5-6 Effective stress in the soil of the Loaded pile model relative to the free-field model

Relative effective stress of the Loaded pile model with respect to the Free-field model.

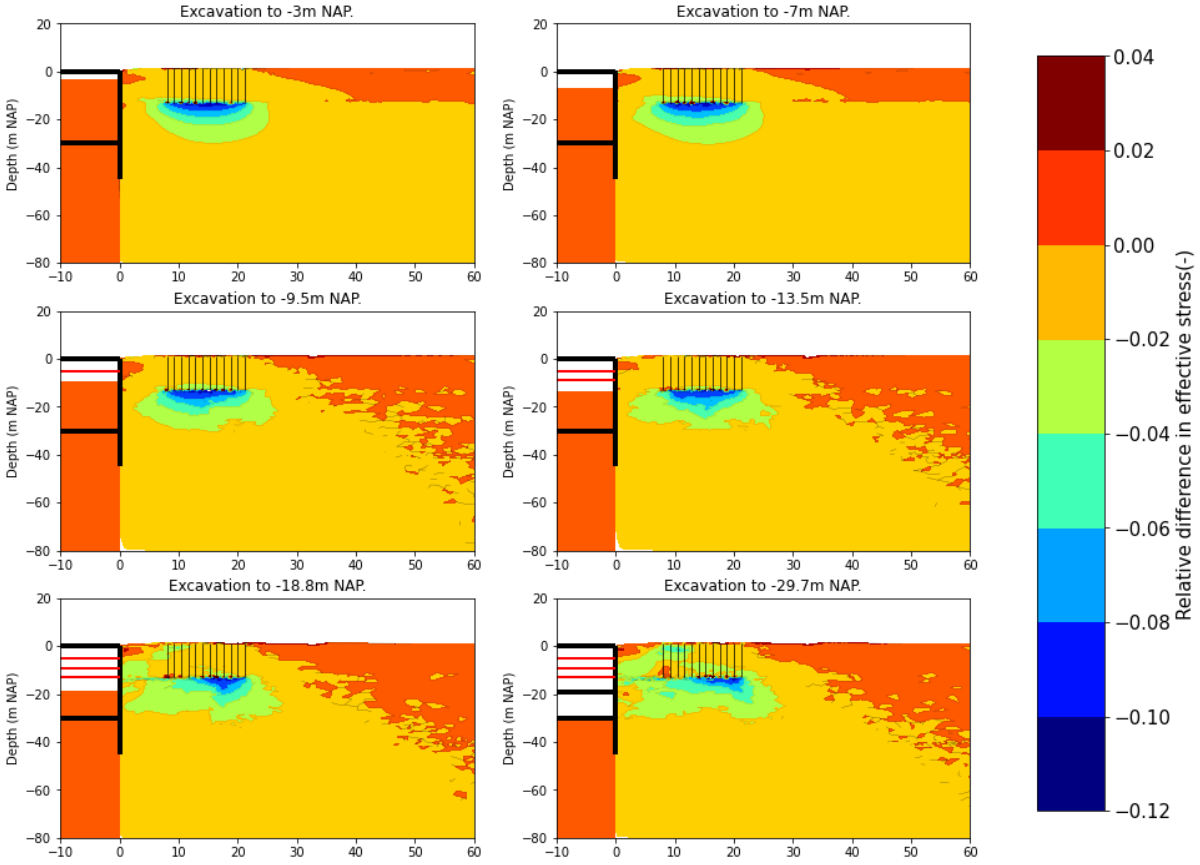

Figure 5-7 Relative effective stress in the soil of the Loaded pile model relative to the free-field model

The results show that during the first few excavation phases there is an increase in vertical stress beneath the piles closer to the excavation. The difference reaches up to 15 $\frac{kN}{m^2}$. This is the result of the settlement of the upper soil layers inducing negative skin friction on the piles. This negative skin friction subsequently results in an increase in the downward force adding pressure on the soil underneath the pile tips, increasing the (effective) stress. As the excavation depth increases, deeper soil layers tend to move accordingly reaching the point where these layers settle more than the upper soil layers. This leads to a decrease of stress beneath the pile tip. The piles further form the excavation undergo a different process. The upper soil layers settle to a larger extent than the deeper soil layers. This results in negative skin friction, which leads to an increase in stress beneath the piles to carry this friction. Hence, the observed increase in stress beneath the piles further form the excavation.

5.2.2 Building effect

Figure 5-8 shows the vertical soil deformation of the Building model relative to the Free-field model. Figure 5-10 shows the horizontal soil deformation of the Building model relative to the Free-field model. This difference is represented by a colour and the magnitude can be derived from the colour bar. The values are derived from calculations performed using PLAXIS FEA. To get a better understanding of the overall development of these influences the results are shown in six intervals. These intervals represent the excavation steps according to chapter 3.5.4. These differences in vertical and horizontal displacements are represented relative to the overall free-field situation in Figure 5-9 and Figure 5-11 respectively. This representation helps to show the proportionality of these differences and is the result of dividing the difference between the loaded pile model and the free-field model by the free-field model:

$$relative\ difference\ in\ displacement = \frac{u_{building} - u_{free-field}}{u_{free-field}}$$

5.2.2.1 Vertical displacements

Vertical soil deformation of the Building model with respect to the Free-field model.

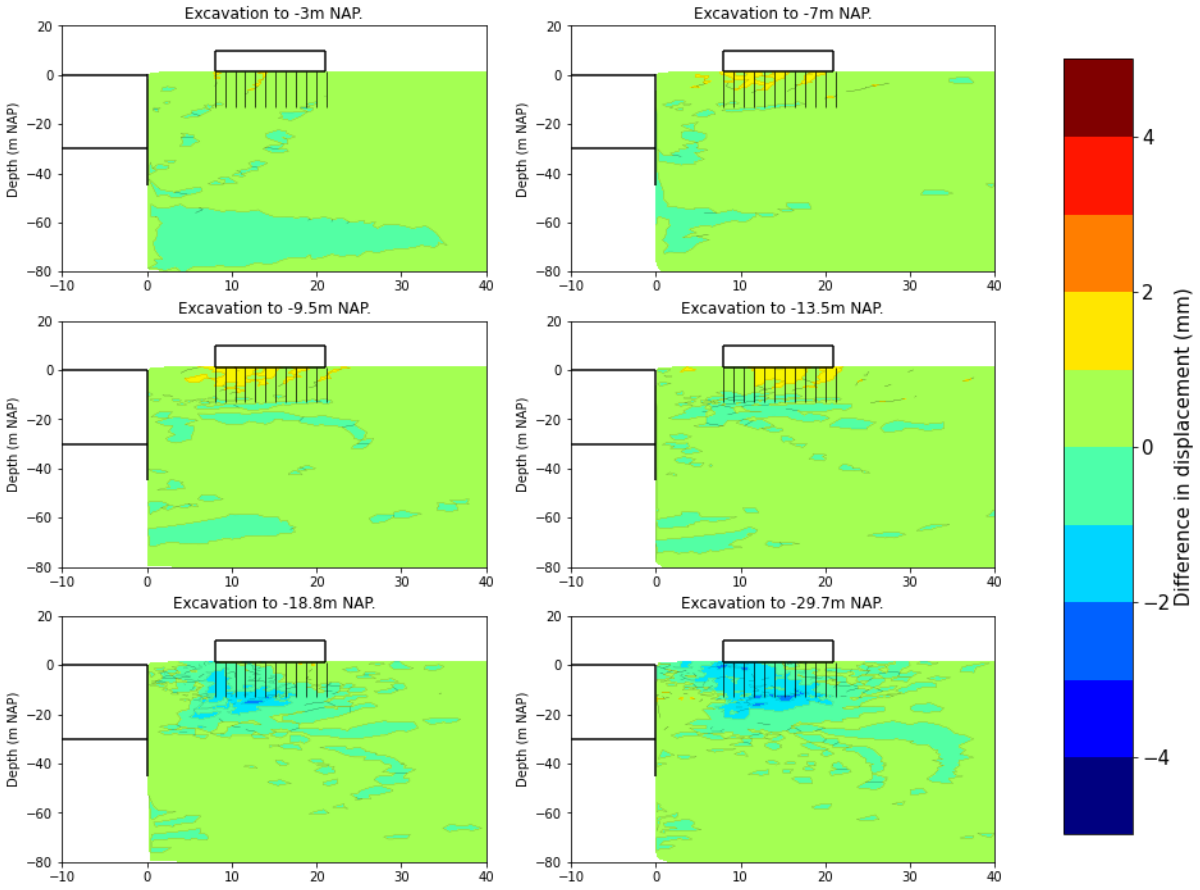

Figure 5-8 Vertical soil deformation of the Building model relative to the free-field model

Relative vertical soil deformation of the Building model with respect to the Free-field model.

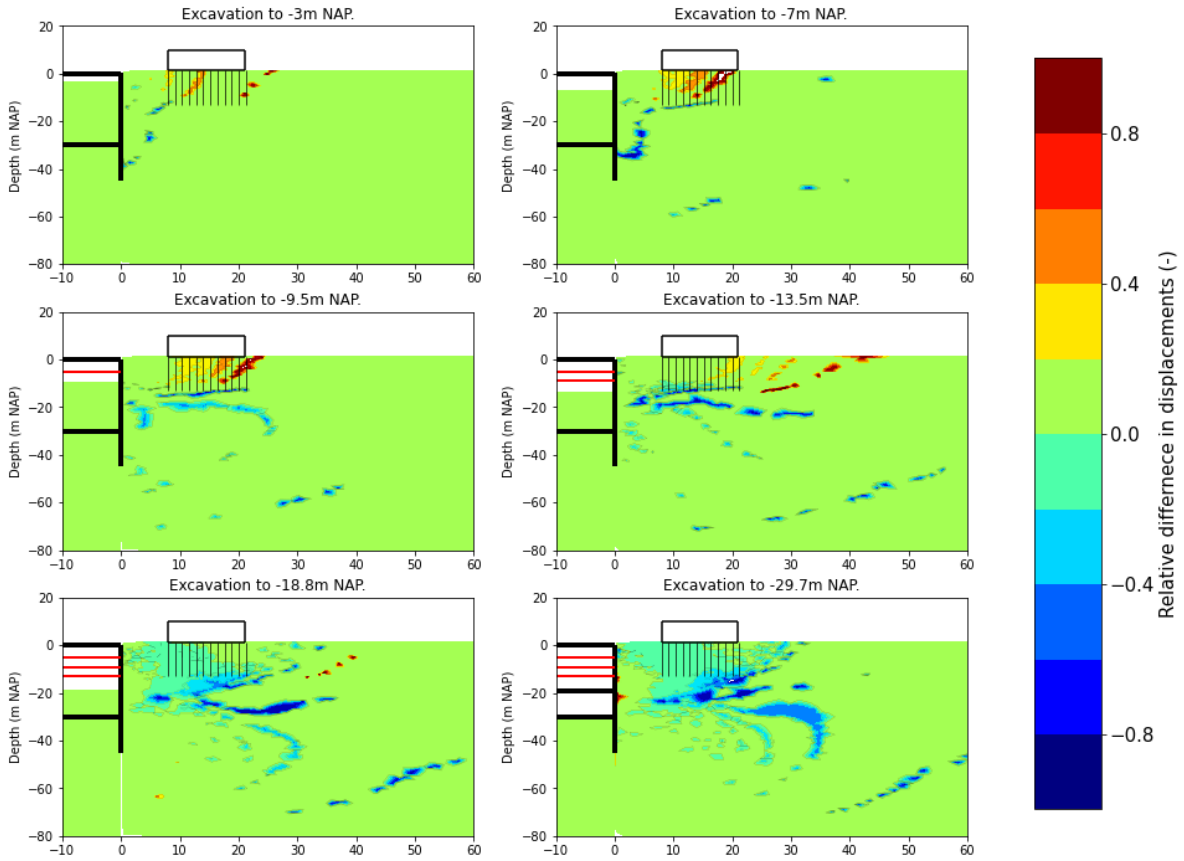

Figure 5-9 Relative vertical soil deformation of the Building model relative to the free-field model

During the first few excavation steps the difference between the models are quite small. With increasing excavation depth difference become more visible, at surface level especially. The settlement at surface level is less for the building model than for the free-field model. This is due to the pile foundation forming an additional constraint (foundation piles are stiffer than soil generally) allowing for less relative displacement between soil layers/bodies in direct contact to the piles. Interestingly the difference is more smeared out when compared with the difference with the uncoupled pile model. This is the result of the building redistributing load according to the movement of the piles relative to the building. As the deeper soil layers start to settle more and the settlement being felt at the pile tip some interesting developments are observable. Similar to the uncoupled pile model the front piles settle more at surface level, due to them being “dragged” by the deeper soil layers. As they are pulled away from the building they are loaded less and the effect of settlement of soil around the pile head is less. This load is then redirected to the other piles by redistribution, leading these piles and the adjacent soil bodies settle more than in a free-field situation and in the uncoupled pile model even the piles are loaded subject to the same load.

5.2.2.2 Horizontal displacements

Horizontal soil deformation of the Building model with respect to the Free-field model.

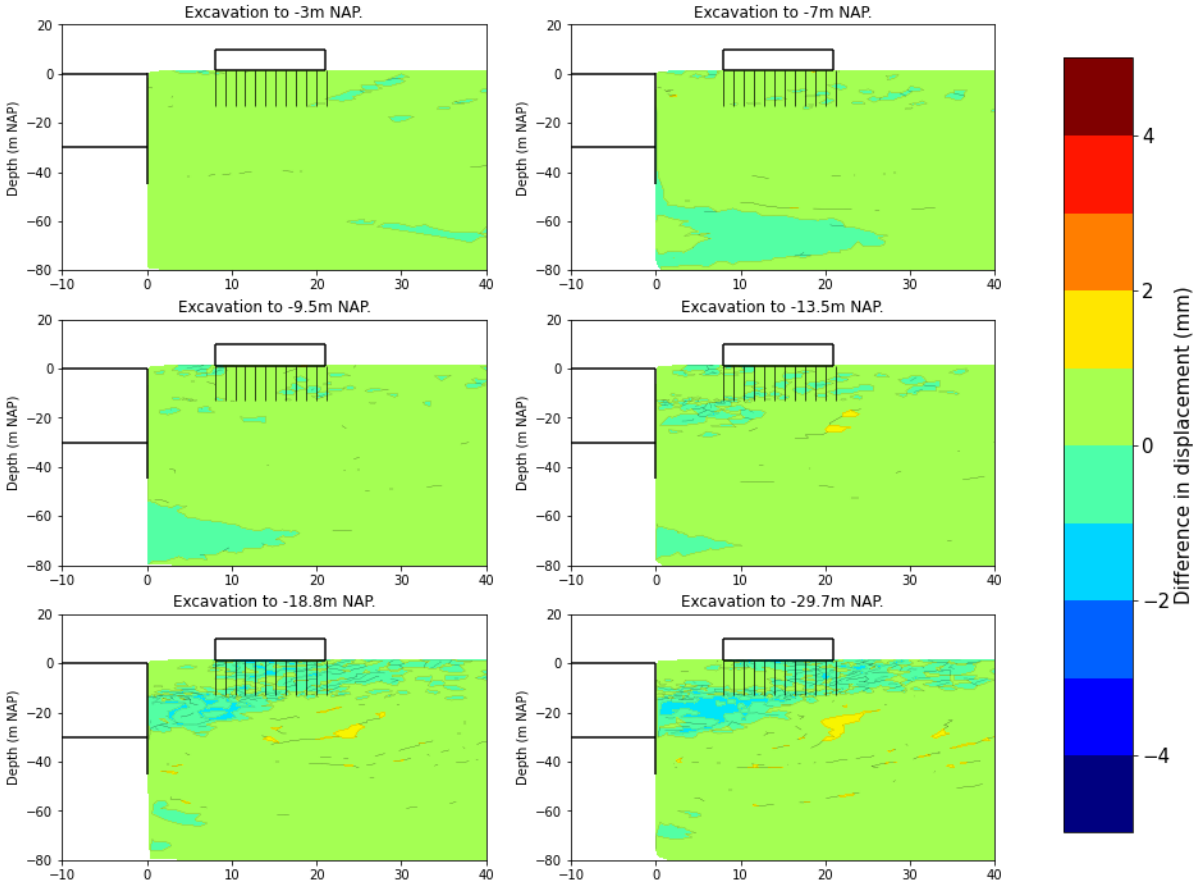

Figure 5-10 Horizontal soil deformation of the Building model relative to the free-field model

Relative horizontal soil deformation of the Building model with respect to the Free-field model.

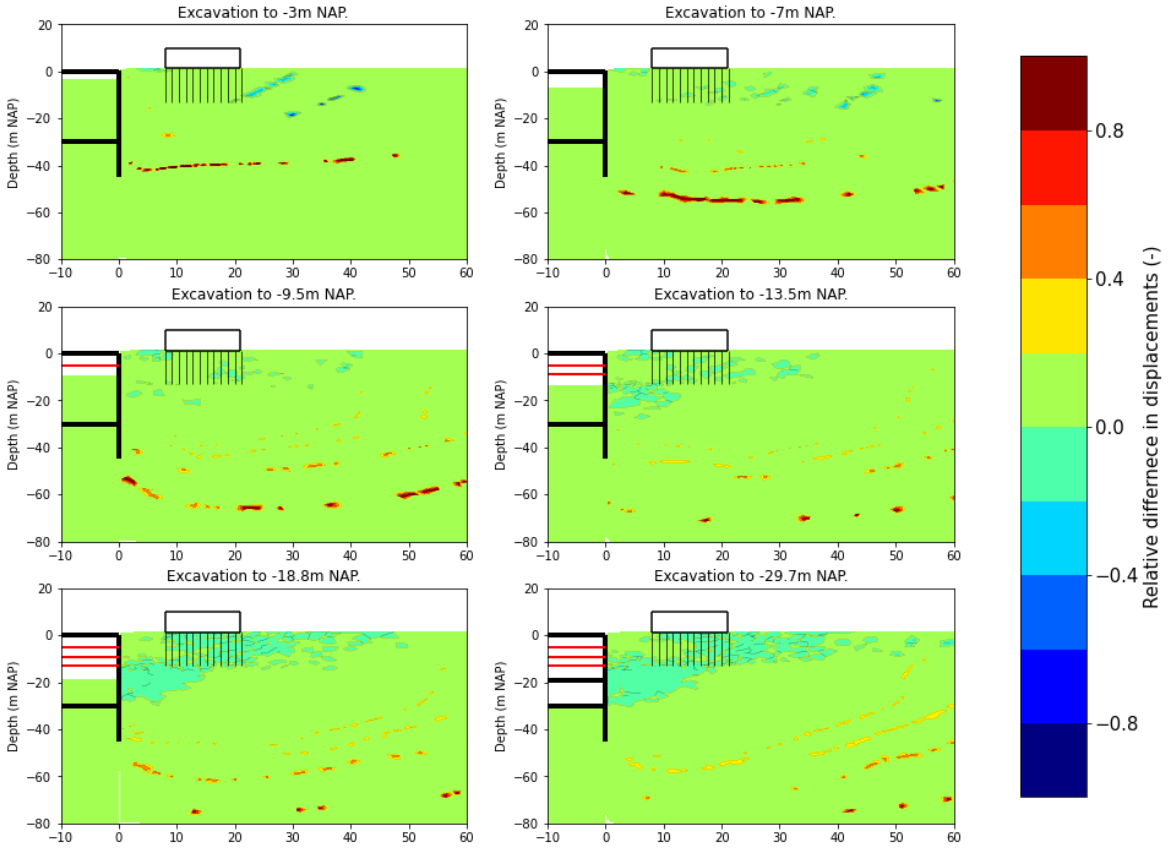

Figure 5-11 Relative horizontal soil deformation of the Building model relative to the free-field model

The difference between the model is initially small and increases with excavation depth. The difference are fairly similar to the differences with the uncoupled pile model. After the deeper excavation phases some deviation can be observed. Again, the deeper soil layers close to the excavation deform more than the in free-field situation. This is similar to the uncoupled pile model, which is described in 5.2.1.2. However, slightly larger deviations are observable in the shallow soil layers near the edges of the building. The piles are now less able to displace, particularly at the pile heads. This is the result of the constraint imposed by the building, which couples the pile heads. In turn, the pile heads are less able to translate independently due to the dependency on all foundation piles, the stiffness of the building and the interface between the pile heads and building. The soil movement around the piles is heavily dependent on the pile movements. Which explains the difference observed between the models at the shallow soil layers.

5.2.2.3 Effective stress

Figure 5-12 shows the difference in effective stress between the Building model and the Free-field model for six excavation steps. This difference is represented by a colour and the magnitude can be derived from the colour bar. A net downward pointing stress has a negative value and an upward pointing stress has a positive value. Figure 5-13 this difference relative to the stress in the free field situation, according to the following scheme:

$$relative\ difference\ in\ stress = \frac{\varepsilon_{building} - \varepsilon_{free-field}}{\varepsilon_{free-field}}$$

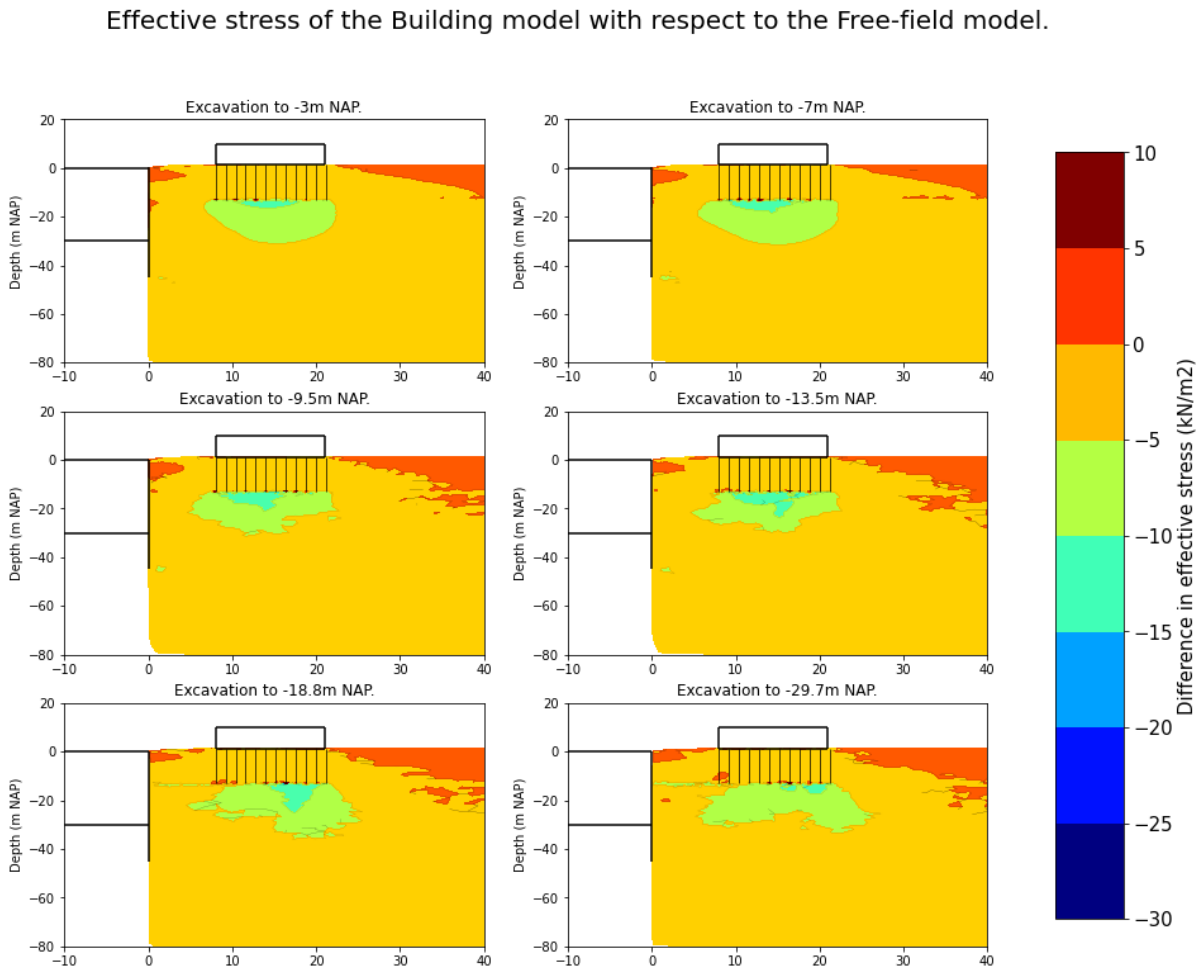

Figure 5-12 Effective stress in the soil of the Loaded pile model relative to the free-field model

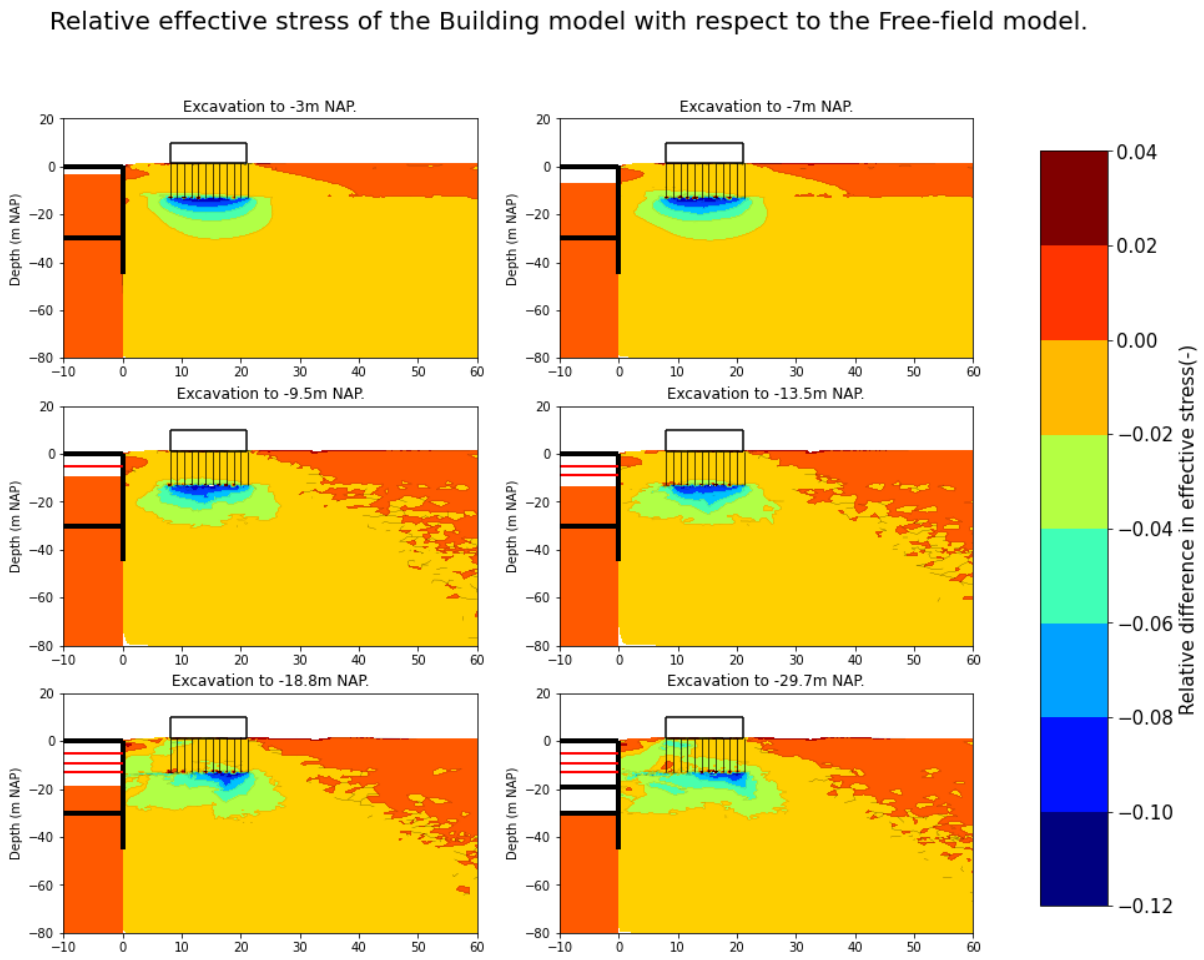

Figure 5-13 Relative effective stress in the soil of the Loaded pile model relative to the free-field model

The stress in the soil beneath and around the pile tips is higher than in the free-field model. This is due to the increased load coming from the building caried by the piles. Similarly, to the Loaded pile model the stress beneath the piles close to the excavation increases with increasing excavation depth due to the development of negative skin friction on these piles. However, this developments has some additional implications. The downward dragging force on the piles close to the excavation leads to redistribution of the load. The building tilts slightly towards the excavation, adding stress pile in the middle of the building (the building is on top of the hogging zone). This load is then transferred to the soil underneath these middle piles leading to an increase in stress. The tilt of the building leads also to a small upward motion of the back-end of the building, lowering the load on these piles leading to a decrease of stress in the soil underneath these piles. This mechanism is clearly visible during four first three excavation depth. Again, during the last two excavation phases deeper soil layers tend to move accordingly reaching the point where these layers settle more than the upper soil layers, leading to a decrease of stress in the soil beneath the pile tip. Also, the soil settlements further from the excavation induce an increased load on these piles leading to increasing soil stress underneath these piles. Still the, compared to the Loaded pile model the differences are fairly small.

5.3 CONCLUSIONS

In terms of vertical displacements, both the loaded pile model and the building model show differences up to 4 mm relative to the free-field model. In the situation where the excavation is shallow the difference in rather small. This difference increases with excavation depth. The first sand layers shows to be of a large influence on the soil displacements of the upper soil layers. In general, the peak of the settlements are smaller for the building, this is the result of the coupled situation of the foundation piles. Differential settlement of the piles leads to redistribution of the loads and therefore displacement that are smeared out over the foundation piles.

The horizontal displacements of the soil are also influenced by the presence of the foundation piles in the Loaded pile model and the building model. The differences reached up to 2-3 mm. This value increases which increasing excavation depth. The load of the piles on the soil leads to an increase of the horizontal force on the retaining wall, which is a major contributor to the difference on horizontal displacements of soil. The difference in vertical displacements could lead to both an underestimation and an overestimation of the potential damages to a building. Whereas the difference in horizontal displacements could lead to an overestimation of the damages. The combination of the both would have significant implications, giving an example of the potential overestimation and the conservativism of the uncoupled damage prediction methods.

The results in effective stresses show, during the first few excavation phases, there is an increase in downward effective stress beneath the piles closer to the excavation. The piles endure negative skin friction. This negative skin friction subsequently results in an increase in the downward force adding pressure on the soil underneath the pile tips. As the excavation depth increases, deeper soil layers tend to move accordingly reaching the point where these layers settle more than the upper soil layers. This leads to a decrease of stress beneath the pile tip. The distance of the pile to the excavation dictates which of the previous mechanisms occur. These are both visible in the loaded pile model and the building model.

6 BUILDING DEFORMATION ANALYSIS

In this chapter a comparison will be drawn between integrated 2D numerical modelling and decoupled analytic modelling. Monitoring data will be used to verify the outcome. The results of integrated 2D numerical modelling of the Vijzelgracht case will be conducted and the results will be verified using monitoring data. This will help to assess whether integrated 2D numerical modelling could be beneficiary and could be a helpful tool for future projects on the prediction of building deformations next to deep excavations. The merging of the otherwise two separate models of these cases (soil deformations and building deformations) into one model could lead to future saving in time and costs.

An unspecified building will be used for this analysis. The building will be modelled using numerical modelling in PLAXIS and analytic modelling. The soil model of the previous chapters will be used. The building will be modelled assigning both linear and nonlinear stiffness. analytic calculations will be done by performing both coupled and uncoupled calculations. The Limiting Tensile Strain Method (LTSM) and the relative stiffness method will be used. Further information on the models is given in Section 6.1.

6.1 THE MODEL

To perform the assessment a two-story building is used. The building façade is facing in the direction parallel to the length of the excavation. The Vijzelgracht Station Case is. Further information about the properties of the excavation and the soil parameters are present in Section 3.5. The soil is again modelled using Hardening Soil Small-Strain. According to the PLAXIS FEA manual (Plaxis 2D Reference Manual), this most suited soil model for the prediction of excavation induced deformations (Section 3.4).

6.1.1 Building Dimensions

A two-story building is modelled using PLAXIS FEA and LTSM. The building façade has a height of 7 meters and a width of 13 m. A schematization of the facade is presented in Figure 6-1. The façade at ground floor level is assumed to have thickness of 330 mm and at higher floors a thickness of 220 mm is assumed. The bottom of the façade is assumed to roughly 1 m below ground level (0.3 m NAP), where it is founded on a typical Amsterdam pile foundation. The building is located at a distance of 8 meters from the retaining wall.

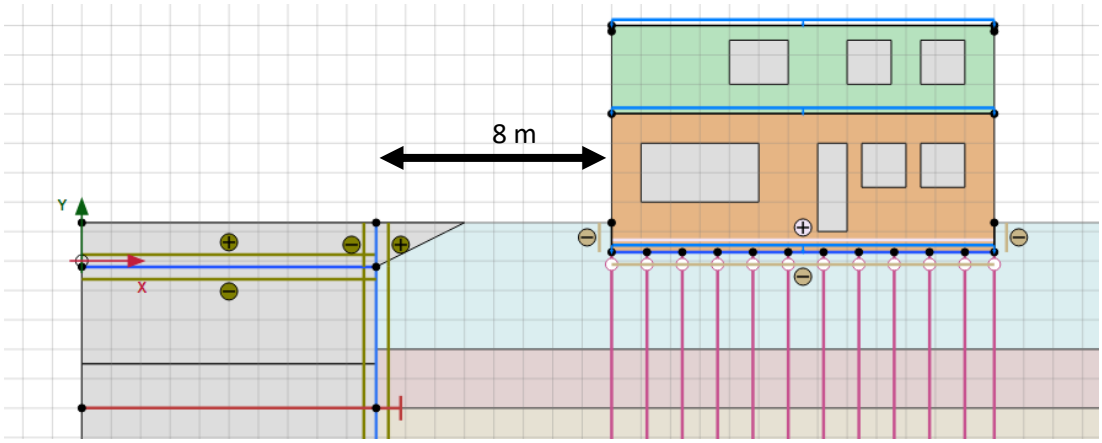

Figure 6-1 Facade as modelled in PLAXIS.

6.1.2 Foundation parameters

Similar to section 4, a typical Amsterdam foundation is assumed. The piles are assumed to have an average diameter of 180 mm and are end-bearing with the tip being in the First sand layer. On average the tip of the piles is assumed to be founded on -13 m NAP. The foundation piles are assumed to have the properties of aged pine wood. These properties correspond a stiffness of $E = 6000\ \frac{N}{mm^2}$ and a specific density of $\gamma = 4.6\ \frac{kN}{m^3}$.

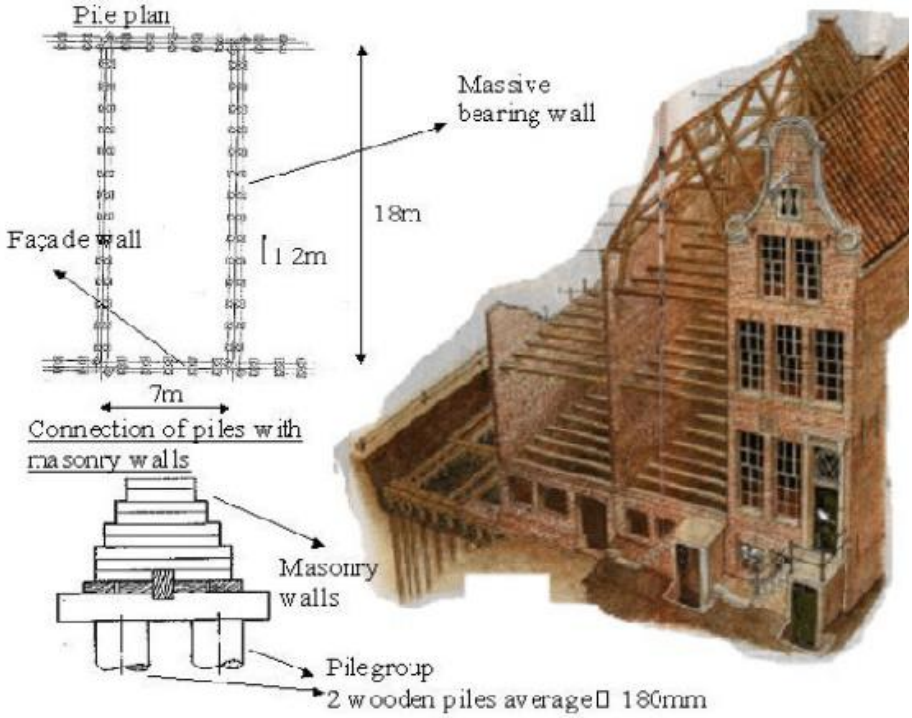

Figure 6-2 Typical Amsterdam Foundation (Zantkuijl, 1993)

Figure 6-2 shows a sketch of a foundation of a typical Amsterdam building. Each wall is supported by a wooden beam on top of a row of pile groups, consisting of two piles spaced 1.2 m out of each other hart-to-hart. The hart-to-hart distance between the pile groups is on average 1.5 meters. The wooden beam is assumed to have a width of 1.5 m and a height of 200 mm . This wooden beam also assumed to be of aged pine wood and the same material properties are considered as for the piles; A stiffness of $E = 6000\ \frac{N}{mm^2}$ and a specific density of $\gamma = 4.6\ \frac{kN}{m^3}$.

The elements forming the foundation are not fully coupled. The wall transferred compression fully to the wooden beam and lateral forces are transferred partially. A friction coefficient of 0.6 is assumed, in accordance with Table F.3 of NP9998:2017. This is a common value used to describe the friction coefficient between brick and wood and gives a good estimate. The connection between the piles and beam needs some modifications. The pile does not transfer tension to the beam. Only compressive forces are transferred between the pile and beam.

6.1.3 Material models

This section discusses the material models used for the assessment and gives a description of the used material models and variations. The building will be modelled with linear material properties and nonlinear material properties. Also, an analytic model will be made using the Limiting Tensile Strain Method (LTSM) and the relative stiffness method. The models will be described further in their respective subsection (6.1.3.1 to 6.1.3.3).

The buildings adjacent to the excavation are predominantly masonry structures. This assessment will model the masonry using the continuum approach. In the continuum models, the masonry is represented as a single material with homogenized properties. The constitutive law describing the material behaviour relates the average stress and strain, and the damage is smeared out in the continuum elements (Giardina, 2013).

Modelling the masonry using the continuum approach is assumed to be sufficient for this thesis. As this thesis does not focus on the failure of the structures but rather the overall deformation of the structures. Not much data is available about the exact characteristics of the failed masonry elements and no detailed documentation is available about the detailed interim repair of façade or foundation.

6.1.3.1 Linear numerical models

Unreinforced masonry consists of a combination of brick and mortar. The brick is often much stronger than the mortar. The strength of masonry is largely dependent on the mortar. Several studies are carried out to determine the strength and stiffness of masonry. Masonry is in essence extremely nonlinear. There are also studies carried out to determine a linear approximations for estimation purposes. Pluijm (1997) has done such a study and found an average stiffness of 1505 MPa and a standard deviation of 1161 MPa for masonry in good condition, with a lognormal distribution. The standard deviation results in a large spread for the stiffness. Similar results were found by Raijmakers (1995), based on the literature review conducted (Raijmakers, 1995). These studies formed the base of the study conducted by Waarts (Waarts, 1997).

Recent studies tend to use higher stiffnesses for the linear approach. This could be the result of analyses including newer masonry, which in general has a larger stiffness Giardina (2013) for example used a range of 1000, 3000 and 9000 MPa for the Young's moduli, with 3000 MPa being the mean value. The stiffness of unreinforced masonry could become as low as 300 MPa (Bull, 2001). In line with the distribution found by Pluijm (1997) and the study conducted by Giardina (2013) the following Parameters are used for the assessment:

Table 6-1 Linear elastic material properties used in the nummerical model

Parameter	Sign	Value	Unit
Stiffness	E	1000/3000/9000	$\frac{N}{mm^2}$
Poisson's ratio	v	0.2	$-$
Density	ρ	20	$\frac{kN}{m^3}$

6.1.3.2 Non-linear material model

PLAXIS comes with a in-built user defined material model for masonry structures. This masonry model is a non-linear (linear elastic perfectly plastic) model aimed to simulate the macroscopic, anisotropic response of unreinforced masonry structures. In this model a coulomb criterion is used to simulate the failure in the predefined directions and an overall Mohr-Coulomb criterion is used to represent a failure of the masonry blocks. It is based on the anisotropic Jointed Rock constitutive model, a user defined model implemented in PLAXIS which has a constitutive law that takes into account the directional properties of the medium and orientation of maximum three failure directions along which a Coulomb failure criterion applies (PLAXIS-UDSM Masonry model).

The material model takes into account up to three joint directions representing the cementation joints. Along those directions a local Coulomb failure criterion apply and a Mohr-Coulomb failure criterion applies to represent failure of the blocks. The Jointed Rock formulation is modified to incorporate the strength enhancement in brick masonry as a result of interlocking effects. This was not incorporated in the original Jointed Rock model. This is the result of combined analysis of the Sapienza and Roma 3 University, which also incorporated several other specific features of the nonlinear mechanics of masonry structures stemming from the interlocking effects of the bricks due to its staggered arrangement in vertical direction (PLAXIS-UDSM Masonry model). These properties are especially relevant during horizontal sliding and overturing of the element(s).

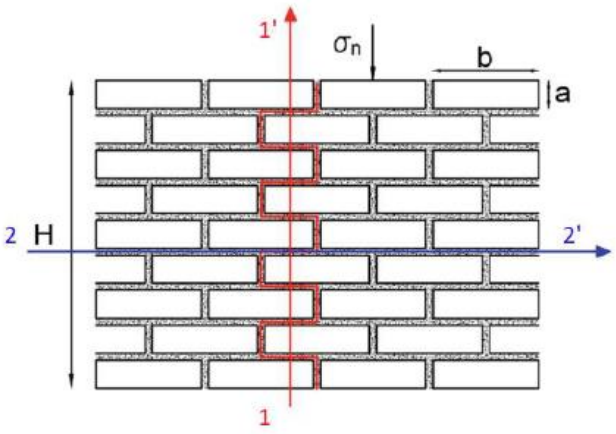

Figure 6-3 Orientation of Plane 1-1' and Plane 2-2' in the Masonry model (Amorosi, 2018)

To determine the material parameters national Dutch guidelines (NPR 9998:2017) is helpful if no laboratory data is available. Table-F2 contains strength and stiffness values of different masonry structures. Poor quality brickwork (pre-1945) material parameters are assumed similar to the case study of a typical Dutch old masonry building (PLAXIS-UDSM Masonry model).

Table 6-2 shows the used model parameters for the analysis.

Table 6-2 Non-linear material parameters

Description	Symbol	Value	Unit
Density	γ	20	kN/m^3
Shear modulus	G	0.89E5	kN/m^2
Poisson's ratio	v	0.21	-
Cohesion	C_{mc}	1649	kN/m^2
Friction angle, Dilatancy angle	ϕ_{mc}, ψ_{mc}	24.2	°
Tensile strength	$tens_{mc}$	3664	kN/m^2
Strength factor	SF_{beta}	0.75	-
Orientation of vertical joints	$1{:}\,\alpha_1, 1{:}\,\alpha_2$	90	°
Cohesion of joints	C_1, C_2	180	kN/m^2
Friction angle and dilatancy angle of joints	$\phi_1, \phi_2, \psi_1, \psi_2$	31	°
Tensile strength of vertical joints	$tens_1$	21	kN/m^2
Tensile strength of horizontal joints	$tens_2$	60	kN/m^2
Orientation of horizontal joints	$2{:}\,\alpha_1, 2{:}\,\alpha_2$	0	°

6.1.3.3 Analytic models

Building deformations are also assessed analytically. To perform the analytic calculations the LTSM Method and the relative stiffness method as proposed by Goh (2010) will be used. Both are discussed respectively in paragraph 3.2.1 and 3.2.2 and 3.2.3. The ratio between the Young's modulus and the shear modulus is assumed to be equal to 12, since the face of the building is significantly perforated. For the relative stiffness method, the building is assumed to have as stiffness of 1000 MPa and the average soil stiffness is assumed to be equal to 9 MPa.

6.1.4 Loads

The building is mainly carrying vertical loads of which a part is redirected towards the façade through the floors and roof. In terms of magnitude, the loads similar assumptions are made as discussed in Section 5.1. The exact connection between the floors and rood and the facade is unknown. Therefore,

the loads from the floor are assumed to act as a distributed load on the facades. The façade is on the lengthy side of the building, meaning that the load is mostly directed towards the façade and the opposing wall. The building has a width of roughly 8 meters. For simplification the 3 meter of these loads are redirected towards the façade on every level. The self-weight of the façade is included via the properties of the masonry wall discussed in 6.1.1 and 6.1.2. The loads on the façade are composed as follows:

- Roof:
  - $Q_{p,Roof} = 0.5 \frac{kN}{m^2}$
  - $Q_{v,Roof} = 0.0 \frac{kN}{m^2}$
- Attic:
  - $Q_{p,Attic} = 0.5 \frac{kN}{m^2}$
  - $Q_{v,Attic} = 1.0 \frac{kN}{m^2}$
- Floors:
  - $Q_{p,Floor} = 0.75 \frac{kN}{m^2}$
  - $Q_{v,Floor} = 1.5 \frac{kN}{m^2}$
- Ground floor:
  - $Q_{p,Ground} = 0.75 \frac{kN}{m^2}$
  - $Q_{v,Ground} = 2.0 \frac{kN}{m^2}$

This results in the following composition of permanent and variable loads:

$$Q_{Attic} = \big((0.5 + 0.5) + (0.0 + 1.0) * .5\big) * 3 = 4.5 \frac{kN}{m}$$

$$Q_{1st\ Floor} = (0.75 + 1.5 * .5) * 3 = 4.5 \frac{kN}{m}$$

$$Q_{Ground\ Floor} = (.75 + 2.0 * .5) * 3 = 5.25 \frac{kN}{m}$$

6.2 RESULTS

The numerical results are presented and discussed in terms of strain during the different excavation steps. The horizontal strain is presented and analysed because this is a main indicator of potential damages. This enables the comparison between the numerical results and the analytic results (Limiting Tensile Strain Method and Relative Stiffness Method) as the horizontal strain can be obtained from the analytic calculations.

6.2.1 Linear elastic material models

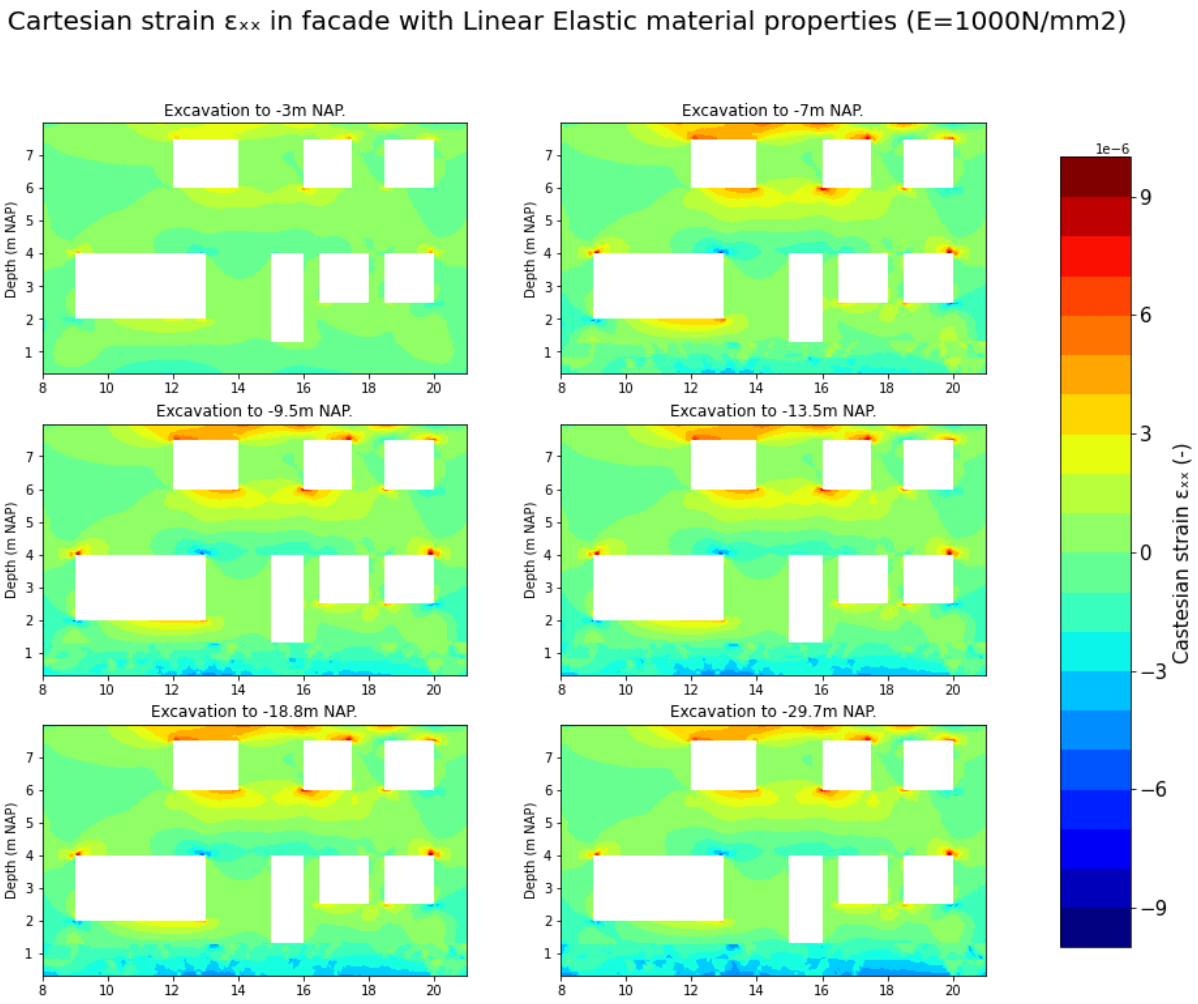

Figure 6-4 Horizontal strains in façade in the Linear elastic model with a stiffness of 1000 MPa

Figure 6-4 shows the development of horizontal cartesian strains during 6 different excavation steps for the model with continuum material properties with a stiffness of 1000 MPa. The colour represents the strain in the façade. A positive value corresponds with tensile strains and a negative value corresponds with compressive strains.

After the first excavation step tensile strains are observed in the upper part of the facade and around perforations as the building is in the hogging zone at this stage. These tensile strains increase during the following excavation step as the building is still in the hogging zone and the curvature of the subsoil increases. After this stage no significant development in strains are observed. The strain reaches local peak values of $9 * 10^{-6}$ $(0.0009\ \%)$. The curvature underneath the building doesn't seem to impose further strains in the façade. The façade seems to rotate as a whole.

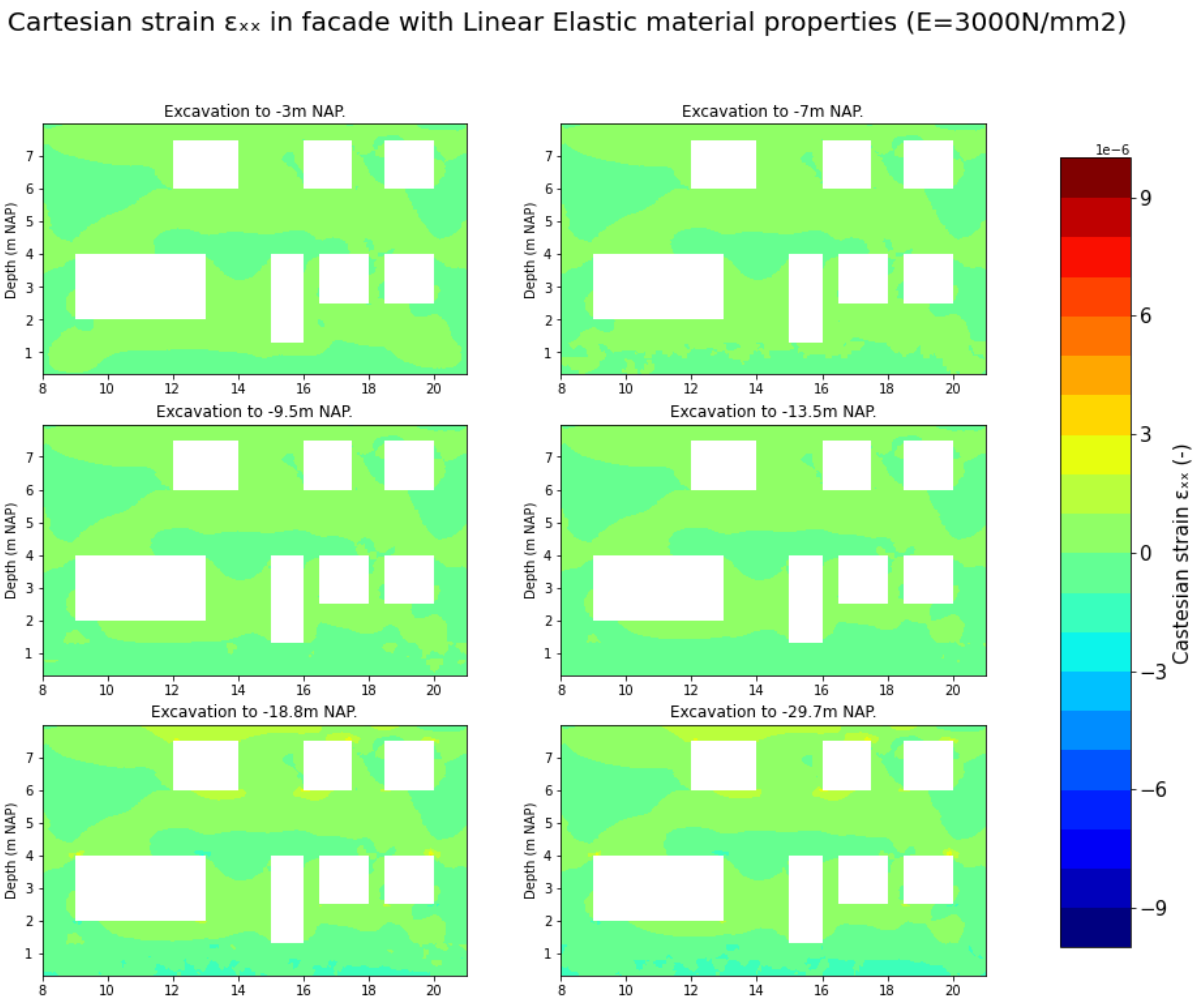

Figure 6-5 Horizontal strains in façade in the Linear elastic model with a stiffness of 3000 MPa

Figure 6-5 shows the development of horizontal cartesian strains during 6 different excavation steps for the model with continuum material properties with a stiffness of 3000 MPa. The colour represents the strain in the façade. A positive value corresponds with tensile strains and a negative value corresponds with compressive strains.

The results show minor strain development over the excavation steps. Peaks are observed after an excavation depth of -18.8 m NAP is reached. After this stage no significant development in strains are observed. The strain reaches local peak values of $3 * 10^{-6}$ $(0.0003\ \%)$.

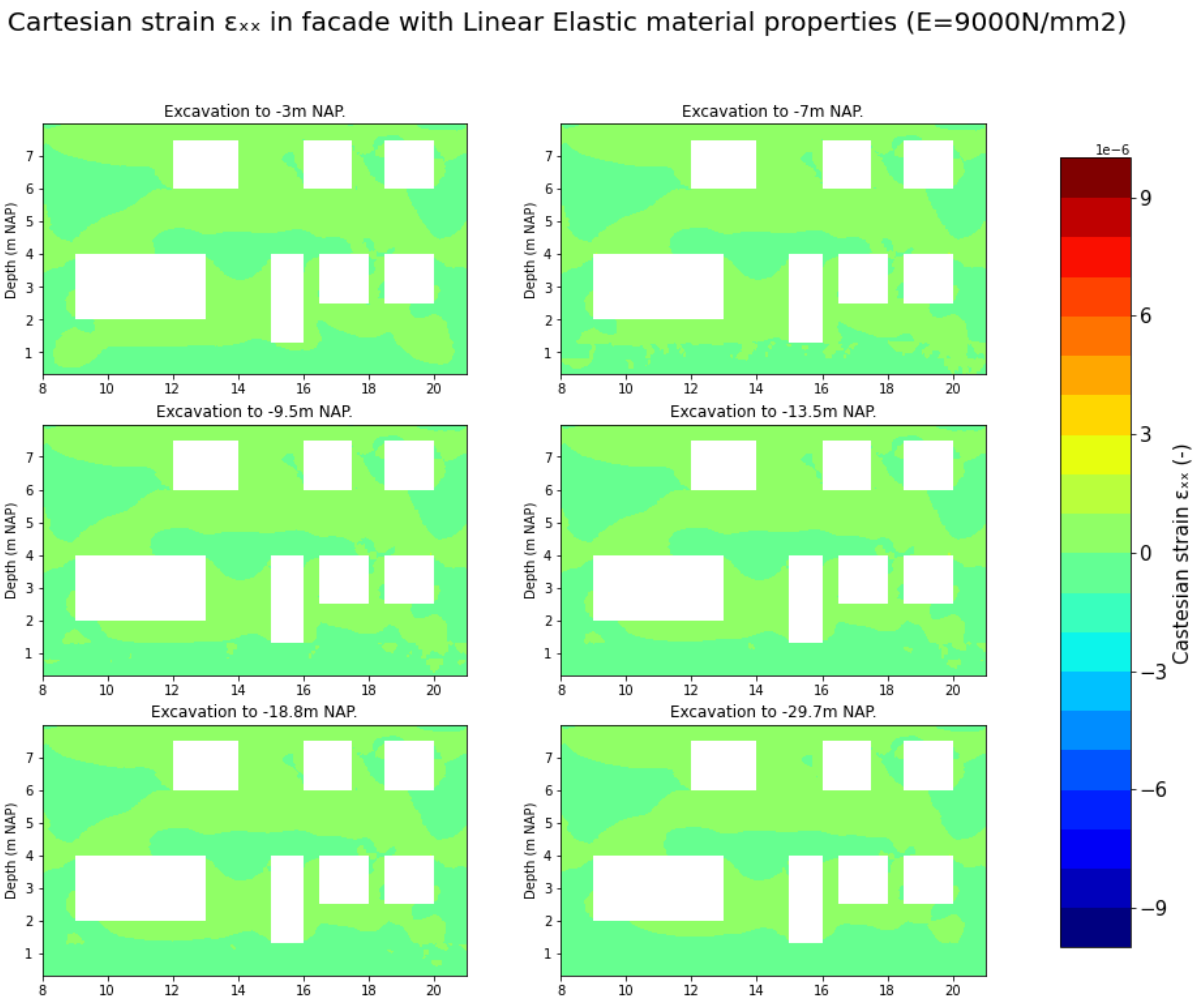

Figure 6-6 Horizontal strains in façade in the Linear elastic model with a stiffness of 9000 MPa

Figure 6-6 shows the development of horizontal cartesian strains during 6 different excavation steps for the model with continuum material properties with a stiffness of 3000 MPa. The colour represents the strain in the façade. A positive value corresponds with tensile strains and a negative value corresponds with compressive strains.

The results show even less strain development over the excavation steps. Peaks are observed after an excavation depth of -18.8 m NAP is reached. After this stage no significant development in strains are observed. The strain reaches local peak values of $1 * 10^{-6}$ $(0.0001\,\%)$.

6.2.2 Non-linear material model

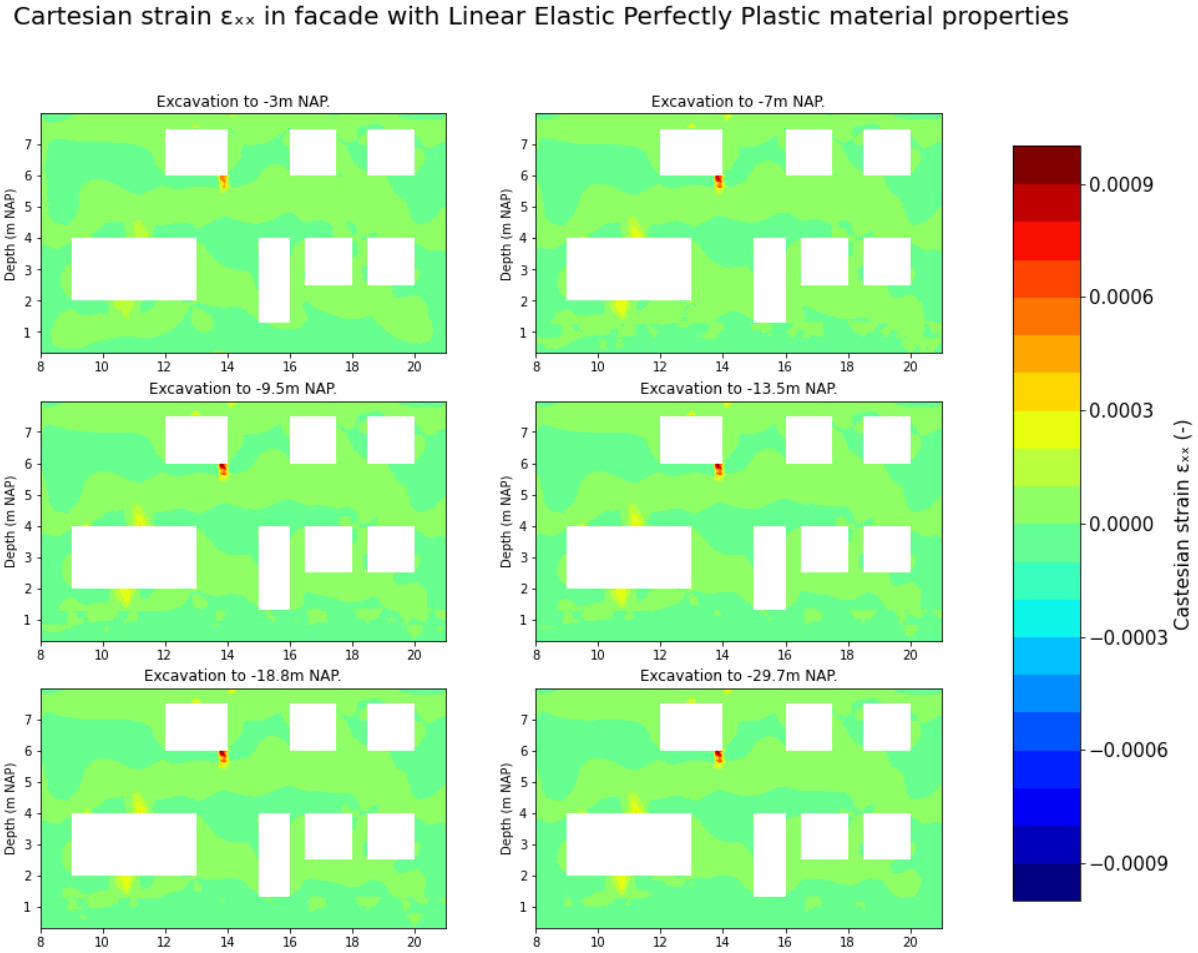

Figure 6-7 Horizontal strains in façade in the Non-linear model

Figure 6-7 shows the development of horizontal cartesian strains during 6 different excavation steps for the model with Non-linear. The colour represents the strain in the façade. A positive value corresponds with tensile strains and a negative value corresponds with compressive strains.

Some interesting observations can be made for this non-linear model. The peak in horizontal strain is observed at the upper left window, with a value of about 0.001 (0.1%). Also, along the lower left window larger strains are observed at the centre. Overall, the strains are larger in the nonlinear model. This is due to the lower shear modulus used in the nonlinear model.

6.2.3 Analytic models

To perform the analytic calculation one particular excavation step will be analysed. The excavation depth in this stage reaches -19.7 m NAP(step 5). The surface settlements in the analytic calculations and the numerical results show great resemblance. The soil deformations from the numerical free-field model follow similar deformations to the deformations in the integrated models. This will help to identify the significance of integrated modelling. The numerical and analytical surface settlements and the settlement at the foundation layer are plotted together with the numerical settlement of the building in Figure 6-8.

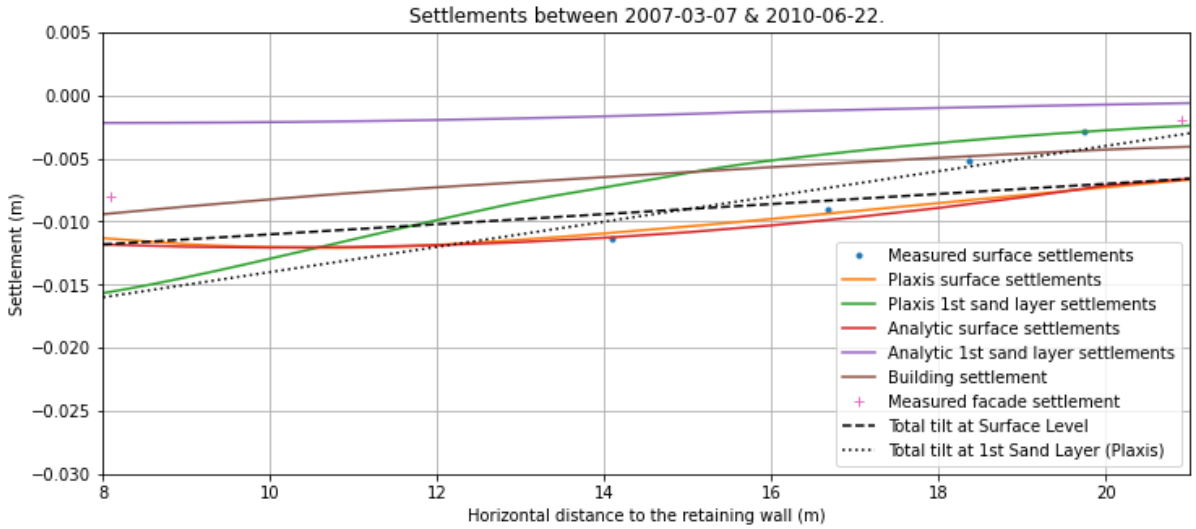

Figure 6-8 Analytic and numerical settlement at surface level and foundation level (1st Sand Layer)

In Section 4.3 the influence of the foundation layer on the overall settlement of a pile was shown. Korff (2013) also analysed the building settlement for several cases along the north-south line in which the buildings are founded on the first sand layer. Korff (2013) compared the settlements of the building with the overall surface settlements and the settlements of the foundation layer. Korff (2013) found that the buildings followed the settlement of the foundation layer for 50~100% relative to the surface settlements depending on the age and safety factor for piles with at least 50% end bearing. Piles with larger percentages of shaft capacity or smaller safety factors settle significantly more, ultimately leading to the maximum pile displacement being equal to the maximum soil settlement, which for excavations is found at the surface (Korff M. , 2013).

The surface settlements impose a sagging settlement mode and the settlement of the foundation layer imposes a hogging settlement mode at the location of the building. The buildings in the numerical models (PLAXIS models) showed a hogging settlement mode during this particular excavation step. Therefore, analytic calculations are performed for both the free-field surface settlements and the settlements at foundation level in order to be able to draw a comparison between analytic and integrated numerical modelling.

The modification factors for the relative stiffness method are determined using the modified formulae as presented by Goh (Goh, 2010). The results are presented below for the modification factors, assuming a building stiffness (E) of 1000 MPa and an average soil stiffness (E_s) of 9 MPa:

$$\rho^*_{exc} = \frac{EI}{E_s L^3} = 0{,}47$$

$$\alpha^*_{exc} = \frac{EA}{E_s B} = 15{,}04$$

$$M^{DR_{sag}}; M^{DR_{hog}} \approx 0{,}15$$

$$M^{\varepsilon_h} \approx 0{,}0$$

The results for the predicted building strains and deformations using the analytic methods (LTSM and Relative Stiffness Method) are presented in Table 6-3. The results are determined using the settlements at surface level and the foundation level separately. Horizontal strain as a result of horizontal deformation of the subsoil is assumed to be equal to 0, because of the level of flexibility of

the piles in combination with the lack of fixation between the building and the foundation piles. The neutral axis is assumed to be in the middle of the building in sagging mode and at the bottom in hogging mode.

Table 6-3 Building strains and deformations following LTSM and Relative Stiffness Method

Criterion	LTSM – surface level (%)	LTSM – foundation level (%)	Relative Stiffness – surface level (%)	Relative Stiffness – foundation level (%)
Maximum slope	0,080	0,150	0,080	0,150
Relative rotation β (average tilt)	0,120	0,121	0,120	0,121
Relative rotation β (maximum tilt)	0,080	0,093	0,080	0,093
Deflection ratio $\frac{\Delta}{L}$	0,015	0,031	0,002	0,005
Horizontal strain ε_h	0,000	0,045	0,000	0,007
Maximum horizontal tensile strain $\varepsilon_{h,max}$	0,023	0,091	0,003	0,014
Maximum diagonal strain $\varepsilon_{d,max}$	0,009	0,018	0,001	0,003
Damage Class[1]	0 – Negligible	2 - Slight	0 – Negligible	0 – Negligible

The results show that there is a significant difference between the LTSM and the relative stiffness method. This is due to the low values for the modification factors, which in turn is the result of the relation between the building stiffness (E) of 1000 MPa and the average soil stiffness (E_s) of 9 MPa. The modification factor for the horizontal strain holds that the building stiffness is significantly larger than the soil stiffness, resulting in modification factor equal to 0. Since the building is founded on flexible piles the transferred horizontal strains in the subsoil to the building is assumed to be zero.

6.3 Validation of Deformations

This section aims to present the building displacements of the different models and use the monitoring data as validation for the results. The damage class is specified in the records of the building. The data does not describe the exact pattern and severity of the cracks and damages. Certain inconveniences occurred during the construction of the diaphragm walls, leading to the majority of the damages.

[1] Associated damage level according to Boscardin et al. (1989) (Table 3-1)

Prisms were placed on the façade of the building to monitor displacements during the construction of the Vijzelgracht Station. Prisms 01 and 12 fell out very early on (during the preparatory works) and prisms 11 and 02 were recalibrated in June 2010. The prism place and name is shown in Figure 6-9. The horizontal and vertical displacements are plotted together in Figure 6-11 and Figure 6-12 respectively. In order to compare the measurement data with the numerical results nodes are placed on the exact same location as the prisms in the numerical model. The displacements of these nodes are plotted together with the measurement data in the same graph, which aids to indicate the differences and similarities.

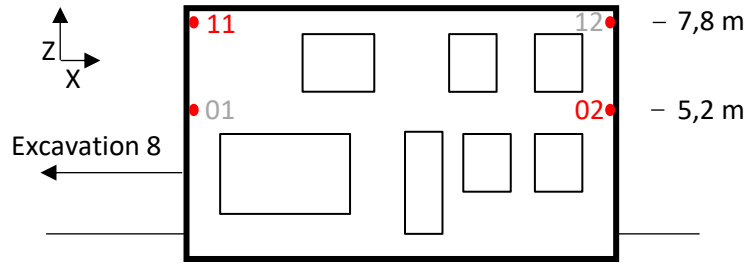

Figure 6-9 Sketch of the prism placement on the building façade

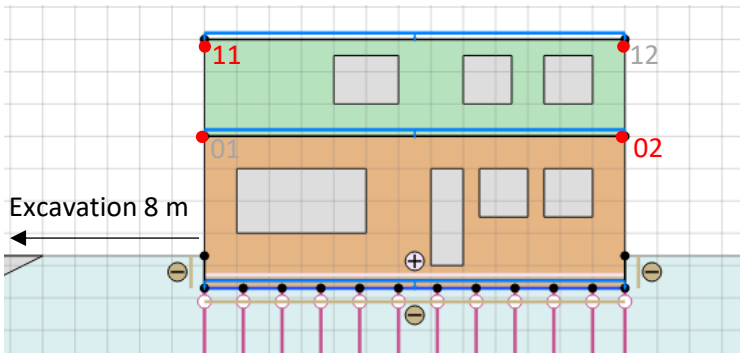

Figure 6-10 Facade as modelled in PLAXIS with indication of the nodes corresponding with the prisms

The monitoring data used starts on the 3rd of march 2007 corresponding with the estimated start of the excavation works. On this starting point the deformations are set to zero. The vertical axis shows the displacement and the horizontal axis shows the corresponding date. The numerical results are plotted along the monitoring data. The six excavation stages and corresponding dates from Section 3.5.4 is used, namely -3 m NAP, -7 m NAP, -9.5 m NAP, -13.5 m NAP, -18.8 m NAP and -29.7 m NAP. The deformation of the masonry facade with a stiffness of 3000 MPa is presented. There were no significant differences in deformations between the different stiffnesses of the linear elastic models. The difference were smaller than 1mm, which is negligible compared to the overall deformations.

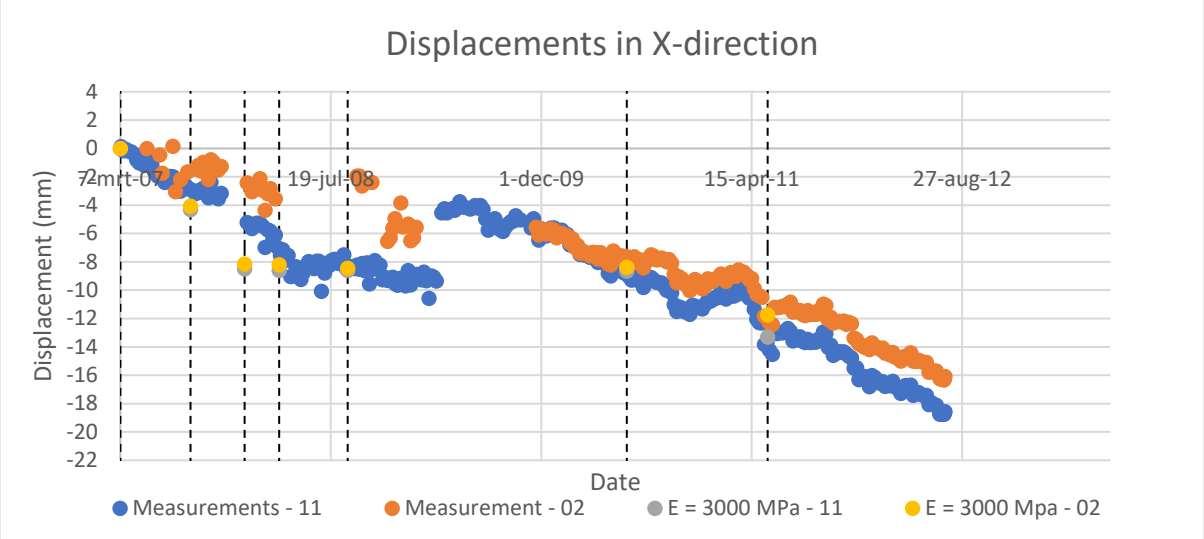

Figure 6-11 Horizontal building displacements

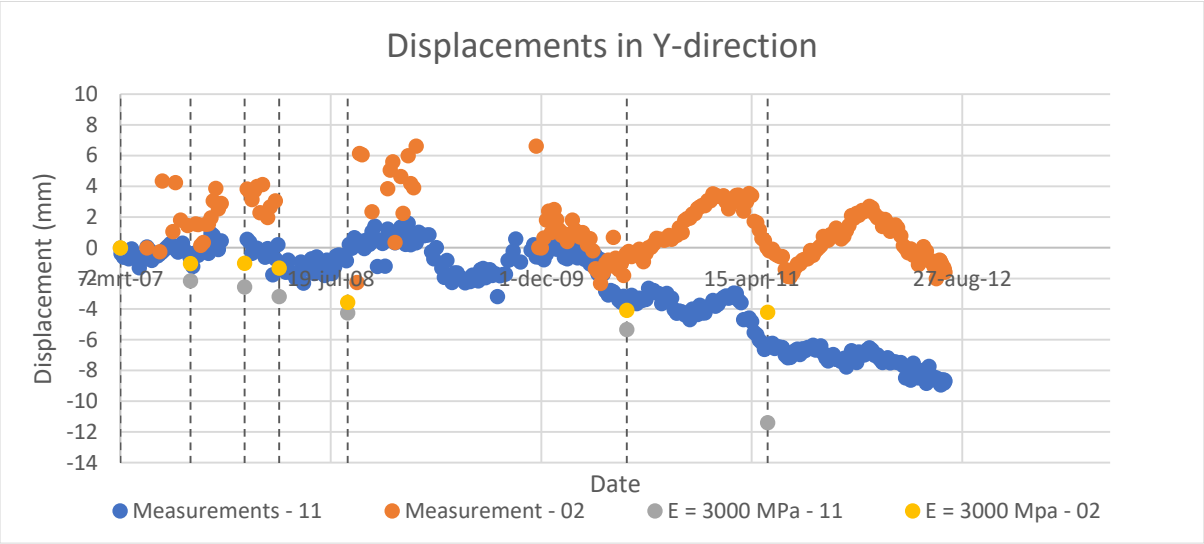

Figure 6-12 Vertical building displacements

The displacement measured correspond very well with the numerical results. The dates corresponding with the different excavation steps are estimates and can vary over the length of the excavation. This could explain some of the difference between the numerical results and the monitoring data. The horizontal displacements especially follow the monitoring data very well. The differences in vertical displacement are larger. At certain stages the façade has moved upwards which is against expectations. No records are available in this matter. The difference could be assigned to measurement errors or foundation restoration in the period of measuring or overall rotation of the façade in which the left side of the building moves down and the right side of the building moves up. After the calibration date the settlements show to increase fairly stable endorsing the possible explanations given. However, the displacements following from the numerical calculations are considered reliable for the given reasons.

6.4 CONCLUSIONS

The results have shown that the building reacts rather stiff on the developments in the deep excavation. This stiffness is observed uniformly over the different stiffnesses in the linear elastic

calculations. No significant differences in deformation are observed between the different stiffnesses. The superimposed forces on the façade seem to be fairly dominant and uniform. This results in a nearly linear relation between the stiffness in the façade and the calculated strains in the façade. However, all these strains do not correspond with any (visible) damages according to Table 3-1.

The nonlinear model showed larger horizontal strains. This could be assigned to the smaller shear modulus assigned to the building in the nonlinear model. The smaller shear modulus and overall conservative parameters resulted in larger strains. The peaks in strain occur at different points in the façade. The peak horizontal strain value is about 0,09%. Which could indicate small damages according to Table 3-1. The results for horizontal strain are presented in Table 6-4 together with the results from the analytic models.

Table 6-4 Comparison of the horizontal building strains following from the numerical and analytic results

Criterion	LTSM – foundation level (%)	Relative Stiffness – foundation level (%)	Linear model - E=1000MPa (%)	Non-linear model (%)
Deflection ratio $\frac{\Delta}{L}$	0,031	0,005	0,000	0,005
Maximum horizontal strain $\varepsilon_{h,max}$	0,091	0,014	0,001	0,09
Damage Class[2]	2 - Slight	2 - Slight	0 – Negligible	0 – Negligible

The analytic results are consistent with the numerical results. The Relative Stiffness-results and the non-linear model show great resemblances. The identified strains at the top of the façade are consistent with the results following the use of relative stiffness method. However, local peak values exceed the values obtained from the relative stiffness method and are comparable to the results from the LTSM. This is the result of the LTSM neglecting the building stiffness and taking perforation of the façade into account in combination with the conservative material parameters assigned to the building in the non-linear model. This lead both results to be dominated by the soil deformations without adding significant stiffness to the subsoil.

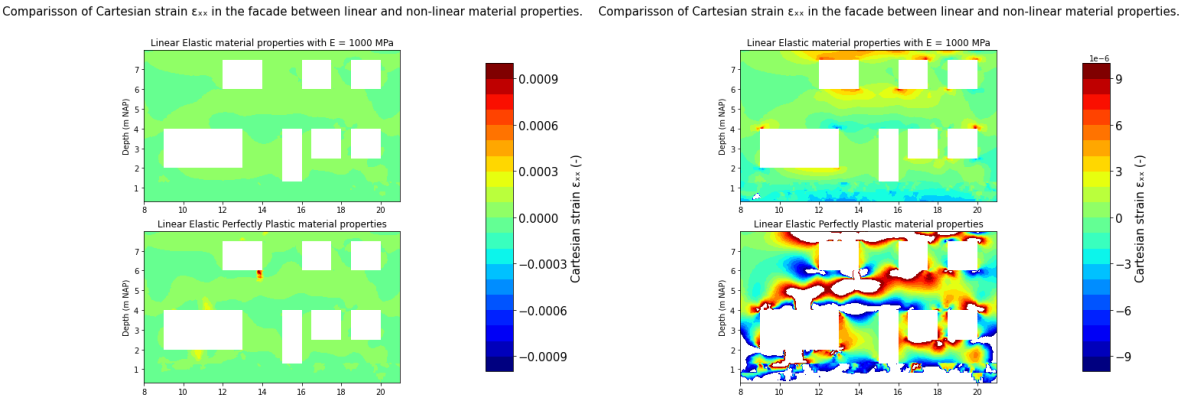

Figure 6-13 Comparison of horizontal strain between the linear elastic and non-linear model with different scales

[2] Associated damage level according to Boscardin et al. (1989) (Table 3-1)

The numerical results from the model with linear elastic material properties and non-linear material properties are both presented in Figure 6-13. The overall shape of the strains are fairly similar. However local peaks differ significantly. This could be assigned to the lower strength used in the non-linear model and the low strength used to account for the joints.

The relative stiffness method takes into account the building stiffness and the stiffness of the subsoil. The modification factor for the horizontal strain already revealed that the building stiffness is significantly larger than the soil stiffness, resulting in modification factor equal to 0. This implies that no horizontal strain in the subsoil is to be transferred to the building. The modification factor for bending is rather small (0.15). This is the result of the relation between the building stiffness and the average soil stiffness, giving a rather stiff response of the building to the soil deformation. The numerical models with linear elastic material parameters gave also stiff results.

The strains following from the relative stiffness method are about 10 times as high as the strains from the linear elastic numerical models. This could be due to the sensitivity of the relative stiffness method. The graph which determines the modification factor has a certain spread. For this calculation only the best fit is selected to determine the building deformations and strain. The numerical results using non-linear material properties resemble the results from the relative stiffness method in general. The strains at the top of the façade are found to be around 0.015%. However, local peaks are observed using numerical modelling that surpass the strains following from the relative stiffness method resembling the results using LTSM. The use of linear elastic material properties in the numerical model has shown to be limited in its reliability due to the magnitudal difference in result compared to the other methods.

When comparing the results from the relative stiffness method and the numerical model with non-linear material properties it becomes clear that the relative stiffness method is still rather conservative. Although, similar material properties are used in both models for modelling the difference in result is large (factor 10). This could be due to the fact that the proposed modified relative stiffness method by Goh (2010) is derived for shallow foundations and this case regards a piled foundation. For the analytic calculations solely the settlements of the foundation layer are used. Although, the piles are assumed to be predominantly end-bearing, influences of the upper soil layers are expected. In this case the deflection of the base of the façade would diminish. The foundation layer induces a hogging settlement mode and at surface level a sagging settlement mode is observed. this should result in less hogging or sagging at the base of the building as both the foundation layer and surface counteract each other, resulting in mainly tilt and less overall strain.

7 CONCLUSION & RECOMMENDATIONS

Over the past decades an increase in underground construction is observed. Deep excavations are among the structures used for underground construction. The construction of such structures often affect nearby existing structures and causes possibly even damages.

2D integrate numerical modelling could be a useful solution for assessing building damage next to deep excavations.

7.1 RETURNING TO THE RESEARCH QUESTIONS

This section aims to formulated the answers on the questions identified in Section 2.2 based on the performed research.

1. ***What is the state of the art of predicting building deformations?***
   The prediction of these damages are usually done by following these steps:
   a. Determining the free-field ground displacements
   b. Imposing the displacements on the structure
   c. Determining the deformations of the structure
   d. Assess potential damages following these deformations

   The ground and the structure are often modelled separately taking no (LTSM) or a factor (Relative Stiffness Method) into account for interaction between soil and structure. Taking no interaction into account is especially conservative when looking at vertical displacements. Also, the non-linear behaviour of structural elements is neglected by these methods. This could lead to errors when assessing deformations of a masonry building due to the extreme non-linear behaviour of masonry structures.

2. ***What are important parameters in modelling piled foundations using 2D Finite Element Analysis?***
   Based on the analysis performed in Section 4 the load on the pile is the dominant factor determining the vertical displacements of the pile relative to the soil around the pile. An increase in load leads to an increase in settlement of the pile. Increasing the load has led to an increase in displacement of 8mm relative to an unloaded pile and 12mm relative to free-field vertical soil deformations. These deviances amount to an increase of roughly 80% and 50% respectively. increasing the load on a pile has also led to increased horizontal deformations of the pile. The difference could amount to 4 mm, which is roughly a 25% increase or decrease. Varying the diameter and stiffness has had a negligible influence on horizontal pile displacements relative to the free-field soil deformations (smaller than 1 mm). However, these parameters do influence the vertical deformations of the pile. The deviation could reach up to 4 mm. This amounts to a difference of 30~50%.

3. ***How do foundation loads and or building stiffness impact soil deformations next to deep excavation?***
   Grouped uncoupled piles stiffen the soil surrounding the piles. This effect increases when the piles are coupled by a structure. There is more interaction between the different soil layers leading to the soil body around the pile group to act more like single element. This has led to decrease in settlement of 20%. Increased distortion in the subsoil on the other hand has led to an increase of deformation of roughly 40% at surface level. The presence of piles allows for the transfer of stress and even deformations over the length of the foundation. Loading on a

structure results in additional load on the subsoil. This load is partially transferred to the retaining wall, increasing the deflection and therefore overall soil deformations. The inclusion of a pile foundation in the soil has led to a decrease in horizontal displacement at the pile head of around 2mm (10~20%). Including stiffness between the piles in the form of a building has increased the rigidity leading to a decrease in horizontal displacement at surface level of around 4mm (20~30%). This is mainly the results of reduced freedom of motion between the pile heads, reducing the possible relative displacements between the piles.

4. ***What are the forces acting on a building foundation during every excavation step?***
   The forces acting on a building foundation are composed of the load induced by the structure on top of the foundation and the forces induced by the soil on the foundation. Generally, the load form the structure on a piled foundation could be assumed to be evenly distributed over the supporting piles. This changes as differential settlement of the piles occurs. Piles that are moving away from the structure starts to carry less load. This difference is than redistributed over the remaining piles. These differences increase with increasing differential settlement of the piles. Differential settlement of the ground also leads to differences in loads on a foundation. Increased soil deformation leads to increased skin friction (until a certain threshold, often 10mm difference between soil and pile). This occurs especially when a pile row is orientated perpendicular to the excavation as differential settlement occurs especially in this plane.

5. ***What is possible in modelling masonry buildings into PLAXIS and how do these compare?***
   Two main possibilities have been identified to use a masonry model in PLAXIS. A linear elastic and a non-linear (linear elastic perfectly plastic) model are available material models. Modelling a masonry building with linear elastic material properties could be risky due to masonry's extreme non-linear behaviour. Given that the strains are small, a linear elastic material model could give reliable first estimation. The non-linear material model is a user defined model based on an soil model. The model is able to incorporate the shear and tensile strength of the masonry elements. This leads to improved representation of the expected failure patterns. This is observed in Section 6, where the strains using the linear elastic material model were underestimated. The non-linear model describes a more realistic strain development and subsequential damages. Therefore, the non-linear material model enables a better and more detailed simulation of the behaviour of the masonry structures.

6. ***How do the numerical and analytical models compare to real data?***
   Comparing the numerical results with the analytic results showed that the analytic method are conservative. The use of numerical modelling also gave differing results depending on the used material model for the masonry elements. The linear elastic material model showed a relatively stiff response, resulting in significantly small strains in the façade (0.001%). This amounts to no damage. The use of a non-linear material model has resulted in significantly larger strains in the façade (0.09%, slight damage). The results obtained, using the non-linear material model are in line with the results from the analytic calculations. The observed strains at the top of the façade are in line with the results obtained using the relative stiffness method (0.01-0.02%, negligible damage). However, local peak values around perforations in the façade exceed these values, reaching up to 0.09%. These peak values indicate local cracks occurring.
   The relative stiffness method does not take perforation of the façade into account. The LTSM does take perforation into account. Using the LTSM has resulted in strains up to 0.091%, which

are similar to the strains observed in the numerical model with non-linear material properties and implying slight damages in the façade. The overall deformation following from the numerical calculations have been validated using measurement data and found to give a good representation. The analytic calculations have been based on the numerical result of the free-field soil deformations, which also have been validated using measurement data.

As for the main research questing which is stated below:

"What are the important parameters for predicting building deformation next to deep excavations using integrated 2D numerical modelling?"

The answer is presented below:

Integrated numerical modelling could be a viable option for future projects ware building damage is prediction next to deep excavation. This study has shown that it is possible to do damage assessment using an integrated 2D numerical model. Although, the results are similar to the more accessible analytic models, integrated modelling could be very helpful in future projects. The numerical model has given similar results to the analytic models. The analytic methods present an absolute value for the expected strains, but fail to identify possible local weak points within a structure. This is where integrated numerical modelling could be a helpful method to identify these weak spots within a structure and allow to take measures on time. Because it is less time consuming than the frequently used decoupled numerical modelling of structures. The important factors in modelling such projects are first and foremost reliable soil deformations. The settlement of the deeper soil layers beneath structures founded on deeper soil layers can not be overlooked. The interface between the foundation and the structure is important, together with the correct description of the behaviour of the foundation in the subsoil. In the case of a piled building the horizontal constraint of the pile head needs to be identified and whether or not tension is transferred. Lastly, the shape and material parameters of the structure are of importance as these are the most important parameters in describing the behaviour of the building as a response to induces by the foundation.

7.2 RECOMMENDATIONS

7.2.1 Experimental modelling:

Experimental modelling could be used to model the mechanisms involved during excavatory works next to piled structures. Different scales, geometries, material parameters and settlement profiles could be modelled. This could help the validation of the integrated numerical models and identify necessary adjustments to the numerical models.

7.2.2 3-Dimensional approach:

Integrated numerical modelling could be applied in three-dimensional models. At the edges of an excavation the problem is particularly three-dimensional as biaxial differential settlement occurs. Integrated numerical modelling could become helpful tool in modelling these kinds of situations. A study should be conducted to identify the possibilities of using an integrated numerical modelling in these types of situations

7.2.3 Integrated modelling of piled building next to tunnelling:

Building deformation are not solely a problem next to deep excavation. Tunnelling underneath structures could also lead to damages to these structures. The assessment of these damages are also dominated by uncoupled methods. The possibility of using integrated numerical modelling for buildings close to tunnel construction should be analysed.

…

REFERENCES

(BRE), B. R. (1981; revised 1990). *Assessment of damage in low rise buildings with particular reference to progressive foundation movements.* Garston: BRE.

Albers, B. (2012). *2D Numerical Analysis of Settlement Damage to Buildings: Including a non-linear Masonry Model and Soil-structure Interface .* Delft: TU Delft.

Amorosi, A. B. (2018). Analisi geotecnica e strutturale del Ninfeo di Genazano. *Rivista Italiana di Geotecnica*, 49(1), 29-44.

BEK, M. S. (2018). *Modelling piles in FEM-Design.* Gothenburg: CHALMERS UNIVERSITY OF TECHNOLOGY.

Brassinga, O. O. (2009). *Predicted and measured settlements due to installation and removal of sheet piles .* Rotterdam: Rotterdam Public Works.

Bull, J. W. (2001). *Computational Modelling of Masonry, Brickwork and Blockwork Structures.* Saxe-Coburg Publications.

Burland, J. a. (1974). Settlements of buildings and associated damage. *State of the art review.* Cambridge: Pentech Press.

Burland, J. B. (1975, January). Settlement of Buildings and Associated Damage.

Burland, J. B. (1977, January). Behaviour of foundations and structures.

Chieh-Wen Sun, C.-T. C. (sd). *Prediction of Ground Settlements Due to Deep Excavations.*

Clough, G. a. (1990). Construction induced movements of in-situ walls. *ASCE Geotechnical special publication No.25 – Design and Performance of Earth Retaining structures*, 439-470.

COB, D. &. (2011). *Data set Vijzelgracht Station.* NoordZuidlijn: COB.

Cording, M. D. (1989, January). Building Response to Excavation-Induced Settlement. *Journal of Geotechnical Engineering*.

Delfgaauw, S. B. (2009). Jet Grout Strut for Deep Station Boxes of the North/South Metro Line Amsterdam - Design and Back Analysis. Budapest, Hungary: Proceedings ITA world conference.

Dhanjal H.S., T. P. (2001). Building settlement on the Copenhagen metro project. *Proc. of Int. Conf. at Imp. Coll. of London.* London.

Everaars M.J.C., P. M. (2013). Finite Element Modelling of D-wall Supported Excavations. *Proceedings of the 18th International Conference on Soil Mechanics and Geotechnical Engineering, Paris 2013.* Paris: Grontmij Nederland BV.

F531, D. &. (2011). *Soils, Buildings and foundations in Amsterdam, Background information for Dataset NoordZuidlijn.* NoordZuidlijn: COB.

Frankenmolen, S. (2006). *Analyse Noord/Zuidlijn monitoringsdata - Effecten van de beïnvloeding van de Holocene Laag op het zettingsgedrag van vooroorlogse panden .* Delft: TU Delft.

Franzius, J. (2003). *Behaviour of buildings due to tunnel induced subsidence.*

Giardina, G. (2013). *Modelling of settlement induced building damage.* Delft : TU Delft.

Goh. (2010). *Response of ground and buildings to deep excavations and tunnelling.* UK: Cambridge University.

Horatiu Popa, L. B. (2010). study, Using Finite Element Method in geotechnical design. Comparison between soil constitutive laws and case. *Proceedings of the 3rd WSEAS Int. Conference on FINITE DIFFERENCES - FINITE ELEMENTS - FINITE VOLUMES - BOUNDARY ELEMENTS.* Bucharest: Technical University of Civil Engineering of Bucharest.

Hsieh, P. G. (1998). Shape of ground surface settlement profiles caused by excavation. *Canadian Geotechnical journal*, pp. 1004-1017.

Korff, M. (2009). *Deformations and damage to buildings adjacent to deep excavations in soft soils.* Delft: Deltares.

Korff, M. (2013). *Response of piled buildings to the construction of deep excavations.* Cambridge: University of Cambridge.

Korff, M., & Tol, F. A. (sd). Failure cost analysis of 50 deep excavations in The Netherlands.

Korff, M., Mair, R. J., VanTol, A., & Kaalberg, F. (2012). *The response of piled buildings to deep excavations*. Opgeroepen op 10 15, 2019, van http://issmge.org/images/joomd/tc204/2011_108.pdf

Kunst, D. (2017). *Modelling construction phases of bored tunnels with respect to internal lining forces - A comparison of fiite element programs.* Delft: TU Delft.

M. Boonpichetvong, H. N. (2006). *Numerical analyses of soil-foundation-building interaction due to tunneling.* Delft: TU Delft.

M. Minno, R. P. (2015, Sptember). Finite element modeling of a piled raft for a tall building on cohesionless soil.

Mitew-Czajewska, M. (2017). FEM modelling of deep excavation – parametric study, Hypoplastic Clay model verification .

Moorman, C. a. (2002). A study of wall and ground movements due to. *Proc. 3rd intern. symp. on Geotechnical Aspects of Underground Construction in Soft Ground, Toulouse.* Lyon.

Netzel, H. (2009). *Building response due to ground movements.* Delft: TU Delft.

O'Rourke, T. (1993). Base stability and ground movement prediction for excavations. In T. Telford, *Retaing Structures* (pp. 131-139). London.

Ou C.-Y., T. F.-C.-G.-C. (2013). Mechanism of Settlement Influence Zone due to Deep Excavation in Soft Clay. *Proceedings of the 18th International Conference on Soil Mechanics and Geotechnical Engineering, Paris.* Paris.

Pallavi Ravishankar, D. D. (sd). *Finite Element Modelling to Study Soil Structure Interaction of Assymmetrical Tall .*

Peck, R. (1969). Deep excavations and tunneling in soft ground. *Proc. 7th International Conference on Soil Mechanics and Foundation Engineering.* Mexico City: Sociedad Mexicana de Mecanica de Suelos, A.C.

Pickhaver, J. (2006). *Numerical modelling of building response to tunneling.*

Plaxis 2D Reference Manual. (sd).

PLAXIS-UDSM Masonry model. (sd).

Pluijm, R. v. (1997). *Non-Linear Behaviour of Masonry under Tension.*

Potts, & Addenbrooke. (1997). *A structure's influence on tunnelling-induced ground movements.*

Raijmakers, T. (1995). *Eigenschappen metselwerkvan rond 1900.*

Schipper, F., Visser, A., & Wieser, W. (2011, Februari). Proactieve risicobeheersing door verzekeraars Noord/Zuildlijn. *LAND+WATER*.

Son, M. a. (2005). Estimation of building damage due to excavation-induced ground movements. *SCE Journal of Geotechnical and Geoenvironmental Engineering* , pp. 162-177.

Stoel, A. v. (2003-05-23). *Parameters jet grouting stempels diepe bouwkuipen stations.*

Surjadinata, J., Hull, T. S., Carter, J. P., & Poulos, a. H. (2006, September/October). Combined Finite- and Boundary-Element Analaysis of the Effect of Tunneling on Single Piled. *International Journal of Geomechanics*.

T. Ulrich, C. N. (2011). Comparison of different numerical methodologies to derive fragility curves of RC buildings with soil-structure interactions. *Proceedings of the 8th International Conference on Structural Dynamics, EURODYN 2011.* Orleand Cedex 2, France: BRGM (French Geological Survey).

Thevaneyan K. David, R. R. (2015, May). Finite element modelling of soil-structure interaction.

Timoshenko, S. (1957). *Strength of Materials – Part I.* London, England: D. Van Nostrand Co. Inc.,.

Timoshenko, S. a. (1971). *Mechanics of materials.* Van Nostrand Reinhold Company.

Verruijt, P. d. (2006). *Numerical Geomechanics.* Delft: TU Delft.

Waarts, P. (1997). *Kans op schade aan bouwwerken door trillingen.*

Whittle A.J., H. Y. (1993). Analyses of a deep excavation in Boston. *Journal of Geotechnical Engineering*.

Whittle A.J., H. Y. (1993). Analyses of a deep excavation in Boston. *Journal of Geotechnical Engineering*, 69-90.

Whittle, Y. M. (1996, June). Ground Movement Prediction for Deep Excavations in Soft Clay. *Journal of Geotechical Engineering*.

Woods, R. I. (2003). *The application of finite element analysis to the design of embedded retaining walls.* Surrey: University of Surrey.

Yih, C. C. (2003). *Finite Element Study of Tunnel-Soil-Pile Interaction.* Singapore: National University of Singapore.

Zantkuijl, H. (1993). *Bouwen in Amsterdam – Het Woonhuis in de stad (Building in Amsterdam).* Amsterdam: Architectura & Natura.

Zhou, T. (2015). *3D FEM analysis for sequential excavation.* Delft: TU Delft.

APPENDIX A

Web-diagram

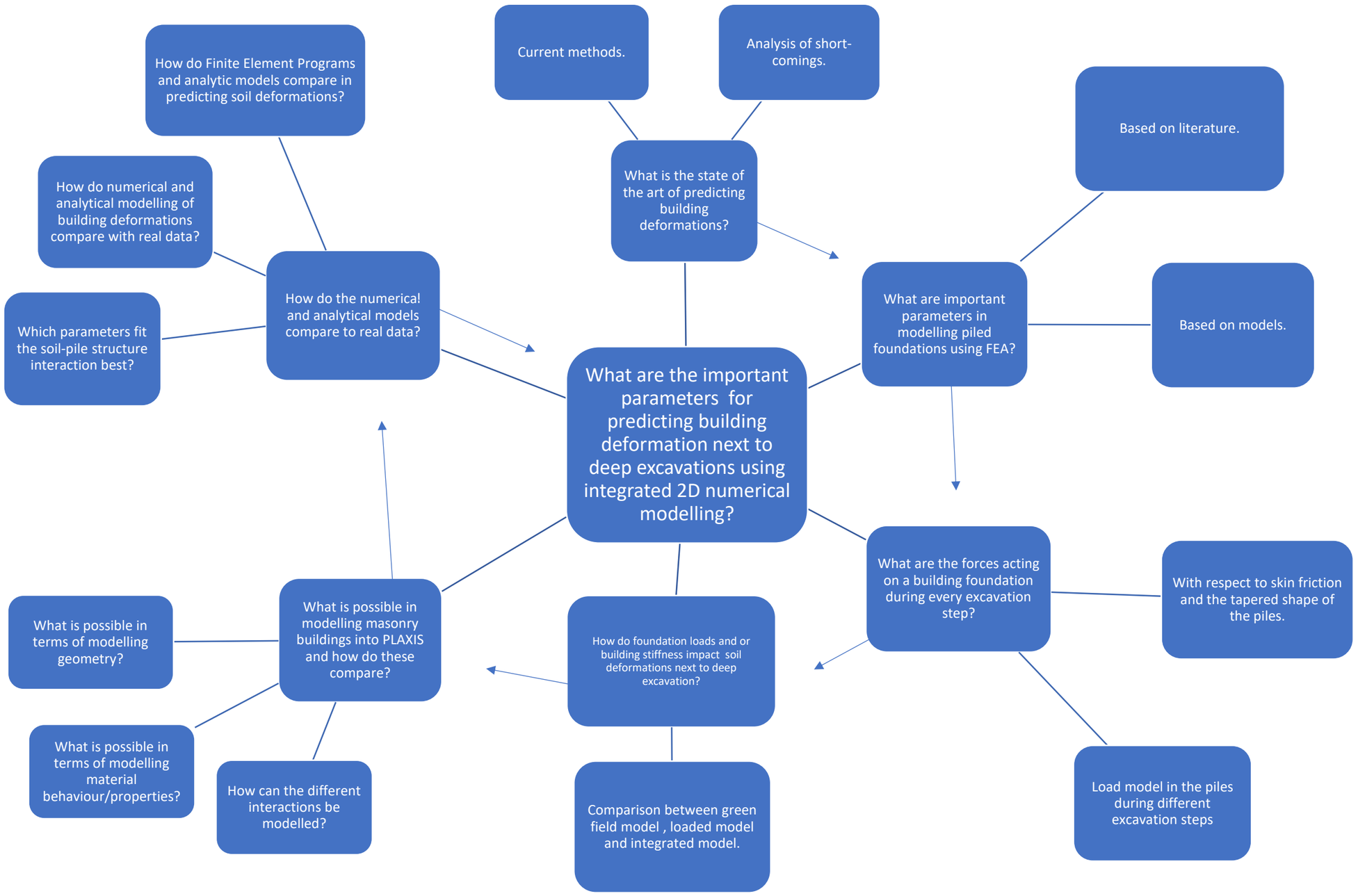

APPENDIX B

PLAXIS input

Initial phase

The start of the analysis is done right after the completion of the preliminary worked. This means that the analysis is started right before the construction of the diaphragm walls. The soil profile used is presented in Section 3.5. The water levels and piezometric levels are presented in Table 3-3.

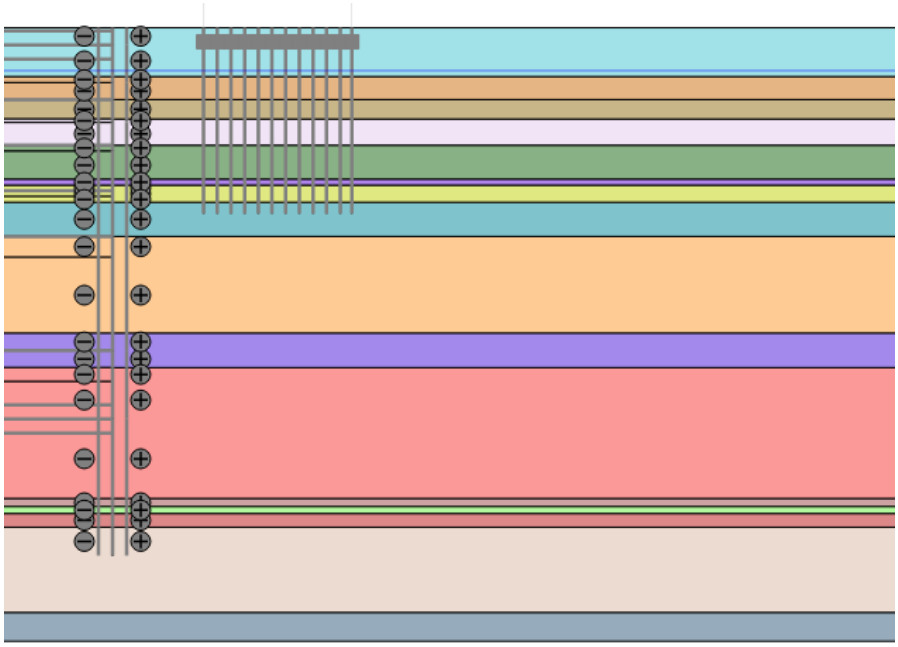

Phase 2 – Placement of the diaphragm walls

In this phase the diaphragm walls are placed. The characteristics of the diaphragm walls are presented in Table 3-4. The average values are used.

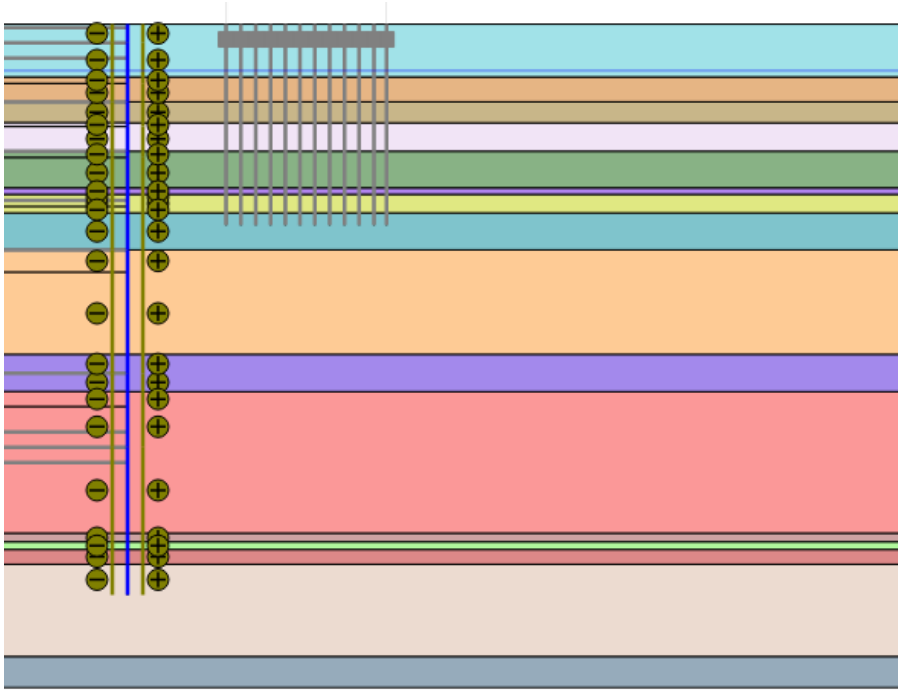

Phase 3 – Placement of grout strut

The grout strut is constructed in this phase. As shown in Figure 3-22 the grout strut doesn't have one thickness over the width of the cross-section. At the connection with the diaphragm walls the grout strut has a thickness approximately. Further from the walls the grout strut has a thickness of 1.5 m and at the centre the grout strut has a thickness of approximately 1 m. Since the construction of the grout strut is quite a difficult project the grout strut will show quite some imperfections. To simplify the grout strut characteristics the grout strut in the PLAXIS model is modelled having a thickness of 1 m. The characteristics of the grout strut are presented Table 3-10. The values presented by PIP are used since these where the characteristic that were expected to be present before construction.

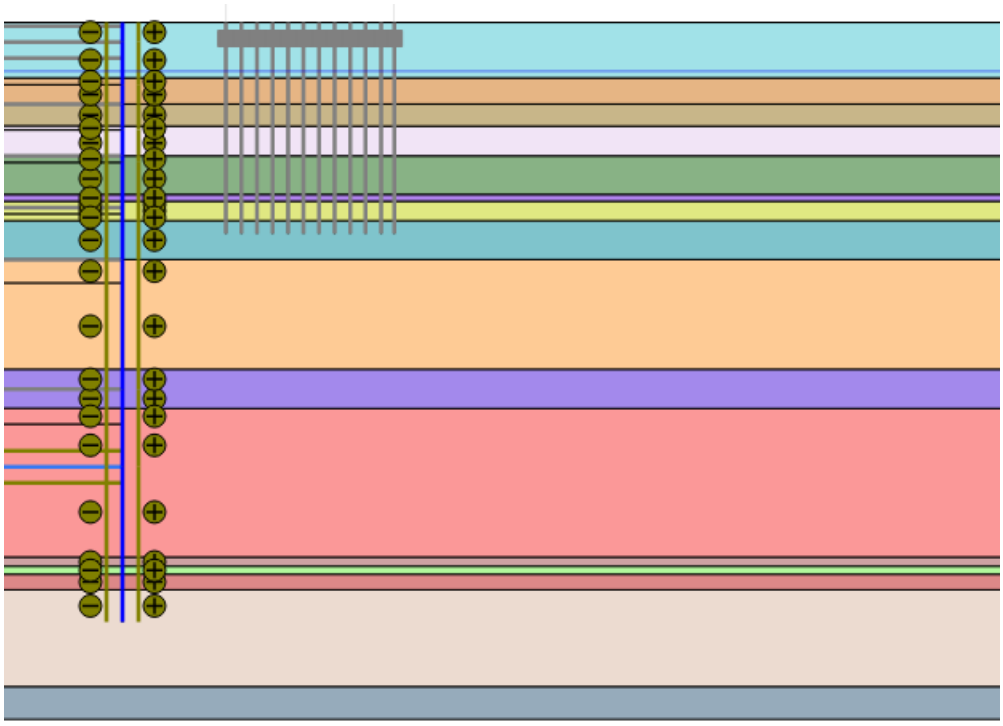

Phase 4 – Excavate to -3.0 m NAP

The building pit is excavated to -3 m NAP. Also, the water level is lowered to -3.5 m with respect to NAP.

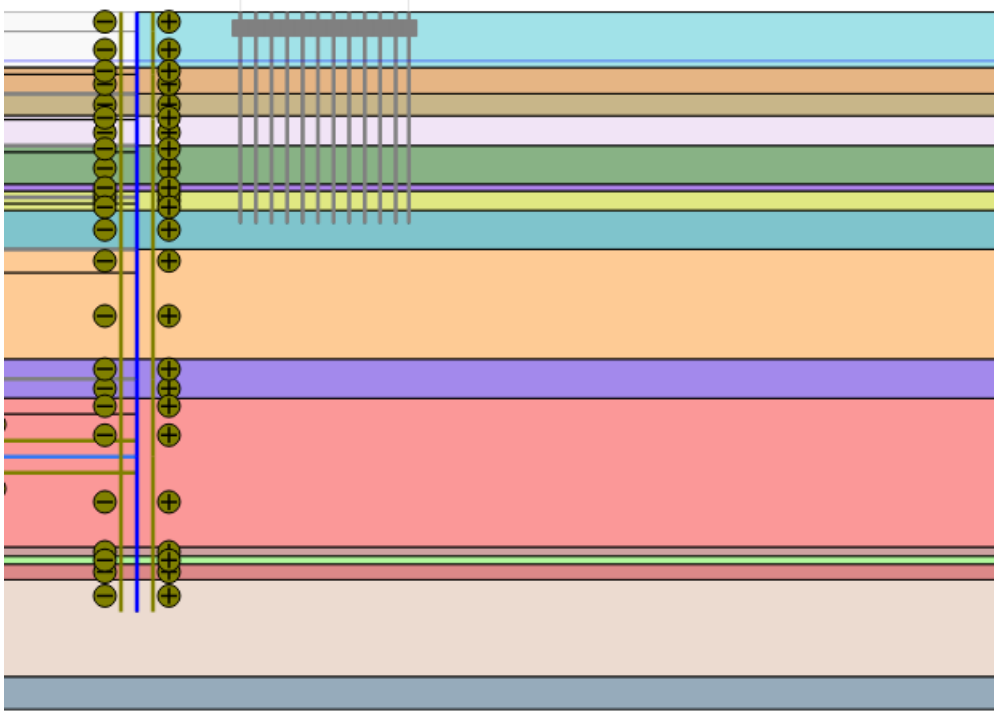

Phase 5 – Excavate to -3.5 m NAP & placement of the roof

The building pit is further excavated to -3 m NAP. Also, the water level is kept at -3.5 m in order to avoid heave. Furthermore, the roof is constructed in order to support the diaphragm walls. The roof has a thickness of 1 m and the top of the roof is situated at -0.2 m NAP. Further characteristics are presented in Table 3-9.

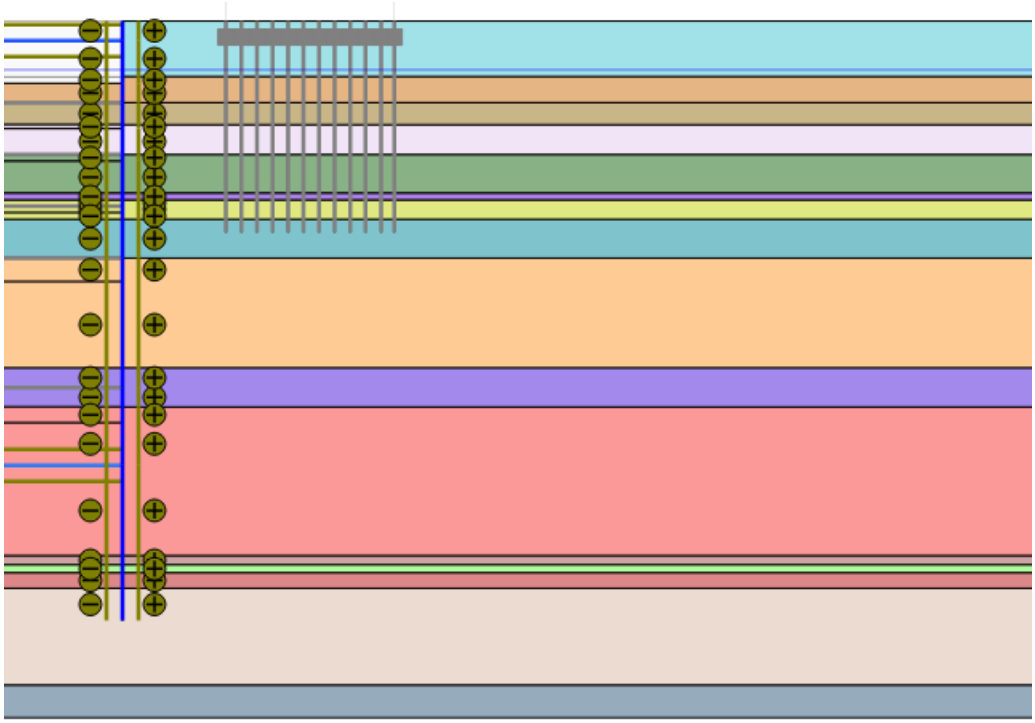

Phase 6 – Sand backfill

The roof is covered with backfill sand. The assumption is made that the original material is used as backfill.

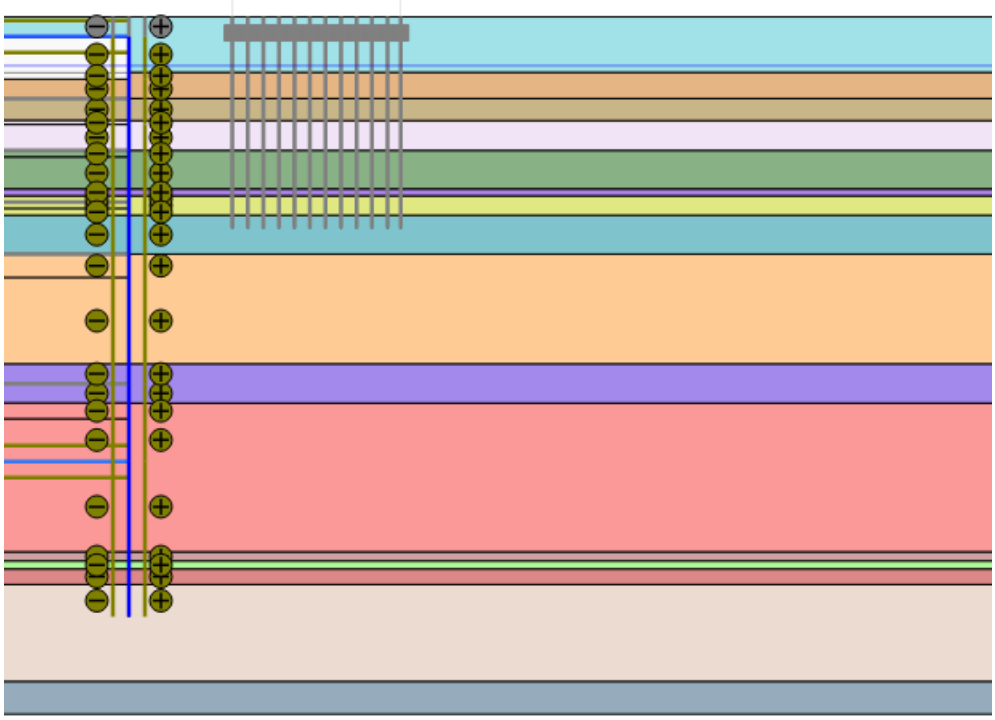

Phase 7 – Excavate to -7.0 m NAP

The building pit is excavated to -7 m NAP. Also, the water level is lowered to -11 m with respect to NAP as described in Section 3.5.

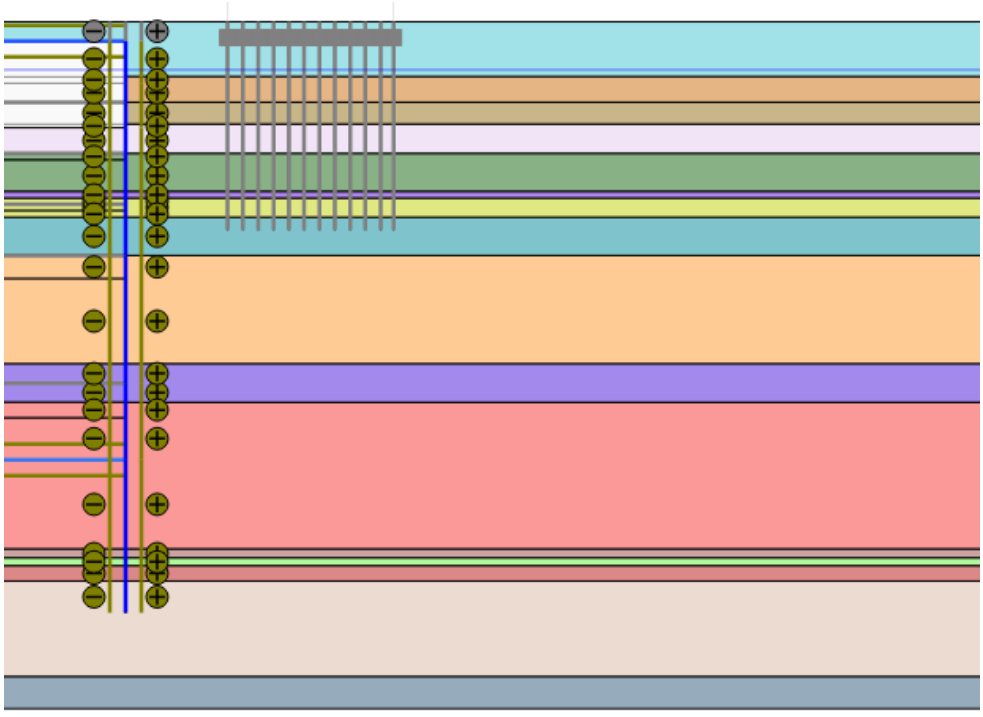

Phase 8 -Steel strut placement at -5.5 m NAP

Steel struts are placed at -5.5 m NAP and prestressed with 1000 kN/m. The distance between different struts is roughly 5 meters. Further details about the cross-sectional properties of the steel struts is presented in

Table 3-7 and details about the material used is presented in Table 3-5.

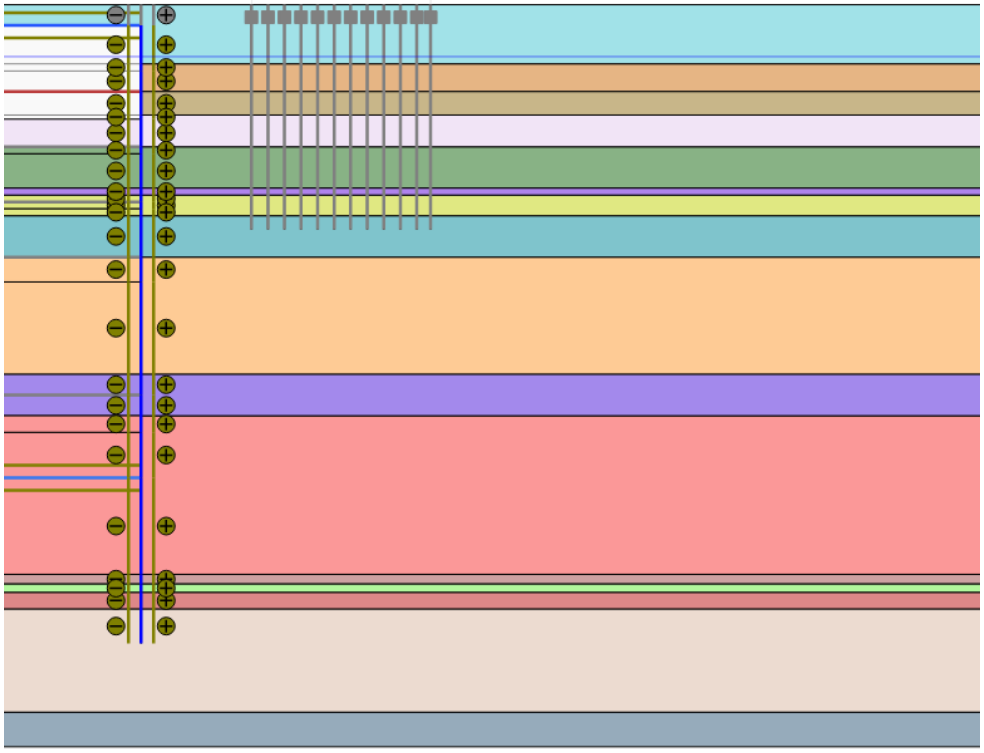

Phase 9 – Excavate to -9.5 m NAP

The building pit is excavated to -9.5 m NAP. Also, the water level is lowered to -15 m with respect to NAP as described in Section 3.5.

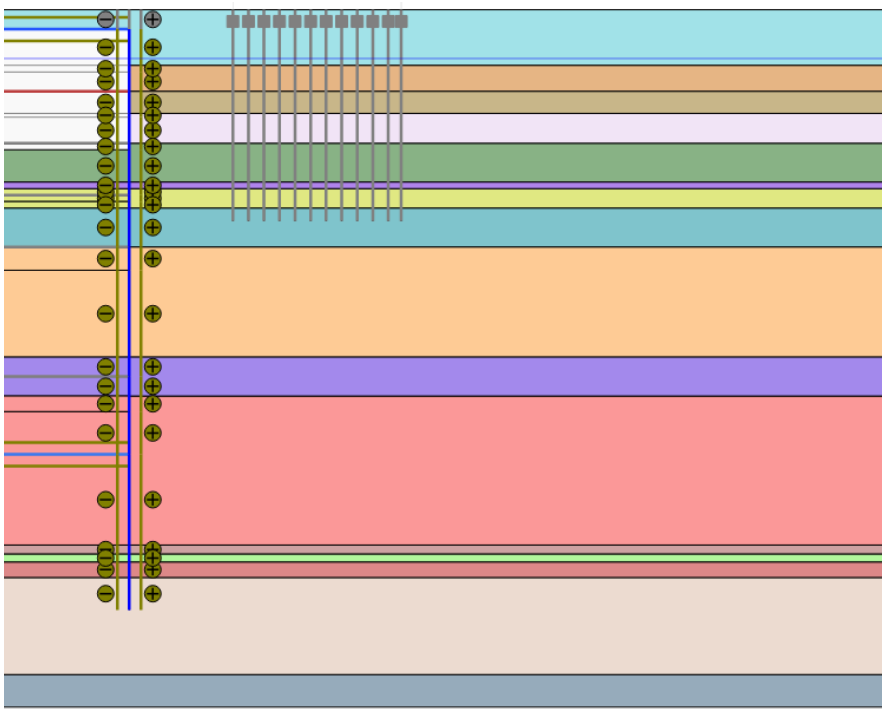

Phase 10 -Steel strut placement at -8.5 m NAP

Steel struts are placed at -8.5 m NAP and prestressed with 1500 kN/m. The distance between different struts is roughly 5 meters. Further details about the cross-sectional properties of the steel struts is presented in

Table 3-7 and details about the material used is presented in Table 3-5.

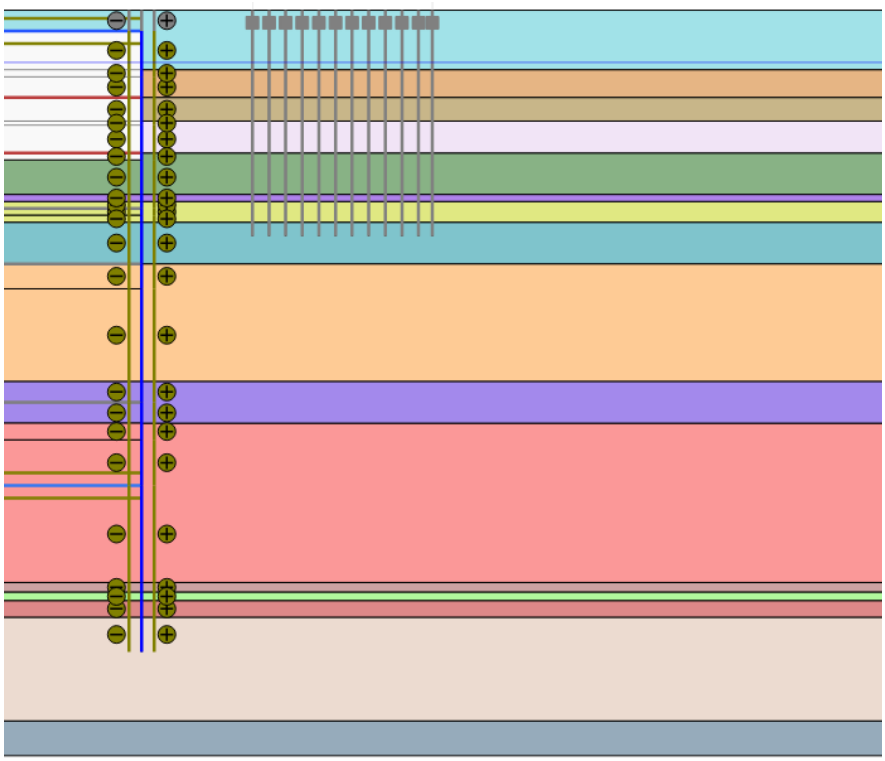

Phase 11 – Excavate to -13,5 m NAP

The building pit is excavated to -13,5 m NAP. Also, the water level is lowered to -19 m with respect to NAP as described in Section 3.5.

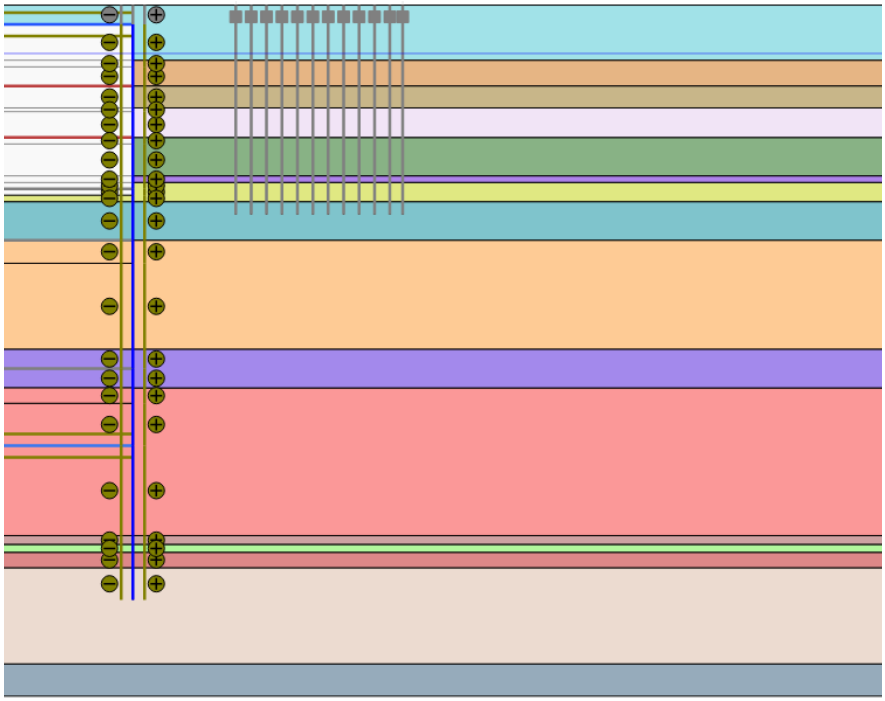

Phase 12 -Steel strut placement at -12 m NAP

Steel struts are placed at -12 m NAP. The distance between different struts is roughly 5 meters. Further details about the cross-sectional properties of the steel struts is presented in

Table 3-7 and details about the material used is presented in Table 3-5.

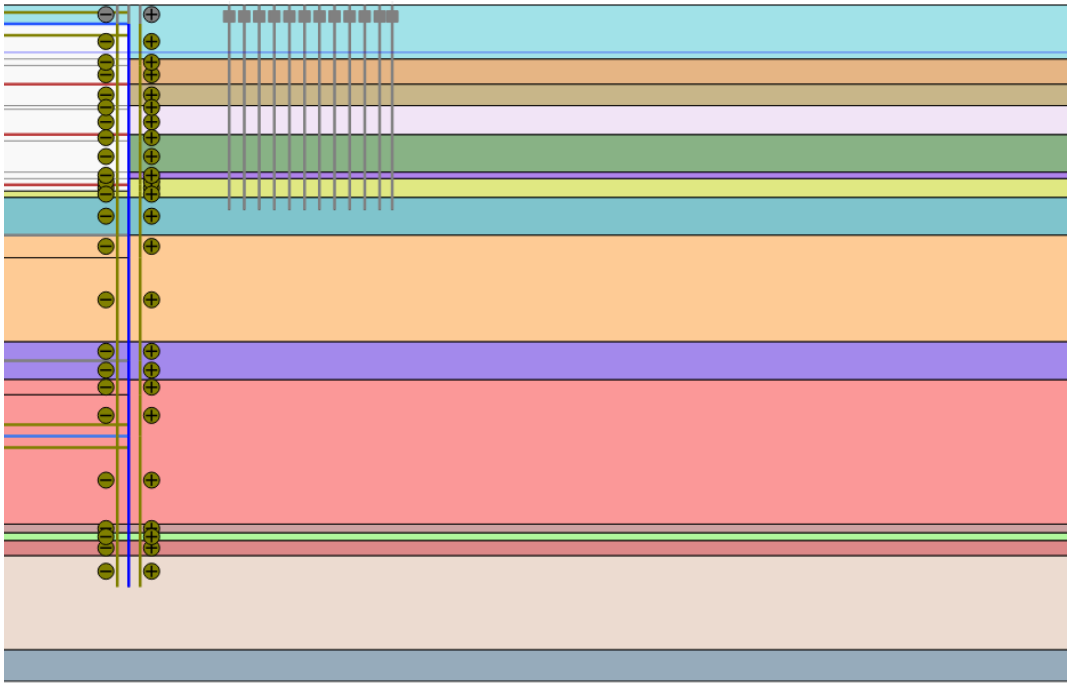

Phase 13 – Excavate to -18.8 m NAP

The building pit is excavated to -18.8 m NAP and prestressed with 1500 kN/m. Also, the water level is lowered to -25.7 m with respect to NAP as described in Section 3.5.

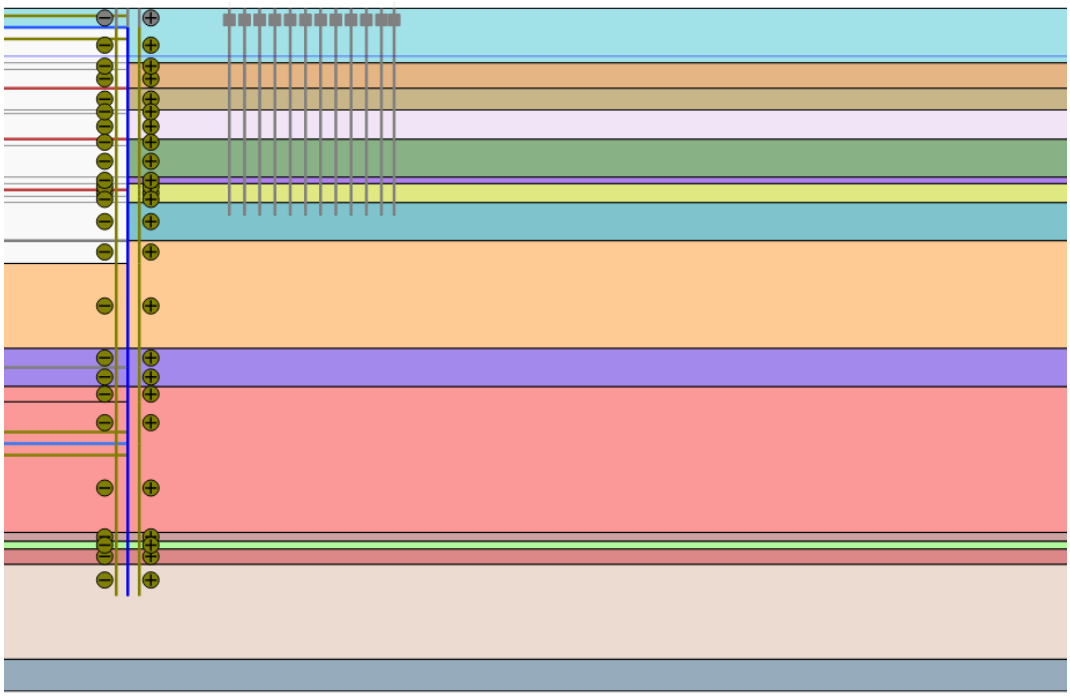

Phase 14 – Place first floor

The first floor is constructed, which also acts as a support to the diaphragm walls. The floor has a thickness of 1.5 m and the top of the roof is situated at -18.25 m NAP. Further characteristics are presented in Table 3-9.

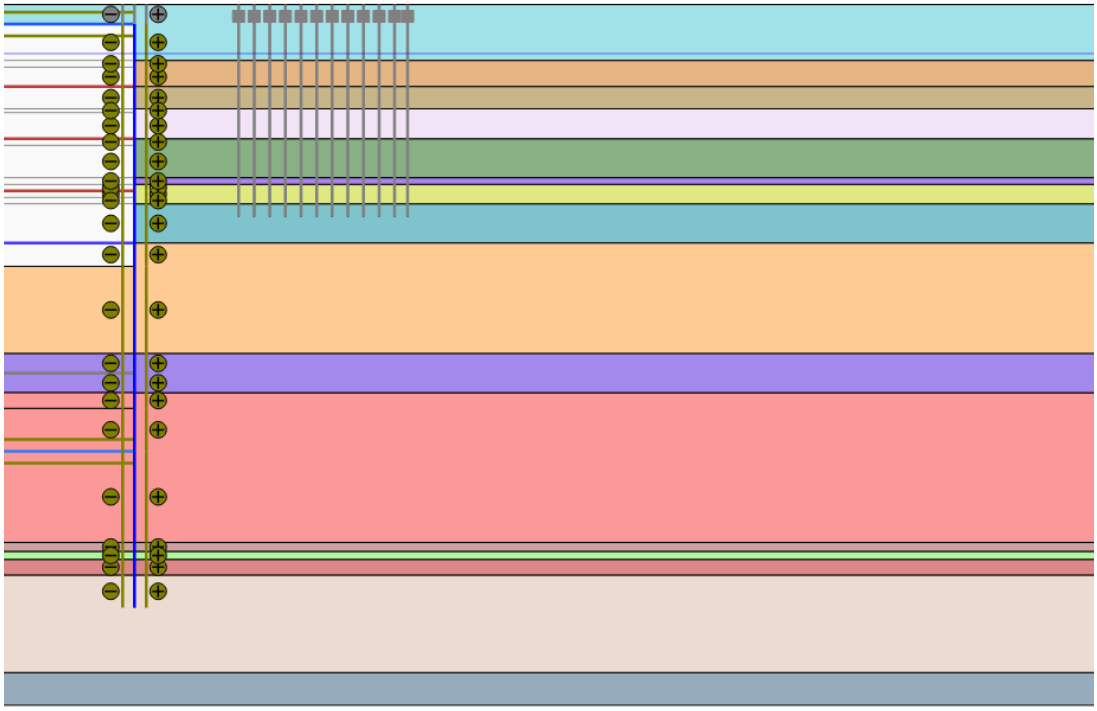

Phase 15 – Excavate to -29,7 m NAP

The building pit is excavated to -29.7 m NAP. Which is also the final excavation step.

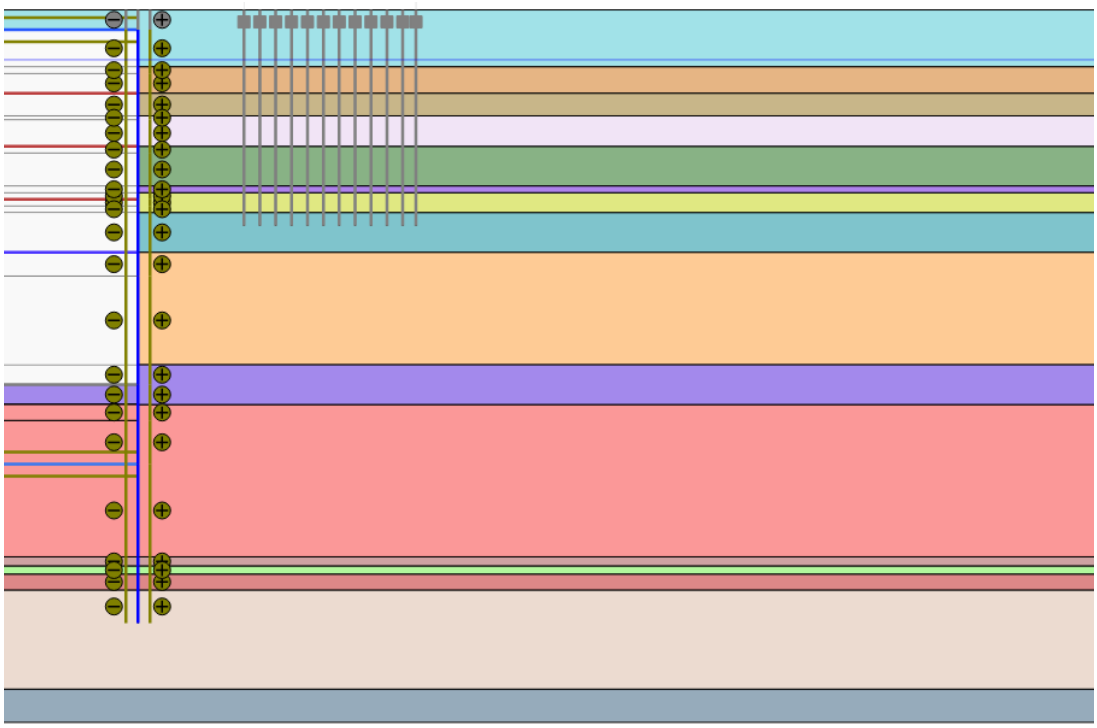

APPENDIX C

Numerical results Soil effect

Horizontal displacements

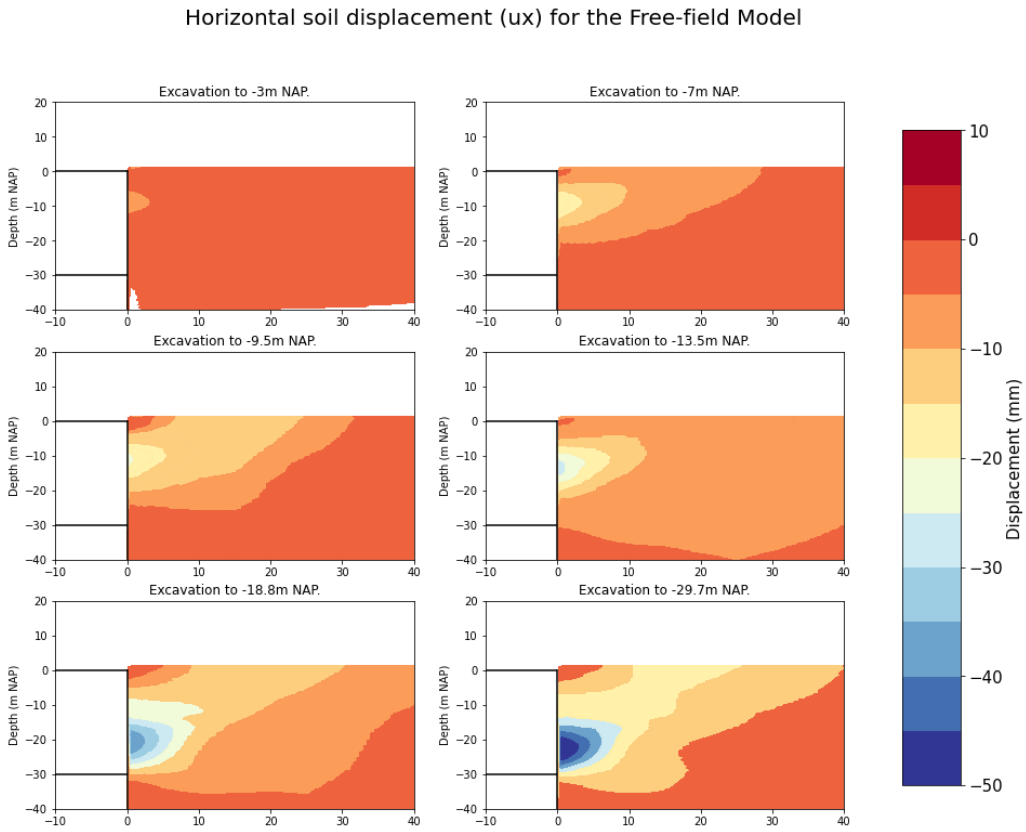

Horizontal soil displacement (ux) for the Loaded Pile Model

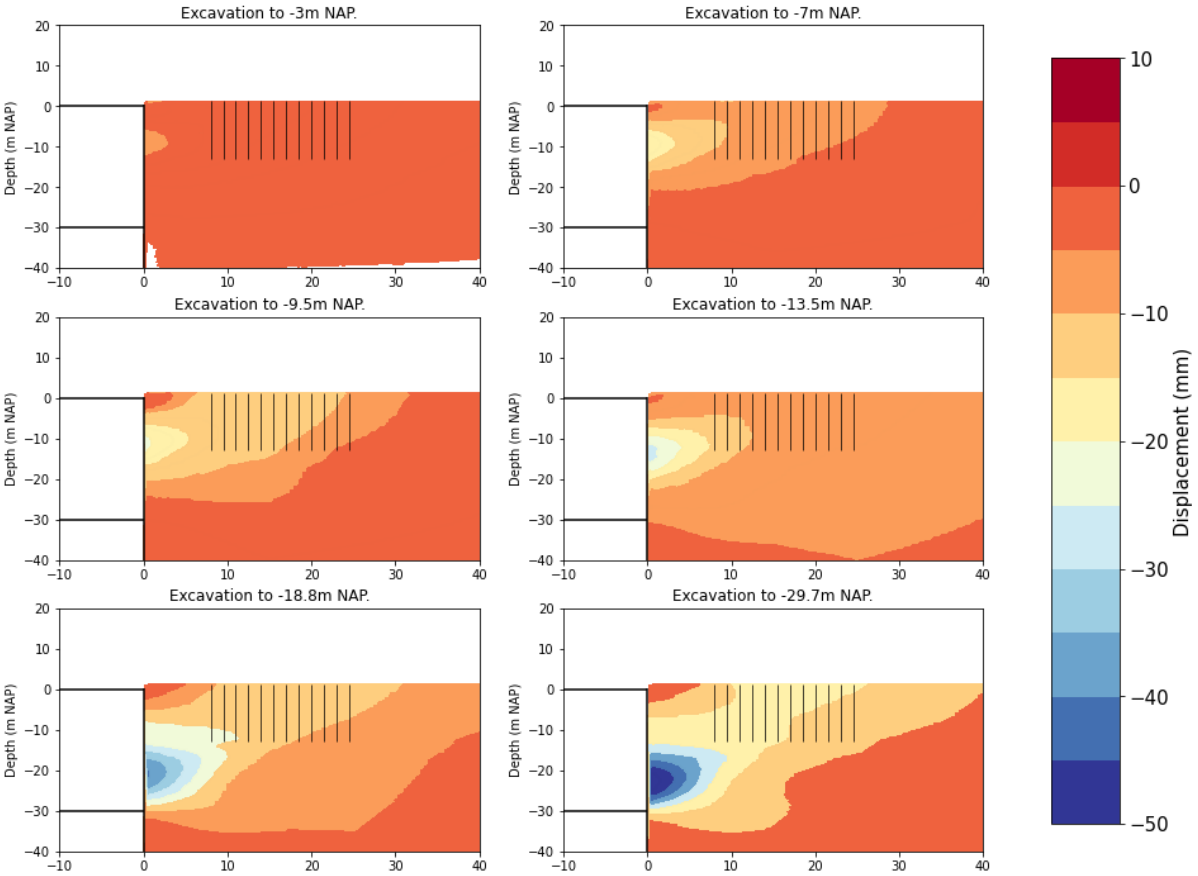

Horizontal soil displacement (ux) for the Building Model

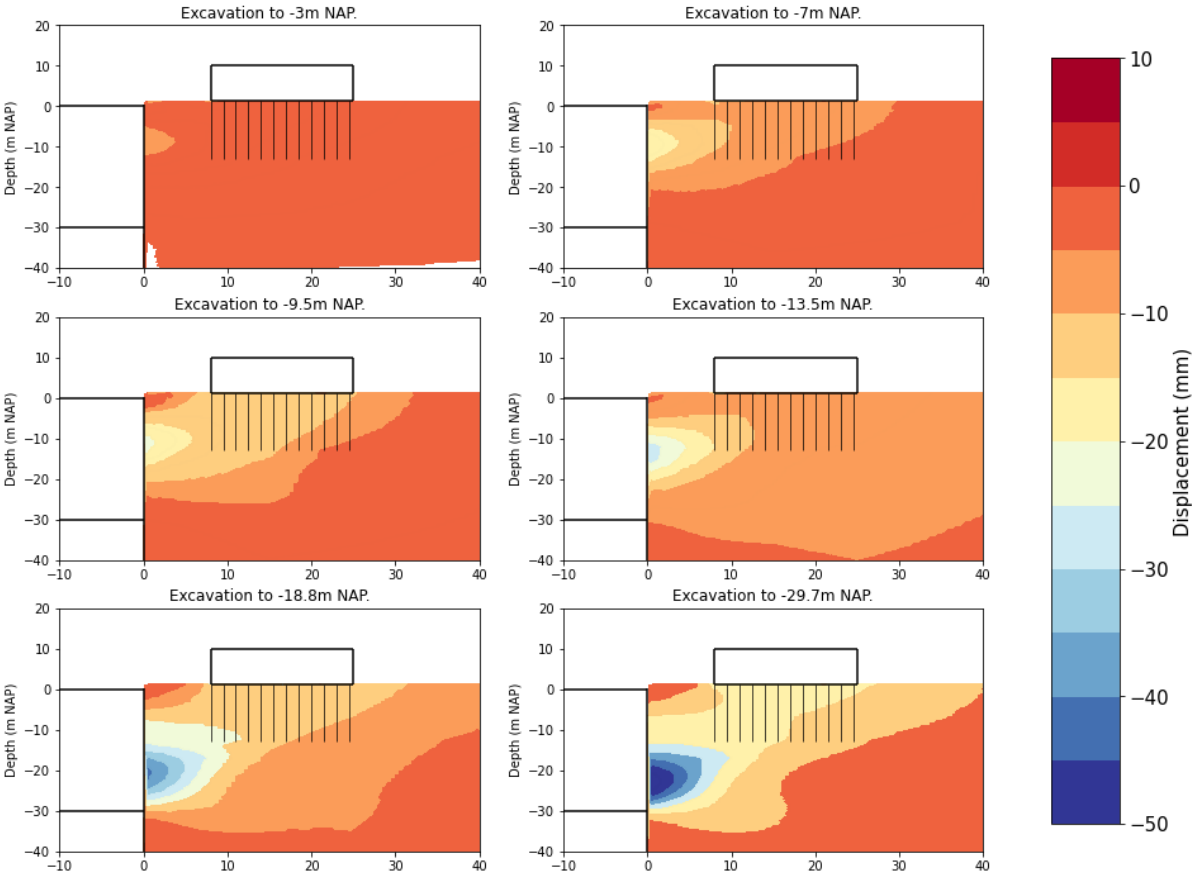

Vertical displacements

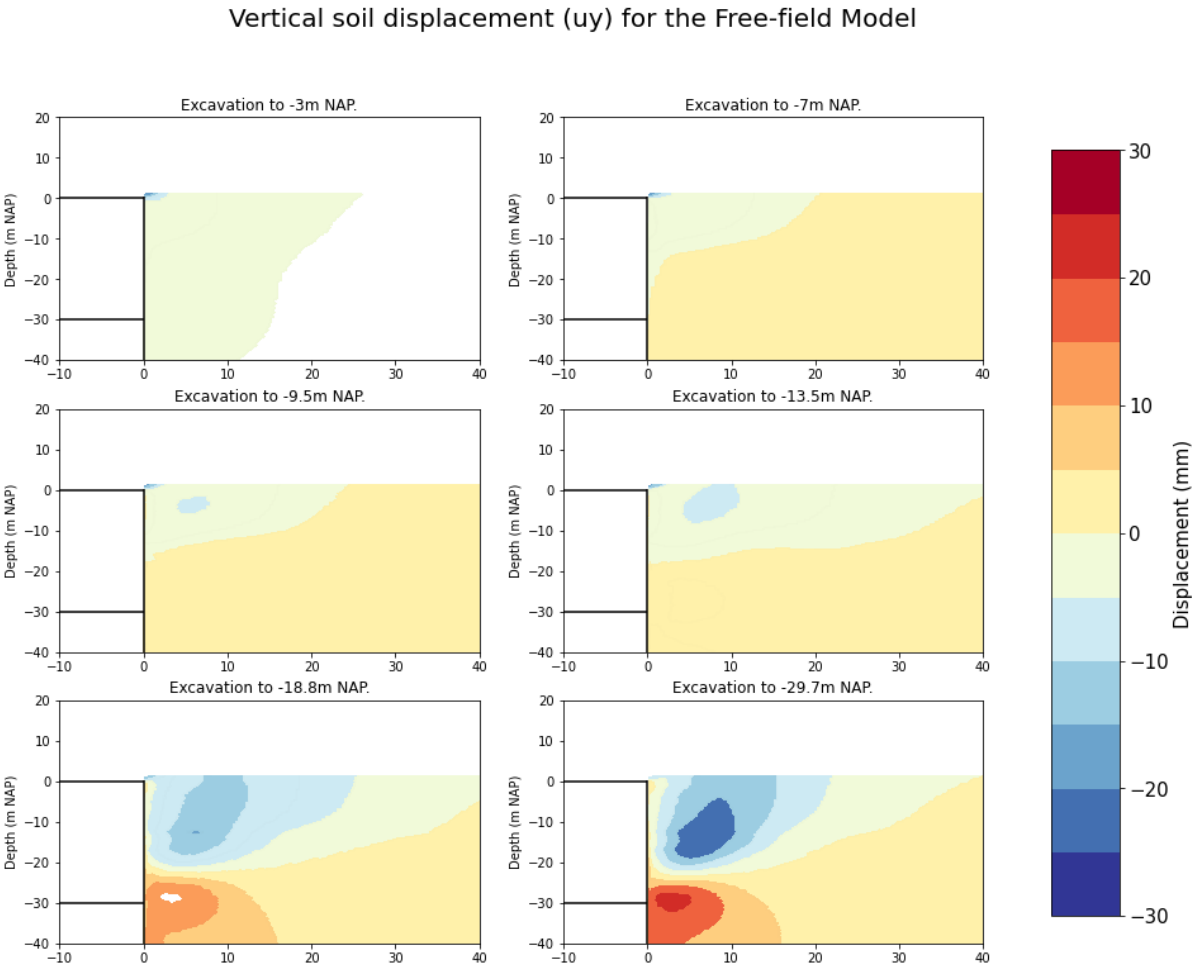

Vertical soil displacement (uy) for the Loaded Pile Model

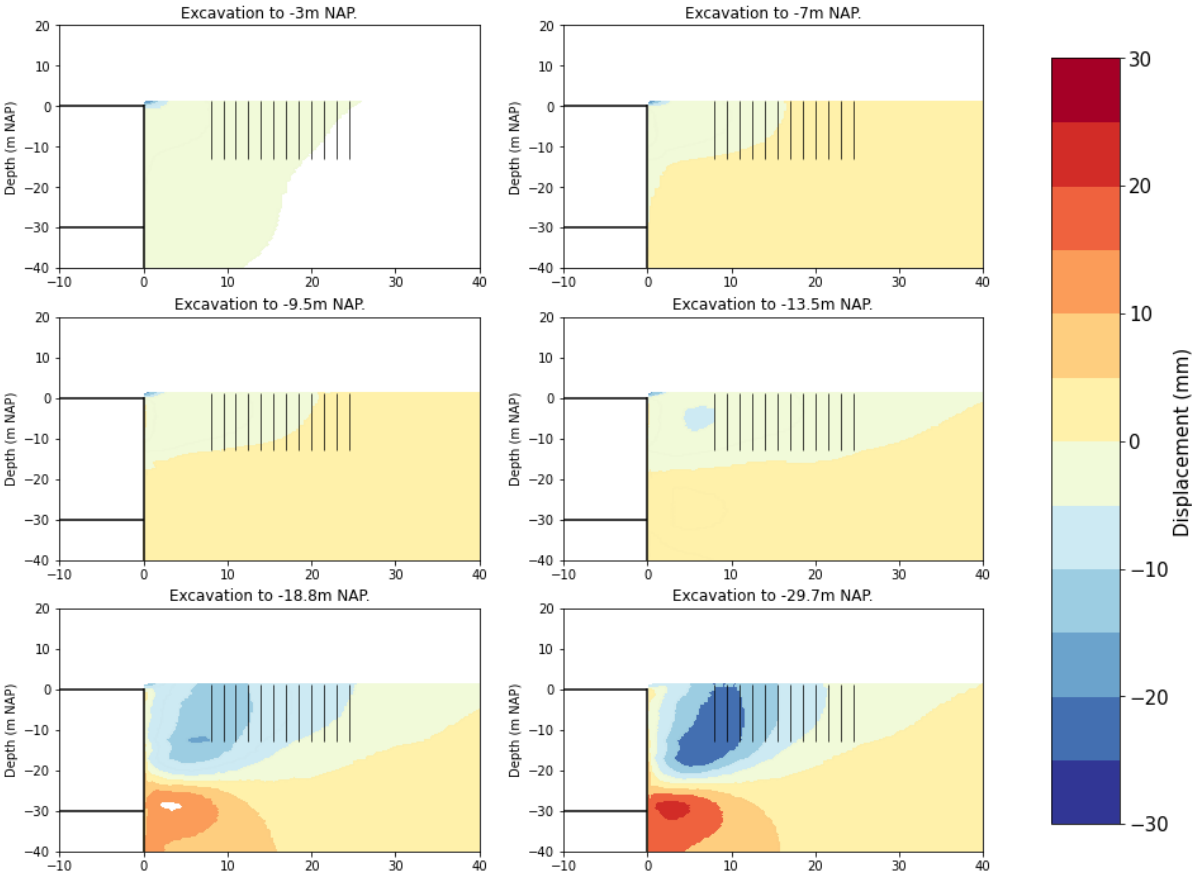

Vertical soil displacement (uy) for the Building Model

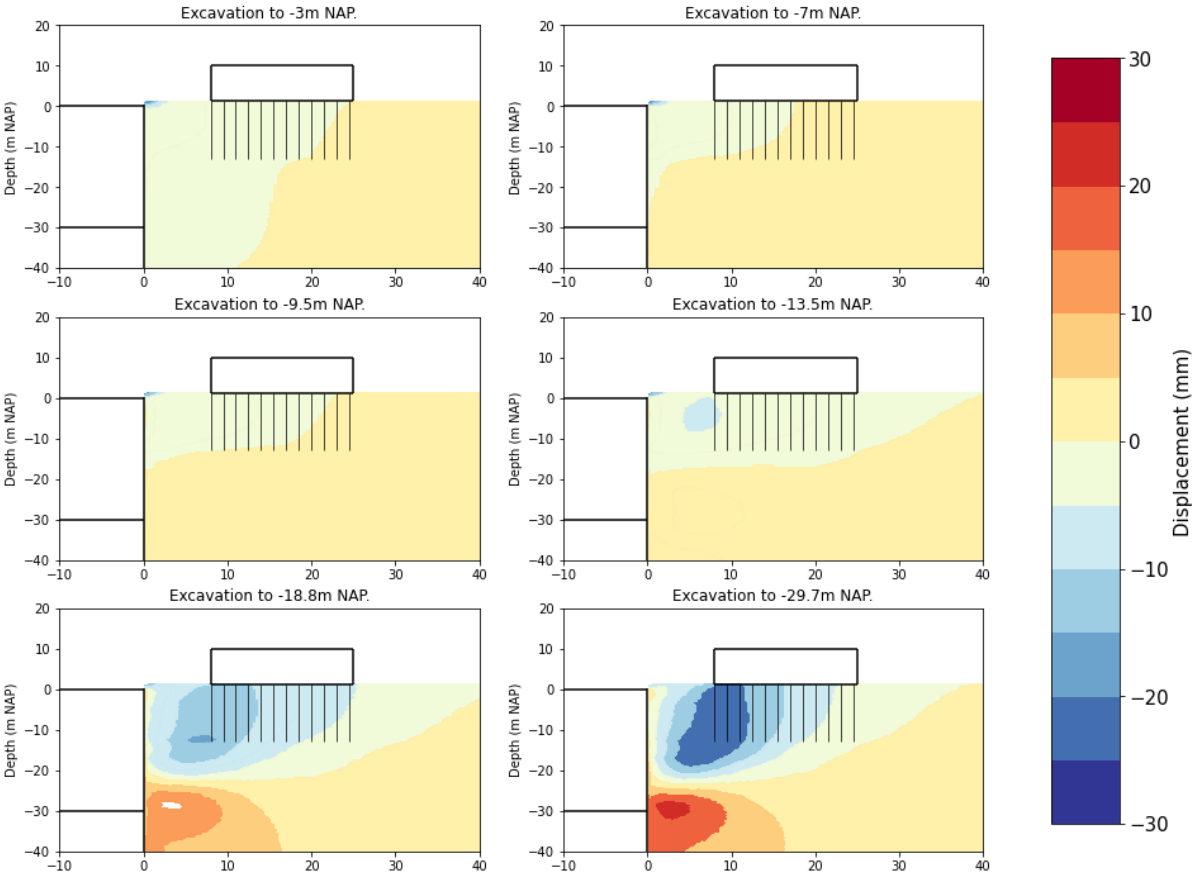

Total stress

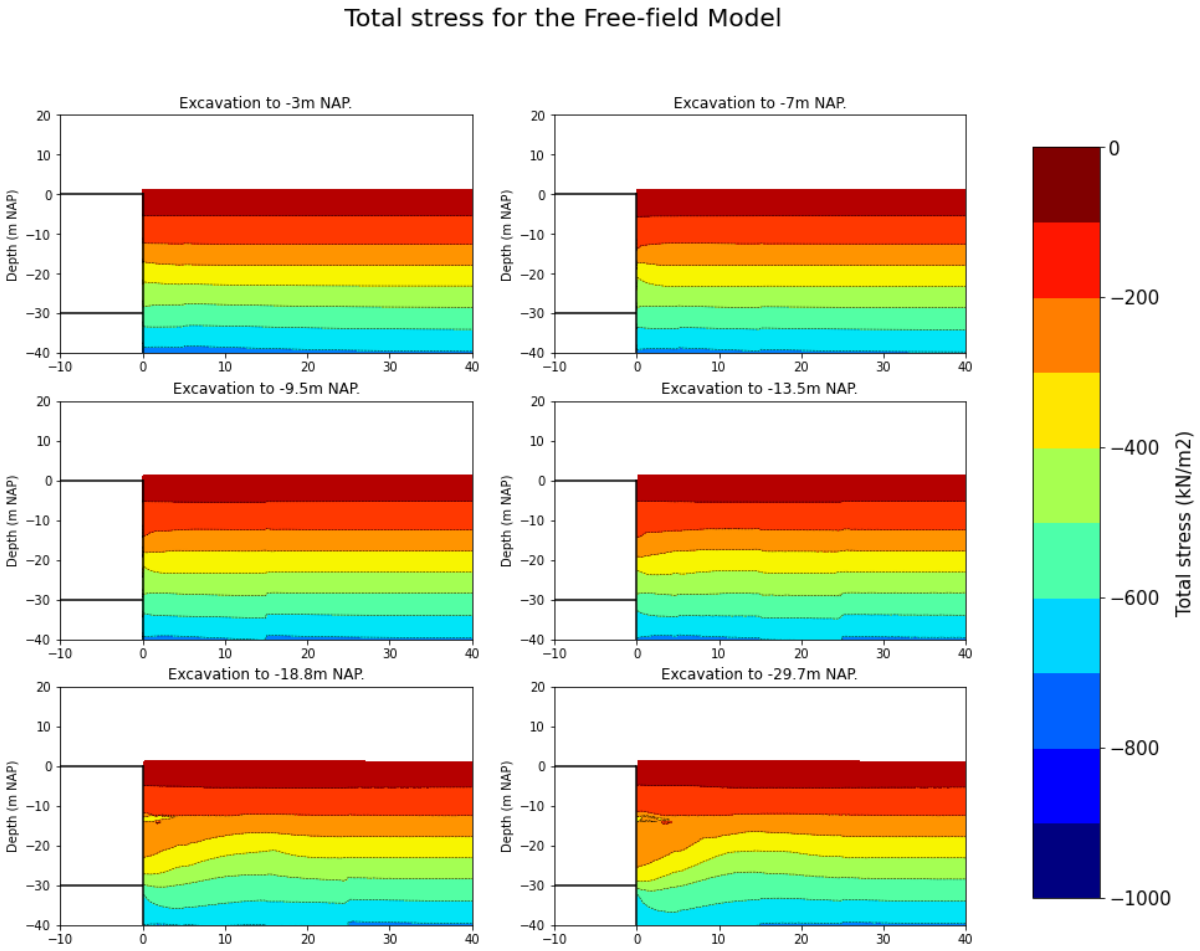

Total stress for the Loaded Pile Model

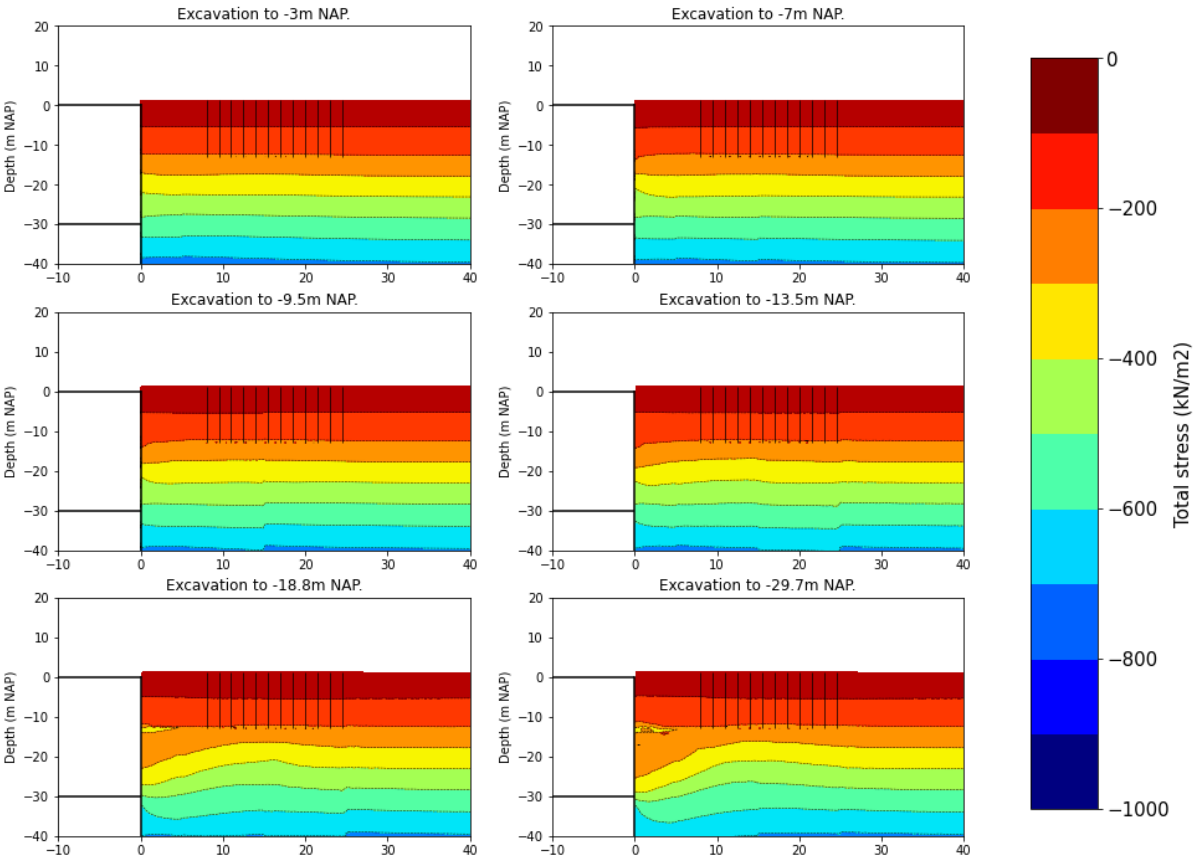

Total stress for the Building Model

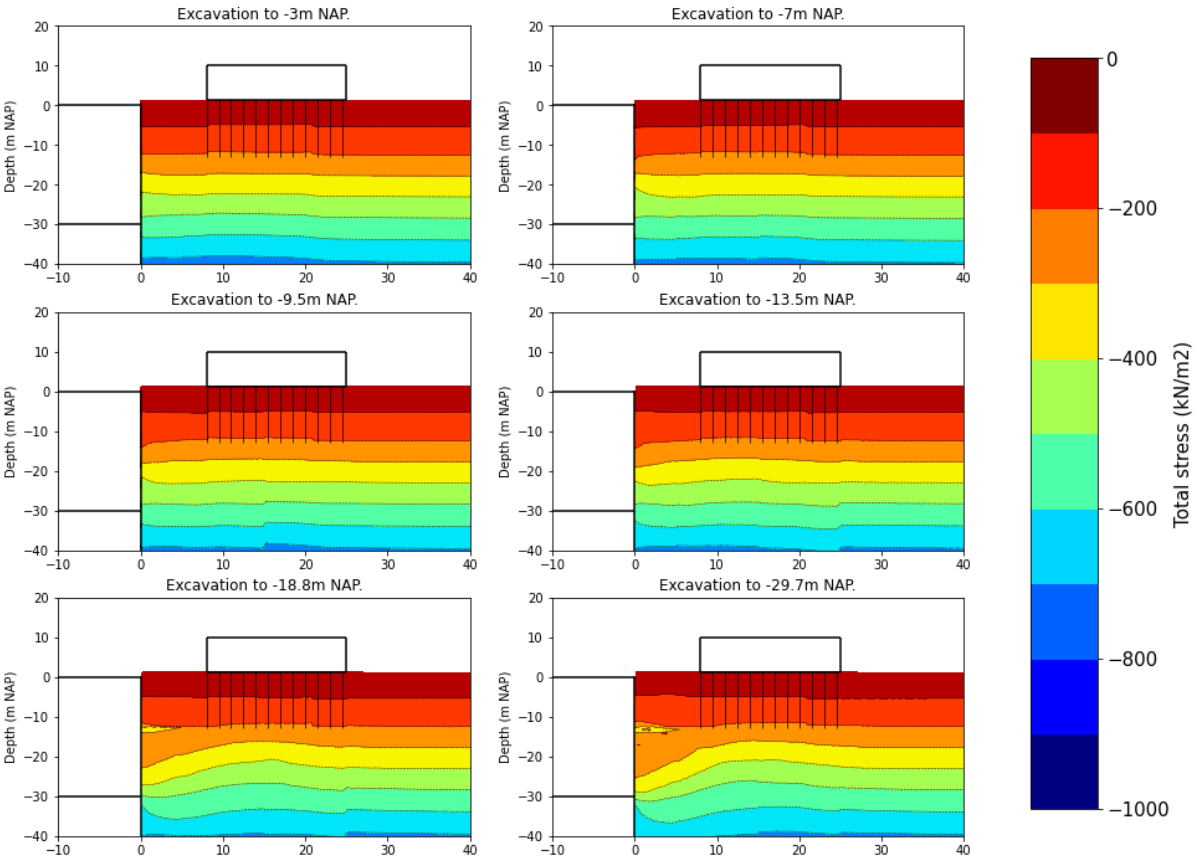

Effective stress

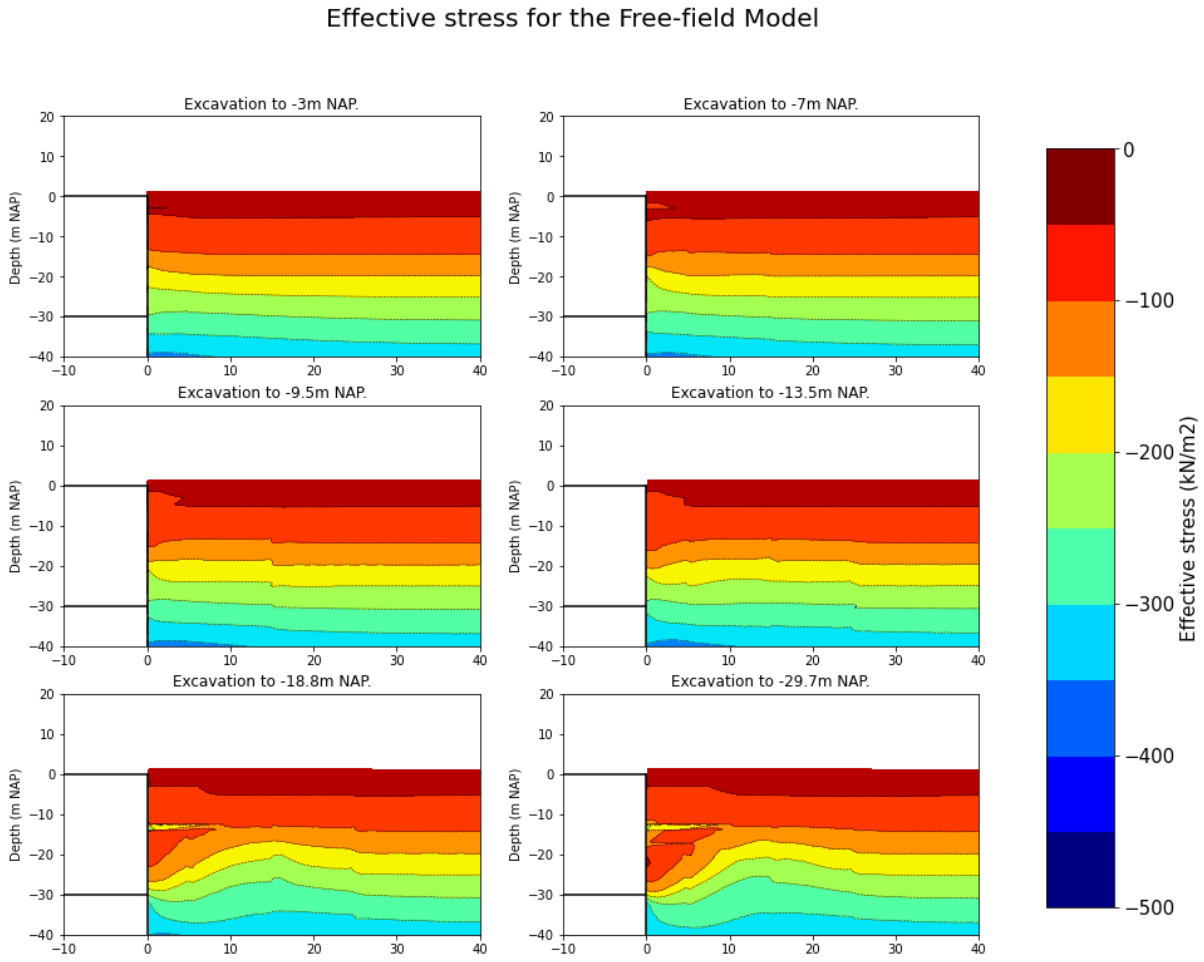

Effective stress for the Loaded Pile Model

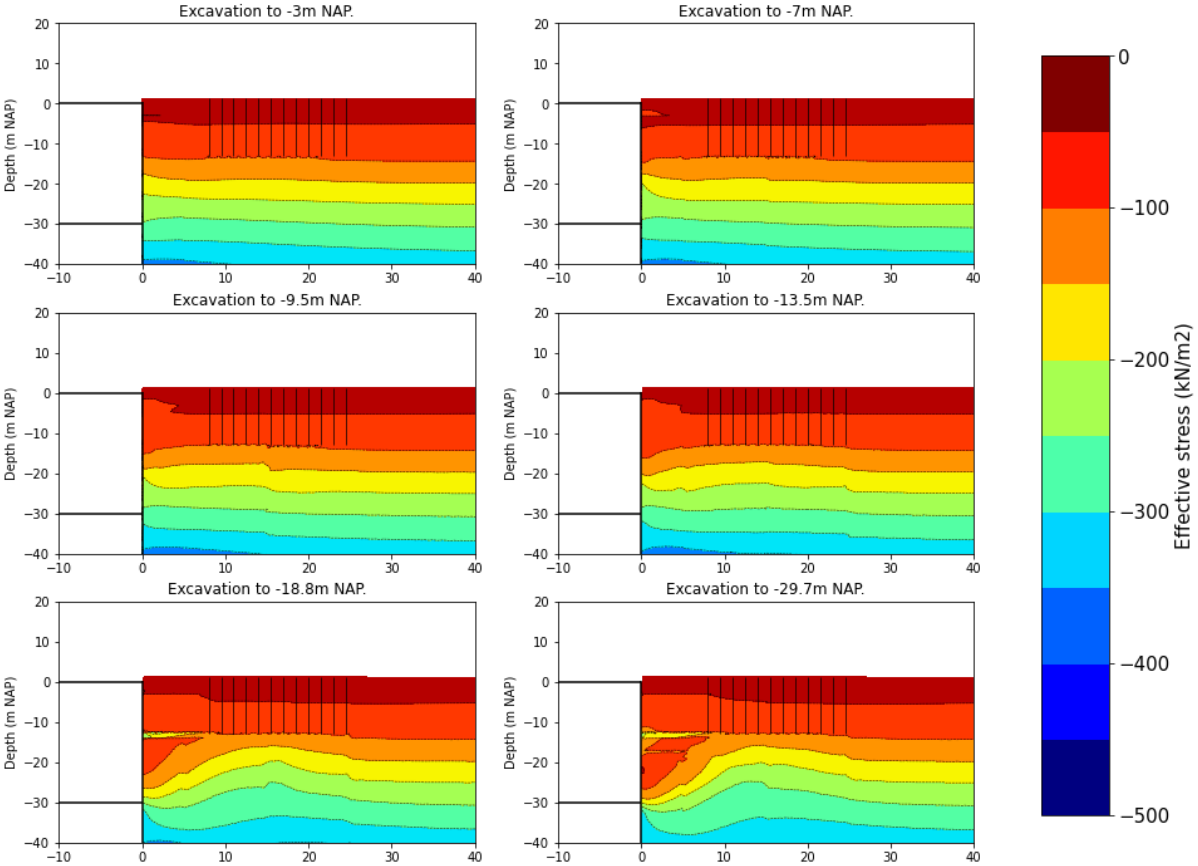

Effective stress for the Building Model